

Genetic dissection of the 11q13 amplicon
in squamous cell carcinoma

Céline Ismay Mahieu

Genetic dissection of the 11q13 amplicon in squamous cell carcinoma

Céline Ismay Mahieu

Colofon

Genetic dissection of the 11q13 amplicon in squamous cell carcinoma

Cover illustration Ellee Vikram

Design/Lay-out Proefschriftenbalie, Nijmegen

Print Ipskamp Printing, Nijmegen

ISBN 978-94-6473-419-5

© 2024, Céline Ismay Mahieu

Genetic dissection of the 11q13 amplicon in squamous cell carcinoma

Genetische dissectie van het 11q13 amplicon in plaveiselcelcarcinoom
(met een samenvatting in het Nederlands)

Proefschrift

ter verkrijging van de graad van doctor aan de
Universiteit Utrecht
op gezag van de
rector magnificus, prof. dr. H.R.B.M. Kummeling,
ingevolge het besluit van het college voor promoties
in het openbaar te verdedigen op

donderdag 25 april 2024 des middags te 12.15 uur

door

Céline Ismay Mahieu

geboren op 18 juli 1992
te Utrecht

Promotor

Prof. dr. R. Bernards

Copromotor

Dr. A.D. Tward

Beoordelingscommissie

Dr. E. van den Boogaard

Prof. dr. R.H. Brakenhoff

Prof. dr. P.J. van Diest

Prof. dr. E.M.D. Schuurin

Prof. dr. S.M. Willems

**When we try to pick out anything by itself,
we find it hitched to everything else in the universe**

John Muir

Contents

CHAPTER 1	General introduction	9
CHAPTER 2	Keratinocyte engineering for disease modeling and therapy development	25
CHAPTER 3	11q13 amplification drives squamous cell carcinoma through 3 distinct oncogenic events	51
CHAPTER 4	11q13 amplification-mediated rewiring of the cyclin D1 regulatory network in squamous cell carcinoma	85
CHAPTER 5	Discovery of ORAOV1 as a novel oncogene	115
CHAPTER 6	General discusscion	133
APPENDIX	References	149
	Nederlandse samenvatting	175
	Curriculum Vitae	179
	Dankwoord	180

Chapter 1

General introduction



Keratinocyte function in health and disease

Epithelial tissue is a layer of compacted cells lining organs, blood vessels, and the body cavities, as well as the outside of the body, which protects the underlying tissue from the environment. The oral mucosa and the skin are the most protective epithelial tissues as they form a physical barrier between the internal and external environment of the human body¹. Through this barrier function, these epithelia protect against damage caused by external factors such as chemicals, UV, allergens, and mechanical and physical injuries². Furthermore, epithelial tissues can have functions in water retention and absorption, vitamin D production, sensation, and regulation of the body temperature³⁻⁶.

The skin is comprised of 3 main layers. The epidermis is the epithelium that forms the outermost layer of the skin (Fig. 1). This is the main protective layer and consists of four cell types: Melanocytes for UV protection and pigmentation, Langerhans cells that guide the adaptive immune response, Merkel cells for somatosensation, and keratinocytes that form the structural barrier component. Of these four cell types, keratinocytes are the most predominant cells of the epidermis.

The basement membrane separates the epidermis from the layer underneath, the dermis. The dermis forms the supportive layer that is important for elasticity and holding appendages such as hairs and nails. Fibroblasts form the main component of this layer, alongside blood vessels, immune cells, and the extracellular matrix. The deepest layer is the hypodermis, which is mainly made of the subcutaneous fat layer and is important for thermal insulation, mobility, and mechanical protection⁷. In addition to white adipose tissue, the hypodermis also contains blood vessels, inflammatory cells, and mesenchymal stem cells.

Oral mucosa is similarly divided in layers (Fig. 1). The top layer is the epithelium, which closely resembles the epithelium in the epidermis. This epithelium consists of the same 4 cell types, with keratinocytes being the most abundant one, and is likewise separated from the supportive layer beneath - the lamina propria - by the basement membrane¹. The lamina propria consists mostly of connective tissue, fibroblasts, and blood vessels. Beneath the oral mucosa we find the submucosa, that typically forms a layer between the mucosa and muscle layers.

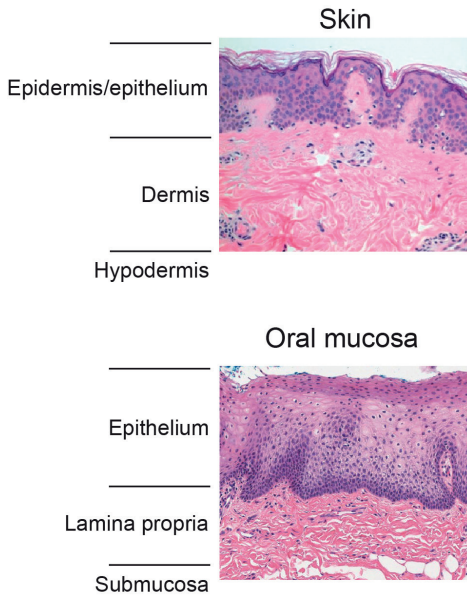


Figure 1 | Architecture of the skin and oral mucosa

The skin and oral mucosa display a comparable architecture. The skin consists of 3 layers: the epidermis (epithelial tissue), the dermis, and the hypodermis. The oral mucosa consists of 2 layers: the epithelium and the lamina propria, which are on top of the submucosa. The epithelial tissue layer is the top layer of these tissues that protects the underlying tissue from the external environment. This layer is mainly composed of keratinocytes. *Adapted from Ji et al. and Eisenberg et al*^{488,489}.

Keratinocytes in the epidermis and oral mucosa

The epidermis and oral mucosa are stratified epithelia that consist of layers of keratinocytes that are characterized by their specific morphology and biochemical and genetic markers^{8,9}. These different layers of keratinocytes show a cohesive cell architecture that is critical to the epithelial barrier function. This protection is established through dead keratinocytes that form a cornified layer at the top of keratinized epithelia, and/or through living keratinocytes that form a protective layer through mechanical cohesion created by desmosomes, adherens junctions, and tight junctions. Although keratinocytes in the dermal and oral epithelium have similar functions, they also show different morphology and behavior - particularly studied in the context of wound healing^{10,11} - and show some intrinsic differences in gene expression patterns¹².

The keratinized epithelium of the epidermis can roughly be subdivided into four layers of keratinocytes that express distinct marker proteins per layer (Fig. 2). The bottom layer of the epidermis is the stratum basale, which contains the proliferating

basal keratinocytes. Their daughter cells migrate upwards through the other layers - the stratum spinosum and the stratum granulosum - until they reach the stratum corneum at the skin's surface and eventually shed off³. The stratum corneum forms the outermost layer of the skin that regulates permeability and water retention. It is organized in a "brick and mortar" architecture, where the bricks are the enucleated, flattened, dead keratinocytes ("corneocytes") and the mortar is formed by a complex structure of linked protein and lipids that create an envelope around the cells^{13,14}.

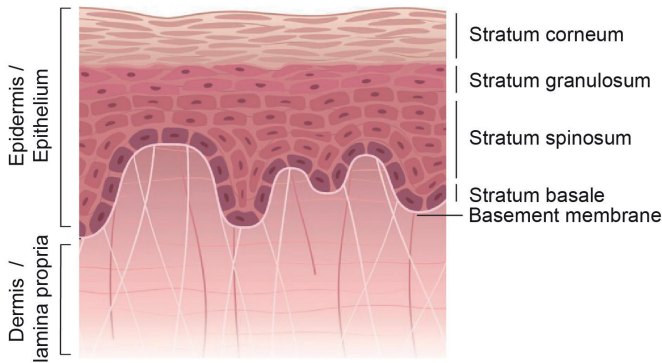


Figure 2 | Architecture of the epithelial layer

Most epithelial tissues, including the epidermis and keratinized oral mucosa, consists of four layers of keratinocytes. These layers exhibit different genetic and phenotypic characteristics that define their different stages of proliferation and differentiation. The Stratum Basale is the bottom layer and contains the proliferating keratinocytes. From here, the keratinocytes move upwards through the Stratum Spinosum and Stratum Granulosum, towards the Stratum Corneum, where they reach the final stage of differentiation and termination as enucleated, flattened, dead keratinocytes. *Adapted from Lawton*⁴⁹⁰.

In the oral mucosa, the epithelium can be either keratinized or non-keratinized. The mucosa that lines soft structures such as the lips, is generally non-keratinized. Mucosa that provide a tougher lining over for example the gingiva and hard palate, as well as specialized mucosa found at the dorsum of the tongue (containing specialized structures such as the tastebuds) are keratinized¹. These keratinized epithelia show the same structure as the epidermal epithelium (Fig. 2), whereas the non-keratinized mucosa is subdivided in the stratum basale, stratum filamentous, and stratum distendum, thus lacking a cornified layer on top¹.

Epithelial tissues are continuously regenerated, through a process of terminal differentiation - also known as cornification or keratinization - of keratinocytes. The basal layer contains distinct stem cell populations which give rise to the mature keratinocytes^{15,16}. As these cells differentiate, they detach from the basement membrane and lose their proliferative capacities. These progenitor cells then go

through a programmed process of differentiation while moving upwards through the epithelial layers, with - in the case of keratinized epithelium - the eventual purpose to form the cornified layer as terminally differentiated, enucleated, flattened keratinocytes¹⁷.

Regulation of keratinocyte proliferation and differentiation

To maintain intact barrier function, it is essential that proliferation and differentiation of keratinocytes are well balanced, as aberrant balance can result in epithelial disorders such as cancer, psoriasis, or defective wound healing. The proliferation rate in the basal layer is regulated by the desquamation rate in the top layer, creating a perfect homeostasis¹³. The epidermal differentiation process is tightly regulated through several transcriptional programs. These programs are in their turn regulated by transcription factors, signaling pathways, and epigenetic modifications on the one hand, and challenged by external factors, such as aging and UV radiation, on the other¹⁸⁻²⁰.

One of the main regulators of terminal differentiation is the epidermal differentiation complex (EDC). EDC is a gene dense region on the 1q21 chromosome that codes for several proteins, including proteins that are expressed by differentiating keratinocytes^{21,22}. Key regulators of the EDC and other proliferation/differentiation programs include P63 and Notch signaling, amongst others. P63 is generally regarded as the master regulator for the development of the epidermis²³⁻²⁵. Its activation prevents continuation of keratinocytes in the cell cycle and p63 deficiency results in aberrant differentiation²⁵⁻²⁸. Similarly, Notch activation makes cells withdraw from cell cycle activity, and upon Notch signaling cells show early differentiation markers such as KRT1 and KRT10²⁷⁻³¹. Other regulators of epidermal differentiation include MAPK signaling pathways and calcium, which is a strong inducer of differentiation^{8,32}.

Keratinocytes in wound healing

Since keratinocytes are the major cell type in the epithelium, they are not only important for maintenance of the epithelial layer, but also its regeneration upon wounding. Re-epithelization is the main characteristic of proper wound healing upon dermal or oral trauma and starts just hours post-injury³³. Dermal and oral keratinocytes show a very similar response to wounding, with the main difference that oral tissue shows faster, shorter, and a less intense healing response with lower inflammation rates and overall faster wound closure¹⁰⁻¹².

Upon epithelial injury, keratinocyte proliferation is activated, but this proliferation only occurs 0.5-1.0 mm away from the leading edge of the wound³⁴⁻³⁶. Rather, at the edge of the wound, only cell migration - not proliferation - occurs and keratinocytes move as a cellular sheet to eventually cover the wound^{35,36}. When a wound is formed,

keratinocytes secrete several immune molecules, such as cytokines, chemokines, antimicrobial peptides and extracellular vesicles, which function in the crosstalk between keratinocytes and hematopoietic immune cells³⁷⁻³⁹. For example, upon epithelial damage, keratinocytes produce IL-1, which recruits macrophages to the wound site⁴⁰. These macrophages in their turn stimulate fibroblasts to produce keratinocyte growth factor (KGF), which stimulates the migration and proliferation of keratinocytes⁴¹⁻⁴³.

Keratinocytes in disease and disease models

As the main cell type of epithelia, keratinocytes are integral to normal epidermal and oral function and regeneration, and aberrant keratinocyte function is at the base of several epithelial injuries or diseases. The epithelial barrier function is a complex culmination of several elements, including lipid content, cell-cell or cell-matrix junctions, keratinocyte proliferation, and epidermal differentiation. Alterations at any level of these cell elements or processes can result in impairment of the barrier function³.

Wounding of the epithelial layer results in disruption of the barrier and it is important that this wound heals quickly to restore the barrier. Wound healing prevents excess water loss or infection-induced sepsis, which in severe cases such as burn wounds or several genetic skin diseases ultimately can result in death. The importance of an intact barrier is exemplified by the increased survival rate of burn victims when an artificial barrier is placed over the wounds⁴⁴.

Genodermatoses are rare, monogenic skin diseases that present with defective skin morphology. Over 560 different genetic skin disorders have been identified, which have been associated with mutations in over 500 unique genes, frequently affecting the keratinocyte population⁴⁵. Examples of genodermatoses that find their cause in faulty keratinocyte function are Netherton Syndrome (NS), Harlequin Ichthyosis, and specific types of Epidermolysis Bullosa (EB). Although the cause of these hereditary diseases lays within the epithelium, they often come with systemic effects due to the importance of the epithelial layer for overall health. This severely affects the patients quality of life and in many cases reduces life expectancy⁴⁶. Current treatment strategies are mostly in the field of wound and/or skin treatment, without targeting the cause of the disease. However, thanks to sequencing efforts in the past decade, the current understanding about underlying genetics has significantly improved, thereby paving the way for better understanding of the molecular pathways and potential treatment options⁴⁶.

In order to identify precise pathogenic mechanisms and establish therapeutic opportunities, it is important to use appropriate disease models using human cells. For a number of genodermatoses there are transgenic and gene knockout mice models, although they frequently fall short in accurately recreating the clinical and histological

aspects of human skin conditions⁴⁷. Proof of principle for the idea of using primary human cells to model these diseases is presented in a recent study that modeled NS into human keratinocytes through CRISPR-Cas9 mediated disruption of the *SPINK5* gene. NS is characterized by a defective skin barrier due to inactivating mutations in *SPINK5*, resulting in faulty control of kallikrein expressions and excessive degradation of the stratum corneum⁴⁸⁻⁵⁰. Disruption of the *SPINK5* gene resulted in a hyperkeratic phenotype and other hallmarks of NS. Moreover, subsequent application of a lentiviral based *ex vivo* gene therapy reversed these phenotypes⁴⁷.

Similarly, primary keratinocytes can be used to model and treat forms of EB. There are several types of EB that differ and are classified dependent on the type of mutation, but they have in common that the epidermal layer has deficient adhesion to the dermal layer, resulting in blistering of the skin. Patients with Recessive Dystrophic EB (RDEB) carry a loss of function mutations in the *COL7A1* gene, resulting in dysfunctional or absent Type 7 Collagen (C7) production by keratinocytes and fibroblasts⁵¹. In healthy skin, C7 assembles in homotrimers to form a network of anchoring fibrils in the basement membrane, that attach the epidermis to the dermis^{52,53}. Therefore, in RDEB patients, the *COL7A1* mutation results in severe and chronic blistering of the skin and other stratified epithelia, including the oral mucosa, reducing life expectancy and increasing the risk of cancer development⁵¹.

Current efforts in the development of therapeutic approaches against RDEB include the delivery of a correct full length *COL7A1* gene, or the *ex vivo* correction of the mutation in patients' cells followed by a transplant of the autograft⁵⁴⁻⁵⁶. To assess the efficiency, safety, and mode of action of such therapies, large numbers of RDEB keratinocytes are needed. However, it can be challenging to acquire sufficient cells from patients as keratinocytes have a limited life span, patients already have a fragile epithelium, and there are many different mutations. Therefore, modeling the mutations as found in patients in primary keratinocytes derived from healthy skin samples can be a solution to provide sufficient material to test and develop novel therapies against EB. This shows that the use of primary human keratinocytes in the modelling of genodermatoses is an attractive option to increase the understanding of the pathogenesis and establish novel therapeutic strategies.

In contrast to the single mutations and hereditary pattern for genodermatoses as described above, a culmination of specific mutations over time can also result in keratinocyte-based diseases. Squamous cell carcinomas (SCC) originate from keratinocytes that - induced by risk factors such as tobacco and UV - over time develop a complex mutational pattern that result in uncontrolled proliferation⁵⁷. Due to the complexity of this mutational pattern, it can be challenging to identify which mutations are the key-drivers of disease development and if the order in which mutations occur affects the pathogenesis. SCC can develop in any epithelial tissue, but the most frequent types are SCC of the skin, lung, and head and neck, due to their

high level of exposure to risk factors⁵⁷. To develop better treatment strategies for SCC, it is essential to understand which genomic alterations are driver events for either the development or progression of the disease. For this purpose, it is insightful to study frequently occurring alterations in the context of normal keratinocytes and assess how these alterations change keratinocyte morphology and behavior. This allows us to study SCC initiation and progression in an early stage, as opposed to the use of cancer cells, which only allows us to study disease progression at later stages. Ultimately, the combination of both early- and late-stage disease models will provide a complete understanding of SCC progression. Below we will further expand on the epidemiology, mutational landscape, and development of head and neck squamous cell carcinomas.

Overall, keratinocytes are an integral part of the epithelial tissue and therefore play an important part in its barrier function. Genomic alterations in these cells can result in severe disorders, including genodermatoses and SCC. Therefore, normal keratinocytes can be an important tool in increasing our understanding of the molecular mechanisms behind these diseases through modeling of their accompanying alterations, moving forward the development of novel therapeutic approaches, and potentially even be part of the solution in restoring the epithelial barrier upon injury.

Head and Neck Squamous Cell Carcinomas

Head and Neck Squamous Cell Carcinoma (HNSCC) develops from keratinocytes in the mucosal tissue lining the mouth, nose, and throat areas and accounts for >90% of all head and neck cancers⁵⁸. In 2020, 930,000 patients were diagnosed with head and neck cancer. HNSCC incidence is still on the rise with new diagnoses expected to surpass the 1,000,000 mark within this decade⁵⁹⁻⁶¹. In the majority of cases, patients are only diagnosed in advanced disease stages, partially explaining the high mortality rate of over 50%⁵⁸⁻⁶¹.

HNSCC is typically associated with tobacco and alcohol consumption, although in recent years there has been an increasing incidence of the human papilloma virus (HPV)-induced subclass. HNSCCs are typically subdivided into HPV-positive and HPV-negative subclasses, as these classes show clear differences in their population statistics, genetic landscape, and prognosis⁶²⁻⁶⁷. Whereas the HPV-negative subtype shows a strong correlation to cigarette pack-years, the HPV-positive subtype affects a younger population that were often “never-smokers” and its occurrence is more frequent in the Western world. Furthermore, HPV-positive HNSCC has a significantly better prognosis⁶⁵⁻⁶⁷, as this disease subclass typically only advances regionally and only 7-9% of patients develop distant metastasis over the course of the disease⁶⁸. Although cigarette/alcohol intake and HPV infection are the biggest risk factors, genetic predisposition can also play a part in disease development, for example in patients that have polymorphisms in carcinogen-metabolizing or immune pathways^{69,70}.

The current standard of care for HNSCC includes surgical resection (if operable), followed by radiation and cisplatin treatment. Although effective at controlling local disease progression, cisplatin treatment comes with serious dose-limiting toxicities and can have long term side effects^{71,72}. Moreover, cisplatin is less effective in reducing the incidence of distant metastasis, and patients often develop treatment resistance^{68,73,74}. Therefore, in most cases a combination of approaches or alternatives is necessary. One alternative approach is the use of cetuximab – an EGFR monoclonal antibody that can function as radiosensitizer – both as stand-alone or combinatorial therapy⁷⁵. Cetuximab is mostly used in patients that are not eligible for cisplatin treatment, as cisplatin is still the preferred chemotherapy with better results^{76,77}. Additionally, several immune checkpoint inhibitors are now available, including pembrolizumab and nivolumab, which are used in recurrent or metastatic disease^{78,79}.

Despite aggressive therapeutic intervention, approximately half of patients develop recurrent disease within two years. Over the past decades, there have been some improvement in the 5 year survival rate of all HNSCCs, but this is largely explained by the relatively increased number of HPV positive cases^{80,81}. If we look at the prognosis of the HPV-negative subset by itself, there has been minimal improvement. The poor prognosis and lack in patient outcome improvement has prompted several studies aiming to further classify HNSCC in subgroups based on their gene expression profiles⁸²⁻⁸⁴. However, these subgroups have not been widely adapted in clinical settings as they showed to only have limited clinical utility⁸⁵. Therefore, a better understanding of how the molecular landscape of HNSCC contributes to disease development and progression is needed.

Mutational landscape of HNSCCs

Over the course of life, cells acquire genetic and epigenetic alterations⁸⁶⁻⁸⁸. Most of these alterations do not affect cell function and are just passive bystanders. However, occasionally an alteration occurs that provides the cell with a growth advantage, resulting in clonal growth. These clones are thought to be at the origin of cancer^{87,88}. To transform a normal cell into a cancer cell, several molecular regulatory changes are necessary. These include induction of genomic instability, sustained proliferation, and evading cell death among others⁸⁶. These changes can be caused by a variety of genetic alterations, depending on the type, origin, and stage of the tumor progression.

The two most prevalent types of mutation are single nucleotide alterations and DNA copy number alterations (CNA). Single nucleotide alterations are the loss, insertion, or substitution of a single nucleotide in a gene. These mutations are typically silent, but can result in either a loss or activation of gene function if they occur in a functional domain of the protein. DNA copy number alterations are a common and important form of genetic instability in which gain or loss of whole chromosomes or chromosomal regions can result in altered expression of oncogenes and tumor suppressor genes⁸⁶.

Although chromosomal deletions in cancer have been extensively studied, much less is known about amplification of chromosomal regions (referred to as ‘amplicons’), due to challenges in comprehensively modeling and studying amplifications. Amplicons can exist either extrachromosomally on double minutes, or intrachromosomally at the original or a new genomic location. The formation of amplicons can be promoted by chromosomal fragile sites, defective DNA replication, and dysfunctional telomeres in a background of aberrant DNA damage control^{189,90}.

Several sequencing efforts have characterized the most frequent genetic alterations in HNSCC⁹¹⁻⁹³. These studies revealed that HNSCC is a heterogeneous disease, characterized by a wide variety of mutations and genetic instability with frequent loss or gain of chromosomal regions. The most comprehensive analysis of the mutational landscape of HNSCC so far is the The Cancer Genome Atlas (TCGA) study, in which 520 tumors were analyzed for CNA, mutations, mRNA and miRNA expression⁹². This study confirmed previous findings showing that the mutational landscape is very different between HPV-positive and HPV-negative tumors and thus these two types of HNSCC should be considered different diseases⁹¹⁻⁹³.

Analysis of HPV-negative tumors shows that these tumors carry a high mutational burden, with the most frequent alterations in the tumor suppressor genes *TP53* (84%) and *CDKN2A* (58%)⁹². The latter gene is also frequently silenced through epigenetic mechanisms, making the total frequency of loss of *CDKN2A* function even higher. *TP53* is a key tumor suppressor, found dysregulated in virtually all tumors, that couples the activation of apoptosis and suppression of the cell cycle to DNA damage⁹⁴. *CDKN2A* codes for the P16 protein, which is an inhibitor of the cell cycle at the G1-S checkpoint that functions through inhibition of the phosphorylation and degradation of the cell cycle repressor RB1⁹⁵. Thus, through inactivation of both *TP53* and *CDKN2A*, cells activate cell cycle progression while avoiding cell death and allow for further accumulation of genetic alterations. Other frequent mutations in HPV-negative HNSCC are found in *FAT1*, *NOTCH1*, *KMT2D*, *NSD1*, *CASP8*, and *PIK3CA*⁹².

Moreover, HPV-negative HNSCC carries frequent CNA⁹⁶. These CNA can span both large chromosomal regions, such as loss of chromosomal arms 3p and 8p, or gain of chromosomal arms 3q, 5p and 8q. The CNA can also be focal, as is the case for deletions found for some of the aforementioned tumor suppressor genes, including *CDKN2A* and *NOTCH1*. Moreover, HNSCC displays frequent focal amplification in, for example, receptor tyrosine kinases (*EGFR*, *FGFR1*, *ERBB2*) or oncogenes such as *MYC* or *CCND1*. *CCND1* is part of a wider focused amplification in the 11q13 region that includes several genes with potential oncogenic functions. The 11q13 amplification is a frequent focal amplification in HNSCC, found in 31% of HPV-negative HNSCCs⁹².

In contrast, HPV-induced tumors show a low frequency of alterations in tumor suppressor genes such as *TP53* and *CDKN2A*, but a relatively high incidence of

alteration of the Pi3K pathway, either through amplification or gain of function mutation in PIK3CA, or through loss of function mutations in *PTEN*^{92,93,97}. However, the main oncogenic alterations in these tumors are caused by the HPV-virus. The majority of HPV-positive HNSCCs is associated with HPV-16, although some are associated with HPV-18 or other high risk HPV types⁹⁸. HPV is a double stranded DNA virus that carries several genes, including the E6 and E7 oncoproteins, which are important for the malignant phenotype of HPV-positive cells⁹⁹. The E6 and E7 oncoproteins associate with and stimulate degradation of P53 and Rb1, respectively, resulting in evasion of cell death and releasing the break on the cell cycle. Thus, HPV-infection provides an alternative mechanism to affect the *TP53* and *CDKN2A-RB1-CCND1* pathways.

Development and progression of HNSCC

Cancer formation is a complex process in which cells accumulate somatic mutations at random. Subsequent positive selection for the presence of driver mutations results in a progressively more cancerous state of the cells⁹⁸. The development from normal keratinocytes to metastatic HNSCCs follows a series of steps (Fig. 3). From a histopathological perspective, the first step is hyperplasia of keratinocytes, followed by dysplasia, carcinoma *in situ*, and eventually invasive carcinoma as the carcinogenic keratinocytes break through the basement membrane⁵⁸. Advancement through these stages comes with increasing frequency of oncogenic mutations¹⁰⁰.

As described above, numerous extensive analyses on the genetic landscape of HNSCC exist. However, these analyses typically focus on mutations found in the final stages of HNSCC, making it difficult to interpret at which stages these mutations occur and how they affect tumor progression. Moreover, it remains unclear if these mutations need to occur in a specific temporal sequence, or whether simply accumulating these mutations is sufficient for disease progression. Lastly, sequencing efforts such as TCGA have enabled the discovery of many mutated genes. Dependent on the used analysis platform, data show 50-100 significantly mutated genes, which are then classified as 'candidate drivers'. However, many of these genes only show low frequency occurrence or have unknown functions in tumorigenesis. Thus, it is important to acquire experimental evidence on the contribution of frequently occurring genetic alterations in HNSCC to assign driver functions.

Normally seeming tissue can already contain several oncogenic mutations. For example, studies in skin show that normal dermal keratinocytes display many mutations^{101,102}. Normal aged skin carries approximately 2-6 mutations per megabase, with a positive selection for mutations in cancer-associated genes such as *TP53*, *NOTCH1*, and *FAT1*^{101,102}. This selection results in mutant clones, which can spread laterally throughout the skin, thereby outcompeting neighboring cell clones¹⁰². Despite the presence of cancer-favoring mutations, these patches of skin do not

display a cancerous phenotype, likely because they are space constraint and therefore forced to behave normally^{103,104}. Similarly keratinocytes in normal aged esophageal tissue show a high level of mutational burden, especially in cancer genes such as *TP53* and *NOTCH1*¹⁰⁵. Cells with these mutations can form mutant clones that colonize the esophagus, but still are displaying normal cellular behavior. Thus, in order to transition to a cancerous phenotype, these keratinocytes require additional genetic alterations.

Only a few studies have aimed to compare the genetic landscape of normal, neoplastic, and cancerous oral tissues^{100,106,107}. These studies find that in HNSCC, mutations in tumor suppressor genes such as *TP53*, *CDKN2A*, *NOTCH1*, and *FAT1* are some of the earliest events and can already be detected in potentially premalignant lesions^{100,107}. However, many somatic CNA are found only in later stages of tumorigenesis^{100,106,107}. For example, deletion of *CSMD1*, deletion of *NOTCH1*, or amplification of *PIK3CA* is frequently found in the transitioning stage from potentially premalignant lesion towards malignant tissue¹⁰⁷. Amplification of the 11q13 region coincides with the transition to a severely malignant and metastatic stage^{100,107}. Thus, whereas single nucleotide mutations are already present in normal and pre-neoplastic tissue, CNA characteristically occur during the late stages in carcinogenesis (Fig. 3). Therefore, further investigation into the contribution of commonly occurring CNA - such as the 11q13 amplification - to the progression of HNSCC will increase the understanding of the pathogenesis of this morbid and lethal disease.

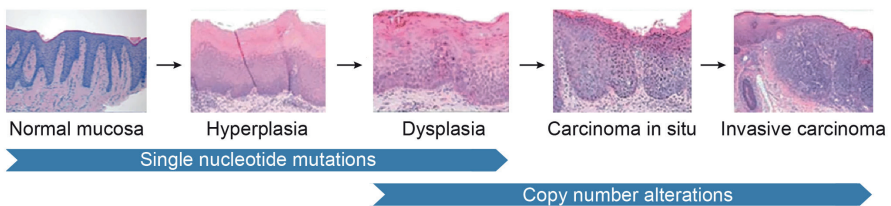


Figure 3 | Development of HNSCC

The development and progression of HNSCC from normal mucosa goes through several stages, which include hyperplasia, dysplasia, carcinoma in situ and eventually invasive carcinoma. Progression is caused by an accumulation of oncogenic mutations, amongst which single nucleotide mutations and copy number alterations are the most important contributors. Although all types of mutations can be found to arise in any stage, single nucleotide mutations are commonly found in the earlier stages of HNSCC development, whereas copy number alterations, such as amplification of the 11q13 region, are more frequently found to arise in and contribute to the later stages of cancer progression. *Adapted from Johnson et al.*⁵⁸.

Thesis outline

As described in this introduction, genomic alterations in keratinocytes are at the base of several epidermal diseases, including HNSCC. Improved disease modeling will enhance our molecular understanding of such diseases and create novel therapeutic strategies. The work described in this thesis aimed to first provide a better tool to study the effects of genomic alterations on keratinocyte function, and second apply this tool in the genomic dissection of the 11q13 amplicon in HNSCC.

In **Chapter 2** we describe a novel workflow for the efficient transfection and engineering of primary adult keratinocyte through electroporation. We demonstrate near 100% efficiencies for transfection and engineering of adult primary keratinocytes by mRNA and CRISPR-RNPs and show efficient knockout of some of the most frequently altered tumor suppressor genes. Lastly, we apply this technology towards a proof of concept for the development of universal donor keratinocytes for use in allogeneic cell therapies.

In **Chapter 3** we report the genetic dissection of the 11q13 amplicon in SCC. A combination of CRISPR-interference, CRISPR-knockout, lentiviral overexpression, and computational analysis finds that 3 genes - *CCND1*, *ORAOVI*, and *MIR548K* - are the main contributors to the oncogenic effects of the 11q13 amplification.

In **Chapter 4** we study the role of amplified *CCND1* in SCC development and progression and find that its amplification induces *CCND1* oncogene dependence. This dependence is in contrast to primary cells, which show higher expression and dependence on *CCND2*. We find that cyclin D1 largely acts in a CDK-independent manner, suggesting that direct cyclin D1 targeting is favorable over CDK targeting. Lastly, we identify *RRM2* as a downstream target of *CCND1* and suggest *RRM2* as an alternative target in *CCND1* amplified tumors.

In **Chapter 5** we describe the discovery of *ORAOVI* as a pan-cancer essential oncogene and show that its inhibition might be specifically effective in cancer cells as opposed to primary cells. Mechanistically, we find that *ORAOVI* is involved in protection against oxidative stress and identify that *ORAOVI* induces expression of Thioredoxin, a key regulator of oxidative stress.

Finally, **Chapter 6** summarizes the main findings of this thesis and discusses these findings in the context of previous work on the topic. This chapter has a particular focus on the future perspectives of the use of CRISPR-Cas technologies in the understanding and treatment of skin diseases, interpreting copy number alterations in cancer, and the implications of the work described in this thesis for therapeutic approaches for 11q13-amplified HNSCC.

Chapter 2

Keratinocyte engineering for disease modeling and therapy development

Céline I Mahieu¹, Andrew G Mancini², Aaron D Tward¹

¹Department of Otolaryngology - Head and Neck Surgery, University of California
San Francisco, San Francisco, USA

²MaxCyte, Inc., Gaithersburg, MD, USA

Parts of this chapter are protected under invention disclosure SF2023-128
(*University of California*)



Abstract

Many skin diseases or conditions are caused by defective or damaged epidermal tissue due to loss of normal keratinocyte function. To gain better insights into these conditions, the development of representative genetic models is essential. Moreover, engineered keratinocytes are an attractive option for cell therapies for a variety of dermal conditions. Therefore, we need the ability to engineer keratinocytes to study the effect of mutations on keratinocyte function and develop keratinocyte-based cell therapies.

Current strategies to generate engineered keratinocytes are constrained by the lack of efficient delivery of genome editing machinery. Here, we describe a new electroporation-based cell engineering workflow that results in highly efficient delivery of mRNA and CRISPR RNPs to primary keratinocytes derived from four distinct anatomical sites. Using this new strategy, we are able to routinely achieve gene editing efficiencies between 85 and 100% in under one week, thereby eliminating the need for any downstream sorting or selection during the keratinocyte engineering process. Importantly, our novel cell engineering process preserves normal keratinocyte morphology and does not compromise cell viability or growth potential. Finally, we show the scalability of the electroporation process, therefore enabling the manufacturing of millions of engineered keratinocytes in a GMP-compliant process with no loss in efficiency. We show that we can use this workflow to generate accurate genetic models for squamous cell carcinoma. Moreover, we demonstrate a proof of concept generation of universal donor primary adult keratinocytes for the use in cell therapies.

Overall, we establish an improved workflow for the production of engineered keratinocytes, decreasing engineering time down to under one week, while significantly increasing efficiency and viability. These improvements open the door for the development of robust keratinocyte-derived disease models and engineered keratinocyte-based cell therapies.

Introduction

Keratinocytes are the major cell type of the epidermis and are fundamental for both the epidermal barrier function and wound healing of the tissue, as discussed in chapter 1. Many skin diseases or conditions – including squamous cell carcinoma (SCC), epidermolysis bullosa (EB), pressure ulcers, and burn wounds – are caused by defective or damaged epidermal tissue due to loss of normal keratinocyte function. In disease, this loss of keratinocyte function is often caused by mutations in specific genes, such as the *KRT5*, *KRT14*, or *COL7A1* genes in EB, or *TP53* and *CDKN2A* in SCC. To gain better mechanistic and therapeutic insights into these conditions, the development of representative genetic models is essential. High fidelity disease models allow us to study the effect of mutations on normal keratinocyte function in their appropriate genetic context. Additionally, conditions that cause wound formation or defective wound healing could benefit from keratinocyte-based cell therapies to improve and restore the epidermal barrier function. For both the development of genetic models and keratinocyte-based cell therapy, the ability to efficiently engineer keratinocytes is essential.

Limitations in keratinocyte engineering

Keratinocytes are hard to transfect and current strategies to generate engineered keratinocytes are constrained by the lack of efficient delivery of genome editing machinery. The low efficiency transfection methods used by current cell engineering workflows necessitate the inclusion of time-consuming single cell sorting or selection steps to achieve a highly pure edited cell population. However, due to the fragile and adherent nature of keratinocytes, these types of selection processes typically result in growth arrest, phenotypic changes, or cell death, thus placing additional limitations on the manufacturing of engineered keratinocytes. These limitations thereby constrain studying keratinocytes in health and disease and block the development of keratinocyte-based cell therapies.

Keratinocytes in disease modeling

As discussed in Chapter 1, we have a good understanding of the mutational landscape for many genetic keratinocyte diseases. For diseases that have a simple mutational pattern, such as EB, we already have a good understanding of the contribution of these mutations to disease development, but genetic models can still contribute to new therapeutic insights. However, for diseases with more complex mutational patterns, such as SCC, it is more challenging to ascribe driver and passenger function to genetic alterations. Head and Neck SCC (HNSCC) tumors have high genomic instability, with reported average copy number alterations and coding mutations of 141 and 130 per tumor, respectively^{92,91}. Some of the most frequent mutations, however, have also been found in non-cancerous epithelial tissue, raising the question to what extent single

mutations contribute to tumorigenesis^{101,105}. It is challenging to study the effect of a single mutation on cancer progression in the context of a cancer cell, as signaling pathways may be affected in several ways. Moreover, cancer cell lines are subject to both genetic and phenotypic instability, which can result in selection of subclones as cells are adapting to the *in vitro* culturing conditions.

Modeling the effect of single mutations on the oncogenic transformation process in primary cells has several advantages over working with cell lines. First, cancer cell lines have often been around for decades, the origin and subtype may not be fully documented, and there is a risk that the cells over time have become contaminated with either micro-organism, or other cell types, such as the HeLa cell line¹⁰⁸⁻¹¹⁰. In contrast, primary cells have a defined origin and limited lifespan. Additionally, these cells have not fully adapted to the cell culturing conditions and remain their primary cell identity. This retention of primary cell identity allows us to study the process of transformation from a normal to a cancerous cell at the intermediate stages in a more representative model, instead of studying only the final stage of the cancer cell. Thus, efficient keratinocyte engineering will allow for studying the effect of oncogenic alterations in a representative cell type and help elucidate essential alterations in the oncogenic transformation process.

Keratinocytes in cell therapy - restoring the epithelial barrier function

Faulty keratinocyte function is not only a cause of several epithelial disorders, it can also be a consequence of epithelial barrier damage. This damage can be caused by either epithelial or systemic diseases, such as diabetic foot ulcers, or through external damage, such as burns or scrapes. As keratinocytes are the major affected cell type upon this epithelial barrier damage, keratinocyte-based cell therapies can be used to restore the epithelial barrier function.

The use of engineered keratinocytes for cell therapy has long been an attractive option to treat various dermatological, oral, and aural disorders. Keratinocytes are easily adapted to *in vitro* culture and expanded from even small tissue specimens, making them an ideal cell source for a range of autologous and allogeneic cell therapy products. Although the first generation of keratinocyte-based cell therapies showed some promise in treating certain skin diseases, they were generally not more effective than standard of care and therefore not widely adopted.

Cell therapies to restore the epithelial barrier function of the skin have been mostly focused on the culture and development of epidermal grafts. The first successful epidermal graft was cultured in 1979 by Green *et al*, which was quickly followed by the first successful treatment of 3rd degree burn wounds with autologous epidermal grafts^{111,112}. Since this initial work, there have been many studies with epidermal grafts to treat skin wounds caused by burns or due to inherited skin diseases such as EB, with

varied successes (reviewed by Petrof et al.¹¹³). Developments to improve the success rate have mainly focused on several variables in the composite of the skin graft. Examples are addition of other types of skin cells besides keratinocytes (including melanocytes, fibroblasts, and Langerhans cells), the origin of the cells (autologous or allogeneic), composite/addition of a matrix (fibrin, collagen, acellular dermis), and the way of administration (graft or spray).

Despite these developments, the standard in the field remains the split thickness or full thickness autograft, sometimes combined with *ex vivo* keratinocyte proliferation to increase available donor material^{114,115}. However, the skin autograft has serious limitations, and *ex vivo* proliferation costs valuable time (2-3 weeks) in which the patient is susceptible to inflammation and scar formation. Moreover, autografts are not always suitable, for example for patients where the wound covers large areas of the body, elderly patients, or patients with inflammatory conditions. Therefore, the use of allogeneic 'off the shelf' cells is an interesting option, as these cells could be readily available and decrease the burden on the patient.

Already in 1983 the first patients were treated with allogeneic keratinocytes from unrelated donors¹¹⁶. Although initially it was thought that these allografts successfully incorporated into the patients dermis, later reports showed that allogeneic donor cells quickly disappeared, and it is now well established that allogeneic keratinocytes only persist for a couple weeks after transplantation¹¹⁷⁻¹²¹. Recognition of allogeneic keratinocytes as non-self by the hosts T-cells results in elimination by the immune system, limiting the persistence of these cells in the skin. Administration of immunosuppressants to receiving patients does increase the survival of the graft, but the added risks on e.g. inflammation and toxicity, make this a precarious alternative¹²². Although allogeneic keratinocytes do not engraft, they still provide some healing properties that are attributed to secreted factors¹²³. Therefore, currently the use of allogeneic keratinocytes is limited to conditions where temporary dressing can suffice, such as small burns. For larger and more severe wounds, however, current allogeneic cell therapies insufficiently stimulate full reepithelization.

Another strategy in the field of gene and cell therapy to treat genetic skin diseases is through *ex vivo* gene repair. In this approach, the patients' cells are engineered *ex vivo* to repair the faulty gene, and then placed back. This approach is of particular interest in the treatment of EB, where currently TALEN and CRISPR are being explored as a viable strategy to edit keratinocytes^{55,56,120,124-127}. For example, deletion of exon 80 of a faulty *COL7A1* gene or homology-directed repair (HDR)-based correction of mutations in the *COL7A1* gene using CRISPR-Cas9 or TALENs showed restored expression of *COL7A1*^{55,56,125,126}. However, correction efficiencies were only 11-15%, limiting the use of this approach for clinical applications.

Overall, the development of keratinocyte-based disease models and cell therapies is very promising but is being held back by the lack of efficient genome engineering methods for primary adult keratinocytes. Here, we present a novel workflow for very efficient transfection and genome engineering of primary adult keratinocytes from distinct anatomical sites. We apply this workflow to the development of HNSCC models and demonstrate the production of universal donor adult keratinocytes through deletion of MHC-I and MHC-II complexes through CRISPR-Cas9, paving the way for keratinocyte-based allogeneic cell therapies.

Results

High Efficiency Delivery of RNA and CRISPR RNPs to Primary Keratinocytes

To achieve highly efficient transfection of primary adult keratinocytes, we explored several chemical and electroporation-based transfection methods (see **Table 1**). We achieved the highest transfection efficiency with the ATX electroporation instrument (MaxCyte). Therefore, we explored these transfection options and conditions further. For the purpose of transfection (and gene editing, see figure 2) optimization, we used primary foreskin keratinocytes (FKC), as these keratinocytes have a low mutational burden and are - comparably - easier to obtain and culture. Transfection of primary FKC with mRNA-GFP at two different concentrations and at three different energy levels resulted in transfection efficiencies over 90%. mRNA uptake increased with higher energy and higher mRNA concentrations, with up to 97% transfection efficiency under optimal transfection conditions (**Fig 1a**). Similarly, transfection of ATTO-550 labeled CRISPR RNPs resulted in highly efficient transfection, with uptake efficiencies of >99% at the higher energy and higher RNP concentration (**Fig 1b**). Whereas transfection of plasmids has more challenges because of plasmid size and DNA-toxicity, compared to fully optimized transfection under previous standard best conditions (**Fig S1a**), here too we were able to achieve significantly higher transfection efficiencies of up to 43% (**Fig S1b**). Plasmid transfection of keratinocytes requires higher energy than RNA and RNP transfection, as lower energy resulted in less plasmid uptake (data not shown).

Whereas other transfection methods require the use of single cell selection or sorting to improve population purity, significantly decreasing cell viability and inducing cell death, this step is not necessary upon RNA or RNP transfection with the ATX. The high transfection efficiency of CRISPR RNPs or mRNA did not affect cell viability or morphology (**Fig 1c**), nor did the electroporation itself decrease cell proliferation (**Fig 1d**). Only upon electroporation of a *CCR5*-targeting Cas9:RNP did we observe a mild decrease in cell growth, which is likely explained by the introduction of double strand breaks into the DNA and activation of the DNA repair machinery. Furthermore, ATX-mediated electroporation induced less oxidative stress in keratinocytes compared to chemical transfection (**Fig S1c**).

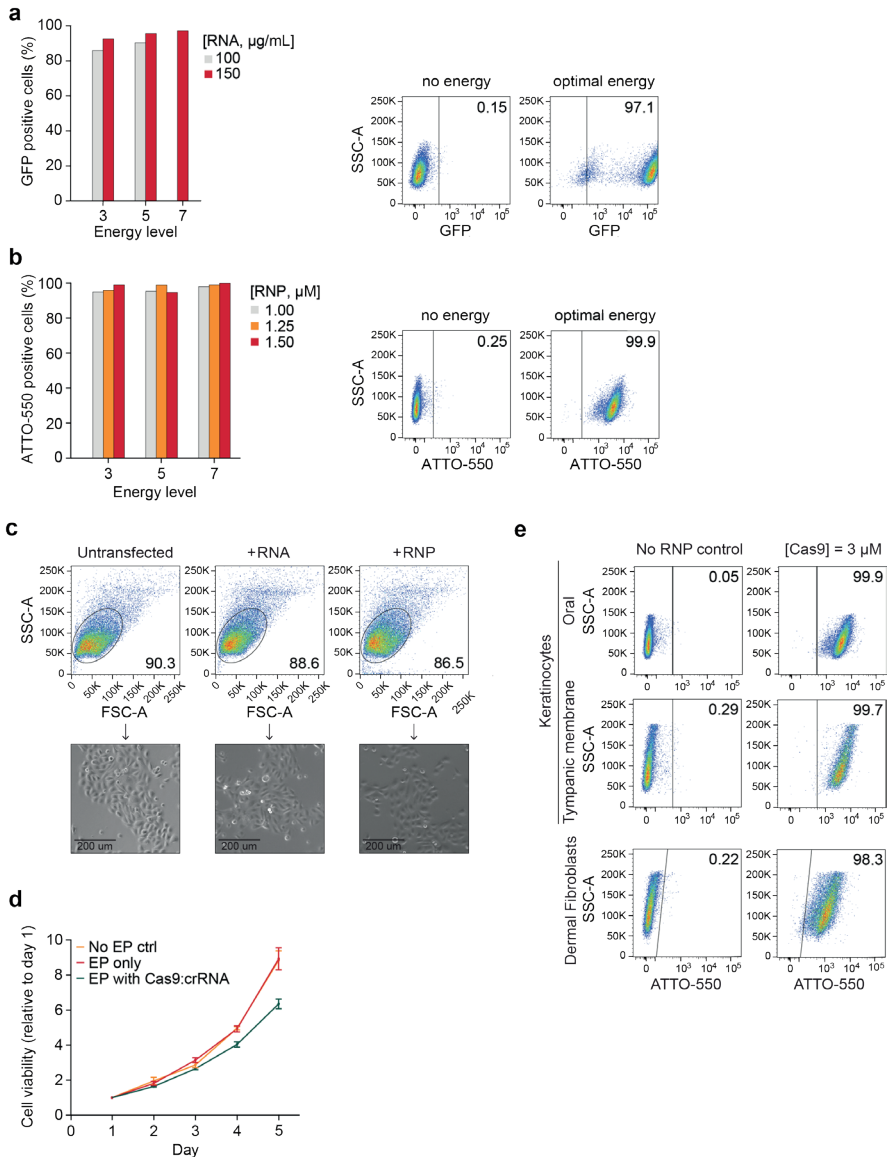


Figure 1 | High efficiency delivery of RNA and CRISPR RNPs to primary keratinocytes

a Left: transfection efficiencies of primary FKCs 24 hrs post electroporation of mRNA-GFP. Right: flow cytometry data on uptake at optimal energy.

b Left: transfection efficiencies of primary FKCs 24 hrs post electroporation of ATTO-550 labeled Cas9:crRNA:tracrRNA. Right: flow cytometry data on uptake at optimal energy.

c Top: viable cell population of transfected keratinocytes from (A) and (B) as detected by SSC-A versus FSC-A flow cytometry 24 hrs post electroporation. Bottom: accompanying representative brightfield images of keratinocytes.

d Relative cell viability values based on Alamar Blue assay upon electroporation of primary FKCs (crRNA targeting the *CCR5* locus).

e Flow cytometry data on transfection of primary OKC, TMKC, and primary dermal fibroblasts by ATTO-550 labeled Cas9:crRNA:tracrRNA 24 hours post-transfection.

Lastly, while we optimized transfection conditions in primary foreskin keratinocytes, we demonstrate that we can easily adapt this workflow to keratinocytes of the tonsil and the tympanic membrane, as well as primary dermal fibroblasts (Fig 1e), the main cell type in the dermis. Thus, here we establish a highly versatile strategy for transfection of primary human keratinocytes, with high efficiencies and without compromising cell viability.

Table 1 | Efficiencies of pSpCas9 transfection in primary keratinocytes using different transfection methods

Transfection method		Uptake
Chemical	TransIT-X2 Transfection reagent (Mirus Bio)	15%
	DNA-In CRISPR Transfection Reagent (Amsbio)	7%
	TransIT-Keratinocyte Transfection reagent (Mirus Bio)	7%
	Lipofectamine 2000 Transfection Reagent (Life Technologies)	5%
	FuGENE HD Transfection Reagent (Promega)	4%
Electroporation	ATX (MaxCyte)	43%
	4D-Nucleofector X (Lonza)	4%

Efficient gene knockout in primary keratinocytes enables modeling of squamous cell carcinoma

Many conditions that originate from dysfunctional keratinocyte function - including SCC - are caused by mutations in the genome. To gain better understanding of the causes of these diseases and the effects of these mutations, it is essential to be able to develop disease models that accurately represent the mutational landscape found in these diseases. SCCs present with deleterious mutations in many cancer genes, but we don't have a full understanding of which of these genes are essential for tumor formation. Therefore, we aimed to engineer primary keratinocytes with high efficiency to carry deleterious indels via CRISPR. We first transfected cells with a SpCas9-GFP plasmid targeting *CDKN2A*. Consistent with the transfection efficiency for a reporter plasmid, we observed better editing efficiencies at higher energy levels, with up to 47% editing efficiency at the higher DNA concentration (Fig S2a), although concentrations beyond 100 $\mu\text{g}/\text{mL}$ show toxic effects and induce cell death (data not shown). Although we were able to significantly increase the editing efficiency by pSpCas9 plasmids compared to optimized chemical transfection, we aimed to get editing efficiencies that omit the need for population purification. Therefore next, we tested the efficiency of *TP53*- and *CDKN2A* targeting Cas9:RNPs in editing the genome. Primary FKCs were electroporated with the ATx with different Cas9:RNP concentrations at different energy levels. 96 hours post electroporation, DNA was collected and indel frequency was measured through TIDE assay¹²⁸. Whereas we

already demonstrated that transfection of Cas9:crRNPs is highly effective at all shown conditions, the percentage of deleterious indels created in the respective loci is significantly affected by the energy level and RNP concentration (Fig 2a). At the lower energy and lower concentration, editing efficiencies balance around 60-70%, whereas at the higher concentration and energy, we observed editing efficiencies up to 99% in both FKC and OKC (Fig 2a, Fig 2b, Fig 2c), with especially the higher energy level being critical for good efficiency.

Since both *TP53* and *CDKN2A* are tumor suppressor genes, the introduction of deleterious indels in these genes might provide the cells with a proliferative advantage, skewing the actual initial editing efficiency. Therefore, we tested next the editing efficiency of two cell cycle genes and a “neutral” gene under optimized conditions (Fig 2d). We were able to repeat the engineering process to achieve similar editing efficiencies with all targets. Importantly, editing efficiencies were stable over time (Fig 2e), indicating that this engineering workflow is not affecting cell viability or cell growth in a manner that promotes the selection of non-transfected or unedited cells. This method thereby allows us to efficiently model specific deleterious mutations in primary keratinocytes with far greater efficiency than previous methods.

Keratinocytes that accumulate a variety of specific mutations can give rise to SCCs. SCCs display a remarkable genetic homogeneity, even between tissues of origin, and we find similar mutational patterns in different types of SCCs⁹². Amongst SCCs we find that some of the most frequently altered genes are *TP53*, *CDKN2A*, *NOTCH1*, *FAT1*, and *KMT2D* (Fig 2f)^{92,129,130}. Typically, the introduction of somatic mutations in these genes induces gene disruption through, for example, activation of the nonsense mediated decay (NMD) process or induction of missense mutations that result in a dysfunctional protein. Together with homozygous deletions and promotor methylation (frequent for *CDKN2A*) the result is decreased or absent gene activity.

Through electroporation of crRNA:Cas9, we were able to achieve high gene knockouts for the most frequently mutated genes in SCCs (Fig 2f), thus allowing us to model the evolution of SCCs in a way that accounts both for the timing and the genetic context in which mutations occur during SCC tumorigenesis. Together with increased transfection efficiencies that we were able to achieve in keratinocyte-derived cancer cells (Fig S2c), this now provides us with a robust toolset to study the role of cancer genes in SCCs.

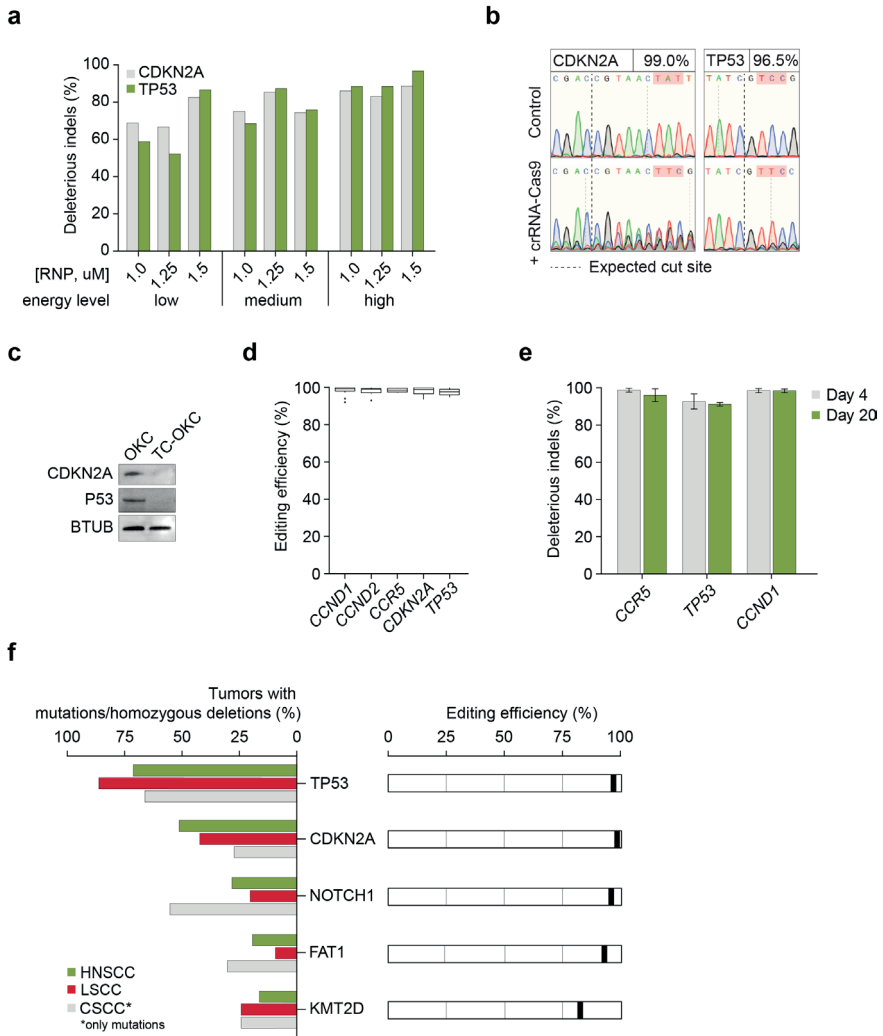


Figure 2 | Efficient gene knockout in primary keratinocytes enables modeling of squamous cell carcinoma

a Percentage of indels measured via TIDE 96 hrs post electroporation with *CDKN2A*- and *TP53* targeting CRISPR RNPs in primary FKC.

b Sanger Sequencing traces of engineered OKC 96 hrs post electroporation with *CDKN2A*- and *TP53* targeting CRISPR RNPs.

c Immunoblot analysis for P53 and *CDKN2A* expression in OKC 96 hrs post electroporation of *CDKN2A*- and *TP53* targeting CRISPR RNPs.

d Percentage of deleterious indels measured via TIDE 96 hours post electroporation of 5 different CRISPR RNPs targeting either negative, neutral, or positive cell cycle genes in primary keratinocytes.

e Percentage of deleterious indels measured via TIDE 4 days or 20 days post electroporation of 3 different CRISPR RNPs.

f Most significantly mutated genes in 3 types of SCC and their percent deleterious indels upon electroporation in KCs. HNSCC: TCGA PanCancer (496 tumors), LSCC: TCGA: PanCancer Atlas (469 tumors), CSCC: UCSF, NPJ Genom Med 2021 (83 tumors).

Adaptable strategies for the development of keratinocyte-based cell therapies

Our results presented thus far show a highly efficient workflow to engineer primary keratinocytes. The use of engineered keratinocytes for cell therapy is an attractive option to treat a variety of dermal conditions. However, engineered keratinocyte-based cell therapies have been limited by the lack of efficient transfection methods for adult keratinocytes. Engineering strategies for the development of cell therapies can be more complicated than for other purposes. Therefore, we next aimed to see if we can use our electroporation process for more complex engineering strategies. First, we show that the cell engineering process is gentle enough to allow for multiple rounds of genome editing without sacrificing efficiency or cell health (Fig 3a). Further, multiplexed electroporation of CRISPR-RNPs resulted in high transfection and is equally efficient in creating indels compared to transfection of a single target (Fig 3b). Thus, this allows us to target multiple genes in either sequential or multiplexed editing strategies.

For the development of cell therapies, it is important to consider the manufacturing scale. Depending on the application of the cell therapy product, it can be desirable to be able to produce very high numbers of engineered keratinocytes in a single manufacturing run. Therefore, we aimed to scale up our process. MaxCyte's electroporation platform has instruments for different scales, including closed system cGMP-compliant instrumentation that allows for the engineering of tens of billions of cells at a single time. We show that our engineering process is highly scalable, enabling the electroporation of up to 8×10^6 keratinocytes in a single reaction (Fig 3c) with no further optimization. This is a 16-fold scale up compared to our previous runs - using electroporation of 0.5×10^6 keratinocytes - without any loss in transfection or editing efficiency, and with significant capability for further up-scaling. Moreover, we show that the indel pattern created upon electroporation is nearly identical between the smaller and larger scale (Fig S3a). These data corroborate the consistency and seamless scalability of the engineering process, enabling the manufacturing of millions of engineered keratinocytes in a GMP-compliant process.

The production of high number engineered keratinocytes is of particular interest for the production of universal donor cell therapies, as cells can be engineered, preserved, and serve as "off the shelf" allogeneic therapies. However, non-engineered allogeneic cell therapies are typically hampered by low persistence of the donor cells post-engraftment. Therefore, the first challenge to overcome in the development of such cell therapies lies in preventing an immune response upon patient engraftment by using gene editing to create hypimmune allogeneic keratinocytes. The immune response by the host develops from T-cells that get activated upon recognition of antigens presented on major histocompatibility class I or class II (MHC-I / MHC-II) protein complexes present on the surface of the cells, where MHC-I present antigens to CD8+ cytotoxic T cells, and MHC-II to CD4+ helper T cells.

To create hypimmune allogeneic keratinocytes, we therefore aimed to engineer cells that have defective MHC-I and MHC-II expression. MHC-I complexes are expressed on all nucleated cell types and consist of 4 chains (α 1-3, and β 2-microglobulin (*B2M*)), of which the *B2M* locus is located on a different chromosome. MHC-II is only constitutively active on antigen presenting cells, but some other cell types may also express these proteins upon induction by interferon- γ (IFN- γ). Expression of MHC-II is tightly positively regulated by the class II major histocompatibility complex transactivator (CIITA), which is activated by IFN- γ . To verify the necessity of MHC-II depletion in allogeneic keratinocytes, we first tested whether keratinocytes express MHC-II upon induction with IFN- γ . Incubation of keratinocytes with different concentrations of IFN- γ induced expression of MHC-II in a significant part of the keratinocyte population (Fig S3b). We confirmed this observation in keratinocytes from distinct anatomical sites (Fig S3c), supporting the need to target both MHC-I and MHC-II to create universal donor allogeneic keratinocytes. To target these complexes, we engineered dermal and oral keratinocytes with deleterious indels in the *B2M* and *CIITA* loci using a multi-guide CRISPR knockout strategy. Flow cytometry on expression of MHC-I (*B2M*) and MHC-II (HLA-DR) shows very effective depletion of MHC-I, and reasonable depletion of MHC-II (Fig 3d). Accounting for only partial activation of the MHC-II in the population, 80% of total cells does not express MHC-I nor MHC-II, thus creating a significant hypimmune allogeneic keratinocyte pool that can be used for allogeneic cell therapies.

Keratinocytes both in the skin and in culture have a limited lifespan. After a set number of cell divisions, keratinocytes undergo differentiation and keratinization, thus eventually leading to cell death and senescence. To assess whether we can culture sufficient numbers of engineered keratinocytes for use as an off-the-shelf cell bank, we calculated the total number of engineered cells obtained from 1 vial of cells upon *B2M* and *CIITA* knockout engineering (Fig 3e). Based on these numbers, we then did a conservative calculation on the number of cells we could produce when starting from fresh donor material. *In vitro* expansion for 20 or 23 days (P5/P3 to P11) would produce up to 1.6E9 oral keratinocytes (OKC) and 1.9E9 tympanic membrane keratinocytes (TMKC), respectively. For an allogeneic cell therapy manufacturing process, we would target cryopreservation to create a cell bank of engineered keratinocytes after approximately 3 weeks (8 passages) in culture in order to guarantee functional and healthy keratinocytes post-thaw. This strategy would reduce the amount of preserved engineered keratinocytes overall, but still allows manufacturing of at least 3.2E7 (TMKC) and 1.5E8 (OKC) engineered cells from a small specimen.

In summary, here we present a novel and improved workflow for the very effective transfection and engineering of primary adult keratinocytes, decreasing engineering time down to under one week, while significantly increasing efficiency and viability. These improvements allow for rapid development of robust keratinocyte-disease models and engineered keratinocyte-based cell therapy processes (Fig 3f, Fig S3d).

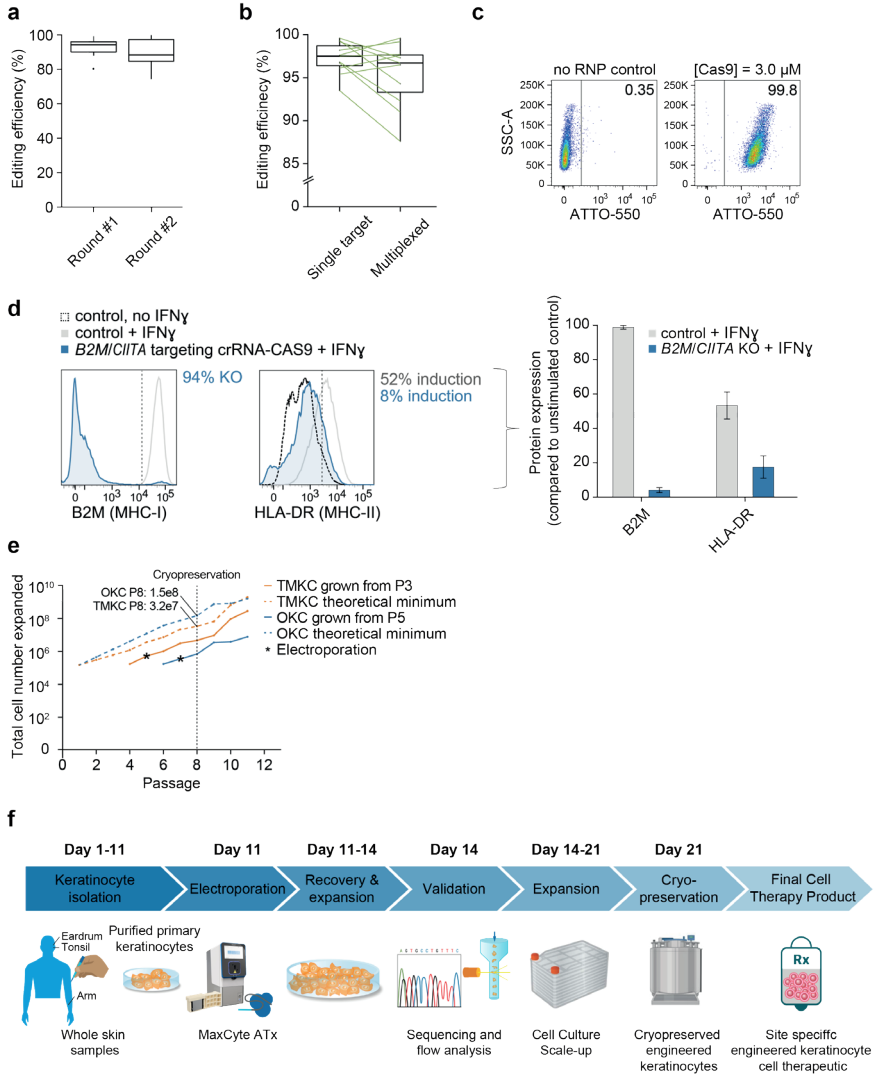


Figure 3 | Adaptable strategies for the development of keratinocyte-based cell therapies

a Percentage of indels created 96 hrs post electroporation at 1st or 2nd round of sequential editing of primary oral keratinocytes, measured through TIDE. Upper and lower whiskers represent the largest and smallest observed values within 1.5 times the interquartile range from the ends of the box.

b Matched percentage of indels created 96 hrs post electroporation of either single or dual CRISPR RNPs of 6 different targets in primary oral keratinocytes. Upper and lower whiskers represent the largest and smallest observed values within 1.5 times the interquartile range from the ends of the box.

c Flow cytometry data on transfection of 8×10^6 primary foreskin keratinocytes by ATTO-550 labeled Cas9:crRNA:tracrRNA 24 hours post-transfection.

d Left: representative flow cytometry data on expression of B2M (MHC-I) and HLA-DR (MHC-II) 5 days post electroporation of 6 CRISPR RNPs using the Synthego multi-guide knockout kit in

>>

- primary forearm-derived skin keratinocytes. Right: pooled expression data upon knockout in oral and skin keratinocytes relative to their control cells without IFN γ .
- e Total number of keratinocytes expanded from 1 vial (approximately 0.8×10^6 cells) of P3 (TMKC) and P5 (OKC) cells up to P11 including 1 round of electroporation targeting *B2M* and *C/ITA*, and the theorized total minimum cell numbers expanded from 1 small specimen to P11.
- f Optimized workflow to create engineered keratinocyte-based cell therapies.
-

Discussion

In this study, we established a novel workflow for the efficient transfection and genome engineering of primary adult keratinocytes. We demonstrate robustly high transfection efficiencies of 90 - 100% with mRNA and CRISPR-RNPs in keratinocytes of different anatomical origins, without compromising cell viability or morphology. Delivery of CRISPR-RNPs resulted in equally high editing efficiencies of target genes. We demonstrate that we can induce efficient gene knockouts in some of the most frequently mutated tumor suppressor genes in SCCs, opening possibilities to study cancer genes in more appropriate genetic contexts. Ultimately, we utilize this new workflow to generate universal donor keratinocytes, opening up novel strategies for the development of keratinocyte-based cell therapies for the treatment of a variety of epidermal conditions.

Keratinocytes are at the center of epidermal conditions that are caused by either injuries or genetic skin diseases. Thus, the ability to engineer keratinocytes to study specific mutations or create cell therapy products will help to gain better mechanistic and therapeutic insights into these conditions. However, keratinocytes are hard to transfect, and current strategies are not efficient enough to create a high purity cell population, thus necessitating lengthy and harmful selection steps. Over the years, many different strategies have been explored, with the highest success rates coming from lipid-based transfection methods, viral gene delivery, and electroporation¹³¹. However, even in more efficient transfection protocols, cell viability remains a key issue^{132,133}. Here we report high transfection efficiencies in primary adult keratinocytes, with transfection rates of 97% (RNA) and 100% (RNPs) for keratinocytes of multiple origins. Importantly, our electroporation-based workflow does not affect cell viability, growth, or morphology. Electroporation is generally accepted as the most efficient way to transfect keratinocytes, yet the high efficiencies we report here have never been shown before.

Other studies have also found that after electroporation keratinocytes still express keratinocyte stem cell markers, suggesting that they retain their stemness features^{47,133}. In our study, we show plasmid transfection rates of up to 43%. Although this is higher than plasmid transfection efficiencies using alternative methods, it is significantly lower than the transfection rates that we found for RNA and RNPs. This

is to be expected, as plasmids are not only bigger, but also more toxic to cells. Using RNPs instead of plasmids for CRISPR-Cas9 based genome engineering also has other benefits, such as the higher stability of RNPs and a lower rate of off target effects as RNPs only have transient Cas9 expression and thus shorter nuclease activity, avoiding the risk of (partial) integration into the genome^{134,135}.

The high transfection efficiencies that we obtained also translate to high editing efficiencies in primary keratinocytes, as under optimized conditions we routinely achieve 90-100% deleterious indel creation.

The unprecedented efficiency enables new strategies to study keratinocyte function in health and disease. Here we show efficient knockout of the most frequently altered tumor suppressor genes in SCC. Through combined or sequential gene knockout of these genes we can accurately model SCC progression and identify key events that progress keratinocytes from healthy, to neoplastic, to cancerous. This is particularly important as many cancerous mutations have also been found in non-cancerous skin^{101,105}. Previous work from our lab using CRISPR-mediated knockout of cancer genes in keratinocytes showed that only specific combinations of gene knockout create oncogenic phenotypes such as invasion and *in vivo* tumor growth (Planells Palop *et al.*, submitted). Thus, identification of progression events will give us new mechanistic and therapeutic insights for SCC.

Besides SCCs, there are over 560 identified genetic skin disorders that are caused by alterations in over 500 different genes⁴⁵. Many of these conditions are caused by loss of function (LOF) mutations in genes essential for normal keratinocyte function, such as LOF of *NFI* (neurofibromatosis type I), LOF of *ABCA12* (Harlequin Ichthyosis), and LOF of *Spink5* (Netherton disease)¹³⁶⁻¹³⁸. Furthermore, diseases can also be driven by gain of function (GOF) mutations that activate genes or alter their function, such as *PI3KCA* in cancer. Current efforts in the field aim to broaden the genomic tool set in primary keratinocytes to study these types of mutations as well, using e.g. prime-editing techniques to create specific mutations¹³⁹. Overall, modeling these LOF or GOF mutations in keratinocytes in cell- or organotypic culture will enhance our understanding of these genetic skin diseases.

Next, we show the use of the engineering workflow for the development of novel cell therapies. The development of CRISPR/Cas9 (and associated) technologies have accelerated the developments in the field of gene- and cell therapies. In recent years, the use of TALEN and CRISPR have been explored as a way of correcting patients defective keratinocytes *ex vivo* in epidermal diseases such as EB^{55,56,120,124-127}. The results of these studies are promising, as they for example show restored expression of the *COL7A1* gene^{55,56}. However, low efficiencies and cell viability issues limit the use of this strategy in clinical applications. With the improved transfection efficiencies that we show here, future studies can focus on higher efficiencies of these strategies.

As opposed to *ex vivo* gene repair of the patients' affected cells, a distinct approach is to transplant either autologous or allogeneic healthy keratinocytes. In recent years, there have been few developments in this application of epidermal grafts as a cell therapy for epidermal conditions. Most grafts used in the clinic are still autografts, as allografts only persist for a couple weeks and their contribution to wound healing is limited to their secreted factors^{119,121,123}. Furthermore, autologous grafts increase the burden on patients and have limitations in use in patients with wounds that cover large parts of the body, inflammatory conditions, or elderly patients. On the other hand, allogeneic grafts are limited to the use where temporary dressing can suffice. Despite their limited contribution, allogeneic keratinocytes still support wound healing in diabetic foot ulcers and 2nd degree burns, although this can also be (partially) attributed to other factors in the product that stimulate wound healing^{120,140}. Allogeneic cell therapies with bone marrow concentrate, mesenchymal stromal cells, or fibroblasts also benefited EB patients, but HLA matching remains an issue and only the patients faulty COL7 was produced¹⁴¹⁻¹⁴³.

Therefore, here we aimed to overcome these limitations through the development of universal donor hypimmune allogeneic keratinocytes that can be used for all patients, without getting rejected.

There are several strategies to manipulate the antigen presenting capacity of cells to prevent CD4+ and CD8+ T cell recognition. Here, we chose to create deleterious indels in *B2M* and *CIITA*, to inhibit the expression of MHC-I and MHC-II complexes, respectively. MHC-I is constitutively expressed on all nucleated cells, so deletion of MHC-I is always needed to prevent immune cell recognition by the host. However, complete loss of MHC-I can also stimulate recognition by natural killer (NK) cells. To overcome this problem, alternative strategies can include expression of a non-classical HLA to prevent NK-cell recognition, or MHC-I knockout with HLA-C7 retention by targeting HLA-A, HLA-B, and non-7 HLA-C¹⁴⁴⁻¹⁴⁶. MHC-II is less actively expressed on keratinocytes. Generally, in the epidermis only Langerhans cells express MHC-II, and a few studies also report expression by keratinocytes under normal homeostatic conditions^{147,148}. However, keratinocytes are more robustly found expressing MHC-II under certain conditions, such as skin disorders or when stimulated with IFN γ ¹⁴⁹⁻¹⁵⁵. So it is likely that MHC-II expression can get induced in pro-inflammatory situations, which is supported by the positive correlation between expression and lymphocyte infiltration^{151,156}.

Here, we show a decrease of 96% in *B2M* (MHC-I) expression upon B2M knockout, and a 67% decrease in HLA-DR expression upon CIITA knockout, resulting in only 17% of cells expressing HLA-DR upon IFN- γ stimulation. Effectively, this means that 80% of the keratinocyte population does not present antigens, being of low immunogenicity and thus can be used as universal donor cells. Previous studies in iPSC derived MHC-I and MHC-II deficient endothelial cells, cardiomyocytes,

and smooth muscle cells, show that these cells can successfully be transplanted, as these cells avoid recognition by the immune system without the need for immunosuppressants¹⁵⁷. No such studies have been done in keratinocytes, but viral overexpression of US11 has been shown to downregulate MHC-I expression and improve cell survival¹⁵⁸. However, this downregulation only lasted for 24 hours, thus limiting the usage of these cells. Alternative approaches could include the expression of immune suppressive molecules such as PD-L1 and CTLA4-Ig, as keratinocytes can modulate CD4+ T cell proliferation through surface expression of immune checkpoint proteins, although this is particular for the progenitor population and less so for differentiated keratinocytes^{159,160}.

We calculated that from a single small specimen, we can obtain between $3.2E7$ and $1.5E8$ universal donor keratinocytes at an early passage. The selection of early passage keratinocytes is important, as keratinocytes increase in size over time and lose progenitor markers such as keratin 5 and 15, which is indicative for keratinocyte differentiation¹⁶¹. Thus, for cell therapy purposes it could be preferred to use younger keratinocytes as these population include more progenitor-like cells. Additionally, factors that should be considered to optimize keratinocyte culture for such purposes include the addition of agents that can transiently stimulate cell growth and expansion in a safe manner, such as ROCK-inhibitors, KLF-4 inhibitors, or SMAD inhibitors¹⁶²⁻¹⁶⁵.

Studies would be needed to determine how long the universal donor cells remain in the skin, as part of normal keratinocyte function is to differentiate and shed off. This shedding is likely dependent on the progenitor state/ keratinocyte stem cell fraction of the population. On the other hand, a limited lifespan may reduce the risk for neoplastic growth originating from the engineered cell product.

A previous *in vitro* study indicated that 750,000 keratinocytes in spray formulation were sufficient to re-epithelialize an area of 10-15 cm² within 7 days¹⁶⁶. Therefore, the above-mentioned numbers equate to enough keratinocytes for approximately 200 doses in single-cell suspension application. This form of application is a very practical one, as it is easy to transport and store. For comparison, keratinocyte sheets are vulnerable as they are only 8-10 cells thick. Therefore, they need a backing for transport and once detached from the culture vessel, they need to be transplanted the same day. Lastly, in the transplant process there is an enhanced risk on blister- and tear formation. Application through a spray does not affect cell viability and previous studies showed more success compared to keratinocyte delivery through a fibrin membrane transfer, and cells showed evidence of proliferation^{166,167}.

It is hypothesized that in suspension, keratinocytes are not contact inhibited, and are therefore more proliferative and provide better support in the wound healing process. Keratinocytes in suspension can be applied in medium or in fibrin as a delivery vehicle. The rationale behind delivery in fibrin is that fibrin will instantly clot upon

application, reducing the likelihood that the applied cell suspension runs out of the wound. Moreover, the fibrin could theoretically stimulate cell growth when combined with growth factors. There have been several successful studies and clinical trials that show improved wound healing upon application of keratinocytes in suspension^{166,168-172}. Some of these studies combine keratinocytes with other cell types, such as fibroblasts, melanocytes, or Langerhans cells^{168,169,172}. For example, clinical trials by Kirsner *et al.* found that suspension-applied allogeneic keratinocytes and fibroblasts improved wound closure of venous leg ulcers in a phase II clinical trial¹⁶⁸. However, in the subsequent phase III clinical trial they did not observe a difference between treated and control subject, most likely due to the quality of the keratinocytes¹⁷³.

To create better keratinocyte-based cell therapies, genome engineering can also be used to engineer keratinocytes with specific properties - such as enhanced wound healing or improved antimicrobial activity - that enable better treatment of targeted indications. For example, one study showed that introducing a host defense peptide (LL-37) in keratinocytes in mice improves woundhealing¹⁷⁴, whereas in another the introduction of keratinocyte growth factor 1-a (KGF1-a) in the epidermis of rats also showed faster wound closure¹⁷⁵. Furthermore, keratinocytes from different anatomical sites - although genetically and phenotypically very similar - show some intrinsic differences, and dermal keratinocytes transplanted into the oral cavity maintain their skin morphology^{176,177}. Using allogeneic approaches provides more possibilities to site-match and thus maintain site-specific properties.

With the above-described approaches for new “off the shelf” allogeneic keratinocyte-based cell therapies, patients with a variety of epidermal conditions can benefit. Evident indications would be patients with 2nd- or 3rd degree burns, diabetic foot ulcers, venous leg ulcers, and patients with genetic skin disorders such as EB. However, one could also imagine to topically apply allogeneic keratinocytes upon tympanic membrane (TM) perforation, as an alternative to tympanoplasty, to enable regeneration of the TM. Similarly, upon resection of (oral) SCCs, allogeneic keratinocytes in a matrix such as fibrin or collagen can be applied on the site of resection to stimulate regeneration of the area.

In summary, we describe a novel workflow for the efficient transfection and genome-engineering of primary adult keratinocytes, creating possibilities for the generation of new models for genetic skin disorders and the development of novel keratinocyte-based cell therapies.

Materials and methods

Cell culture

Human primary keratinocytes were collected and isolated from patient derived mucosal (5 donors), foreskin (2 donors), or tympanic membrane (1 donor) samples and cultured in Medium 154 and Keratinocyte Serum Free Medium (1:1, Life Technologies cat#M154500 and cat#17005042), supplemented with 5 mL/L Human Keratinocyte Growth Supplement (Life Technologies cat#S0015), 25 mg/L Bovine Pituitary Extract (Life Technologies cat#17005042), 2.5 µg/L EGF Human Recombinant (Life Technologies cat#17005042), and 1% Penicillin/Streptomycin (P/S, Corning cat#MT30002CI). Human primary fibroblasts were isolated and collected from patient derived skin samples and cultured in DMEM supplemented with 5% FBS (Corning cat#MT3501OCV) and 1% P/S. FaDu (ATCC cat#HTB-43, male) and Detroit562 (ATCC cat#CCL-138, female) cells were grown in Eagle's Minimal Essential Medium with L-glutamine (Fisher Scientific cat#50983283) supplemented with 10% FBS and 1% P/S.

Electroporation protocol

Cells were transfected via electroporation using the MaxCyte ATX electroporation platform using a variety of settings and conditions, of which some have been described in the results section. Here we will describe only the optimal conditions. For electroporation, sub-confluent cells were trypsinized and washed 1x in DMEM and 1x in Opti-MEM (Life Technologies cat#31985070). Cells were resuspended to a concentration of 2.5×10^7 cells/mL in Opti-MEM.

CRISPR-Cas9 RNP

Gene-specific crRNAs (table 2) were designed and tested to maximize disruption of gene expression. crRNAs and Alt-R CRISPR-Cas9 tracrRNA (Integrated DNA Technologies) were hybridized in a 1:1 ratio to a final concentration of 50 µM. crRNA:tracrRNA were complexed with Cas9-RNP (Macrolab, UC Berkeley) at a 1:1:1 ratio for 20 minutes at room temperature and subsequently mixed with the cells to a final concentrations of 2.5 µM crRNA:Cas9 per sgRNA and 2.0×10^7 cells/mL.

mRNA

GFP-RNA was prepared in water and mixed with the cells at a final concentration of 150 µg and 2.0×10^7 cells/mL.

Plasmid

pSpCas9(BB)-2A-GFP plasmid (Addgene cat#48138) targeting *CDKN2A* (gRNA: CACCGAATAGTTACGGTCGG) and pGFP plasmid (provided by MaxCyte) were

prepared in water at a concentration of 3000-10.000 ng/ μ L. Plasmids were mixed with the cells at a final concentration of 100 μ g plasmid and 2.0E7 cells/mL.

Cells were electroporated in 25 μ L or 400 μ L reactions with the 'Optimization 7' (Keratinocytes, Fibroblasts and Detroit562) or 'DLD-1' (FaDu) electroporation protocols using OC-25x3 or OC-400 processing assemblies. After electroporation, cells were immediately collected from the processing assembly, plated into a 6 well plate and recovered 20 minutes at 37°C, before resuspending in 2 mL culture medium. Transfection efficiency and cell viability was determined 24 hrs post electroporation on a LSR II Flow Cytometer (BD). For genome engineering, gene disruption was confirmed 96 hours post electroporation through TIDE (Tracking of Indels by Decomposition) analysis¹²⁸ (primers: table 2).

Table 2 | crRNAs and primers for TIDE analysis

Target gene	crRNA sequence	Forward primer	Reversed primer
CCND1	CATTTGAAGTAGACACCGA	CACACGGACTACAGGGGAGT	ACCCCTTCTCCTTCAGAAA
CCND2	CTCGTGGCACAGCAGCTCCA	GGGAGAGCGAGACCAGTTTT	GACCTACCTCCAGCATCCAG
CCR5	AACACCAGTGAGTAGAGCGG	TGCTTGCCAAAAAGAGAGT	CGATTGTCAGGAGGATGATG
CDKN2A	TAACTATTCGGTGCCTGGG	GACTCCCTTTTTATCCCAAACG	CCAGTCTCCTTCTCTGCCAAC
FGF19	CGGTACACATTGTAGCCATC	ACCTACTGTGCCTGGCCTTA	TCTCAAAGCTGGGACTCCTC
OR2B6	TATCAAAGGACATGACGGCC	GCTGGAGTTTCCACTCCTTG	TTCAGCCTCATTGTCTGTTG
ORAOV1	CATATTGATGCCATCGTGA	CCATGTACAGGCTGCTTTGG	ACCAGGCTGAGCAGATGTTT
SC1	TTGGTCCCACGATGACCCAC	GATCGAGGTCCACTCTGAGC	GGTGTGTGACTGGGGGAAC
TP53	CCATTGTTCAATATCGTCCG	ACTGACCGTGAAGTCACAG	CCCTCTGAGTCAGGAAACA

B2M/CIITA knockout keratinocytes

Cells were electroporated following protocol as described above. To target the B2M and CIITA locus, the Gene Knockout Kit V2 (Synthego) was used, combining 3 gRNAs per target (see table 3) at a final concentration of 3.5 μ M crRNA:Cas9 per target and 2.0E7 cells/mL. 4 days post electroporation, cells were stimulated with recombinant human IFN- γ protein (Fisher Scientific cat# 285IF100) at 10 or 40 ng/mL for 24 hrs after which cells were collected for flow analysis. Cells were washed 1x in flow buffer (DPBS (Life Technologies Life Technologies cat#14190250) + 5% FBS + 1% EDTA (Invitrogen)), 1x in PBS, and collected in PBS at 500.000 cells/50 μ L. Cells were incubated at room temperature for 20 minutes with APC anti-human HLA-DR Antibody (BioLegend cat#307610) and PE anti-human B2-microglobulin Antibody (BioLegend cat# 316305, 1:20). Cells were washed 2x in PBS and analyzed on a LSR II Flow Cytometer (BD) for expression of B2M and CIITA. Gating was based on expression of unstimulated WT keratinocytes (CIITA: expression set at "0" in the control, B2M: expression set at "100" in the control).

Table 3 | Gene knockout Kit V2 Target sequences

Target	Sequence (with modified EZ scaffold)
B2M guide #1	C*G*C*AGCGAGAGACACAGCG
B2M guide #2	G*G*C*CGAGAUGUCUCGCUCCG
B2M guide #3	A*C*U*CACGUCGGAUAGCCUCC
CIITA guide #0	C*C*C*CUAACAUACUGGAAUC
CIITA guide #1	G*G*C*UCCUGGUUGAACAGCGC
CIITA guide #2	C*A*C*AGCUGAGCCCCCACUG

Chemical transfection

2 mL of cells were seeded at a density of 80,000 cells/mL in a 6 well plate and transfected 24 hours later at a concentration of 1500 ng pSpCas9(BB)-2A-GFP plasmid (Addgene cat#48138) targeting TP53 (gRNA: GGTGCCCTATGAGCCGCTG) and 2.25 µl TransIT-LT1 Transfection Reagent (Mirus Bio cat#2300)/mL.

Immunoblot analysis

Cell pellets were lysed in Pierce RIPA buffer (Thermo Scientific, 62249), supplemented with phosphatase inhibitor and protease inhibitor cocktail sets (Calbiochem cat#524625 and cat#539134). Protein extracts were resolved on Nu PAGE 4-12% Bis-Tris gradient gels (Invitrogen cat#WG1401A) and transferred to PVDF membranes using the Trans-Blot Turbo system. Membranes were blocked in 5% milk in TBS-T and probed with primary antibodies overnight at 4°C, and then with horseradish peroxidase-conjugated secondary antibodies. Signals were visualized with SuperSignal West Pico PLUS Chemiluminescent Substrate (Thermo scientific cat#PI34577) on the Bio-Rad ChemiDox XRS+ System. The following antibodies were used: Beta-Tubulin (Abcam cat#6046, 1:500), CDKN2A/P16INK4a (Abcam cat#ab108349, 1:300), P53 (Cell Signaling cat#9282, 1:800).

Cell viability assay

Cells were seeded into Black Greiner Cellstar 96 well plates (Sigma-Aldrich cat#M9936). Starting at 72 hours after plating or drug treatment, cells were incubated with 10% Alamar Blue (Bio-Rad cat#100234-634) according to the manufacturer's instruction. Fluorescence was read out on a GloMax Explorer plate reader (Promega) at an excitation of 520 nm and emission of 580-640 nm. Cell viability was calculated relative to untreated or day 1 condition.

Reactive oxygen species assays

ROS levels were detected using CellROX Green flow cytometry assay kits (Life Technologies cat#C10492). Cells were concentrated 5×10^5 cells/mL in complete medium. Negative controls were incubated with N-acetylcysteine at 1000 μM for 60 minutes at 37°C, positive controls were incubated with TBHP hydroperoxide at 400 μM for 30 minutes at 37°C. CellROX Green reagent was added at 500 nM for 40 minutes at 37°C. Samples were analyzed by flow cytometry.

SCC mutational data analyses

Publicly available copy number and mutational data from TCGA was accessed through cBioportal¹⁷⁸. The following datasets were used: HNSCC (TCGA, 496 tumors), Lung SCC (GDC TCGA, 469 tumors), and Cutaneous SCC (UCSF NPJ Genom Med 2021, 83 tumors)^{92,129,130}. For CSCC no copy number data was available.

Statistical analysis

All data are represented as mean \pm SEM unless stated otherwise. Error bars represent variation between at least 3 independent experiments.

Acknowledgements

This work was supported, in part, by the US National Institutes of Health (NIH) grant R01 MOH135632A (A.T.). We thank Vicente Planells Palop and Nancy Joseph for helpful discussions, Caroline Beckett for illustrating figure 3f, and Lesley Eschinger and James Brady for facilitating the collaboration with MaxCyte Inc.

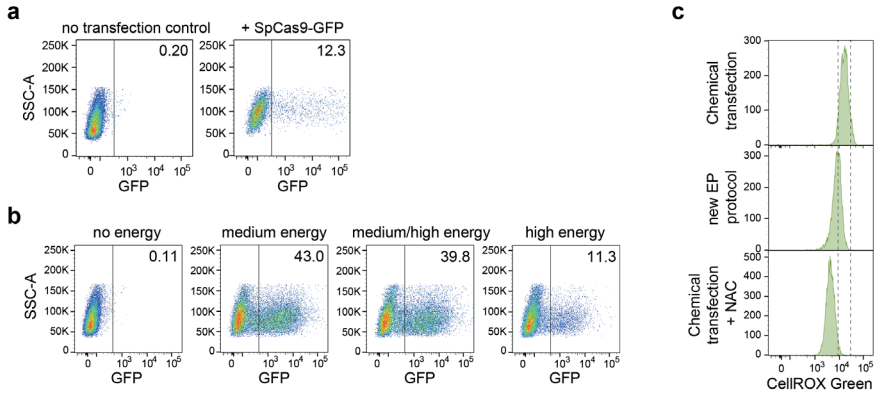
Author contributions

C.I.M. and A.G.M conceived of research. C.I.M. designed and executed all experiments, performed all data analyses, and wrote the manuscript. A.G.M. contributed to electroporation optimization parameters, conceptualization of the engineering of universal donor keratinocytes and provided valuable discussion. A.D.T. supervised the study.

Conflict of interest

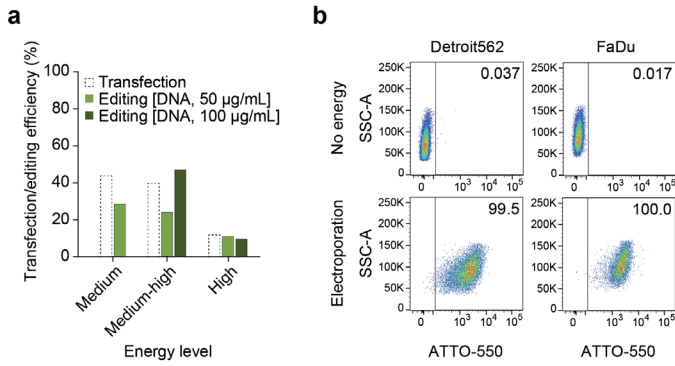
Parts of this chapter are protected under invention disclosure SF2023-128 (*University of California*) (C.I.M, A.G.M, A.D.T.). A.G.M. is an employee of MaxCyte Inc.

Supplemental data



Supplemental figure 1 | Improved transfection efficiencies of primary keratinocytes

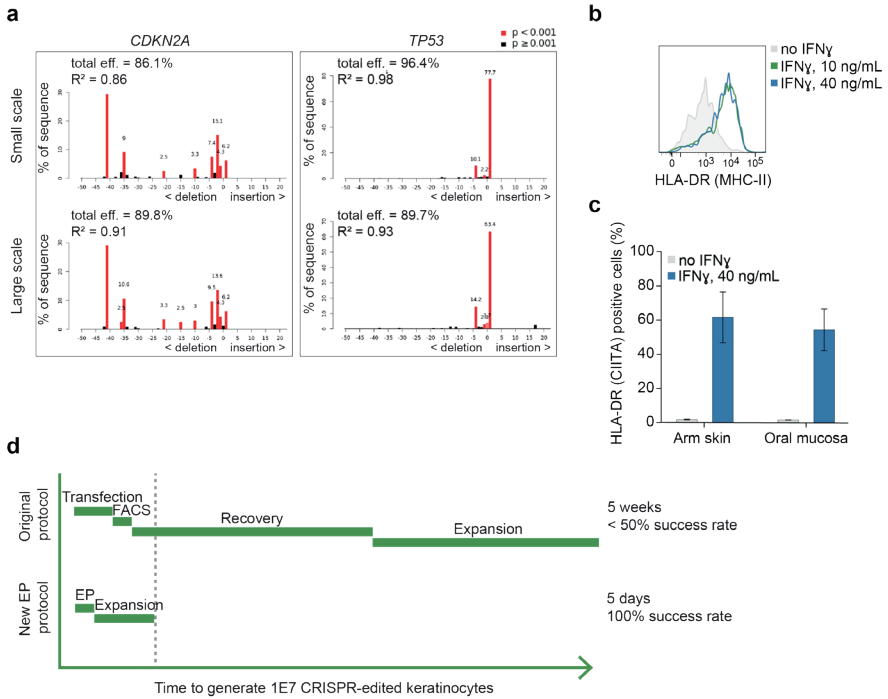
- Flow cytometry data on transfection efficiencies of primary FKCs by a SpCas9-GFP plasmid using chemical transfection under optimized conditions.
- Flow cytometry data on transfection efficiencies of primary FKCs by a GFP reporter plasmid 24 hrs post electroporation at different energy levels.
- Reactive Oxygen Species (ROS) levels as measured by CellROX Green in primary keratinocytes transfected via standard chemical transfection or via electroporation.



Supplemental figure 2 | Genome engineering for cancer modeling

a Percentage of (transfection efficiency and) deleterious indels measured via TIDE assay upon electroporation of primary FKC by a SpCas9-GFP plasmid targeting *CDKN2A*.

b Flow cytometry data on transfection of squamous cell carcinoma lines FaDu and Detroit562 by ATTO-550 labeled Cas9:crRNA:tracrRNA 24 hours post-transfection.



Supplemental figure 3 | Rapid workflow for large-scale production of engineered keratinocytes

a Indel pattern created 96 hrs post electroporation with *CDKN2A*- and *TP53* targeting CRISPR RNPs in primary FKCs at the research- or manufacturing scale.

b HLA-DR expression in arm skin KC upon stimulation with different IFN γ concentrations

c HLA-DR expression in arm skin and oral mucosa KC upon stimulation with IFN γ , relative to unstimulated KC.

d Faster primary keratinocyte genome engineering with reduced risk

Chapter 3

11q13 amplification drives squamous cell carcinoma through 3 distinct oncogenic events

Céline I Mahieu¹, Andrew G Mancini², Ellee Vikram¹, Vicente Planells Palop¹,
Nancy M Joseph³, Aaron D Tward¹

¹Department of Otolaryngology - Head and Neck Surgery, University of California
San Francisco, San Francisco, USA

²MaxCyte, Inc., Gaithersburg, MD, USA

³Department of Pathology, University of California San Francisco, San Francisco, USA

Based on

ORAOV1, *CCND1*, and *MIR548K* are the driver oncogenes of the 11q13 amplicon in
squamous cell carcinoma (Molecular Cancer Research, 2024)



Abstract

11q13 amplification is a frequent event in human cancer, especially in squamous cell carcinomas (SCC). Despite almost always spanning 10 genes, it is unclear which genetic components of the amplicon are the key driver events contributing to SCC tumorigenesis. Here, we present a comparative analysis on the role of each gene in head and neck SCC (HNSCC), leveraging a combination of computational, *in vitro*, *ex vivo* and *in vivo* models using both cancer cell lines and primary cells. We identified *ORAOVI*, *CCND1*, and *MIR548K* as the critical drivers of the amplicon in HNSCC, with each having distinct effects on tumorigenesis. Thus, the 11q13 amplicon drives SCC through at least three independent genetic elements, thereby suggesting therapeutic targets for this morbid and lethal disease.

Introduction

Cancer evolves through distinct types of mutations, including single nucleotide variations, indels, chromosomal gains and losses, focal amplifications, and complex rearrangements, as described in Chapter 1. Among the most common chromosomal amplifications in cancer is the 11q13 amplification. 11q13 amplification occurs in approximately 6% of all tumors previously studied, making it the third most common amplification across cancers, following *MYC* and *PIK3CA* amplifications¹⁷⁹ (Fig 1).

The 11q13 amplification stretches multiple genes, including *CCND1*, in a gene dense region. The amplification was originally described in breast cancer and subsequently in many other cancer types¹⁸⁰. In particular, squamous cell carcinomas (SCC) are enriched for amplification of genes in the 11q13 region^{107,179,181,182}. In contrast to other cancer types, SCCs display a remarkable genetic homogeneity, even between different tissues of origin, suggesting similar oncogenic mechanisms across different types of SCC⁹².

Amplifications of 11q13 tend to be an early event in SCC tumorigenesis, but are exclusively found in cancerous tissue and not in pre-neoplastic lesions^{107,181,182}. Amplification co-occurs alongside loss of function mutations in tumor suppressor genes such as *TP53* and *CDKN2A* - two mutations which occur earlier in the tumor evolution process^{92,91}. Tumors with the amplification contain an average of seven copies of each gene with minimal variation. The amplification is organized intrachromosomally at the original locus, forming a homogeneously staining region which is thought to arise through breakage-fusion-bridge cycles¹⁸³. In this process, dysfunctional telomeres result in fusion of chromosomal ends, leading to double-stranded breaks (DSBs) during anaphase that can result in aneuploidy and chromosomal duplications.

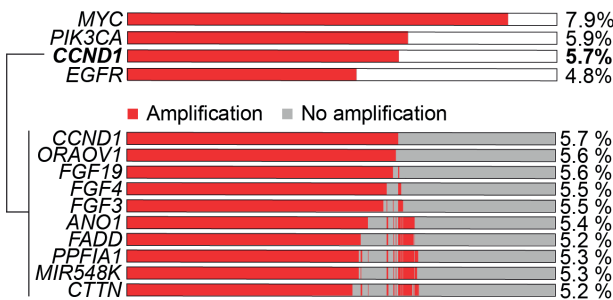


Figure 1 | 11q13 amplification is a frequent event in cancer

Frequency of amplification of *MYC*, *PIK3CA*, *EGFR*, and 11q13 genes across all 32 TCGA PanCancer Atlas Studies tumors ($n = 10950$).

Although several studies have described a role for individual 11q13 genes in SCC tumorigenesis, these studies have been limited by their focus on individual genes on the amplicon without consideration of the roles of other genes on the amplicon and the greater genetic context in which 11q13 amplification occurs. Other studies have aimed to identify the mechanism through which the 11q13 amplicon acts as a driver of tumorigenesis by determining the smallest region of overlap^{184,185}. However, these studies have had conflicting results due to differences in approaches and modeling as well as insufficient cohort sizes. Thus, despite the high frequency of 11q13 amplification, it remains unclear which genes comprise the functional core of the 11q13 amplicon in SCC and through which mechanisms they contribute to SCC tumorigenesis.

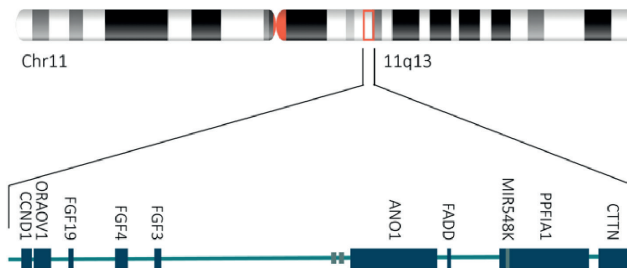


Figure 2 | The 11q13 amplicon
Schematic overview of genes on the 11q13 amplicon

The amplified 11q13 region contains several genes (Fig 2), off which many have previously been implicated as potential oncogenic drivers in cancer in general, or SCCs specifically. Below we describe each of these genes in order from the 5' end to the 3' end of the amplicon.

CCND1 (Cyclin D1) is the most studied of the genes on the amplicon and is a well characterized oncogene across multiple tumor types. Cyclin D1's classical function is to bind to and activate Cyclin Dependent Kinases (CDK) 4 and 6, and the resulting Cyclin-CDK complex promotes cell proliferation by overcoming RB-dependent growth arrest and promoting the G1/S-phase transition¹⁸⁶. However, cyclin D1 also has CDK-independent functions such as stimulating cell proliferation through interaction with nuclear hormone receptors ERa, AR, and PPARg, transcription factors, and chromatin modifiers¹⁸⁷⁻¹⁹². Therefore, *CCND1* is a likely candidate as an oncogenic driver of the 11q13 amplification.

However, most other genes on the amplicon have, to different extents, also been implied in HNSCC tumorigenesis. Located immediately next to *CCND1*, at the 3' side, is *ORAOV1* (Oral Cancer Overexpressed 1, also known as LTO1). Although not much is known about the function of *ORAOV1* in mammalian cells, several studies show an effect on *in vitro* or *in vivo* growth upon knock down of *ORAOV1* in various 11q13-amplified cancer cell lines¹⁹³⁻¹⁹⁶. One study suggests *ORAOV1*'s involvement in

reactive oxygen species (ROS) and proline metabolism, whereas other studies report a function in promoting vascular endothelial growth¹⁹⁴⁻¹⁹⁶.

Of the 3 members of the Fibroblast Growth Factors family on the amplicon (*FGF19*, *FGF4*, and *FGF3*), *FGF19* is the most studied in the context of cancer development. Under normal conditions, *FGF19* is secreted by the ileum, upon which it functions as a hormone by binding *FGFR4*, regulating several metabolic processes, such as bile acid and glycogen synthesis, as well as its function in liver metabolism^{197,198}. Targeting *FGF19* signaling decreases *in vivo* tumor growth of *FGF19*-high liver and colon cancer models, but several studies also report an effect of attenuated *FGF19* levels on *in vivo* growth of SCC lines¹⁹⁹⁻²⁰³.

Anoctamin-1 (*ANO1*, also known as *TMEM16A*) is a large transmembrane protein that functions as a Ca^{2+} -dependent chloride- and bicarbonate channel^{204,205}. The role of *ANO1* in cancer has long been of interest and several studies show the involvement of *ANO1* on cellular growth or invasion via oncogenic signaling pathways^{204,205}. However, these reports show different - and sometimes conflicting - effects in different cancer cells, suggesting cell type specific oncogenic effects of *ANO1*. However, these conflicting results are also prevalent within cancer types. For head and neck SCC (HNSCC), for example, there is no consensus on the contribution of *ANO1* to tumorigenesis, as some reports show that loss of *ANO1* decreases cell proliferation or growth, whereas other reports solely show an effect on migration or invasion upon *ANO1* loss with no impact on cell proliferation. Furthermore, there is also evidence that *ANO1* has a negative effect on cell growth, a phenotype which may be dependent on tumor stage²⁰⁶⁻²¹⁰.

FADD (Fas-Associated Protein with Death Domain) is located right next to *ANO1* and is commonly implicated as a positive regulator of apoptosis^{211,212}. *FADD* is recruited through its death domain by members of the tumor necrosis factor receptor superfamily. Following recruitment, *FADD* functions as an adaptor protein by recruiting procaspases 8 and 10 and together these proteins form the death inducing signaling complex^{213,214}. However, there are also indications that *FADD* can regulate oncogenic signaling pathways such as NF- κ B and MAPK to promote cell cycle progression, proliferation, and inflammation. However it is unclear whether the cell proliferation benefits from *FADD* amplification outweigh its apoptotic effects^{215,216}.

PPFIA1 (Liprin- α 1) is a member of the liprin family that interacts with receptor-like tyrosine phosphatases, localizing at cell focal adhesions and possibly regulating the disassembly of these adhesions²¹⁷. Similar to other liprins, Liprin- α 1 is involved in cell adhesion and motility, and its increased expression in tumors has been linked to invasion and metastasis²¹⁸⁻²²¹.

MIR548K is a micro-RNA located in an intronic region of the *PPFIA1* gene that was only described for the first time in 2014. The targets and cellular function of *MIR548K*

remain elusive. However, due to its frequent amplification in SCC, several studies have focused on its function in ESCC and describe effects on tumor growth and a potential link to *VEGFC* and EGFR-MAPK signaling^{182,222-224}.

Lastly, *CTTN* (cortactin) is located on the 3' end of the 11q13 amplicon and is known for its role in actin cytoskeleton remodeling as an actin binding protein²²⁵⁻²²⁹. Activated cortactin recruits Arp2/3 complexes to actin filaments, a process which facilitates actin branching and ultimately cell migration^{230,231}. Increased levels of *CTTN* have been linked to migratory and invasive phenotypes in several cancers^{207,208,231-233}. Other studies investigating *CTTN*'s role in tumorigenesis report solely an effect on cell proliferation, possibly through activation of the EGFR/MAPK signaling pathways²³⁴⁻²³⁷.

Thus, for almost all genes on the amplicon there are studies showing oncogenic benefits upon increased expression. However, the majority of studies are still association studies and experimental results are inconsistent and narrow in scope, making it unclear which genes are the primary oncogenic drivers of the 11q13 amplicon.

In this study, we comprehensively characterize the role of the 11q13 amplicon during tumorigenesis of HNSCC, a common and morbid type of SCC that originates from epithelial cells lining the upper aerodigestive tract (see Chapter 1). Using a combination of engineered primary human keratinocytes and established HNSCC cell lines, we created novel *in vitro*, *ex vivo*, and *in vivo* models of HNSCC to systematically analyze the role of each component of the 11q13 amplicon during HNSCC tumorigenesis. Through this approach, we are able to model the 11q13 amplification in a way that accounts both for the timing and the genetic context in which it occurs during SCC tumorigenesis. In doing so, we identified *CCND1*, *ORAOV1*, and *MIR548K* as three independent driver oncogenes present on the 11q13 amplicon.

Results

The 11q13 amplification in SCC spans from *CCND1* to *CTTN*

We first sought to identify the frequency of 11q13 amplification across tumor types. Among tumors analyzed in the TCGA dataset, squamous cell carcinomas harbored the 11q13 amplification most frequently. 37% of esophageal cancers, of which many are SCC, and 25% of head and neck SCCs (HNSCCs) carry amplifications of genes in the 11q13 region, and lung SCCs (LSCC) harbor amplification slightly less frequently¹⁷⁹ (Fig 3a). Splitting out esophageal cancers between SCCs and non-SCCs, revealed that 58% of the esophageal SCC (ESCC) harbor the 11q13 mutation (Fig S1a), as opposed to only 13% of the non-SCC esophageal cancers. This further supports the finding that 11q13 amplification is enriched in SCCs. Therefore, we focus on the contribution of the 11q13 amplification specifically to SCCs.

We next sought to define the genes that mark the edge of the minimal critical region of the amplicon in SCC to determine which genes comprise the amplification. Using TCGA data for ESCC, HNSCC, and LSCC^{92,129,238}, we identified 10 genes (*CCND1*, *ORAOVI*, *FGF19*, *FGF4*, *FGF3*, *ANO1*, *FADD*, *PPFIA1*, *MIR548K*, *CTTN*) as focally co-amplified across a total of 1119 SCC tumors (Fig 3b). From this analysis, we identified that *CCND1* and *CTTN* form the 5' and 3' boundaries of the minimal critical region of the amplicon, respectively, as there is a significant drop in amplification frequency beyond these genes. Therefore, in this work, we define 11q13 amplicon as amplification of these 10 genes. The genes in this 800 kB span are nearly always amplified together, with only rare cases exhibiting a smaller amplicon not containing all 10 genes (Fig S1b).

The frequency with which the 11q13 amplification occurs in SCCs seems indicative for its contribution to tumorigenesis. Furthermore, 60% of HNSCC and 77% of ESCC lines harbor 11q13 amplification (Fig S1c), compared to 25% and 58% of primary tumors, respectively, suggesting further selection for the amplification in either the isolation or propagation of SCC cell lines. The finding that patients whose HNSCC tumors carry the 11q13 amplification have decreased survival gives further evidence that the 11q13 amplification plays an important role in SCC development (Fig 3c), which is consistent with prior reports^{92,96,199,224,239,240}. Previous reports, however, did not separate HPV-positive from HPV-negative cases. The 11q13 amplification almost exclusively occurs in HPV-negative HNSCCs - the population which also has lower overall survival⁶⁵. Here, we show that even within the HPV-negative population, amplification of the 11q13 genes correlates with worse survival.

The particular core of 10 amplified genes at this locus is characteristic of the 11q13 amplicon in SCC, as we - for example - only see the increase in amplification in this window in ESCC, but not in other types of esophageal cancer (Fig S1d). Moreover, analysis of 378 Hepatocellular Carcinoma (HCC) tumors identified a narrower co-amplification window with breakpoints at *CCND1* and *FGF19* (Fig S1e). In HCC *FGF19* is aberrantly expressed and targeting the FGFR4-FGF19 axis has been demonstrated to be a promising strategy for 11q13-amplified HCC^{199,241}. The difference in amplification window thus implies a distinct set of genetic elements driving SCC as opposed to HCC.

The driver oncogenes of the amplicon are likely overexpressed at the transcript and protein levels as a consequence of increased DNA copy number. Using TCGA data, we determined the correlation between expression level and copy number of each protein coding gene in the amplicon in HNSCC⁹². Six of the genes - *CCND1*, *ORAOVI*, *ANO1*, *FADD*, *PPFIA1*, and *CTTN* - were highly expressed and had a significant positive correlation between expression level and copy number (Fig 3d). Similar trends were observed in correlation analysis for ESCC and LSCC (Fig S1f, Fig S1g). Correlation analysis between amplification and protein expression in the HNSCC CPTAC datasets also showed significant correlation for the 5 proteins for which data was available (Fig S1h)²⁴².

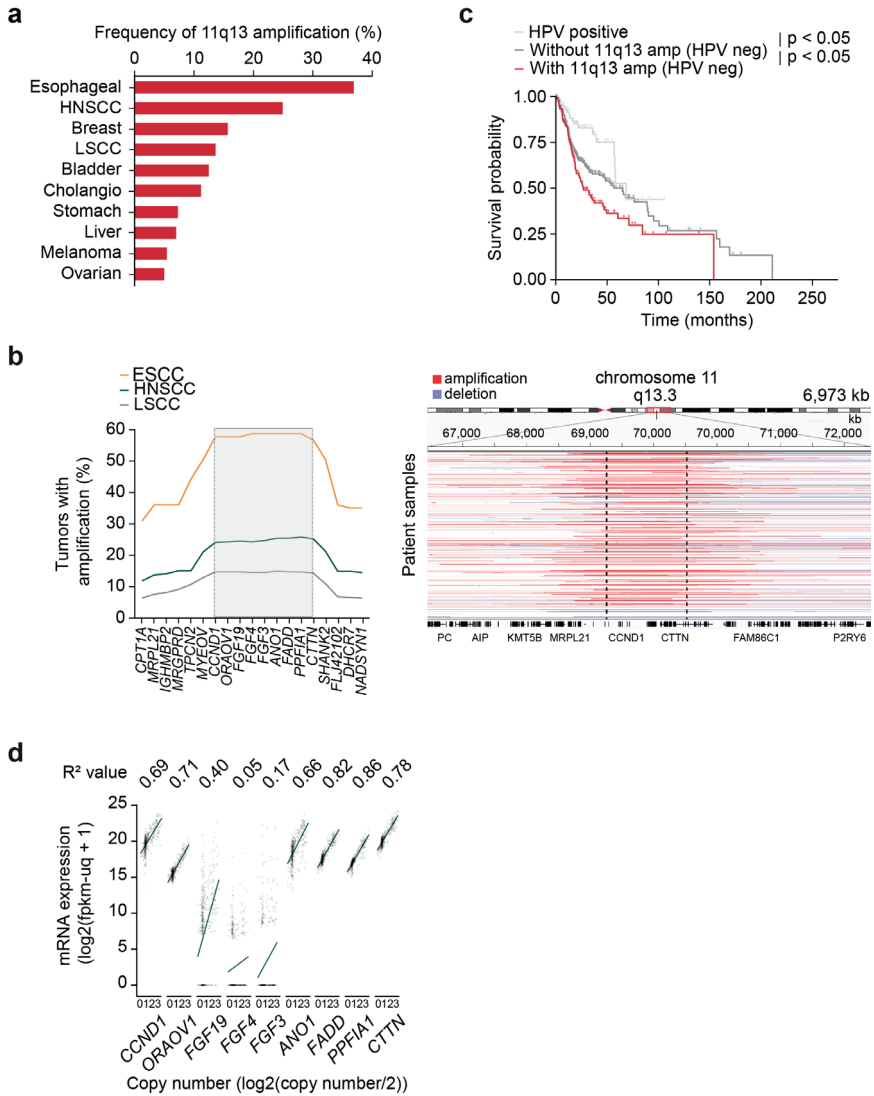


Figure 3 | The 11q13 amplification in SCC spans from *CCND1* to *CTTN*

a Frequency of 11q13 amplification in cancer (TCGA, PanCancer Atlas).

b Left: frequency of amplification of genes in 11q13 region in ESCC ($n = 97$), HNSCC ($n = 519$), and LSCC ($n = 503$). Right: representative integrative genome browser (IGV) view on copy number fragments of 11q13-amplified HNSCCs.

c Kaplan-Meier survival graphs for HNSCC patients, separated by HPV and 11q13 status (HPV negative, $n = 415$. HPV positive, $n = 72$).

d Correlation between gene expression and copy number in HNSCC (TCGA, $n = 496$). R2 value represents Spearman coefficient, p values calculated with Holm correction (all but *FGF3* and *FGF4* significant).

One gene - *FGF19* - was expressed at significantly lower levels and had a weaker correlation with copy number when compared with the aforementioned six genes, an observation we confirmed with qRT-PCR gene expression analysis of the 11q13 genes in HNSCC cell lines (Fig S1i). The other 2 protein coding genes in the amplicon - *FGF4* and *FGF3* - are expressed at low or undetectable levels in tumors with a weak correlation between expression and copy number, thus making them unlikely to be oncogenic drivers of 11q13 amplification.

***CCND1* and *ORAOV1* drive the pathogenic effect of 11q13 amplification**

To study the necessity of the remaining six protein coding genes on tumor associated cellular phenotypes, we utilized two HNSCC cell lines which harbor the 11q13 amplification - FaDu and Detroit562 - in loss of function assays (Fig S2a). For CRISPR interference (CRISPRi) experiments, we compared conditions against the *OR2B6* negative (non-expressed) gene, whereas for CRISPR knockout experiments, we designed a “SCI” negative control that targets the 11q13 region in a non-coding and non-regulating region to control for the multitude of edits introduced in the amplified 11q13 region.

We first aimed to determine the effect of the genes on a cancer defining phenotype. Therefore, we examined the effect of 11q13 gene knockdown on cell invasion in an *ex vivo* organotypic model of SCC. This organotypic model enables us to model cell invasion through the basement membrane by closely recreating the tumor microenvironment with physiological layers of a dermis scaffold, fibroblasts, and keratinocytes at an air-liquid interface²⁴³. CRISPRi-mediated knockdown of the protein-coding 11q13 genes in FaDu cells seeded on the organotypic cultures revealed that only depletion of *CCND1* or *ORAOV1* affected invasion of cells through the basement membrane (Fig 4a, Fig S2b).

In order to identify the phenotypic effect of knockout of 11q13 genes in a larger set of cell lines, we analyzed data using the Cancer Dependency Map (DepMap, project Achilles CRISPR knockout screens) database²⁴⁴. We confirmed *CCND1* and *ORAOV1* as the only protein coding genes on the 11q13 amplicon whose knockout results in lower cancer cell viability across a large panel of LSCC, ESCC and HNSCC lines (Fig 4b). In cell proliferation experiments with the FaDu and Detroit562 cell lines using both CRISPRi and CRISPR-mediated knockout, we were able to recapitulate *in vitro* proliferation effects upon *CCND1* and *ORAOV1* disruption observed in the DepMap data (Fig 4c, Fig 4d, Fig S2c, Fig S2d, Fig S2e, Fig S2f), whereas sphere formation was not affected upon knock down (Fig 4e, Fig S2g).

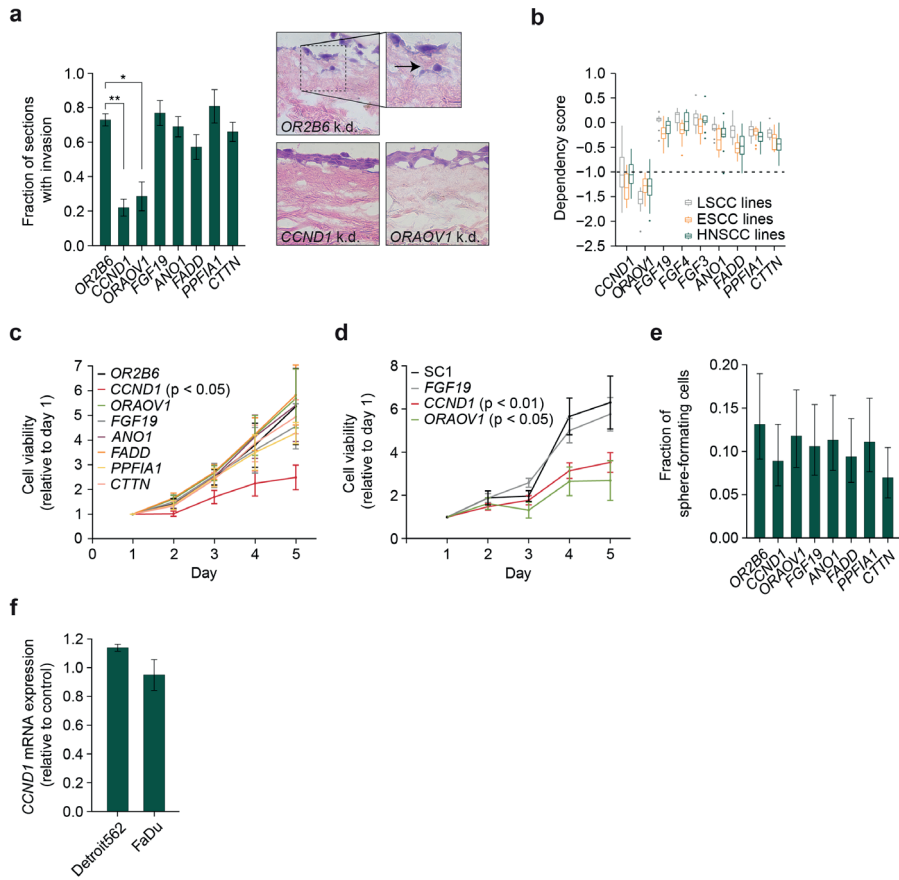


Figure 4 | *CCND1* and *ORAOV1* drive the pathogenic effect of 11q13 amplification

- a Left: Fraction of sections with invading FaDu cells in an organotypic model upon silencing of 11q13 gene expression through CRISPR-i (* $p < 0.05$, ** $p < 0.01$). Right: representative H&E images. Arrow indicates invading cell.
- b Dependency scores on 11q13 genes for LSCC, ESCC and HNSCC cell lines, from CRISPR knockout screens from project Achilles (DepMap). Upper and lower whiskers represent the largest and smallest observed values within 1.5 times the interquartile range from the ends of the box. Scores below -1.0 show significant dependency.
- c Relative cell viability values based on Alamar Blue assay upon CRISPR-i mediated knockdown of 11q13 genes in FaDu cells. P values calculated with two-way ANOVA test.
- d Relative cell viability values based on Alamar Blue assay upon CRISPR mediated knock-out of 11q13 genes in FaDu cells. P values calculated with two-way ANOVA test.
- e Spheroid formation frequency upon CRISPR-i mediated knockdown of 11q13 genes in FaDu cells. Error bars represent 95% confidence interval, p values calculated with chi-square test (none significant).
- f *CCND1* expression upon *ORAOV1* knock-out in FaDu and Detroit562 cells.

Thus, *CCND1* and *ORA0V1* are likely candidates to drive the oncogenic effects of the 11q13 amplification. Considering the genomic proximity between the genes in the 11q13 region, we also sought to verify that the observed effects were gene specific and not due to effects of perturbations on neighboring genes. We validated that silencing of the 11q13 genes does not affect expression of the neighboring genes, confirming the independence of the observed effects, and in particular that the effect of *ORA0V1* on proliferation and invasion is independent of *CCND1* (Fig 4f, Fig S2h, Fig S2i).

***MIR548K* is a putative driver of tumorigenicity on the 3' end of the 11q13 amplicon**

Although we identified *CCND1* and *ORA0V1* as potential drivers of 11q13 amplification in SCC, these two genes are both located on the 5' end of the amplicon and thus are unlikely to explain the selection for the entire 800kb amplicon in SCC when only *CCND1* and *ORA0V1* are amplified in other tumor types (Fig b, Fig S1e). Therefore, we hypothesized that there is an additional genetic element at the 3' end of the amplicon that leads to selection of the full amplicon in SCC and drives the oncogenic effect of the amplicon in cooperation with *CCND1* and *ORA0V1*. The 3' end of the amplicon contains the actively transcribed miRNA *MIR548K*, which was previously implicated in ESCC^{182,222,224}. Analysis of the TCGA PanCancer database revealed that in SCC, *MIR548K* is the most frequently amplified gene on the amplicon (18.73%, versus 17.55% for *CCND1*) (Fig 5a). In SCCs, from *CCND1* onwards, there is an upward trend in amplification rates of the 11q13 genes that reaches until *MIR548K*, after which rates go down again. This is in contrast to non-SCC cancers, where *CCND1* is the most frequently amplified gene, after which we see an immediate decrease in amplification rates. Analysis of TCGA miRNA expression data confirmed that there is a significant positive correlation between copy number and gene expression, indicating that *MIR548K* expression is upregulated upon 11q13 amplification (Fig S3a).

To investigate the functional role of *MIR548K* in SCC tumorigenic behavior, we again utilized to our *in vitro* and *ex vivo* models of SCC. Using our organotypic model of SCC, we found that CRISPR-mediated knockout of *MIR548K* decreases the invasive phenotype of FaDu cells to a similar extent as knockdown of *CCND1* or *ORA0V1* (Fig 5b, Fig S3b). This effect is independent of *CCND1*, as *MIR548K* knockout did not affect *CCND1* levels (Fig S3c). However, unlike knockdown of *CCND1* and *ORA0V1*, knockdown of *MIR548K* using locked nucleic acid antisense oligonucleotides (LNA-ASOs) does not affect growth of the 11q13-amplified cancer cells in 2D culture (Fig 5c, Fig S3d, Fig S3e), but does decrease the tumor sphere formation capabilities of the FaDu and Detroit562 lines (Fig 5d, Fig S3f). These two phenotypes are specific to depletion of *MIR548K*, suggesting a role for *MIR548K* in driving invasion that is distinct from that of *CCND1* or *ORA0V1*.

Invasion is largely a result of the epithelial mesenchymal transition (EMT) process and consists of multiple events. One of the first events during EMT is the loss of cell-

cell adhesion, such as through loss of adherens junction, and activation of a migratory phenotype. E-cadherin is the most prevalent adhesion molecule in normal epithelial tissue, but is typically downregulated or lost in tumors that originate from epithelial cells²⁴⁵. The observed effect of *MIR548K* on invasion is supported by previous studies reporting an essential role for *MIR548K* in migration and invasion in ESCC^{182,222,224}. Here, we further back this up through Gene Set Enrichment Analysis (GSEA)²⁴⁶ on RNAseq data of *MIR548K* knockout in FaDu cells, which points to involvement of *MIR548K* in the EMT process, exemplified by downregulation of the E-cadherin pathway (Fig 5e, Fig S3g). Moreover, downregulation of *MIR548K* resulted in upregulation of *ADAMTS1* and downregulation of *VEGFC*, corroborating previous findings indicating a role for *MIR548K* on EMT through regulation of *VEGFC* levels (Fig 5f)¹⁸². Thus, *MIR548K* appears to exert its effect on cellular invasion via a mechanism that is distinct from *CCND1* and *ORAOVI* and its location on the 3' end of the amplicon can therefore explain the length of the entire 11q13 amplicon in SCC.

***CCND1* and *ORAOVI* drive *in vitro* proliferation of oral keratinocytes**

We next sought to identify whether the 3 candidate oncogenes *CCND1*, *ORAOVI*, and *MIR548K* are sufficient to promote tumorigenic behavior in a primary cell model, using patient derived normal oral keratinocytes (OKCs). To study the effect of amplification of these genes in the genetic background in which 11q13 amplification occurs in HNSCC, we engineered the OKCs to carry deleterious *TP53* and *CDKN2A* mutations (Fig S4a). 88% and 70% of tumors with 11q13 amplification have these genes either mutated or deleted, respectively, making these 2 alterations the most frequently occurring mutations alongside 11q13 amplification (Fig 6a). To engineer the primary OKCs, we used our novel electroporation-based method for efficient delivery of CRISPR ribonucleoproteins (RNP) (see chapter 2).

We determined the effects of amplification of the 11q13 genes on primary OKC cultures from at least two different donors harboring loss-of-function mutations in both *TP53* and *CDKN2A* (TC-OKC) via lentivirus-mediated overexpression of the 11q13 genes (Fig S4b, S4c, for details on experimental set-up also see Fig S4d). Lentiviral expression of either *CCND1* or *ORAOVI* resulted in a competitive proliferation benefit over expression of a control lentivirus (EBFP only) (Fig 6b), further supporting the positive effect that *CCND1* and *ORAOVI* expression have on OKC proliferation. Consistent with previous results, expression of *MIR548K* did not endow the TC-OKCs with a significant proliferation advantage in 2D culture. Furthermore, when we expressed *CCND1* in combination with a second 11q13 gene, the OKCs generally grew more slowly, except when *CCND1* was co-expressed with *ORAOVI* (Fig 6c). Because these effects are additive, these data further suggest that amplification of *ORAOVI* and *CCND1* may drive SCC proliferation through distinct pathways and co-amplification of both *CCND1* and *ORAOVI* can cooperate in SCC tumorigenesis.

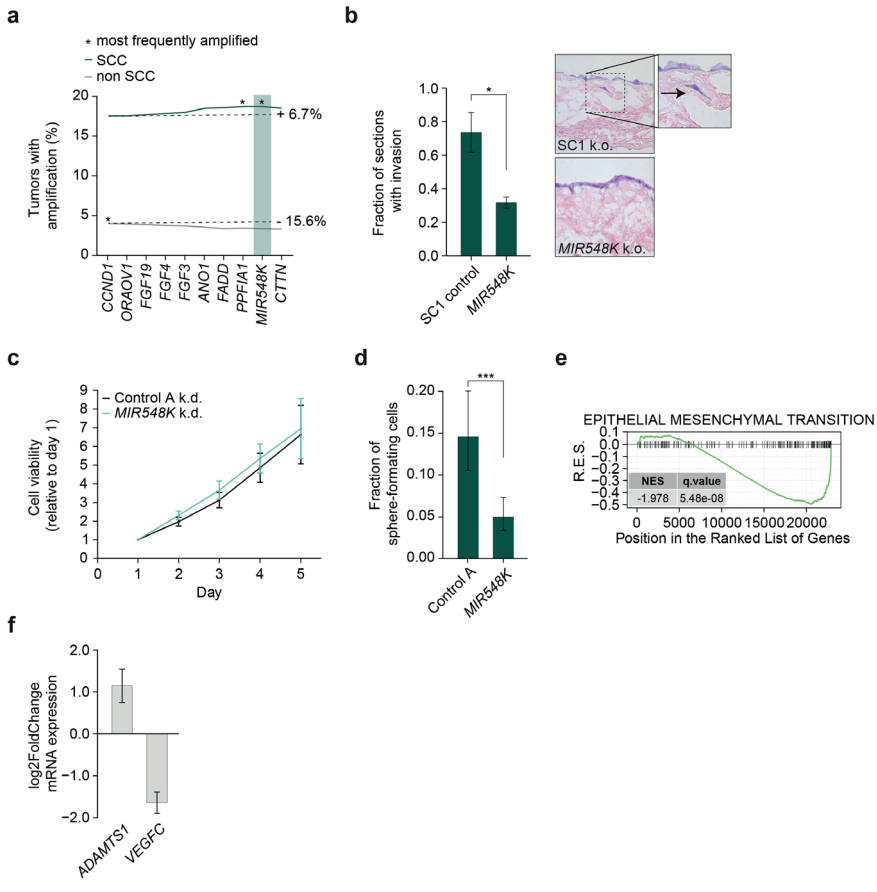


Figure 5 | *MIR548K* is a putative driver of tumorigenicity on the 3' end of the 11q13 amplicon

a Amplification rates of 11q13 genes in all SCC ($n = 1356$) and all non-SCC ($n = 9594$) tumors in TCGA PanCancer database. SCC: *CCND1* amplification rate = 17.55%, *MIR548K* amplification rate = 18.73%. Non-SCC: *CCND1* amplification rate = 3.98%, *MIR548K* amplification rate = 3.36%.

b Left: fraction of sections with invading FaDu cells in an organotypic model upon LNA-mediated knockdown of *MIR548K* (* $p < 0.05$). Right: representative H&E images. Arrow indicates invading cell.

c Relative cell viability values based on Alamar Blue assay upon LNA mediated knockdown of *MIR548K* in FaDu cells.

d Spheroid formation frequency upon LNA mediated knockdown of *MIR548K* in FaDu cells. Error bars represent 95% confidence interval, p value calculated with chi-square test (** $p = 0.001$).

e Running Enrichment Scores of GSEA upon *MIR548K* knockout in FaDu cells for the Hallmark_Epithelial_Mesenchymal_Transition Gene Set.

f Log2FoldChange of *ADAMTS1* ($n = 3$) and *VEGFC* ($n = 2$) expression upon *MIR548K* knockout in FaDu cells.

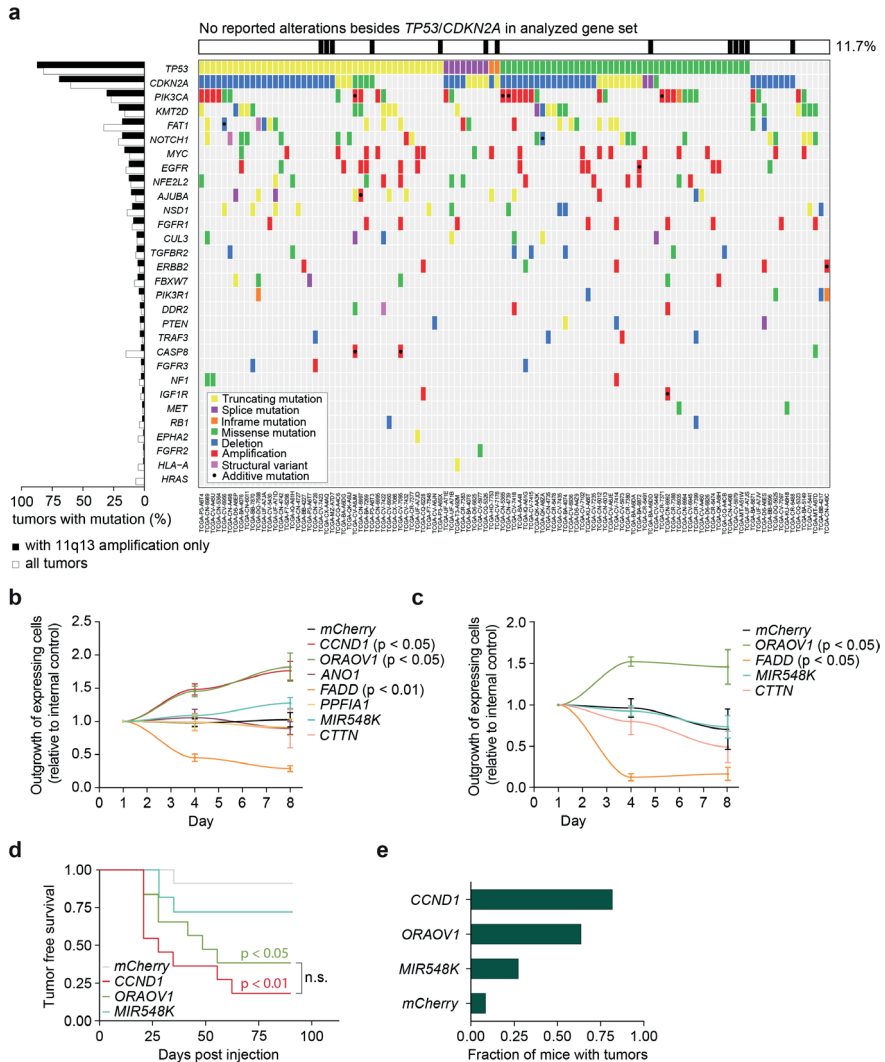


Figure 6 | *CCND1* and *ORAOV1* provide a competitive growth benefit in a novel primary cell model

a Mutational pattern of the most frequently and significantly altered genes in 11q13-amplified HNSCC tumors (TCGA, $n = 111$).

b Outgrowth of 11q13 gene-mCherry or mCherry alone overexpressing TC-OKC versus EBFP overexpressing TC-OKC.

c Outgrowth of *CCND1-EGFP* + 11q13 gene-mCherry or mCherry alone double overexpressing TC-OKC versus EBFP overexpressing TC-OKC.

d Tumor free survival of NSG mice injected with 1E6 human TC-OKC cells overexpressing indicated gene (*mCherry*: $n = 12$, *CCND1*, *ORAOV1*, *MIR548K*: $n = 11$ mice). P values calculated with a Log-Rank Mantel-Cox test with post-hoc P value adjustment for multiple comparisons.

e Fraction of mice with tumors at endpoint (90 days post injection).

Expression of the pro-apoptotic gene *FADD* in the TC-OKCs significantly hindered cell proliferation when compared to control TC-OKCs, suggesting that increased expression of *FADD* is detrimental to SCC proliferation. Indeed, upon expression of *FADD* TC-OKCs show an apoptotic phenotype (Fig S4e). Despite the negative effect that *FADD* amplification has on cell proliferation, virtually all SCCs with 11q13 amplification have an amplification that extends past the 3' boundary of *CCND1/ORAOVI/FGF19*, thereby including the *FADD* gene. The inclusion of the *FADD* gene in the SCC-specific 11q13 amplicon therefore suggests that the oncogenic benefit of the 3' end of the amplicon, which contains *MIR548K*, outweighs the suppressive effects of *FADD*. Additionally, the benefit of the *MIR548K* amplification may be lineage restricted to SCCs as HCCs and other tumor types less frequently exhibit 11q13 amplification beyond focal gain of *CCND1/ORAOVI/FGF19*.

***CCND1* and *ORAOVI* initiate *in vivo* tumor formation from oral keratinocytes**

Finally, we assessed the oncogenic driver potential of *CCND1*, *ORAOVI*, and *MIR548K* *in vivo*. We injected immunocompromised NSG mice with the engineered TC-OKC expressing either *CCND1*, *ORAOVI*, *MIR548K* or mCherry (control). Whereas only 1/12 of the control mice developed a tumor, overexpression of any of these three genes increased tumor formation in multiple mice (Fig 6d). RT-qPCR analysis confirmed that the tumors were highly expressing the target gene, indicating the tumors originated from the injected cells (Fig S4f). *CCND1* was the most potent driver of tumorigenesis, with 82% of mice developing tumors within 9 weeks of injection (Fig 6d, Fig 6e). We found however, that *ORAOVI* is an independent contributor to tumorigenesis, as 64% of mice injected with *ORAOVI*-overexpressing TC-OKC developed tumors. In conclusion, we demonstrate that *CCND1* and *ORAOVI* are strong drivers on the 3' end of the amplicon stimulating proliferation, invasion, and *in vivo* tumor growth. Additionally, we find that *MIR548K*, located on the 5' end of the amplicon, drives invasion probably through effecting an EMT phenotype. Thus, we demonstrate that the 11q13 amplification drives SCC tumorigenesis through at least 3 independent oncogenic events.

Discussion

In this study, we identify the three major genomic features of the 11q13 amplicon - *CCND1*, *ORAOVI*, and *MIR548K* - that contribute to SCC tumorigenesis. Our data reveal that these three genes contribute to SCC tumorigenesis in three independent ways, likely leading to powerful cooperation in tumorigenesis. 11q13 amplification typically occurs as an early genomic event during SCC tumorigenesis, following loss of *TP53* and *CDKN2A*^{107,181,182}. As these previous two events are insufficient to robustly induce tumors (Fig 6d, Fig 6e), we believe that the amplification of the 11q13 locus - and associated amplification of *CCND1*, *ORAOVI*, and *MIR548K* - is a critical

oncogenic event during SCC tumorigenesis of 11q13-amplified tumors. Previous studies have identified loss of *TP53* or *CDKN2A* occurring at some level in normal skin or premalignant lesions, yet 11q13 amplification has not been detected in premalignant HNSCC lesions^{101,107,247}. Moreover, analysis of the mutational pattern of 11l HNSCC tumors carrying the 11q13 amplification, shows that 13/111 (11.7%) of tumors have no mutations in the most frequently altered genes analyzed, besides *TP53* and/or *CDKN2A* (Fig 6a). Lastly, whereas SCC progression is characterized by an increase in somatic copy number alterations, it is particularly the 11q13 amplification that marks progression to a later stage in the tumorigenic process¹⁰⁷. Therefore, amplification of 11q13 likely represents a critical event that drives neoplastic growth during the early stages of SCC tumorigenesis.

11q13 amplification correlates strongly to lymph node metastasis and to a poorer prognosis in general^{107,182,239,240} (Fig 3c). Moreover, 11q13 amplification in HNSCC is negatively correlated with response to PD-1 therapy, limiting therapeutic options^{248,249}. Combined with the frequent occurrence of the amplification, this is illustrative for the need of better therapeutic strategies. Dissection of the amplicon and identification of the key drivers is an important step in discovering novel therapeutic options.

The 11q13 amplicon consists of 10 genes. Studies have reported that each of these 10 genes contribute to tumorigenesis in some capacity, but a comparative analysis to the relative contribution of each gene has never been done. Our data show an important role for the 3 identified genes in important oncogenic phenotypes such as proliferation, invasion, sphere formation, and *in vivo* growth. For the other genes, we did not observe consistent and strong effects of these genes in our models, but they might still contribute to tumorigenesis in a more specific or subtle fashion. For example, although we did not find any evidence in our model systems for the involvement of *CTTN* in the development of HNSCC, hitherto *CTTN* has often been considered to be the main oncogene candidate next to *CCND1*^{250,251}

However, many studies that find *CTTN* to be an oncogenic driver were performed with breast cancer (BC) models. In BC it was observed that amplification of *CTTN* can occur independently from *CCND1*, to an extent where there is no correlation between *CCND1* and *CTTN* amplification²⁵². In contrast, in HNSCC we see a very strong correlation between *CCND1* and *CTTN* amplification, where 96% of HNSCCs with *CTTN* amplification, also have *CCND1* amplification (Fig S1b), compared to only 35.5% in the study by Hui *et al.* in BC. Now techniques and resolution to determine copy number alterations have improved, it would be worthwhile to investigate if *CTTN* amplification indeed occurs more frequently independent in BC, as this would be indicative for a BC-specific function of *CTTN*.

We observed that the amplification in the 11q13 region in SCC differs from the length of the amplicon in other tumor types, such as HCC. While 11q13 amplification in SCC

represents the larger region that we analyzed in this study, 11q13 amplification in HCC is typically restricted to *ORAOVI*, *CCND1*, and *FGF19*, with *FGF19* being a critical component of the amplicon in HCC in comparison to SCC^{199,241}. We identify that the 3' end of the amplicon has a functional role that is likely mediated by amplification of the *MIR548K* locus. Since miRNAs are known to have significant pleiotropy dependent on cellular context²⁵³⁻²⁵⁵, it is feasible that the *MIR548K* exhibits its tumorigenic effect selectively in squamous epithelia, and therefore the miRNA-containing 3' end of the 11q13 amplicon is only selected for in the context of SCC tumorigenesis. Indeed, previous studies reporting a role for *MIR548K* in tumorigenesis and metastasis, predominantly do so in the context of SCC^{182,222,224}.

GSEA on RNA-seq data upon *MIR548K* knockout indicates a role in EMT, potentially by regulation of *CDH1* or *VEGFC* expression. Epithelial cell-derived tumors often lose E-cadherin expression in the tumorigenic process, and restoring expression of this adhesion molecule can inhibit the invasive phenotype in several tumor types^{245,256,257}. Analysis of E-cadherin expression data from the Human Protein Atlas in either esophageal/head and neck tissues or liver tissue, reveals that hepatocytes at baseline express lower CDH1 levels (Fig S5a, Fig S5b)²⁵⁸. This could be one possible explanation of tissue specific effects of *MIR548K* amplification and why it is selected for in ESCC and HNSCC, but not in HCC. Furthermore, similarly to what was previously established by Zhang *et al.*, we find that *MIR548K* expression increases *VEGFC* levels (Fig 5f)¹⁸². A previous study found that specially for HNSCC, but not other tumors, 11q13 amplification correlates with angiogenesis²⁴⁸. These finding further suggest tissue-specific effects of *MIR548K* in tumorigenesis. However, future studies directly evaluating the role of *MIR548K* across different cellular contexts and how *MIR548K* elicits its effects in these scenarios are needed to clearly establish this relationship.

Lastly, we show that increased expression of *FADD* induces apoptosis of TC-OKC, yet nearly all SCCs with 11q13 amplification have an amplification that extends past *CCND1/ORAOVI*, therefore including *FADD*. This inclusion suggests that the 3' end of the amplicon has oncogenic benefits that outweigh or compensate the effects of *FADD* expression. This can be explained by the above described effect of *MIR548K* on EMT/adhesion, but another additive possibility is that *MIR548K* can inhibit the apoptotic phenotype, which has indeed been suggested by a previous report²⁵⁹.

The primary focus of previous studies investigating the function of 11q13 amplification has largely been on *CCND1* due to its established role as a canonical oncogene across multiple tumor types. Our study further supports the role of *CCND1* as a key oncogene in 11q13-amplified SCC, with 11q13 amplified cancer cells exhibiting *CCND1* oncogene addiction similar to what has been described in other *CCND1*-dependent tumors²⁶⁰⁻²⁶². We show for the first time that increased *CCND1* expression is sufficient to drive tumorigenesis in TC-OKC. However, we also show that *ORAOVI* has almost equally oncogenic effects.

Despite both *CCND1* and *ORAOVI* being co-amplified in >98% of tumors with the 11q13 amplification, previous studies have largely overlooked the role of *ORAOVI* and the relationship between these two genes. We have now identified that *ORAOVI* and *CCND1* drive cancer growth through two distinct pathways with an additive effect, creating a potent oncogenic combination that occurs in over 6% of all tumors, regardless of tissue of origin. Although previous studies in yeast and plants have positioned *ORAOVI* as a putative oncogene, our study provides a direct line of evidence that gain of *ORAOVI* is sufficient to drive SCC tumor growth. Indeed, in each of our *in vitro*, *ex vivo*, and *in vivo* models of SCC tumorigenesis, *ORAOVI* had a similar magnitude of oncogenic effect as *CCND1*.

In conclusion, our study identifies *CCND1*, *ORAOVI*, and *MIR548K* as putative oncogenes that drive the pathogenic effect of 11q13 amplification through three independent oncogenic events. Continuing to investigate the role of these three oncogenes will provide critical information about potential anti-cancer therapeutic strategies for 11q13-amplified SCC and may help guide current treatment paradigms.

Material and Methods

Cell culture

FaDu (ATCC cat#HTB-43, male) and Detroit562 (ATCC cat#CCL-138f, female) cells were grown in Eagle's Minimal Essential Medium with L-glutamine (Fisher Scientific cat#50983283) supplemented with 10% FBS (Corning cat#MT35010CV) and 1% Penicillin/Streptomycin (P/S, Corning cat#MT30002CI). A-253 (ATCC cat#HTB-41, male) cells were grown in McCoy's 5A (Modified) Medium (Fisher Scientific cat#16-600-082) supplemented with 5% FBS and 1% P/S. SCC-15 (ATCC cat#CRL-1623) and SCC-9 (ATCC cat#CRL-1629, male) cells were cultured in Dulbecco's Modified Eagle medium (DMEM):F12 (Gibco cat#11039021) supplemented with 400 ng/mL hydrocortisone (EMD Millipore cat#386698), 10% FBS, and 1% P/S. HEK293T (ATCC cat#CRL-3216, female) cells were grown in DMEM (Gibco cat#12491023) supplemented with 5% FBS and 1% P/S. All cell lines were purchased and authenticated at ATCC in 2016 and tested yearly for mycoplasma through PCR. Human primary fibroblasts were isolated and collected from patient derived skin samples and cultured in DMEM supplemented with 5% FBS and 1% P/S. Human primary keratinocytes were collected and isolated from patient derived mucosal samples and cultured in Medium 154 and Keratinocyte Serum Free Medium (1:1, Life Technologies cat#M154500 and cat#17005042), supplemented with 5 mL/L Human Keratinocyte Growth Supplement (Life Technologies cat#S0015), 25 mg/L Bovine Pituitary Extract (Life Technologies cat#17005042), 2.5 µg/L EGF Human Recombinant (Life Technologies cat#17005042), and 1% P/S. No cells were passaged for longer than 5 weeks.

CRISPR interference (CRISPRi) constructs and cloning

Stable dCas9 cells were generated by transducing cells with pHR-SFFV-dCas9-BFP-KRAB (Addgene cat#46911) lentivirus. Stable dCas9 cells were transduced with pU6-sgRNA EF1Alpha-puro-T2A-BFP (Addgene cat#60955) lentivirus to introduce guideRNAs (table 1). *OR2B6*-targeting guideRNAs were used as negative control.

Table 1 | CRISPR interference gRNA sequences

Target gene	Protospacer sequence
ANO1	GCGCACAGGCGGCCACGATG
CCND1	GGTCCGCACGCTCCGGCGAG
CTTN	GGCTGGCGCGGCGGAATCCA
FADD	GAGGCACCGAGTGCAGGTT
FGF19	GGCGCTGCGTCCAGGATCTA
OR2B6	GGGAGTGAAACTCCAGCCA
ORAOV1	GGGTCTGCTACGGCACCGCG
PPFIA1	GCCGGCCTTAGTGACTGGGG
ANO1	GCGCACAGGCGGCCACGATG

Genome engineering

To generate gene knockouts, cells were transfected via electroporation using the MaxCyte ATX electroporation platform with Clustered Regularly Interspaced Short Palindromic Repeat (CRISPR) Cas9- ribonucleoproteins (RNPs) and gene-specific guideRNAs (table 2). For electroporation, sub-confluent cells were trypsinized and washed 1x in DMEM and 1x in Opti-MEM (Life Technologies cat#31985070). Cells were resuspended to a concentration of 2.5×10^7 cells/mL in Opti-MEM. crRNAs and Alt-R CRISPR-Cas9 tracrRNA (Integrated DNA Technologies) were hybridized in a 1:1 ratio to a final concentration of 50 μ M. crRNA:tracrRNA were complexed with Cas9-RNP at a 1:1:1 ratio for 20 minutes at room temperature and subsequently mixed with the cells to a final concentrations of 2.5 μ M crRNA:Cas9 and 2.0×10^7 cells/mL. Cells were electroporated in 25 μ l or 400 μ l reactions with the 'Optimization 7' (keratinocytes and Detroit562) or 'DL-D-1' (FaDu) electroporation protocols. After electroporation, cells were immediately collected from the processing assembly, plated into a 6 well plate and recovered 20 minutes at 37°C, before resuspending in 2 mL culture medium. Transfection efficiency was determined 24 hrs post electroporation through flow cytometry. After 96 hours, gene disruption was confirmed through TIDE (Tracking of Indels by Decomposition) analysis (primers: table 2). To control for multiple edits in the amplified 11q13 region, a negative control "Safe Control" SC1 crRNA was designed to target the 11q13 region in a non-coding and non-regulating region.

Table 2 | CRISPR crRNA sequences and primers for TIDE analysis

Target gene	crRNA sequence	Forward primer	Reversed primer
CCND1	CATTGAAGTAGGACACCGA	CACACGGACTACAGGGGAGT	ACCCCTTCTCTCTCAGAAA
CCR5	AACACCAGTGAGTAGAGCGG	TGCTTGGCCAAAAAGAGAGT	CGATTGTCAGGAGGATGATG
CDKN2A	TAACTATTCCGGTGCCTGGG	GACTCCCTTTTATCCCAAACG	CCAGTCTCTCTCTTGGCCAAC
FGF19	CGGTACACATTGTAGCCATC	ACCTACTGTGCCTGGCCTTA	TCTCAAAGCTGGGACTCCTC
MIR548K	CTCAAGTATTGCTGTAGGT	AACCTGGCGGAATTGTGTAG	TGTTTGCAGCACTCAACAAA
OR2B6	TATCAAAGGACATGACGGCC	GCTGGAGTTTCCACTCCTTG	TTCAGCCTCATTTGCTGTTG
ORAOV1	CATATTCGATGCCATCGTGA	CCATGTACAGGCTGCTTTGG	ACCAGGCTGAGCAGATGTTT
SC1	TTGGTCCCACGATGACCCAC	GATCGAGGTCCACTCTGAGC	GGTGTGTGACTGGGGGAAC
TP53	CCATTGTTCAATATCGTCCG	ACTGACCGTGCAAGTCACAG	CCCCTCTGAGTCAGAAACA

LNA knockdown

Non targeting scrambled control A and *MIR548K* targeting 3' FAM miRCURY Locked Nucleic Acid (LNA) miRNA Power Inhibitors were obtained from Qiagen (cat#339160). 2 mL of cells were seeded at a density of 80,000 cells/mL in a 6 well plate and transfected 24 hours later at a final concentration of 50 nM Inhibitor and 2.5 μ L TransIT-LT1 Transfection Reagent (Fisher Scientific cat#MIR2300). Cells were plated for the appropriate assay 48 hours after transfection. To control for target inhibition during lysis, 50 nM inhibitor was added to control cells during lysis.

Exogenous 11q13 gene constructs and cloning

To clone overexpression constructs, RNA was purified from oral keratinocytes (OKCs) and total cDNA was synthesized with poly-A specific primers using SuperScript III First-Strand Synthesis System (Invitrogen cat#18080051) according to the manufacturer's instructions. To create Gateway compatible PCR products of the gene of interest, coupled to an mCherry tag through a T2A sequence, primers were designed with AttB and T2A adapters (table 3). PCRs were performed to create AttB-gene-T2A and T2A-mCherry-AttB products from whole genome cDNA (for larger coding sequences and fluorescent tags, PCRs were performed using the following plasmids as template: *CTTN*: pGFP Cortactin, Addgene cat#50728; *FADD*: pCI-hFADD-FLAG, Addgene cat#31814; EBFP: pU6-sgRNA EF1Alpha-puro-T2A-BFP, Addgene cat#60955; EGFP: pSPCas9(BB)-2A-GFP, Addgene cat#48138; mCherry: pHR_Gal4UAS_pGKmCherry, Addgene cat#79124). PCR products were purified and coupled in a subsequent PCR. Full *attB* products were cloned into the pDONR221 Vector (Thermofisher Scientific cat#12536017) using Gateway Technology according to the manufacturer's instruction. Coding sequences were transferred into the pLEX_307 vector (Addgene cat#41392).

To create a *MIR548K* gBlock gene fragment for the *MIR548K* overexpression system, the 5' oligo (GAAGGCTCGAGAAGGTATATTGCTGTTGACAGTGAGCGG GCAAAATCCGCAAGTACTTTTTAGTGAAGCCACAGATGTAA) and 3' oligo (AGTGAAGCCACAGATGTAAAAAGTACTTGC GGATTTTGCTTGCC TACT GCCTCGGACTTCAAGGGGCTAGAATTCGAGCA) were annealed and cloned into the SGEF vector (Addgene cat#111170) using *EcORI* and *XhoI* restriction sites. As negative control, pLEX_307-EBFP was generated.

Table 3 | Lentiviral overexpression cloning primers

Gene for fusion cloning pLEX_307		
Target gene		AttB insert forward primer / T2A insert reversed primer
ANO1	AttB Forward	GGGACAAGTTTGTACAAAAAAGCAGGCTTAATGAGGGTCAACGAGAAGTACTCG
	T2A Reversed	CACGTCACCGCATGTTAGCAGACTTCCTCTGCCCTCCTCCGCTCCAGAGCGCCCGTGGTA
CCND1	AttB Forward	GGGACAAGTTTGTACAAAAAAGCAGGCTTAATGGAACACCAGCTCCTGTG
	T2A Reversed	CACGTCACCGCATGTTAGCAGACTTCCTCTGCCCTCCTCCGATGTCCACGTCCCGCAC
CTTN	AttB Forward	GGGACAAGTTTGTACAAAAAAGCAGGCTTAATGTGAAAGCTTCAGCAGG
	T2A Reversed	CACGTCACCGCATGTTAGCAGACTTCCTCTGCCCTCCTCCGCTCCCTGCCGAGCTCCACATAG
FADD	AttB Forward	GGGACAAGTTTGTACAAAAAAGCAGGCTTAATGGACCCGTTCTGGTG
	T2A Reversed	CACGTCACCGCATGTTAGCAGACTTCCTCTGCCCTCCTCCGCTCCGGAGCTTCGGAGGTAGATGC
ORAOV1	AttB Forward	GGGACAAGTTTGTACAAAAAAGCAGGCTTAATGGCTGGCAGTCAGGAC
	T2A Reversed	CACGTCACCGCATGTTAGCAGACTTCCTCTGCCCTCCTCCGCTTCCAAATGAAAGTCCGGAACTTCTGC
PPFIA1	AttB Forward	GGGACAAGTTTGTACAAAAAAGCAGGCTTAATGATGTGCGAGGTGATGCC
	T2A Reversed	CACGTCACCGCATGTTAGCAGACTTCCTCTGCCCTCCTCCGCTCCGCAGGAGTAAGTCTGACTGTAG
Label for fusion cloning pLEX_307		
Label		T2A insert forward primer / AttB insert reversed primer
EGFP	T2A Forward	CTAACATGCGGTGACGTGGAGGAGAATCCCGGCCCTGCTAGCATGGTGAGCAAGGGCGAG
	AttB Reversed	GGGGACCACTTTGTACAAGAAAGCTGGGTTCTTGACAGCTCGTCCATGCC
mCherry	T2A Forward	CTAACATGCGGTGACGTGGAGGAGAATCCCGGCCCTGCTAGCATGGTGAGCAAGGGCGAGG
	AttB Reversed	GGGGACCACTTTGTACAAGAAAGCTGGGTTTACTTGTACAGCTCGTCCATGCC
Label only cloning pLEX_307		
Label		AttB insert forward primer / AttB insert reversed primer
EBFP	AttB Forward	GGGACAAGTTTGTACAAAAAAGCAGGCTTAATGGTGAGCAAGGGCGAG
	AttB Reversed	GGGGACCACTTTGTACAAGAAAGCTGGGTTTACTTGTACAGCTCGTCCATGCC
mCherry	AttB Forward	GGGACAAGTTTGTACAAAAAAGCAGGCTTAATGGTGAGCAAGGGCGAG
	AttB Reversed	GGGGACCACTTTGTACAAGAAAGCTGGGTTTACTTGTACAGCTCGTCCATGCC

Lentiviral production and infection

HEK293T cells were transfected with 750 ng transfer plasmid, 375 ng psPAX2 (Addgene cat#12259), 750 ng pMD2.G (Addgene cat#12260), and 5.5 μ L Lipofectamin 2000 Transfection reagent (Life Technologies cat#11668027) per mL culture medium. Medium was replaced 16 hours post transfection and viral supernatant was collected 72 hours later, filtered through a 0.45 μ m PVDF filter (MilliporeSigma cat#SLHVM33RS), concentrated using LentiX concentrator (Takara Bio cat#631231) and stored at -80°C . Cells were transduced with viral pellets resuspended in appropriate medium with 8 μ g/ml Polybrene Transfection reagent (EMD Millipore cat#TR1003G) for 16 hours.

Copy number and RT-qPCR

For Reversed Transcriptase quantitative PCR (RT-qPCR), RNA was isolated with the RNeasy Plus Mini Kit (Qiagen cat#74136) and converted into cDNA using SuperScript III First-Strand Synthesis SuperMix for qRT-PCR (Thermo Fisher Scientific cat#11752250). PrimeTime qPCR Probe-based assays and Gene Expression Master Mix were purchased from Integrated DNA Technologies with 6-FAM/ZEN/IBFQ labeling (**table 4**). *ACTB* probes and primers for loading control were designed with JOE NHS/ZEN/3' IBFQ labeling to allow multiplex RT-qPCR. 10 μ L RT-qPCR reactions were prepared containing 500 nM of each primer (gene of interest, *ACTB*: forward and reversed), 250 nM of each probe, 5 μ L Mastermix, and 10-50 ng cDNA. Reactions were run in triplicates on the Quantstudio 6 (Applied Biosystems). Relative gene expression levels were calculated using the ΔCT method against *ACTB*. For DNA Copy number qPCR, DNA was isolated using the QIAamp DNA mini kit (Qiagen cat#51306). Custom PrimeTime qPCR Probes (Integrated DNA Technologies, **table 4**) were designed such that primers and probes are spanning an intronic region of the DNA. qPCR reactions were prepared and run as described above, but with 20-40 ng DNA. Copy number was determined using the ΔC_T method against RNase P. For RT-qPCR of *MIR548K*, small RNAs were isolated using the miRNeasy Mini Kit (Qiagen cat#217004). cDNA was synthesized using the Mir-X miRNA First Strand Synthesis Kit (Takara Bio cat#638315). Each 10 μ L reaction contained 100 (cell lines) - 200 (OKC) ng cDNA, 5 μ L TB Green Advantage qPCR premix (Takara Bio cat#639676), 10 μ M forward and reversed primer for U6 and target (*MIR548K* specific forward primer: aaaaguecuugcggauuuugcu).

Immunoblot analysis

Cell pellets were lysed in Pierce RIPA buffer (Thermo Scientific, 62249), supplemented with phosphatase inhibitor and protease inhibitor cocktail sets (Calbiochem cat#524625 and cat#539134). Protein extracts were resolved on Nu PAGE 4-12% Bis-Tris gradient gels (Invitrogen cat#WG1401A) and transferred to

PVDF membranes using the Trans-Blot Turbo system. Membranes were blocked in 5% milk in TBS-T and probed with primary antibodies overnight at 4°C, and then with horseradish peroxidase-conjugated secondary antibodies. Signals were visualized with SuperSignal West Pico PLUS Chemiluminescent Substrate (Thermo scientific cat#PI34577) on the Bio-Rad ChemiDox XRS+ System. The following antibodies were used: Anoctamin 1 (Cell Signaling cat#14476, 1:500), Beta-Tubulin (Abcam cat#6046, 1:500), Cortactin (Cell Signaling cat#3503, 1:1000), Cyclin D1 (Abcam cat#134175, 1:5000), FADD (Cell Signaling cat#2782, 1:1000), ORAOV1 (Invitrogen cat#PA5101219, 1:400), PPFIA1 (Abcam cat#204406, 1:200).

Table 4 | Copy number and RT-qPCR probes and assays

Copy number qPCR			
Target gene	Probe sequence	Forward primer	Reversed primer
CCND1	TCACACGCTTCTCTCCAGAGTGA	CAACAACCTCCTGTCTACTACC	CTAGGTGTCTCCCCCTGTAAG
CTTN	ATTAATTACCAGAGGGCCAGCCA	GGGAGAGAGATGGAGCAAAC	CTCACGCATTAGGAACTAGGG
FADD	AACTTATTTCGAGGTTGCAGGGCGT	CAGATGGGAGAGCCAGAAAC	ATTTACCCGGGCAGAAGTG
GIF	TAGTACCAGACCCAGAGTTCATGCT	CTCTACCTCCTGAGCCTTCT	CAACTGCTTCCCTGACCTC
ORAOV1	CCCTAACTCTGGCTCAAACCAGA	GGGCTAGTGCTACTTGAACAC	TCTGGCCCGGAATCTACTT
RNAse P	TCTGACCTGAAGGCTCT	AGATTTGGACCTGCGAGC	GCGGCTGTCTCCACAA
SORL1	AGTGCATTAACCCATGGCTTGGC	CCCAGAGGCATCTCCTATTA	CCTGTGAGGGCAGCTATAAAC
RT-qPCR			
Target gene	Probe sequence	Forward primer	Reversed primer
ACTB	AGTTTCGTGGATGCCACAGGACTC	CACTCTCCAGCCTTCCTTC	GTACAGGTCTTTGCGGATGT
Target gene	Assay number		
ADAMTS1	Hs.PT.58.1452444		
ANO1	Hs.PT.58.3276970		
CCND1	Hs.PT.56a.4930170		
CTTN	Hs.PT.58.707045		
FADD	Hs.PT.58.14661368.g		
FGF19	Hs.PT.58.27249369		
OR2B6	Hs.PT.58.27730835.g		
ORAOV1	Hs.PT.58.40145225		
PPFIA1	Hs.PT.58.14730583		
VEGFC	Hs.PT.58.14602240		

Organotypic invasion model

Frozen human dermis was thawed in DPBS (Life Technologies cat#14190250) for 48 hours at 37°C, and dermis was separated from epidermis. Dermis was treated with 0.1% Peracetic Acid (Sigma-Aldrich cat#77240) in DPBS for 2 hours and washed 3x 60 minutes with DPBS. Dermis was cut into ~1cm² pieces to fit stands, placed in individual wells of a 12 well plate with the dermal side up and left to air dry for 2 hours. 1 mL of fibroblasts at a concentration of 36,000 cells/mL was added to each well and plates were spun down at 1000 rpm for 60 minutes. Dermis and fibroblasts were co-cultured for 8 days before the dermis was placed on stands with the epidermal side face up. 50-60 µL Matrigel (Corning cat#354234) was added to cover the dermal side. After polymerization of the Matrigel, 500 µL of 3D organotypic media (3:1 DMEM:Ham's F12 medium (Thermo Scientific cat#12-615F) with 10% FBS, 1% P/S, and 1% antibiotic-antimycotic (Gibco cat#15240062), supplemented with 24 µg /mL adenine (Sigma cat#A9795-1G), 8.4 ng/mL cholera toxin (EMD Millipore cat#227036), 0.4 µg/ml hydrocortisone (EMD Millipore cat#386698), 5 µg/mL insulin (Sigma cat#I1882-100MG), 10 ng/mL EGF (Life Technologies cat#PHG0315), 1.4 ng/mL triiodothyronine (Sigma cat#T5516), 1 µg/mL ciprofloxacin hydrochloride (Sigma cat#PHR1044) was added. 50 µL FaDu cells were added on top of the dermis at a concentration of 3.75x10⁶ cells/mL. Media was changed every 2 days. After 10 days, dermis was removed from stand and fixed in 10% Neutral Buffered Formalin (Thermo Scientific cat#22050104) overnight, followed by an overnight wash in DPBS. Dermis was subsequently incubated in 15% sucrose in DPBS, 30% sucrose in DPBS, and 1:1 30% sucrose in DPBS mixed with Optimal Cutting Temperature compound (OCT, Fisher Scientific cat#23730571), 60 minutes each. Dermis was embedded in OCT and stored at -80°C until sectioning. OCT blocks were sectioned on a CryoStar NX70 cryostat (Thermo Scientific) at 5µm, with 500 µm between planes. Sections were stained with Gill III Hematoxylin (Thermo Scientific cat#72611) and Eosin-Y (Fisher Scientific cat#22220104). Each organotypic resulted in approximately 10 sections. Invasion was quantified as the fraction of sections with cells that show invading cells.

Cell growth assays

For viability assays, cells were seeded into Black Greiner Cellstar 96 well plates (Sigma-Aldrich cat#M9936). Starting at 72 hours after plating or drug treatment, cells were incubated with 10% Alamar Blue (Bio-Rad cat#100234-634) according to the manufacturer's instruction. Fluorescence was read out on a GloMax Explorer plate reader (Promega) at an excitation of 520 nm and emission of 580-640 nm. Cell viability was calculated relative to untreated or day 1 condition. For Spheroid assays, serial dilutions were made to concentrate cells at 200, 100, 50, or 20 cells/mL. 100 µL of cells were transferred to an Ultra-Low Attachment Multiwell Plate (Corning cat#3474), with 5 replicates per concentration. 72 hours after seeding, wells were qualified to be either positive or negative for sphere formation. Percentage of cells with

sphere forming capacity was determined using Extreme Limiting Dilution Analysis²⁶³. Statistical power was calculated with chi-square test. For Competition assays, *TP53* and *CDKN2A* knockout OKC (TC-OKC) were transduced with pLEX_307 or SGEP lentivirus for the gene of interest or EBFP control. 72 hours post transduction, gene and EBFP control overexpressing OKCs were mixed 1:1 and immediately analyzed on a LSR II Flow Cytometer (BD) to determine the ratio of gene-mCherry:EBFP. Cells were kept in culture and analyzed over time to determine the change in ratios. Ratios were normalized to day 1. Experiments were performed with OKC from at least 2 different donors (1 donor per replicate).

***In vivo* experiments**

NOD *scid* gamma (NSG) mice were purchased from the Jackson laboratory (cat#005557). All experimental procedures were approved by and in compliance with UCSF IACUC. *TP53* and *CDKN2A* knockout OKCs were transduced with pLEX_307 virus to induce expression of target genes. 6 days post transduction, cells were resuspended in a 1:1 ratio of Matrigel and OKC culture medium at a concentration of $1.0E^7$ cells/mL. NSG mice ($n = 45$, mixed male and female) were subcutaneously injected in the hind flank with $1.0E^6$ cells. Tumor growth was monitored weekly until endpoint and tumors were measured using a caliper. Tumors were dissected and origin was confirmed through RT-qPCR on target genes.

TCGA data analyses

Publicly available copy number and gene expression data from The Cancer Genome Atlas (TCGA) was accessed through diverse applications. For overall 11q13 amplification frequencies in tumors or cancer cell lines, TCGA PanCancer data and the Cancer Cell Line Encyclopedia were analyzed through cBioPortal, respectively^{178,264,265}. To determine individual gene amplification frequencies in tumors, TCGA data sets (GDC TCGA Esophageal (stratified for SCC tumors), GDC TCGA HNSCC, GDC TCGA LUSC, GDC TCGA Liver HCC) were explored for copy number through the Xenabrowser^{92,129,238,266}. Copy number amplification was called at > 3.0 copies. To determine correlations between copy number and gene expression, TCGA HNSCC, TCGA LUSC, and TCGA ESCC data were downloaded from the Genomic Data Commons and mined for copy number, RNA expression, and miRNA expression data. Shapiro Wilk tests showed that data were not linearly distributed, thus pairwise Spearman coefficient between expression and copy number was computed. P-values were corrected for multiple testing with the Holm method.

For correlations between copy number and protein expression, HNSCC data were downloaded from CPTAC²⁴². For survival analysis, TCGA HNSCC 92 data was mined for HPV status, 11q13 gene copy number, and survival in months. Kaplan Meier curves were computed with the Survival and Survminer packages for R. For cancer

dependency analysis, the Cancer Dependency Map was accessed via the depmap package for R. DepMap Release: DepMap, Broad (2020): DepMap 20Q3 Public. figshare. Dataset doi:10.6084/m9.figshare.9201770.v2 (CRISPR knockout screens from project Achilles)²⁴⁴. For HNSCC and Esophageal SCC (ESCC) specific analysis, the following cell lines were analyzed: HNSCC: BHY, BICR18, BICR22, BICR31, BICR6, CAL27, DETROIT562, FADU, HSC3, HSC4, PECAPJ15, PECAPJ41CLONED2, SCC15, SCC25, SCC4, YD38, YD8. ESCC: COLO680N, KYSE140, KYSE180, KYSE410, KYSE510, OE19, OE21, TE10, TE11, TE14, TE15, TE4, TE5, TE6, TE8, TE9, TDOTT. LSCC: HCC15, LK2, HARA, NCIH2170, NCIH2882, HCC95, SW900, SQ1, EBC1, LUDLU1, CORL32, NCIH520, NCIH1869, VMRCLCP, NCIH1703, HCC2450, GT3TKB, LOUNH91, HCC1897, KNS62, EPLC272H, RERFLCAI, LC1SQ, LC1F, NCIH1385, SKMES1, RERFLCSQ1, CALU1, HCC2814, LC1SQSF, NCIH157DM.

Statistical analysis

All data are represented as mean \pm SEM unless stated otherwise. All experiments were independently reproduced at least 3 times. Statistical significance is indicated as follows: * $p < 0.05$, ** $p < 0.01$, *** $p < 0.001$

Acknowledgements

This work was supported, in part, by the US National Institutes of Health (NIH) grant R01-DE029890 (A.T.). The authors thank René Bernards and Nancy Joseph for helpful discussions, and Andrea Yeung for technical assistance.

Author Contributions

C.I.M., A.G.M and A.D.T. conceived of research. C.I.M. designed and executed all in vitro and in vivo studies, performed all data analyses, and wrote the manuscript. A.G.M. contributed to DepMap data analysis and provided valuable discussion. E.V. assisted with the organotypic models. V.P. conceptualized the use of TC-OKC and provided guidance in the use of the organotypic models. A.D.T. supervised the study. All authors edited the manuscript.

Conflict of interest

C.I.M., E.V., V.P., and A.D.T. declare no competing interest. A.G.M. was an employee of MaxCyte Inc.

Supplemental data

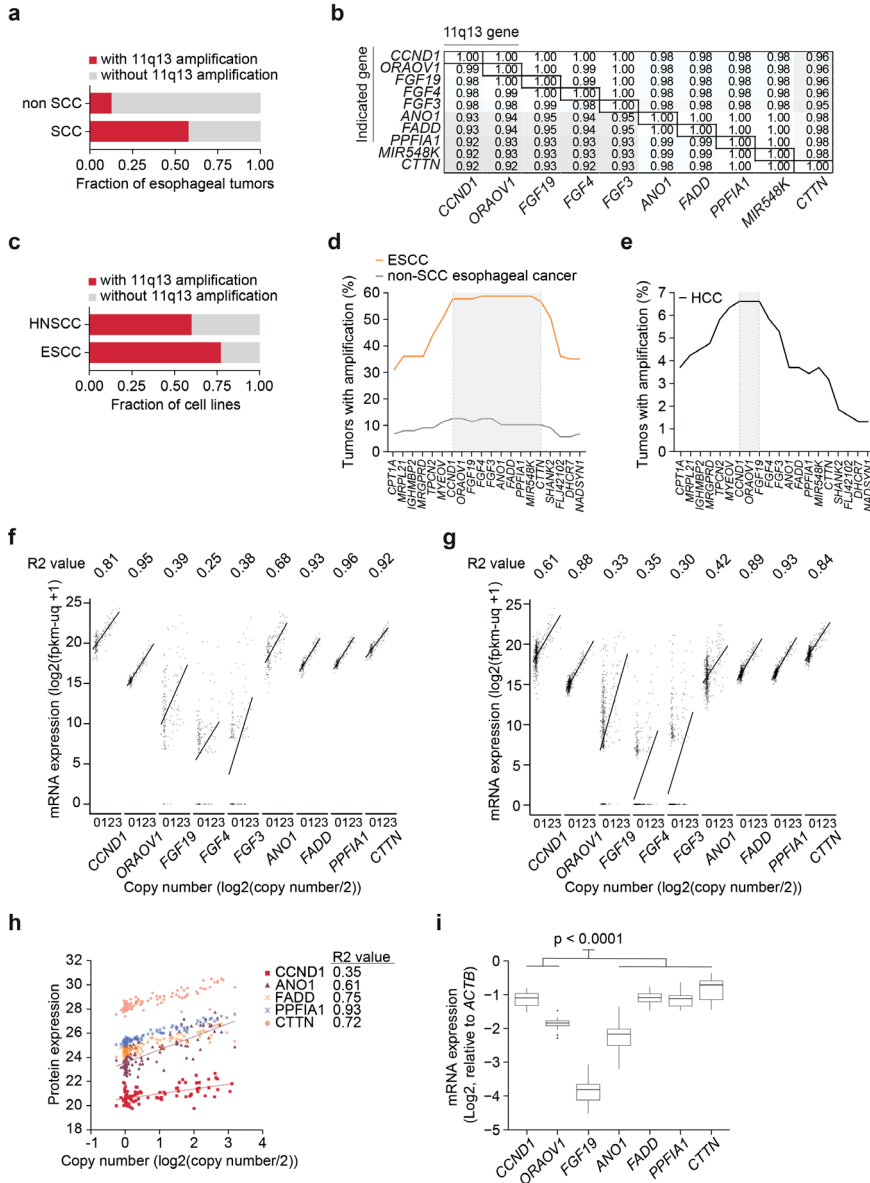


Figure S1 | 11q13 genes are frequently co-amplified in SCC

- a Fraction of esophageal tumors with 11q13 amplification (TCGA, non-SCC: $n = 88$, SCC: $n = 97$).
- b Fraction of tumors that have indicated gene amplified when 11q13 gene is amplified ($n = 519$).
- c Fraction of HNSCC ($n = 30$) and ESCC ($n = 24$) CCLE cell lines with 11q13 amplification.
- d Frequency of amplification of genes in 11q13 region in SCC- and non-SCC esophageal cancers (non-SCC: $n = 88$, SCC: $n = 97$).
- e Frequency of amplification of genes in 11q13 region in hepatocellular carcinoma (HCC, $n = 378$).

>>

- f Correlation between gene expression and copy number in ESCC (TCGA, $n = 161$). R2 value represents Spearman coefficient, p values calculated with Holm correction.
- g Correlation between gene expression and copy number in LSCC (TCGA, $n = 500$). R2 value represents Spearman coefficient, p values calculated with Holm correction.
- h Correlation between copy number and protein expression in HNSCC (CPTAC, CCND1: $n = 96$. Others: $n = 109$). R2 value represents Spearman coefficient.
- i Gene expression of 11q13 genes relative to ACTB expression in FaDu cells. D. Upper and lower whiskers represent the largest and smallest observed values within 1.5 times the interquartile range from the ends of the box. *** $p < 0.001$.

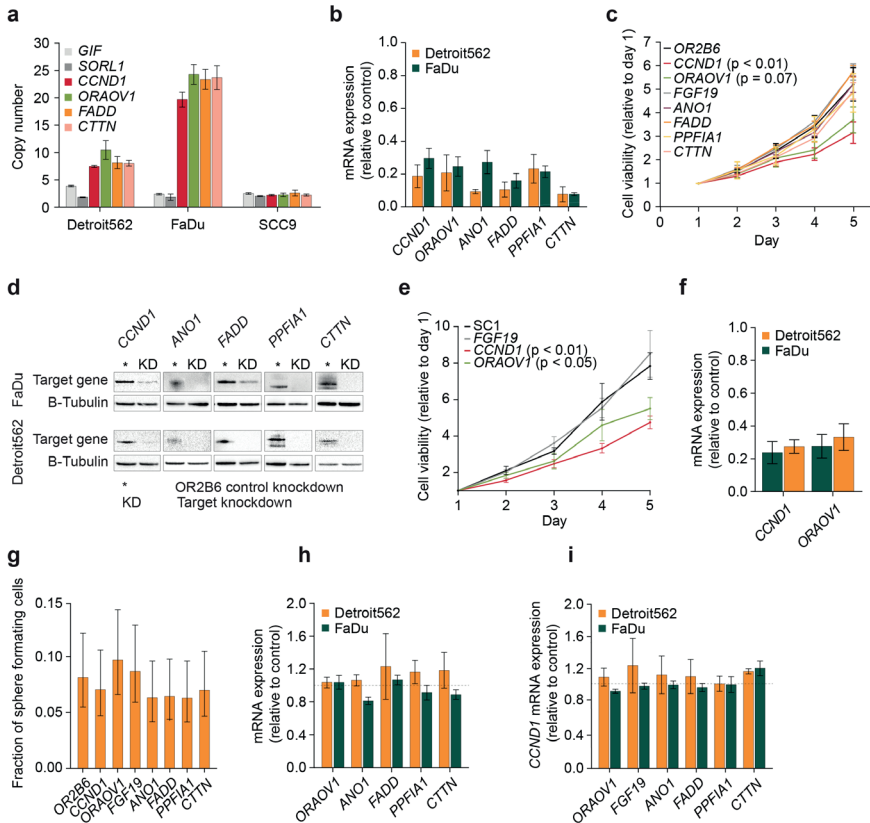


Figure S2 | Growth analyses upon gene specific and efficient knock down in 11q13 amplified cells.
a RT-qPCR copy number values of *GIF* (11q12), *SORL1* (11q24), and 11q13 genes, calculated relative to primary oral keratinocytes.
b Gene expression values 72 hrs post transduction with guideRNA, relative to control.
c Relative cell viability values based on Alamar Blue assay upon CRISPR-i mediated knockdown of 11q13 genes in Detroit562 cells. P values calculated with two-way ANOVA test.
d Immunoblot analysis of 11q13 genes in FaDu and Detroit562 cells upon CRISPRi-mediated knockdown of target genes.
e Relative cell viability values based on Alamar Blue assay upon CRISPR mediated knock-out of 11q13 genes in Detroit562 cells. P values calculated with two-way ANOVA test.
f Gene expression values 96 hrs post respective gene knockout, relative to SC1 control.
g Spheroid formation frequency upon CRISPR-i mediated knockdown of 11q13 genes in Detroit562 cells. Error bars represent 95% confidence interval, p values calculated with chi-square test (none significant).
h Gene expression of 11q13 genes upon CRISPR-i mediated knockdown of *CCND1* in FaDu and Detroit562 cells.
i *CCND1* gene expression upon CRISPR-i mediated knockdown of 11q13 genes in FaDu and Detroit562 cells.

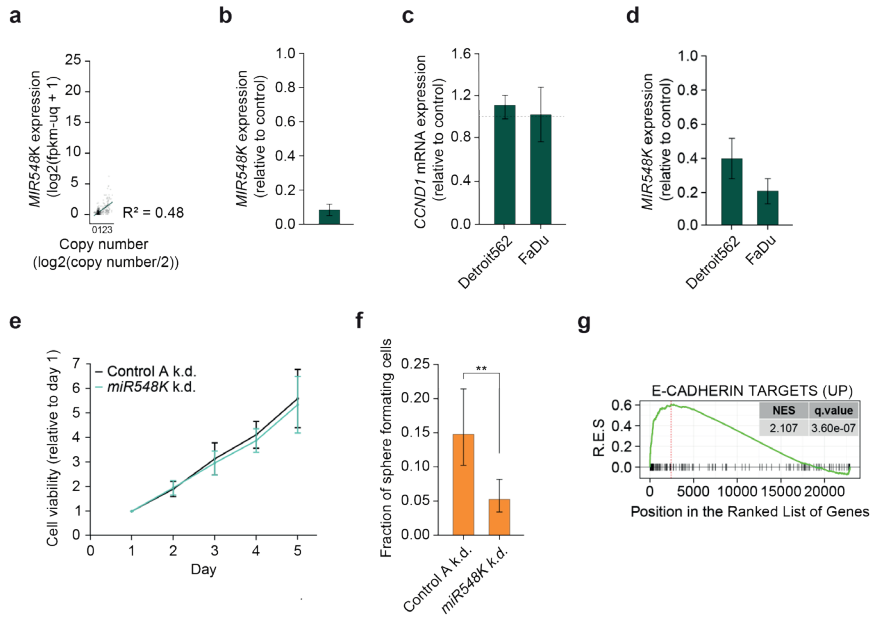


Figure S3 | Growth analyses upon abrogation of *MIR548K*

- a Correlation between *MIR548K* copy number and expression in HNSCC (TCGA, $n = 457$). R2 value represents Spearman coefficient, p value calculated with Holm correction (significant).
- b *MIR548K* expression values 96 hrs post transfection with CRISPR-RNP, relative to control.
- c *CCND1* expression values upon *MIR548K* knockout in FaDu and Detroit562 cells.
- d *MIR548K* expression values 72 hrs post LNA transfection, relative to control.
- e Relative cell viability values based on Alamar Blue assay upon LNA mediated knockdown of *MIR548K* in Detroit562 cells.
- f Spheroid formation frequency upon LNA mediated knockdown of *MIR548K* in Detroit562 cells. Error bars represent 95% confidence interval, p value calculated with chi-square test (**p < 0.01)
- g Running Enrichment Scores of GSEA upon *MIR548K* knockout in FaDu cells for the CDH1_ Targets Gene Set.

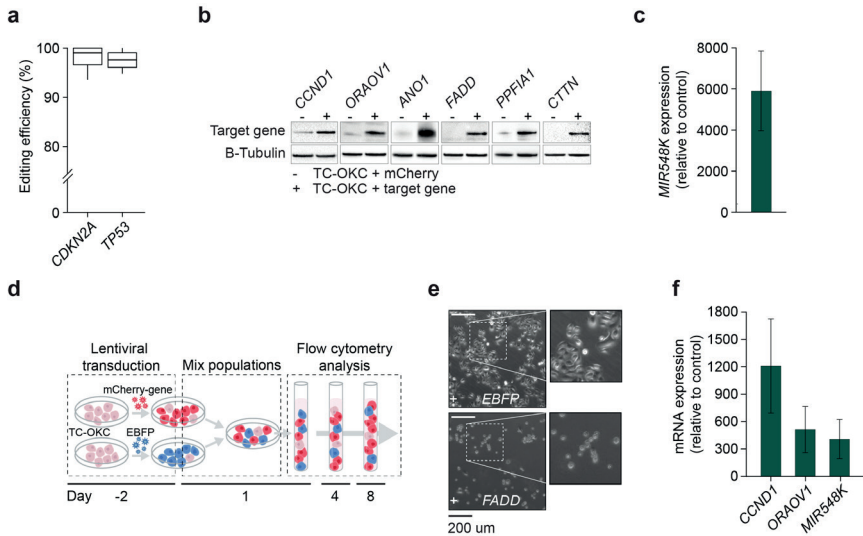


Figure S4 | Expression of 11q13 genes in TP53/CDKN2A knockout OKC

a Percentage of indels measured via TIDE 96 hrs post electroporation with *CDKN2A*- and *TP53* targeting CRISPR RNPs in primary OKC.

b Immunoblot analysis of 11q13 genes in TC-OKC 6 days post transduction with lentivirus.

c *MIR548K* expression levels in OKC relative to control 96 hrs post transduction with lentivirus.

d Schematic overview of experimental set-up for competitive growth assay. TC-OKC are transduced with lentiviral construct for gene of interest (with mCherry) or control (EBFP). After 72 hours, the gene-mCherry and control-EBFP OKC populations are mixed and analyzed through flow cytometry. Cells are kept in culture and analyzed over time.

e Light microscopy pictures of TC-OKC 72 hrs post transduction of *EBFP*- or *FADD*-expression inducing lentivirus.

f Gene expression values of dissected tumors, relative to control cells from pre-injection.

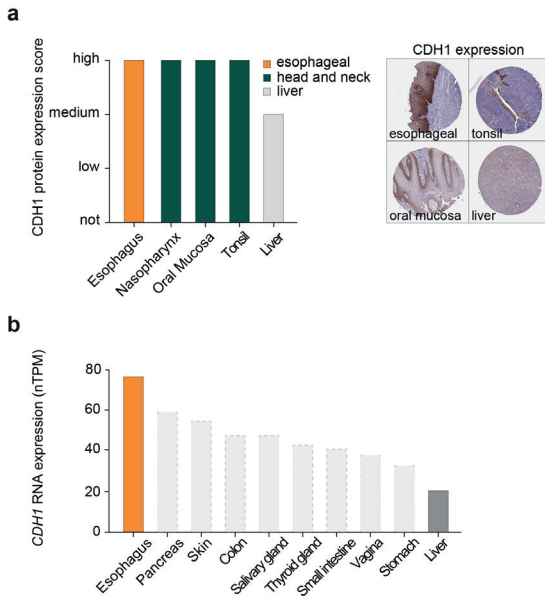


Figure S5 | CDH1 expression in esophageal, nasopharyngeal, and liver tissue

a Left: CDH1 protein expression data for 5 different tissues. Right: Representative immunohistochemistry images from CDH1 staining (all CAB000087 antibody). All data and images from The Human Protein Atlas (<https://www.proteinatlas.org/ENSG00000039068-CDH1/tissue,v22.0.proteinatlas.org>)

b *CDH1* RNA expression in selected tissues, expressed in normalized protein-coding transcripts per million) based on RNA-seq tissue data from the Genotype-Tissue Expression (GTEx) project. Dataset does not include nasopharyngeal tissue. Data obtained through The Human Protein Atlas (<https://www.proteinatlas.org/ENSG00000039068-CDH1/tissue,v22.0.proteinatlas.org>)

Chapter 4

11q13 amplification-mediated rewiring of the cyclin D1 regulatory network in squamous cell carcinoma

Céline I Mahieu¹, Andrew G Mancini², Ellee Vikram¹, Aaron D Tward¹

¹Department of Otolaryngology - Head and Neck Surgery, University of California
San Francisco, San Francisco, USA

²MaxCyte, Inc., Gaithersburg, MD, USA

Based on

ORAOV1, *CCND1*, and *MIR548K* are the driver oncogenes of the 11q13 amplicon in squamous cell carcinoma (Molecular Cancer Research, 2024)



Abstract

11q13-mediated amplification of *CCND1* occurs frequently in squamous cell carcinomas (SCC), and particularly in head and neck SCCs (HNSCCs). *CCND1* is one of the driver oncogenes of the 11q13 amplification, but the effect of amplified *CCND1* in HNSCCs has not yet been fully elucidated. Here, we identify that *CCND1* amplification induces *CCND1* oncogene addiction in amplified cancer cells, whereas primary oral keratinocytes only show dependency on *CCND2*. Moreover, *CCND1* amplification rewires the cyclin D1 regulatory network, such that cyclin D1 drives the cell cycle in a CDK4/6/RB-independent fashion. Lastly, we identify that cyclin D1 induces *RRM2* expression, which may confer a novel dependency on *RRM2*, as we show that *RRM2* inhibitors suppress cyclin D1-mediated tumor growth. Thus, this work provides new insights into viable strategies for targeting *CCND1*-amplified HNSCC tumors.

Introduction

Cell proliferation is crucial in development and normal cell health, but dysregulation of this process can give rise to over-proliferative cells and eventually cancer²⁶⁷. Therefore, progression through the cell cycle is tightly regulated by the cyclin/cyclin dependent kinase (CDK) system. Cyclins are expressed in a cyclic manner, being the limiting step in the formation of the cyclin-CDK complex that stimulates advancement through the cell cycle. There are different classes of cyclins that each display substrate specificity towards their specific CDK partners and are activated in different phases of the cell cycle. Although other classes have also been implicated in tumorigenesis, particularly the D-type cyclins play a significant role in cancer development and maintenance, as responders to signals of several oncogenic pathways^{95,268}. The three types of cyclin D (D1-D3) share significant overlap in amino acid sequence, but cyclin D1 is the most frequently dysregulated in cancer and therefore the best studied amongst the cyclins. Cyclin D1 is a key regulator of cell cycle progression from the G1- to S-phase, through integration of extracellular signals such as growth factor receptor activation and adhesion signaling into progression of the cell cycle through DNA synthesis²⁶⁹. Cyclin D1 levels increase late in the G1 phase to stimulate advancement to the S-phase for DNA synthesis, at which point cyclin D1 levels fall again.

Protein interaction analysis have identified that cyclin D1 interacts with over 100 different proteins. These datasets are particularly enriched for its cell cycle partners and proteins that are involved in transcriptional regulation^{192,270}. However, analysis of interactors in human cancer cell lines also shows presence of proteins that are involved in, for example, DNA repair, cellular organization, protein folding, and RNA metabolism²⁷⁰. Thus, although the most prominent function of cyclin D1 is in cell proliferation, cyclin D1 is also involved in other cellular processes, and it exerts its regulatory function both in a CDK-dependent and -independent fashion.

CDK dependent- and independent functions of cyclin D1

The most well-known function of cyclin D1 is its catalytic function, where it complexes with its CDK4 or CDK6 partners to interact with and phosphorylate several substrates. CDK4/6 activity is regulated through interaction with cyclin D1, phosphorylation and through CDK inhibitors of the INK4 (including p16ink4a and p15ink4b) and CIP/KIP (P21, P27) family members¹⁸⁶. CDKs are integral to the checkpoint that prevents continuation of the cell cycle in response to DNA damage and defects in the formation of the mitotic spindle. Upon stimulation by extracellular growth factors and subsequent expression of cyclin D1, assembly of the cyclin D1-CDK complex results in phosphorylation of the retinoblastoma tumor suppressor protein (RB) and RB-like proteins p107 and p130. RB phosphorylation results in the release of E2F transcription factors, which in turn induce several target genes that are required for S-phase entry and DNA replication⁹⁵.

Since the initial descriptions of this pathway, the model has been further expanded to include several feedback interactions, such as between the RB- and E2F proteins²⁷¹. Other substrates for the cyclin D1-CDK complex include SMAD3 - resulting in subsequent downregulation of genes in the TGF- β family that are involved in inhibition of cell cycle progression -, the PRMT5/MEP50 complex - resulting in a decrease of the CUL4 E3 ligase and subsequent stabilization of CDT1 levels, which is involved in DNA replication -, CDK inhibitors P21 and P27, and several other proteins involved in cell cycle progression, such as RUNX, GATA4, BRCA1, and MEF2 family members²⁷²⁻²⁷⁸.

Besides its catalytic functions, cyclin D1 also regulates cell growth and differentiation through direct - CDK independent - interaction with a number of DNA binding proteins, such as the nuclear hormone receptor family and their co-activators. Cyclin D1 can directly bind and activate the estrogen receptor (ER) in both a CDK- and estrogen- independent manner and also recruit steroid receptor co-activators (SRCs) to the ER187,188,279. This has mainly been observed in breast cancer (BC), where in cells with both high cyclin D1 and ER expression, cyclin D1 activates the transcriptional functions of the ER, stimulating cell growth. In contrast with ER activation, cyclin D1 also directly interacts with but inhibits the Androgen Receptor (AR), and the peroxisome proliferator-activator receptor gamma (PPAR γ) - which inhibits adipocyte differentiation^{189,190,280}. Other DNA binding- and transcription factor proteins that cyclin D1 interact which include MYB, DMP1, MYOD, RAD51, and C/EBP β ^{270,281-286}. Cyclin D1 can further control transcription through interaction with chromatin modifying enzymes such as histone acetyltransferases (HACs) and histone deacetylases (HDACs), forming a bridge between these proteins and transcriptional regulators^{190,191,287,288}.

Dysregulation of cyclin D1 activity in cancer

One of the hallmarks of cancer is that cells display continuous proliferation while evading signals of growth regulation, and dysregulation of the cell cycle is one of the key events in tumorigenesis to drive tumor cell proliferation⁸⁶. Due to its central role in the cell cycle, dysregulated cyclin D1 disrupts checkpoint-induced cell cycle arrest and permits replication of damaged DNA^{272,289,290}. Thus, high levels of cyclin D1 through either overexpression or compromised degradation, stimulate cell cycle progression through the G1-S transition. Ultimately, this can stimulate uncontrolled proliferative growth, endowing cancer cells with a fitness advantage.

Human cancers show frequent dysregulation of cyclin D1, and high CCND1 expression generally correlates with poor prognosis²⁹¹⁻²⁹⁸. Dysregulation of the P16/cyclin D1/CDK pathway has been observed in nearly all cancers, but the mode of dysregulation varies. Dysregulation can be a result of amplification of *CDK4* or *CDK6*, homozygous deletion or deleterious indels of inhibitors such as *CDKN2A* (P16), or inactivation of

RB proteins. Specific activation of cyclin D1 activity can be achieved through *CCND1* amplification, translocation, protein stabilization, or activation through oncogenic signaling pathways.

Cyclin D1 activity is regulated through several signaling pathways, of which the main ones include WNT/ β -catenin, MAPK, PI3K-AKT, EGFR, JAK-STAT, and NF- κ B signaling pathways²⁹⁹⁻³⁰⁵. Furthermore, in cancer, mutations have been observed in genes that regulate the ubiquitination and degradation of cyclin D1. For example, several cancers, including 14% of esophageal squamous cell carcinomas (ESCC), display mutations in *Fbx4*, which is part of a cyclin D1-targeting ubiquitin protein ligase complex, resulting in increased cyclin D1 stability^{306,307}. Another example of cyclin D1 stabilizing mutations observed in cancer are mutations at the Thr-286 site of the *CCND1* gene itself, which prevent phosphorylation by GSK-3 β and subsequent degradation^{302,308,309}. Translocation of *CCND1* to the immunoglobulin heavy chain (IGH) locus can also increase *CCND1* expression and is a defining genetic event in Mantle Cell Carcinoma, where over 90% of the tumors display this translocation³¹⁰.

However, after *CDKN2A* inactivation, the most frequent mode of cyclin D1 activation is through amplification of the 11q13 locus, which includes *CCND1* amongst other genes. 11q13 amplification occurs in approximately 6% of all tumors, making it the third most common amplification across cancers, only trailing *MYC* and *PI3KCA* amplifications¹⁷⁹ (see Chapter 3). 11q13 - and thus *CCND1* - amplifications are particularly enriched in squamous cell carcinomas^{107,179,181,182}.

***CCND1* amplification in HNSCC**

24% of HNSCCs carry 11q13/*CCND1* amplifications, and this amplification correlates significantly with poor prognosis and lymph node metastasis²³⁹ (see Chapter 3 for more details on 11q13 amplification). In HPV-negative HNSCCs, there is a significant overlap in tumors with *CDKN2A* inactivation and *CCND1* amplification^{92,91}. In contrast, HPV-positive HNSCC are associated with E6/E7 viral oncogenes, which bind and inactivate RB in the absence of further mutation³¹¹.

The frequency of this *CCND1* amplification generated enthusiasm for the use of CDK4/6 inhibitors, such as palbociclib, as potential therapeutics in SCC. This is based upon the assumption that CDK4 and/or CDK6 are critical downstream targets of amplified *CCND1* in SCC. One phase II study of palbociclib in lung SCC (LSCC) patients with known amplification of *CCND1* failed to demonstrate significant disease controlling activity³¹². A double-blind randomized placebo controlled trial in 125 patients of palbociclib in combination with cetuximab in patients with HPV-negative recurrent or metastatic head and neck SCC (HNSCC) failed to demonstrate any additive benefit of palbociclib³¹³. Further, a phase II study of palbociclib and cetuximab in patients who previously progressed on cetuximab yielded minimal, if

any, response³¹⁴. These disappointing results raise the possibility that mechanisms other than CDK4/6 activation may be the critical events downstream of *CCND1* amplification in SCC.

Here, we aimed to get a better understanding of the function of cyclin D1 in 11q13-amplified HNSCC. Through comparison of sensitivity of *CCND1*-amplified cancer cells and non-amplified primary cells to either *CCND1* deletion or treatment with CDK-inhibitors, we found that in contrast to primary cells, amplified HNSCC cells show high sensitivity to *CCND1* loss, but in a CDK-independent manner. Furthermore, we identify a novel activity in which *CCND1* amplification results in *RRM2* upregulation that drives tumorigenesis. We show that *RRM2* inhibition decreases tumorigenicity, thus identifying novel potential treatment opportunities and strategies for *CCND1*-amplified HNSCC.

Results

11q13-mediated amplification of *CCND1* induces *CCND1* dependency

Increased *CCND1* expression through 11q13 amplification has been presumed one of the major tumor-driving events of the 11q13 amplification in SCC. To assess the contribution of *CCND1* to *in vivo* tumor growth, we measured tumor growth of *FGF19* (control) and *CCND1* knockout in *CCND1*-amplified FaDu cells. Loss of *CCND1* significantly decreased tumor growth in NSG mice, confirming that cyclin D1 is an important driver of tumor growth in *CCND1* amplified cancer cells (Fig 1a). However, the understanding of the effect of *CCND1* expression on the oncogenic transformation of normal keratinocytes is very limited. Therefore next, we assessed the effect of increased *CCND1* expression on *in vivo* tumor formation and growth of oral keratinocytes (OKCs). OKCs bearing *TP53*- and *CDKN2A* deleterious indels (TC-OKCs) were transduced with *CCND1* or *mCherry* (control) expression inducing lentivirus and injected into NSG mice. Whereas the control mice did not show any tumor formation, induction of *CCND1* expression was sufficient to induce tumors *in vivo* from TC-OKCs (Fig 1b). Moreover, the level of *CCND1* expression was directly correlated to tumor growth, emphasizing the effect of *CCND1* on the tumors (Fig S1a).

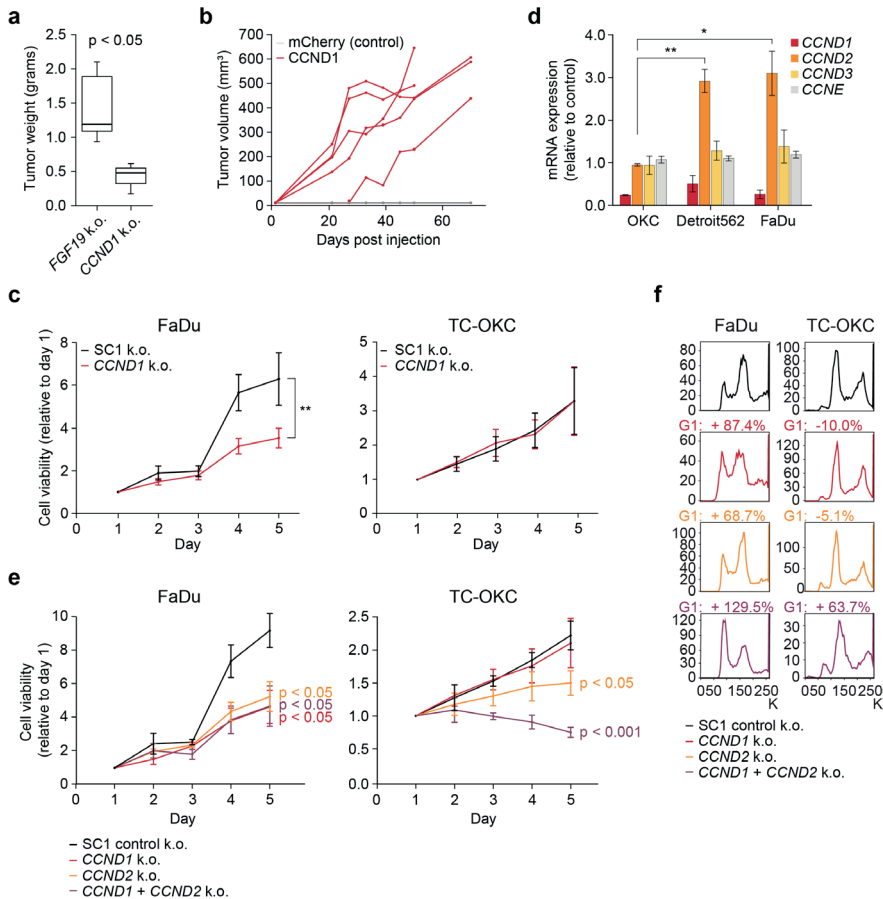


Figure 1 | 11q13-mediated amplification of *CCND1* induces *CCND1* dependency

- a Weight of tumors grown in NSG mice injected with 1E6 FaDu cells bearing either *FGF19* or *CCND1* k.o. mutations. Tumors were dissected 33 days post injection (*FGF19*: *n* = 5, *CCND1*: *n* = 3).
- b *In vivo* tumor growth in NSG mice injected with 1E6 human TC-OKC cells overexpressing indicated gene (*mCherry*: *n* = 5, *CCND1*: *n* = 5) as measured with a caliper.
- c Relative cell viability values based on Alamar Blue assay upon *CCND1* knockout in primary TC-OKC and FaDu cells.
- d Gene expression values 96 hrs post *CCND1* knockout, relative to control (**p* < 0.05, ***p* < 0.01).
- e Relative cell viability values based on Alamar Blue assay upon knockout of Control SC1, *CCND1*, *CCND2*, or *CCND1+CCND2* in FaDu cells (left) and primary TC-OKC (right).
- f Cell cycle profile through DNA staining with FxCycle Violet Ready Flow upon knockout of Control SC1, *CCND1*, *CCND2*, or *CCND1+CCND2* in FaDu cells (left) and primary TC-OKC (right).

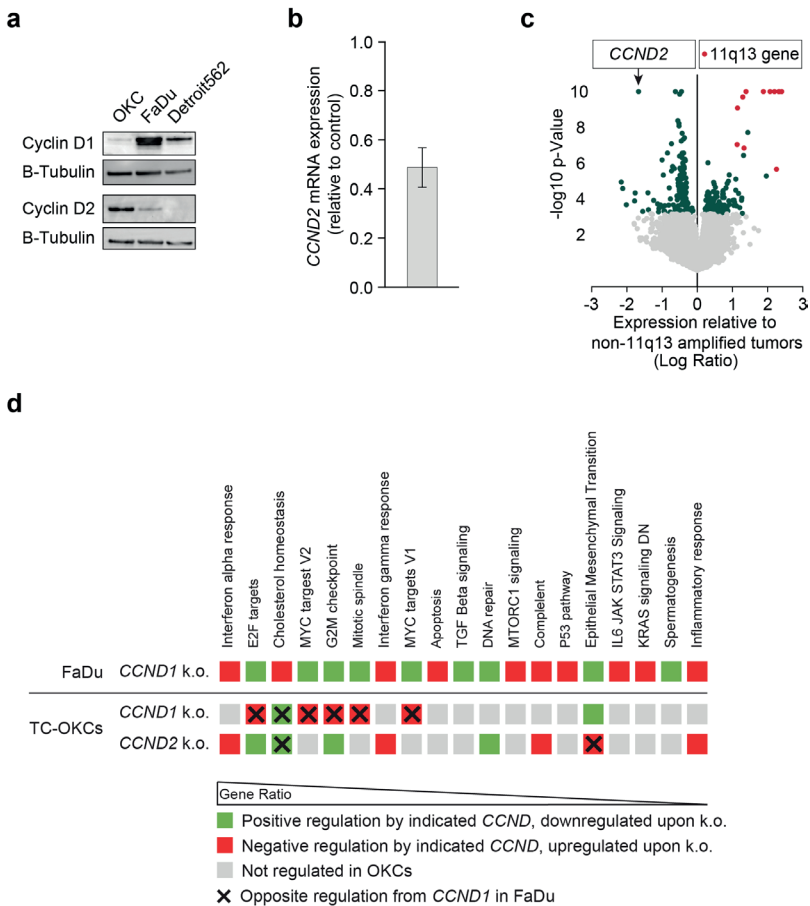


Figure 2 | Amplified *CCND1* takes over *CCND2* function

- a Immunoblot for cyclin D1, cyclin D2 and B-tubulin in OKC, FaDu, and Detroit562 cells
- b *CCND2* expression values in TC-OKC upon lentiviral induced expression of *CCND1*
- c Volcano plot on TCGA expression data of *TP53/CDKN2A* mutated ($n = 139$) vs. *TP53/CDKN2A* mutated + 11q13 amplified tumors ($n = 69$). Red dots indicate genes that are located in the 11q13 region.
- d Pathways regulated by *CCND1* in FaDu cells versus regulation by *CCND1* or *CCND2* in TC-OKC as extracted from GSEA “Hallmark gene sets” analysis on RNAseq data upon respective gene/cell knockout combinations.

Having established *CCND1* as a driver of SSC growth (see also Chapter 3), we next investigated the mechanism through which *CCND1* promotes proliferation in cancer in an amplified setting and how this relates to its normal function in non-malignant cells. To compare the effect of *CCND1* on proliferation between non-cancerous and cancerous cells, we generated *CCND1* knockout TC-OKCs through electroporation of CRISPR-RNPs and compared growth profiles to a “SC1” negative control that targets

the 11q13 region in a non-coding/non-regulating region. In contrast to the necessity of *CCND1* in SCC cells, knockout of *CCND1* in TC-OKCs had no effect on cell proliferation (Fig 1c, Fig S1b). We identified that loss of *CCND1* expression in SCC lines results in a strong upregulation of *CCND2* expression (Fig 1d, Fig S1c), implying the activation of a compensatory mechanism. In contrast, TC-OKCs did not upregulate any members of the cyclin family upon loss of *CCND1*. CRISPRi-mediated knockdown of *CCND1* in the SCC lines recapitulated the *CCND2* compensation, establishing that this effect is intrinsic to the 11q13 amplified lines and not an artifact of CRISPR-mediated gene cutting (Fig S1d). Thus, these data suggest that 11q13 amplification induces *CCND1* oncogene dependence as only *CCND1*-amplified lines exhibit a dependence on *CCND1* for cell proliferation and increased *CCND2* levels fail to rescue the growth defect.

To gain understanding of the effect of the increased *CCND2* levels upon *CCND1* knockout, we next investigated whether *CCND2* is necessary in the 11q13-amplified setting. Knockout of *CCND1* and *CCND2* - either individually or in combination - in both 11q13-amplified lines resulted in significantly slowed cell proliferation with accompanying G1/S cell cycle arrest (Fig 1e, Fig S1e, Fig 1f, Fig S1f). In contrast, TC-OKCs exhibited a modest proliferation defect with no cell cycle arrest upon *CCND2* knockout and only display a robust proliferation defect upon dual *CCND1/2* knockout. Because 11q13-amplified cell lines require both *CCND1* and *CCND2* for proliferation, and knockout of both *CCND1* and *CCND2* results in additive G1/S cell cycle arrest, *CCND1* and *CCND2* therefore may be acting through distinct pathways in the 11q13-amplified setting. The difference in cyclin D dependence between our non-cancerous and cancerous cell models thus suggest that amplification of 11q13 in SCC induces *CCND1*-dependent oncogene addiction.

Amplified *CCND1* takes over *CCND2* function

To gain further understanding of the interaction between *CCND1* and *CCND2* in OKCs and how this interaction changes upon *CCND1* amplification, we first sought to determine the relative expression levels of both cyclin D1 and cyclin D2 in primary and cancer cells. Analysis of basal cyclin D1 and cyclin D2 levels in TC-OKCs and 11q13-amplified SSC lines revealed cyclin D2 as the primary expressed cyclin D in OKCs, in contrast to the high cyclin D1 levels in FaDu and Detroit562 (Fig 2a). Both FaDu and Detroit562 cells express very low levels of cyclin D2 relative to cyclin D1, thereby leading us to investigate whether there is a negative correlation between *CCND1* and *CCND2* levels in these cells. Whereas perturbation of *CCND1* levels leads to increased levels of *CCND2* in cells with high *CCND1* (Fig 1d, Fig S1c, Fig S1d), increased expression of *CCND1* in TC-OKCs suppresses *CCND2* levels (Fig 2b). Furthermore, analysis of publicly available RNA-seq data of HNSCC tumors (139 without *CCND1* amplification, 69 with *CCND1* amplification, all *TP53* and *CDKN2A* mutant) revealed that tumors with *CCND1* amplification have much lower expression of *CCND2* compared to non-amplified tumors (Fig 2c)⁹². Thus, these data suggest that at high level, *CCND1* suppresses *CCND2* expression.

To better understand the change in function of cyclin D1 upon 11q13-driven amplification, we compared transcriptional signatures of *CCND1* knockout in FaDu cells with signatures of either *CCND1* or *CCND2* knockout in TC-OKCs. As expected, we find that in FaDu cells, cyclin D1 positively regulates several cell cycle-adjacent processes, and inhibits inflammatory responses. This is in contrast to its function in TC-OKCs, where cyclin D1 has an opposite effect on the cell cycle processes and no effect on inflammatory responses. However, the transcriptional signature of cyclin D2 in TC-OKCs is more similar to that of cyclin D1 in FaDu cells, with positive effects on several of the cell cycle gene sets, and inhibition of the inflammatory responses. Thus, in TC-OKCs cyclin D1 might have a negative effect on cell cycle progression, whereas cyclin D2 has a positive effect. However, upon *CCND1* amplification in cancer cells cyclin D1 levels go up, suppressing cyclin D2 levels, and instead positively regulate cell cycle processes to progress tumorigenic growth.

Amplified *CCND1* functions through CDK-independent functions

The acquired dependence on cyclin D1 that we observed in the cancer cells compared to the non-cancerous cells suggests that *CCND1* amplification rewires cyclin-dependent proliferation pathways, thereby leading *CCND1* to have a distinct role in amplified SCC cells compared to non-amplified OKCs. Because *CCND1* amplified cancer cells depend on high levels of cyclin D1 (Fig 1c), we hypothesized that they would be sensitive to treatment with the CDK4/6 inhibitor palbociclib. As palbociclib inhibits both cyclin D1 and D2 function via targeting CDK4/6, we observed a proliferation defect upon palbociclib treatment in TC-OKCs (Fig 3a). In contrast, neither 11q13-amplified SSC cell line showed sensitivity to palbociclib despite their sensitivity to combined *CCND1/2* knockout. This disconnect between the CDK4/6-i and *CCND1/2* knockout phenotypes suggest that the cyclin D dependency in these cells may be independent of CDK4/6 activity. To validate this hypothesis, we expressed the *CCND1* mutant *CCND1*^{K112E}, which is unable to bind to CDK4/6 in TC-OKCs³¹⁵. Overexpression of *CCND1*^{K112E} still showed a competitive proliferation benefit in TC-OKCs, consistent with a CDK4/6 independent activity of *CCND1* amplification (Fig 3b).

If cyclin D1 solely functions through interaction with CDK4/6 and subsequent inhibition of RB1, the proliferation inhibitory effect of *CCND1* knockout in 11q13 amplified cells should be rescued by loss of RB function. Therefore, we generated RB1/*RBL1*/*RBL2* triple knockout FaDu and Detroit562 lines and assessed whether *CCND1* deletion would cause inhibition of proliferation (Fig S2a). However, *CCND1* knockout on this background still abrogated proliferation in these cells (Fig 3c, Fig S2b). Moreover, immunoblot analysis of pRB levels shows no change in RB1 phosphorylation upon *CCND1* knockout in these cells (Fig 3d). These findings are consistent with the interpretation that elevated levels of *CCND1* in the 11q13-amplified setting rewire its function to become independent of the CDK4/6-RB1 axis.

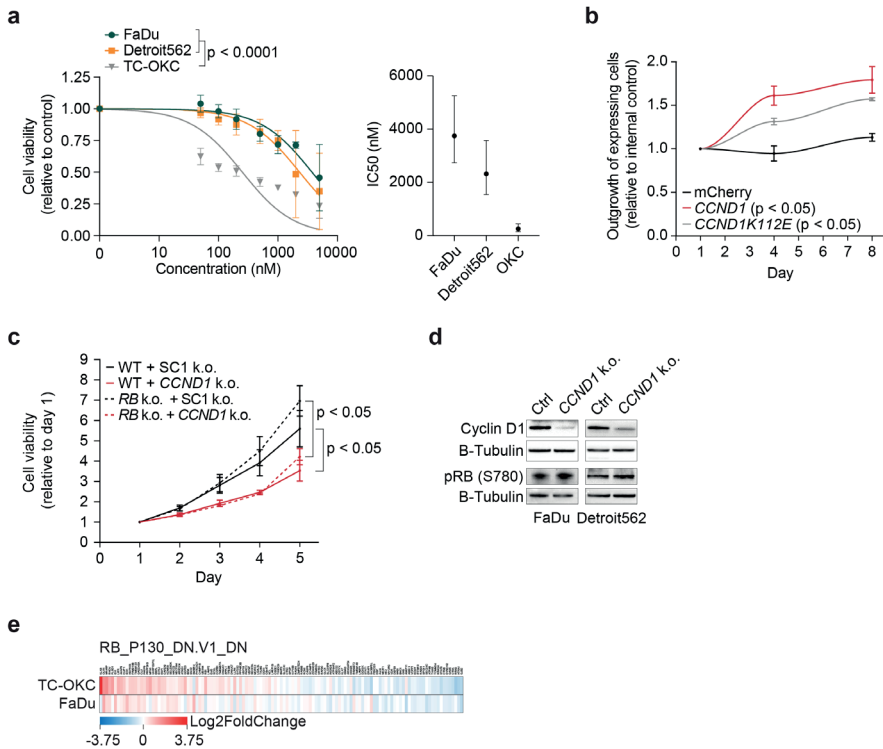


Figure 3 | Amplified *CCND1* functions through CDK-independent functions

- Dose-response curve fitted to a non-linear regression model in TC-OKC, FaDu, and Detroit562 depicting the effect of Palbociclib treatment for 72 hrs (0.5-5 μ M). P value calculated with extra sum of square F-test.
- Outgrowth of *CCND1*-mCherry or *CCND1*^{K112E}-mCherry overexpressing TC-OKC versus EBFP overexpressing TC-OKC.
- Relative cell viability values based on Alamar Blue assay upon *CCND1* knockout in *RB1/RBL1/RBL2* knockout FaDu cells.
- Immunoblot for phosphoRB upon *CCND1* knockout in FaDu and Detroit562 cells.
- RNA-seq expression data on the RB_P130 gene set upon *CCND1* knockout in TC-OKC and FaDu cells.

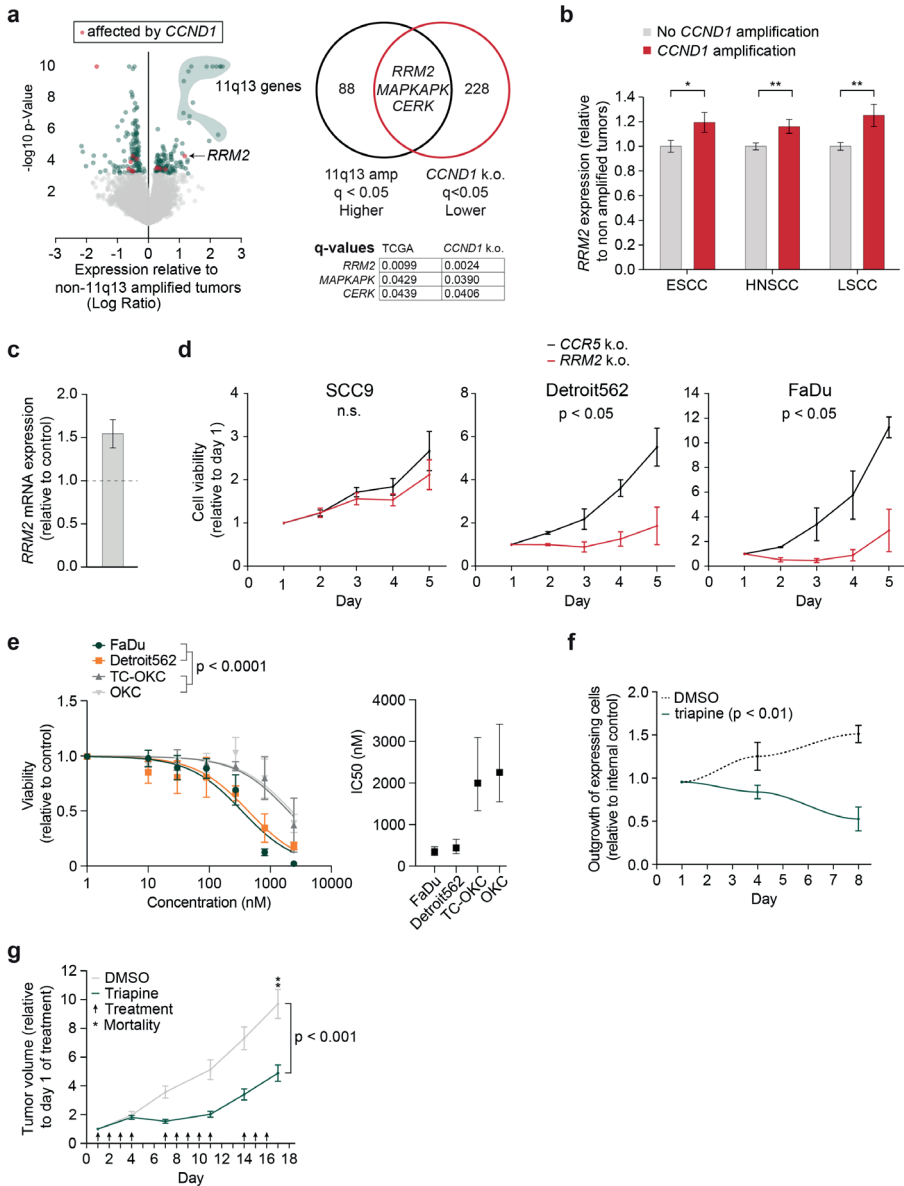


Figure 4 | *RRM2* is a potential target in 11q13-amplified SCC

a Left: Volcano plot of TCGA expression data of *TP53/CDKN2A* mutated ($n = 139$) vs. *TP53/CDKN2A* mutated + 11q13 amplified tumors ($n = 69$). Red dots indicate genes that are also affected upon *CCND1* knockout in FaDu cells. Right: Venn diagram depicting overlapping differentially expressed genes between TCGA 11q13 amplified genes and *CCND1* knockout RNAseq and their q-values.

b *RRM2* gene expression levels in SCC tumors with *CCND1* amplification relative to tumors without *CCND1* amplification (TCGA, ESCC: $n = 184$, HNSCC (HPV negative): $n = 412$, LSCC: $n = 550$). * $p < 0.05$, ** $p < 0.01$.

c *RRM2* expression values in TC-OKC 96 hrs post transduction with *CCND1* overexpression lentivirus, relative to control.

- d Relative cell viability values based on Alamar Blue assay upon *RRM2* knockout in SCC9, Detroit562, and FaDu cells.
- e Left: Dose-response curve fitted to non-linear regression model in OKC, TC-OKC, FaDu, and Detroit562 cells depicting the effect of triapine treatment for 72 hrs (1-7.3 μ M). P value calculated with extra sum of square F-test. Right: IC50 concentration range of the 4 cell types.
- f Outgrowth of *CCND1* overexpressing TC-OKC versus EBFP overexpressing TC-OKC in the presence or absence of 500 nM triapine, p-value calculated by one-sample t-test.
- g Tumor growth relative to 1st day of treatment of either triapine (10 mg/kilo, $n=9$) or control (2% DMSO, $n=7$) treated FaDu tumor xenograft bearing NSG mice.

Lastly, we used RNA sequencing to compare the transcriptomes of TC-OKCs with *CCND1* knockout versus 11q13-amplified FaDu cells with *CCND1* knockout. Gene set enrichment analysis (GSEA) revealed that, although loss of *CCND1* in TC-OKCs significantly affects RB-related genes, these gene-sets are not affected in the FaDu cells (Fig 3e, Fig S2c, Fig S2d). Thus, in *CCND1*-amplified SCC cells, *CCND1* amplification of 11q13 in SCC induces *CCND1*-dependent oncogene addiction and rewires *CCND1* to act primarily through a CDK-independent pathway that is distinct from its role in non-cancerous OKCs.

RRM2 is a potential target in 11q13-amplified SCC

To identify downstream mechanisms through which *CCND1* drives tumorigenesis in 11q13-amplified SCC, we compared RNA-seq data generated from *CCND1* knockout FaDu cells with expression data of 208 HNSCC tumors⁹² (139 without amplification, 69 with amplification, all *TP53* and *CDKN2A* mutant). This comparative analysis identified *RRM2* as a gene whose expression is significantly affected by *CCND1* amplification/expression status in both data sets (Fig 4a). The ribonucleotide-diphosphate reductase subunit M2 (*RRM2*) is the rate-limiting subunit of the ribonucleotide reductase (RNR) enzyme that catalyzes the generation of deoxyribonucleotides. *RRM2* has previously been shown to be a potential target for treatment of several cancers³¹⁶⁻³¹⁹. Analysis of *RRM2* expression in 1146 SCC tumors shows a significantly higher expression of *RRM2* in *CCND1* amplified tumors amongst all 3 analyzed SCC types (Fig 4b). Furthermore, *RRM2* levels are significantly increased in 11q13-amplified HNSCC cell lines compared to non-amplified OKCs (Fig S3a). Lentiviral expression of *CCND1* in TC-OKCs was sufficient to increase *RRM2* expression to similar levels as found in the amplified cell lines, confirming *RRM2* as a downstream target of *CCND1* (Fig 4c). To assess the role of *RRM2* in tumor-proliferation, we knocked out *RRM2* in SCC9, Detroit562, and FaDu cells using CRISPR-Cas9 gene editing. Whereas *RRM2* knockout in SCC9 cells - which have normal *CCND1* levels - does not affect cell viability, *RRM2* knockout in Detroit562 and FaDu cells significantly abrogated cell viability when compared to a control edited at the *CCR5* locus (Fig 4d). Thus, the effect of *CCND1* on SCC growth is likely at least in part mediated through its upregulation of *RRM2*.

To assess the potential of therapeutically targeting RRM2 in 11q13-amplified HNSCC, we measured the effect of triapine on proliferation of OKCs, TC-OKCs, FaDu, and Detroit562 cells. Triapine is a potent inhibitor of the RRM2 subunit of the ribonucleotide reductase (RNR) enzyme and is currently being explored as a cancer treatment option in several phase I, II, and III clinical trials³²⁰⁻³²². Whereas both OKCs and TC-OKCs show moderate sensitivity to triapine only at high doses, both 11q13-amplified SCC lines are significantly more sensitive to treatment, with average IC50 values 5 to 7 times lower compared to the non-amplified OKCs (Fig 4e). To validate that targeting RRM2 inhibits proliferation in a *CCND1*-dependent manner, we analyzed the competitive proliferation benefit of *CCND1* overexpression in the absence or presence of triapine. Triapine treatment decreases proliferation of *CCND1* overexpressing TC-OKCs, but not control TC-OKCs (Fig 4f). These data support our hypothesis that the pro-tumorigenic effects of *CCND1* in *CCND1*-amplified cells are dependent on RRM2. To validate these findings *in vivo*, we treated FaDu-xenograft tumor bearing mice with either triapine or control vehicle (2% DMSO). Triapine administration significantly slowed down tumor growth (Fig 4g, Fig S3b, Fig S3c). Whereas in the control group at day 17 2/7 mice died and 4/5 remaining mice reached ethical endpoint due to tumor burden, none of the mice out of the triapine group reached endpoint. Treatment was well tolerated and did not affect weight of the mice (Fig S3d). Thus, inhibition of the *CCND1*-*RRM2* axis using triapine or other RNR inhibitors may be a viable strategy for targeting 11q13-amplified tumors.

Discussion

Amplification of *CCND1* through 11q13 is a frequent event in HNSCCs, and it is believed that this activation of cyclin D1 activity is a driving event in tumorigenesis^{92,95,292}. Due to this frequent dysregulation, targeting the cyclin D1 pathway is an attractive option for the treatment of SCCs. To validate that cyclin D1 can be a therapeutic target, it must be known whether constant high expression is also essential for tumor maintenance or progression. Understanding the way cyclins contribute mechanistically to tumorigenesis will provide further insights into possible treatment directions. In this study, we show that *CCND1*-amplified tumors are dependent on cyclin D1, and that this dependence is restricted to cancer cells. Mechanistically, we show that this dependence is independent of the CDK4/6-RB1 pathways, and that amplification of *CCND1* seems to rewire the cyclin D1 regulatory network, suppressing *CCND2* expression and inducing expression of *RRM2*, which might serve as an alternative target for *CCND1* amplified tumors.

We show that *CCND1* amplified cancer cells exhibit *CCND1* oncogene addiction similar to what has been described in other *CCND1*-dependent tumors (Fig 1)²⁶⁰⁻²⁶². Although *CCND1* is generally regarded as an essential gene, our data reveal that this dependence on high cyclin D1 levels is exclusive to the *CCND1* amplified cancer cells

and that primary OKCs are not affected in their growth performance upon *CCND1* knockout. These findings are supported by a previous study that reports that cyclin D1 is essential for tumor growth in mouse models of ErbB2-driven mammary carcinoma, but largely dispensable for normal cell function¹⁸⁶. Another study showed that loss of *USP2*, which stabilizes cyclin D1 levels, only affects cancer cells with high cyclin D1 levels, but not cancer cells with low cyclin D1 or primary cells²⁶¹. Thus, cyclin D1 appears essential to cyclin D1-high tumor cells, but not universally required.

We identify key differences between the function of *CCND1* in the 11q13-amplified context versus non-amplified settings, supporting the hypothesis that *CCND1* signaling is rewired depending on its level of amplification, expression, or both (Fig 1, Fig 2). Whereas in primary OKCs *CCND1* is only expressed at low levels but might have a suppressive effect on cell cycle progression, in *CCND1*-amplified cancer cells it stimulates cell cycle progression and inhibits inflammatory responses. This fits with the general regarded function of cyclin D1 in cancer cell proliferation and a recent GSEA on TCGA databases that found a general correlation between *CCND1* amplification and immunosuppressive hallmarks²⁴⁸.

However, in these analyses it was found that specifically in HNSCCs the non-amplified tumors showed increased interferon- α and - β signaling, where our GSEA on FaDu cells show a role for *CCND1* in the negative regulation of the interferon response. Previous studies in HaCat cells (immortalized keratinocytes from adult human skin), showed that overexpression of *CCND1* only marginally increases proliferation of these cells, but significantly affects epidermal homeostasis, inducing tissue destruction through an inflammatory response³²³⁻³²⁵. This contrasting result might be explained by the different state of the cells - “immortalized normal” vs “cancer” - which would suggest that the function of cyclin D1 is not only determined by the expression levels, but also the state of the cell.

Amplification status of *CCND1* in SCC also affects the role of *CCND2*, as upregulation of cyclin D1 suppresses cyclin D2 levels (Fig 1, Fig 2). In primary cells, cyclin D2 seems to be the predominant cyclin to stimulate proliferation, a role that may get taken over by cyclin D1 in amplified cancer cells. It could be speculated that cyclin D1 has additional functions besides cell cycle regulation, and this cyclin D2 downregulation prevents cyclin D1 from having to compete with cyclin D2. There are several cancer types in which the *CCND2* promoter is frequently methylated, and loss of *CCND2* expression has also been shown in pancreatic, breast, and prostate cancer³²⁶⁻³²⁸. Further research on the interplay between *CCND1* and *CCND2* could establish potential feedback loops and compensatory mechanisms.

We show that *CCND1* amplified HNSCC tumors are dependent on *CCND1* for proliferation, and that the upregulation of *CCND2* which occurs upon loss of *CCND1* expression is insufficient to compensate (Fig 1). Cancer types display

high heterogeneity in their dependence on cyclins across cancer models and a previous study that showed that ErbB2-driven mammary carcinomas lose *CCND1* dependency after 2 rounds of passaging upon loss of *CCND1*, as they upregulate *CCND3*^{329,330}. In these tumors, the authors note a benefit of combined *CCND1* and *CCND3* inhibition. In our results however, we see that combinatorial loss of *CCND1* and *CCND2* has no additive effect on the cancer cells, but does affect TC-OKCs, making dual cyclin inhibition a less favorable treatment strategy compared to *CCND1* inhibition alone.

Palbociclib is the first FDA approved drug to inhibit CDK4/6 and this drug has been used to inhibit cyclin D1 activity in cancer³³¹. However, we observed that despite being sensitive to *CCND1/CCND2* knockout, *CCND1* amplified cancer cells are less sensitive to treatment with palbociclib than TC-OKC (Fig 3). Since palbociclib targets both cyclin D1 and cyclin D2 activity on CDK4/6, the high cyclin D2 levels and dependency explain the sensitivity to this treatment in TC-OKC. However, the cancer cells are not sensitive, despite their high *CCND1* levels, indicating a CDK-independent effect of cyclin D1 in the amplified cancer cells. It could be hypothesized that the significantly higher cyclin D1 levels lead to saturation of partner CDKs by Cyclin D1, leaving free cyclin D1 to activate its CDK-independent pathways, explaining this rewiring. Furthermore, analysis of a large panel of tumors showed that there was no correlation between *CCND1* expression and an E2F response signature, raising the question if this proliferation pathway is really the driving factor for *CCND1* oncogene addiction²⁸⁵.

In HNSCCs, *CCND1* amplification occurs in a background of *CDKN2A* mutations or deletions and the combination of these *CCND1* and *CDKN2A* events gives a worse prognosis than the events by themselves⁸⁹. Co-occurrence of these 2 events can be explained by (1) cooperation to activate the cyclin D1-RB-E2F pathway further or (2) extra selective pressure as each component also contributes to other oncogenic processes/pathways beyond this pathway. Our results point towards the latter explanation, driven by activation of CDK-independent mechanisms. Furthermore, different cancers can have specific alterations in the cyclin D1-RB-E2F pathway. For example, small cell lung carcinomas often display RB inactivation, whereas non-small cell lung carcinomas more frequently show inactivation of *CDKN2A*. This suggests that these different ways of altering the pathways have different selective tumorigenic pressures. A lot of the initial work in cyclin D1 function and CDK4/6-inhibitor responsiveness has been done in breast cancer. Here, *CCND1* amplification does not occur in combination with *CDKN2A* mutations/deletions³³². Since the genetic contexts of *CCND1* amplification between BC and HNSCCs are different, we should thus be careful with translating mechanisms and therapeutic opportunities between these cancer types.

The differences in cyclin D1 signaling identified in this study may have a direct impact on how we target the cyclin D1 signaling axis for targeted cancer therapy, as *CCND1*-

amplified SCC lines are significantly more resistant to CDK4/6 inhibition relative to non-amplified cells. Indeed, clinical trials of CDK4/6 inhibitors in SCC have proceeded with limited success³¹²⁻³¹⁴. An alternative approach would be the direct targeting or degrading of cyclin D1, as currently is being explored^{291,333}. Since cyclin D1 itself has no enzymatic activity, it is a challenging target to inhibit. Therefore, some of the current concepts to target cyclin D1 are based on enhancing its degradation. Experimental proof for this idea comes from findings that show that for example targeting the cyclin D1-specific de-ubiquitinase USP2 accelerates cyclin D1 protein turnover and decreases its stability specifically in cyclin D1-high cancer cells²⁶¹. Another example is the discovery that proteins that can degrade cyclin D1, such as myostatin or ER- β , induce a growth arrest upon expression^{334,335}. In recent years, the proteolysis targeting chimeras (PROTAC) have been explored to selectively target and degrade oncogenic proteins, including cyclin D1^{336,337}. Testing the effect of direct cyclin D1 targeting on *CCND1* amplified tumors would be an exciting next step.

Lastly, we identified that in HNSCCs, cyclin D1 induces expression of *RRM2* and that inhibition of *RRM2* inhibits HNSCC growth (Fig 4). Notably, the *RRM2*-mediated growth effect of *CCND1* amplification appears to be unique to the *CCND1*-amplified context. As subunit of the RNR complex - *RRM2* - is essential for DNA synthesis and repair. Whereas the *RRM1* subunit is constantly and excessively expressed, *RRM2* expression is cyclic and thus the critical regulator of RNR activity, balancing the production between dNTP production and DNA synthesis^{338,339}. Indeed, *RRM2* expression gets induced in the G1/S transition in a E2F-dependent manner, which is in line with our findings that *CCND1* induces *RRM2* expression^{338,340}. However, whereas we show that upon amplification in HNSCC cyclin D1 might largely function in a CDK-independent function, another study found that treatment of HNSCC lines with palbociclib decreases *RRM2* levels, suggesting that this is a CDK-dependent effect³⁴¹.

RRM2 has a fundamental function and is amongst the most strictly regulated enzymes. This can explain why even though the fold difference in *RRM2* expression between *CCND1* amplified versus non-amplified tumors is not that high, we see a big difference in dependency of these tumors. High *RRM2* levels have been associated with and correlate to poor prognosis of several cancer types, including HNSCCs^{316,319,342-349}. High levels of *RRM2* in cancer not only can increase cell proliferation, but also increase mutational burden through high dNTP levels and thus high misincorporation during DNA synthesis^{339,350}. Experiments in mice show evidence that inhibition of *RRM2* can halt cancer growth, similar to our results. However, several other studies show that inhibition of *RRM2* in the treatment of cancer is particularly effective in combination with chemotherapy or PARP inhibitors^{317,318,349,350}. This combination regimen seems to be effective since *RRM2* protects against DNA damage induced apoptosis. Indeed, *RRM2* is often found upregulated in chemo resistant cancer cells³⁵¹.

In recent years, clinical studies have aimed to test the effect of triapine on several tumor types. Triapine is clinically well tolerated, but its efficacy remains unclear³⁵²⁻³⁵⁴. Triapine seems to be mostly effective in combination with radiation or cisplatin treatment, as clinical trials testing these combinations report good response rates in patients with several cancer types³⁵⁵⁻³⁵⁸. The combination of triapine plus another RNR inhibitor has also showed promising results in some clinical trials^{359,360}, but yielded no or low success in others³⁶¹⁻³⁶³. For HNSCC particularly, one phase I clinical trial that included 5 patients with progressing HNSCC showed that 1 patient responded particularly well with stable disease for over 10 months upon treatment with triapine as a solo agent³⁵². However, a phase II clinical trial showed a low response rate with only one patient having a partial response³⁶⁴. For future studies it would be worthwhile to determine if *CCND1* amplification or *RRM2* expression are correlated to clinical responses.

Gemcitabine is an FDA-approved chemotherapy for several cancer types which targets the RNR complex through RRMI inhibition. Similarly to triapine, gemcitabine is a sensitizer for chemoradiation. Although gemcitabine is not a standard treatment option for HNSCC, several studies - including phase III clinical trials - have showed that the addition of gemcitabine to cisplatin treatment significantly improves survival³⁶⁵⁻³⁶⁷. Furthermore, a phase II clinical trial showed improved survival upon gemcitabine treatment of a heavily pre-treated group of HNSCCs³⁶⁸. Thus, considering the high success rate of gemcitabine treatments, it would be interesting to determine whether patients with *CCND1* amplification would particularly benefit from gemcitabine, either as a single agent or in combination with cisplatin.

Overall, here we show the rewiring of cyclin D1 function upon *CCND1*-amplification in HNSCCs. This rewiring may open up additional avenues for targeting the *CCND1* signaling axis in SSC that have not been explored previously. Two examples of this are direct targeting of *CCND1* and inhibition of the downstream *RRM2* pathway, as described above. We find that these two strategies for inhibiting the *CCND1* axis in 11q13-amplified SCC are significantly more effective to elicit an anti-tumor growth effect compared to a standard CDK4/6 inhibition strategy while avoiding significant toxicity in normal keratinocytes. Therefore, these and other CDK4/6 independent targeting strategies should be investigated further.

Material and Methods

Cell culture

FaDu (ATCC cat#HTB-43, male) and Detroit562 (ATCC cat#CCL-138, female) cells were grown in Eagle's Minimal Essential Medium with L-glutamine (Fisher Scientific cat#50983283) supplemented with 10% FBS (Corning cat#MT35010CV) and 1% Penicillin/Streptomycin (P/S, Corning cat#MT30002CI). A-253 (ATCC cat#HTB-41,

male) cells were grown in McCoy's 5A (Modified) Medium (Fisher Scientific cat#16-600-082) supplemented with 5% FBS and 1% P/S. SCC-9 (ATCC cat#CRL-1629, male) cells were cultured in Dulbecco's Modified Eagle medium (DMEM):F12 (Gibco cat#11039021) supplemented with 400 ng/mL hydrocortisone (EMD Millipore cat#386698), 10% FBS, and 1% P/S. HEK293T (ATCC cat#CRL-3216, female) cells were grown in DMEM (Gibco cat#12491023) supplemented with 5% FBS and 1% P/S. All cell lines were purchased and authenticated at ATCC in 2016 and tested yearly for mycoplasma through PCR. Human primary keratinocytes were collected and isolated from patient derived mucosal samples and cultured in Medium 154 and Keratinocyte Serum Free Medium (1:1, Life Technologies cat#M154500 and cat#17005042), supplemented with 5 mL/L Human Keratinocyte Growth Supplement (Life Technologies cat#S0015), 25 mg/L Bovine Pituitary Extract (Life Technologies cat#17005042), 2.5 µg/L EGF Human Recombinant (Life Technologies cat#17005042), and 1% P/S. No cells were passaged for longer than 5 weeks.

CRISPR interference constructs and cloning

Stable dCas9 cells were generated by transducing cells with pHR-SFFV-dCas9-BFP-KRAB (Addgene cat#46911) lentivirus as previously described³⁶⁹. Stable dCas9 cells were transduced with pU6-sgRNA EF1Alpha-puro-T2A-BFP (Addgene cat#60955) lentivirus to introduce guideRNAs (table 1). *OR2B6*-targeting guideRNAs were used as negative control.

Table 1 | CRISPR interference gRNA sequences

Target gene	Protospacer sequence
CCND1	GGTCCGCACGCTCCGGCGAG
CCND2	GGTGGGCGAGCAGAGCCTCG
OR2B6	GGGAGTGAAACTCCAGCCA

Genome engineering

To generate gene knockouts, cells were transfected via electroporation using the MaxCyte ATX electroporation platform with Clustered Regularly Interspaced Short Palindromic Repeat (CRISPR) Cas9- ribonucleoproteins (RNPs) and gene-specific guideRNAs (table 2). For electroporation, sub-confluent cells were trypsinized and washed 1x in DMEM and 1x in Opti-MEM (Life Technologies cat#31985070). Cells were resuspended to a concentration of 2.5E7 cells/mL in Opti-MEM. crRNAs and Alt-R CRISPR-Cas9 tracrRNA (Integrated DNA Technologies) were hybridized in a 1:1 ratio to a final concentration of 50 µM. crRNA:tracrRNA were complexed with Cas9-RNP at a 1:1:1 ratio for 20 minutes at room temperature and subsequently mixed with the cells to a final concentrations of 2.5 µM crRNA:Cas9 and 2.0E7 cells/mL. Cells were

electroporated in 25 μ l or 400 μ l reactions with the ‘Optimization 7’ (keratinocytes, Detroit562, and SCC-9) or ‘DL-D-1’ (FaDu) electroporation protocols. After electroporation, cells were immediately collected from the processing assembly, plated into a 6 well plate and recovered 20 minutes at 37°C, before resuspending in 2 mL culture medium. Transfection efficiency was determined 24 hrs post electroporation through flow cytometry. After 96 hours, gene disruption was confirmed through TIDE (Tracking of Indels by Decomposition) analysis (primers: **table 2**). To control for multiple edits in the amplified 11q13 region, a negative control “Safe Control” SC1 crRNA was designed to target the 11q13 region in a non-coding and non-regulating region.

Table 2 | CRISPR crRNA sequences and primers for TIDE analysis

Target gene	crRNA sequence	Forward primer	Reversed primer
CCND1	CATTTGAAGTAGGACACCGA	CACACGGACTACAGGGGAGT	ACCCCTTCCTCCTTCAGAAA
CCND2	CTCGTGGCACAGCAGCTCCA	GGGAGAGCGAGACCAGTTTT	GACCTACCTCCAGCATCCAG
CCR5	AACACCAGTGAGTAGAGCGG	TGCTTGGCCAAAAGAGAGT	CGATTGTGAGGAGGATGATG
CDKN2A	TAACTATTCGGTGCCTGGG	GACTCCCTTTTTATCCCAAACG	CCAGTCTCCTCTCCTGGCCAAC
RB1	AGCATTATCAACTTTGGTAC	TCTTCTTGACCCTTCGTTTTC	CCATTGCAAGTGTTTTCTCG
RBL1	GACGACTTTACTGCCATCCG	CAGACGGTGGATGACAACAC	TGAGCTACACCCACCTTTCC
RBL2	GGCGACTGGTCACCTCCCGA	AGCGTGTAGCTTTCGCTCAT	TCGTGAGTACAGCCCTGTTG
RRM2	GACACAAGGCATCGTTTCAA	ACATTTCCGGTGTGAGTTCTCC	GAAAATGTGAGGCCAGGCAT
SC1	TTGGTCCCACGATGACCCAC	GATCGAGGTCCACTCTGAGC	GGTGTGTGTACTGGGGGAAC
TP53	CCATTGTTCAATATCGTCCG	ACTGACCGTGCAAGTCACAG	CCCCTCTGAGTCAGGAAACA

Exogenous 11q13 gene constructs and cloning

To clone overexpression constructs, RNA was purified from oral keratinocytes (OKCs) and total cDNA was synthesized with poly-A specific primers using SuperScript III First-Strand Synthesis System (Invitrogen cat#18080051) according to the manufacturer’s instructions. To create Gateway compatible PCR products of the gene of interest, coupled to an mCherry tag through a T2A sequence, primers were designed with AttB and T2A adapters (**table 3**). PCRs were performed to create AttB-gene-T2A and T2A-mCherry-AttB products from whole genome cDNA (*CCND1*) or the following plasmids as template: *CCND1*^{K112E}; Rc/CMV Cyclin D1 K112E, Addgene cat#8951, EBFP: pU6-sgRNA EF1Alpha-puro-T2A-BFP, Addgene cat#60955; mCherry: pHR_Gal4UAS_pGKmCherry, Addgene cat#79124). PCR products were purified and coupled in a subsequent PCR. Full *attB* products were cloned into the pDONR221 Vector (ThermoFisher Scientific cat#12536017) using Gateway Technology according to the manufacturer’s instruction. Coding sequences were transferred into the pLEX_307 vector (Addgene cat#41392). As negative control, pLEX_307-EBFP was generated.

Lentiviral production and infection

HEK293T cells were transfected with 750 ng transfer plasmid, 375 ng psPAX2 (Addgene cat#12259), 750 ng pMD2.G (Addgene cat#12260), and 5.5 μ l Lipofectamin 2000 Transfection reagent (Life Technologies cat#11668027) per mL culture medium. Medium was replaced 16 hours post transfection and viral supernatant was collected 72 hours later, filtered through a 0.45 μ m PVDF filter (MilliporeSigma cat#SLHVM33RS), concentrated using LentiX concentrator (Takara Bio cat#631231) and stored at -80°C . Cells were transduced with viral pellets resuspended in appropriate medium with 8 μ g/ml Polybrene Transfection reagent (EMD Millipore cat#TR1003G) for 16 hours.

Table 3 | Lentiviral overexpression cloning primers

Gene for fusion cloning pLEX_307		
Target gene		AttB insert forward primer / T2A insert reversed primer
CCND1	AttB Forward	GGGGACAAGTTTGTACAAAAAAGCAGGCTTAATGGAACACCAGCTCCTGTG
	T2A Reversed	CACGTCACCGCATGTTAGCAGACTTCTCTGCCCTCTCCGCTTCCGATGTCACGTCCCGCAC
CCND1K112E	AttB Forward	GGGGACAAGTTTGTACAAAAAAGCAGGCTTAATGGAACACCAGCTCCTGTG
	T2A Reversed	CACGTCACCGCATGTTAGCAGACTTCTCTGCCCTCTCCGCTTCCGATGTCACGTCCCGCAC
Label for fusion cloning pLEX_307		
Label		T2A insert forward primer / AttB insert reversed primer
mCherry	T2A Forward	CTAACATGCGGTGACGTGGAGGAGAATCCCGCCCTGCTAGCATGGTGGAGCAAGGGCGAGG
	AttB Reversed	GGGGACCACTTTGTACAAGAAAGCTGGGTTTTACTTGTACAGCTCGTCCATGCC
Label only cloning pLEX_307		
Label		AttB insert forward primer / AttB insert reversed primer
EBFP	AttB Forward	GGGGACAAGTTTGTACAAAAAAGCAGGCTTAATGGTGAGCAAGGGCGAG
	AttB Reversed	GGGGACCACTTTGTACAAGAAAGCTGGGTTTTACTTGTACAGCTCGTCCATGCC
mCherry	AttB Forward	GGGGACAAGTTTGTACAAAAAAGCAGGCTTAATGGTGAGCAAGGGCGAG
	AttB Reversed	GGGGACCACTTTGTACAAGAAAGCTGGGTTTTACTTGTACAGCTCGTCCATGCC

RT-qPCR

For Reversed Transcriptase quantitative PCR (RT-qPCR), RNA was isolated with the RNeasy Plus Mini Kit (Qiagen cat#74136) and converted into cDNA using SuperScript III First-Strand Synthesis SuperMix for qRT-PCR (Thermo Fisher Scientific cat#11752250). PrimeTime qPCR Probe-based assays and Gene Expression Master Mix were purchased from Integrated DNA Technologies with 6-FAM/ZEN/IBFQ labeling (table 4). *ACTB* probes and primers for loading control were designed with JOE NHS/ZEN/3' IBFQ labeling to allow multiplex RT-qPCR. 10 μ L RT-qPCR reactions were prepared containing 500 nM of each primer (gene of interest, *ACTB*:

forward and reversed), 250 nM of each probe, 5 μ L Mastermix, and 10-50 ng cDNA. Reactions were run in triplicates on the Quantstudio 6 (Applied Biosystems). Relative gene expression levels were calculated using the Δ CT method against *ACTB*.

Table 4 | RT-qPCR probes and assays

Target gene	Probe sequence	Forward primer	Reversed primer
ACTB	AGTTTCGTGGATGCCACAGGACTC	CACTCTCCAGCCTTCCTTC	GTACAGGTCTTTGCGGATGT
Target gene	Assay number		
CCND1	Hs.PT.56a.4930170		
CCND2	Hs.PT.58.28257		
CCND3	Hs.PT.56a.3707837		
CCNE1	Hs.PT.56a.27776605		
RRM2	Hs.PT.58.23237138		

Cell growth assays

For viability assays, cells were seeded into Black Greiner Cellstar 96 well plates (Sigma-Aldrich cat#M9936). Starting at 72 hours after plating or drug treatment, cells were incubated with 10% Alamar Blue (Bio-Rad cat#100234-634) according to the manufacturer's instruction. Fluorescence was read out on a GloMax Explorer plate reader (Promega) at an excitation of 520 nm and emission of 580-640 nm. Cell viability was calculated relative to untreated or day 1 condition. For Competition assays, *TP53* and *CDKN2A* knockout OKC (TC-OKC) were transduced with pLEX_307 lentivirus for the gene of interest or EBFP control. 72 hours post transduction, gene and EBFP control overexpressing OKCs were mixed 1:1 and immediately analyzed on a LSR II Flow Cytometer (BD) to determine the ratio of gene-mCherry:EBFP. Cells were kept in culture and analyzed over time to determine the change in ratios. Ratios were normalized to day 1. Experiments were performed with OKC from at least 2 different donors (1 donor per replicate).

Drug treatments

Palbociclib (MedChem Express cat#HY-50767) was diluted in 0.1 M HCL and triapine (3-AP, MedChemExpress cat#501871763) was diluted in dimethylsulfoxide (DMSO). Drugs were added to culture media for 72 hours at indicated concentrations. A three parameter non linear dose response curve was fit against the cellular viability scores.

Immunoblot analysis

Cell pellets were lysed in Pierce RIPA buffer (Thermo Scientific, 62249), supplemented with phosphatase inhibitor and protease inhibitor cocktail sets

(Calbiochem cat#524625 and cat#539134). Protein extracts were resolved on Nu PAGE 4-12% Bis-Tris gradient gels (Invitrogen cat#WG1401A) and transferred to PVDF membranes using the Trans-Blot Turbo system. Membranes were blocked in 5% milk in TBS-T and probed with primary antibodies overnight at 4°C, and then with horseradish peroxidase-conjugated secondary antibodies. Signals were visualized with SuperSignal West Pico PLUS Chemiluminescent Substrate (Thermo scientific cat#PI34577) on the Bio-Rad ChemiDox XRS+ System. The following antibodies were used: Beta-Tubulin (Abcam cat#6046, 1:500), Cyclin D1 (Abcam cat#134175, 1:5000), Cyclin D2 (Cell Signaling cat#3741, 1:800), RB1 (Abcam cat#181616, 1:1000), RB phospho S780 (Abcam cat#184702, 1:800).

Cell cycle analysis

Cells were fixed for 60 minutes in 70% ethanol, washed with DPBS and stained with FxCycle Violet Ready Flow Reagent (Fisher Scientific cat#R37166) for 30 minutes at room temperature. DNA content was analyzed on a LSR II Flow Cytometer (BD).

In vivo experiments

NOD *scid* gamma (NSG) mice were purchased from the Jackson laboratory (cat#005557). All experimental procedures were approved by and in compliance with UCSF IACUC. For experiments with TC-OKC, cells were transduced with pLEX_307 virus to induce expression of target genes. For mice experiments with engineered FaDu cells, *FGF19* knockout or *CCND1* knockout cells were created through CRISPR-RNP electroporation. 6 days post transduction or electroporation, cells were resuspended in a 1:1 ratio of Matrigel and OKC culture medium at a concentration of $1.0E^7$ cells/mL. NSG mice ($n = 45$, mixed male and female) were subcutaneously injected in the hind flank with $1.0E^6$ cells. Tumor growth was monitored weekly until endpoint and tumors were measured using a caliper. Tumors were dissected and origin was confirmed through RT-qPCR on target genes. For the triapine experiment, parental FaDu cells were injected into mice (mixed males and females, between 4 and 7 months old. DMSO control: $n = 7$, triapine: $n = 9$) as described above. Tumor growth was monitored at least twice per week. Once tumors were palpable, mice were randomized and drug administration started. Triapine (10 mg/kilo, dissolved in SBE- β -CD in saline) or 2% DMSO were administered through an intraperitoneal injection for 5 consecutive days per week until tumors reached endpoint.

RNA-seq and GSEA analysis

Cells were transfected as indicated and RNA was collected 6 days after. RNA-sequencing libraries were prepared with the QuantSeq 3' mRNA-Seq Library Prep Kit (Lexogen cat#O15.24) according to the manufacturer's instructions. Library quality was assessed with a High Sensitivity DNA Assay on the Agilent 2100 Bioanalyzer.

Samples were sequenced by the Center of Advanced Technologies (UCSF) on the HiSeq SE50/65 (Illumina). Samples of sufficient quality were analyzed for Differential Expression analysis using the DESeq2 pipeline. Gene Set Enrichment Analysis (GSEA) on the differentially expressed genes was performed using the BiocManager, fgsea, and clusterProfiler packages for R²⁴⁶.

TCGA data analyses

For RNAseq analysis on HNSCC TCGA PanCancer tumors, publicly available expression data was accessed through cBioPortal^{92,178}. Tumors were selected on bearing *TP53* and *CDKN2A* mutations and stratified based on amplification of all *11q13* genes. See **table 5** for tumor selection. Genes were considered significantly altered at $q < 0.05$. For *RRM2* expression analysis in *CCND1* low vs high SCCs, the GCD TCGA HNSC, GDC TCGA ESCA, and GDC TCGA LUSC datasets were accessed through the Xenabrowser^{92,129,238}. *CCND1* high and *CCND1* low tumors were set as tumors with above and below average *CCND1* expression, respectively.

Statistical analysis

All data are represented as mean \pm SEM unless stated otherwise. All experiments were independently reproduced at least 3 times. Statistical significance is indicated as follows: * $p < 0.05$, ** $p < 0.01$, *** $p < 0.001$

Data availability

RNA-sequencing data generated in this study are publicly available at the Gene Expression Omnibus under accession code GSE216849.

Acknowledgements

This work was supported, in part, by the US National Institutes of Health (NIH) grant RO1-DE029890 (A.T.). The authors thank René Bernards, Vicente Planells Palop, and Nancy Joseph for helpful discussions, and Andrea Yeung for technical assistance.

Author Contributions

C.I.M. and A.D.T. conceived of research. C.I.M. designed and executed all in vitro and in vivo studies, performed all data analyses, and wrote the manuscript. A.G.M. contributed to RNAseq data analysis and provided valuable discussion. E.V. assisted with overexpression cloning. A.D.T. supervised the study. All authors edited the manuscript.

Conflict of interest

The authors declare no competing interest.

Table 5 | TCGA tumor selection

TP53 and CDKN2A mut/homdel with no 11q13 amp				
TCGA-H7-8501	TCGA-CN-4740	TCGA-CV-6941	TCGA-F7-A61S	TCGA-CR-7365
TCGA-BB-A5HY	TCGA-CN-5363	TCGA-BA-6873	TCGA-P3-A5QA	TCGA-CR-7397
TCGA-CN-A640	TCGA-CR-7364	TCGA-CV-7243	TCGA-QK-A652	TCGA-CV-A6K2
TCGA-CN-5359	TCGA-CV-A6JY	TCGA-F7-A61V	TCGA-UF-A7J9	TCGA-CV-A463
TCGA-CN-5360	TCGA-CV-6948	TCGA-UF-A7JK	TCGA-UF-A7JO	TCGA-CV-5966
TCGA-CN-6998	TCGA-CV-7434	TCGA-CV-6436	TCGA-BA-5152	TCGA-CV-5970
TCGA-CQ-A4CD	TCGA-CV-7438	TCGA-CV-7099	TCGA-CN-6996	TCGA-CV-6952
TCGA-CQ-6229	TCGA-F7-A61W	TCGA-BA-A4IF	TCGA-CR-7379	TCGA-CV-7089
TCGA-CR-7386	TCGA-F7-A623	TCGA-BA-5558	TCGA-DQ-5629	TCGA-CV-7177
TCGA-CV-6003	TCGA-IQ-A61O	TCGA-C9-A480	TCGA-QK-A64Z	TCGA-CV-7407
TCGA-CV-6959	TCGA-QK-A6VC	TCGA-CN-4723	TCGA-CN-A6V3	TCGA-CV-7430
TCGA-CV-7101	TCGA-QK-A8Z7	TCGA-CN-4736	TCGA-CQ-6220	TCGA-CX-7219
TCGA-CV-7255	TCGA-TN-A7HJ	TCGA-CN-5373	TCGA-CR-7370	TCGA-D6-A6EQ
TCGA-CV-7424	TCGA-UF-A7JF	TCGA-CQ-6224	TCGA-CV-A465	TCGA-D6-6517
TCGA-H7-A6C4	TCGA-UF-A7JH	TCGA-CV-A6JD	TCGA-CV-5976	TCGA-D6-6823
TCGA-HD-A633	TCGA-CN-5370	TCGA-CV-A45P	TCGA-CV-7180	TCGA-D6-8569
TCGA-QK-A6IG	TCGA-CQ-5331	TCGA-CV-A45R	TCGA-QK-A6II	TCGA-F7-A50G
TCGA-RS-A6TO	TCGA-CV-A45Z	TCGA-CV-6943	TCGA-CQ-5330	TCGA-HD-8634
TCGA-CN-4731	TCGA-CV-5432	TCGA-CV-6951	TCGA-BA-A6DE	TCGA-IQ-A6SG
TCGA-CV-5444	TCGA-BB-A6UO	TCGA-CV-6953	TCGA-BA-A6DL	TCGA-P3-A5Q6
TCGA-QK-A8ZB	TCGA-CN-5355	TCGA-CV-6962	TCGA-BA-6870	TCGA-P3-A6T5
TCGA-BA-5557	TCGA-CN-6022	TCGA-CV-7090	TCGA-CN-A49A	TCGA-P3-A6T8
TCGA-CN-4738	TCGA-CV-A6JU	TCGA-CV-7245	TCGA-CN-4729	TCGA-QK-A8Z9
TCGA-D6-A74Q	TCGA-CV-A6K1	TCGA-CV-7248	TCGA-CN-5367	TCGA-QK-AA3J
TCGA-CV-6942	TCGA-CV-A45Q	TCGA-CV-7254	TCGA-CN-6016	TCGA-UF-A7JT
TCGA-IQ-A6SH	TCGA-IQ-A61E	TCGA-CV-7413	TCGA-CN-6018	TCGA-UF-A719
TCGA-BA-A8YP	TCGA-P3-A6TO	TCGA-D6-A6EM	TCGA-CQ-A4C9	TCGA-CQ-7063
TCGA-CN-A63W	TCGA-UF-A71A	TCGA-D6-6516	TCGA-CQ-5332	

>>

>>

TP53 and CDKN2A mut/homdel with 11q13 amp				
TCGA-BA-A4II	TCGA-CN-4735	TCGA-P3-A6T4	TCGA-CV-A6JM	TCGA-CV-7423
TCGA-BA-A6DA	TCGA-CN-4739	TCGA-P3-A6T7	TCGA-CV-A45U	TCGA-DQ-7588
TCGA-BA-A6DD	TCGA-CN-4742	TCGA-UF-A7JA	TCGA-CV-5430	TCGA-F7-8298
TCGA-BA-A6DG	TCGA-CN-5364	TCGA-UF-A71B	TCGA-CV-5440	TCGA-HD-7753
TCGA-BA-4074	TCGA-CN-5365	TCGA-UF-A71D	TCGA-CV-5973	TCGA-IQ-A61G
TCGA-BA-4076	TCGA-CN-6011	TCGA-UF-A71E	TCGA-CV-5977	TCGA-IQ-A61H
TCGA-BA-4078	TCGA-CN-6012	TCGA-CN-6997	TCGA-CV-6936	TCGA-KU-A66T
TCGA-BA-6872	TCGA-CN-6013	TCGA-CQ-A4C6	TCGA-CV-6956	TCGA-MZ-A7D7
TCGA-BA-7269	TCGA-CN-6989	TCGA-CQ-5326	TCGA-CV-7102	TCGA-P3-A6T3
TCGA-BB-4227	TCGA-CV-7435	TCGA-CR-6478	TCGA-CV-7178	TCGA-QK-A6IJ
TCGA-BB-7870	TCGA-CX-A4AQ	TCGA-CR-6491	TCGA-CV-7235	TCGA-QK-A8ZA
<i>TCGA-CN-A498</i>	<i>TCGA-D6-A4Z9</i>	<i>TCGA-CR-7380</i>	<i>TCGA-CV-7414</i>	<i>TCGA-QK-AA3K</i>
TCGA-CN-4727	TCGA-D6-A6EP	TCGA-CR-7383	TCGA-CV-7415	TCGA-T3-A92M
TCGA-CN-4728	TCGA-D6-6825	TCGA-CV-A6JE	TCGA-CV-7418	

Supplemental data

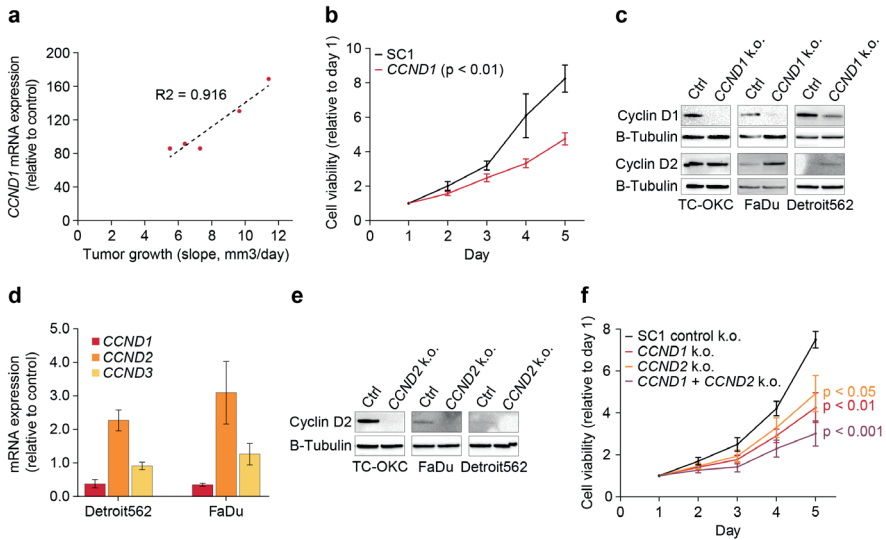


Figure S1 | *CCND1* dependence in amplified cell lines

- Correlation between *CCND1* expression levels and *in vivo* tumor growth in mm³/day.
- Relative cell viability values based on Alamar Blue assay upon *CCND1* knockout in Detroit562 cells.
- Immunoblot for cyclin D1 and cyclin D2 for FaDu, Detroit562 and TC-OKC cells upon *CCND1* knockout.
- Gene expression values 72 hrs post *CCND1* knockdown, relative to control.
- Immunoblot for cyclin D2 for FaDu, Detroit562, and TC-OKC cells upon *CCND2* knockout
- Relative cell viability values based on Alamar Blue assay upon knockout of Control SC1, *CCND1*, *CCND2*, or *CCND1+CCND2* in Detroit562 cells.

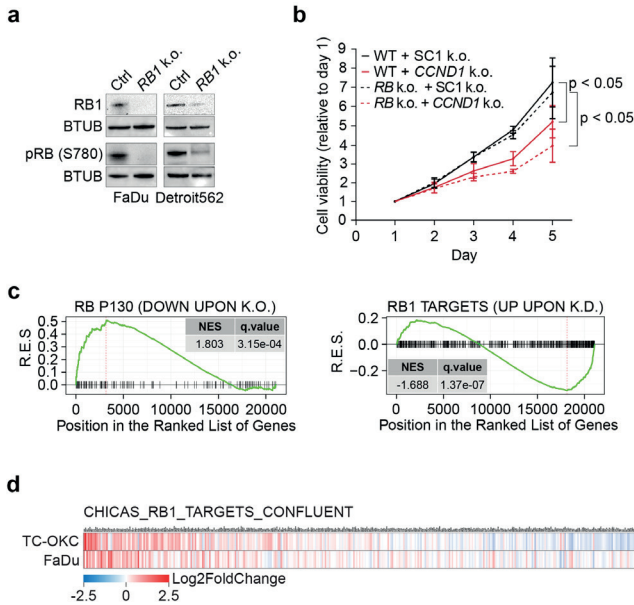


Figure S2 | Expression and growth analysis upon *CCND1* or *RB1* loss

- a Immunoblot for RB1, pRB S780, and B-tubulin for FaDu and Detroit562 cells upon RB1/RBL1/RBL2 knockout.
- b Relative cell viability values based on Alamar Blue assay upon *CCND1* knock-out in RB1/RBL1/RBL2 knockout Detroit562 cells.
- c Running Enrichment Scores of GSEA upon *CCND1* knockout in TC-OKC for the RB_P130_DN.V1_DN (left) and Gene Set and Chicas_RB1_targets (right) gene sets.
- d RNA-seq expression data on the Chicas RB1 target confluent upon *CCND1* knock-out in TC-OKC and FaDu cells.

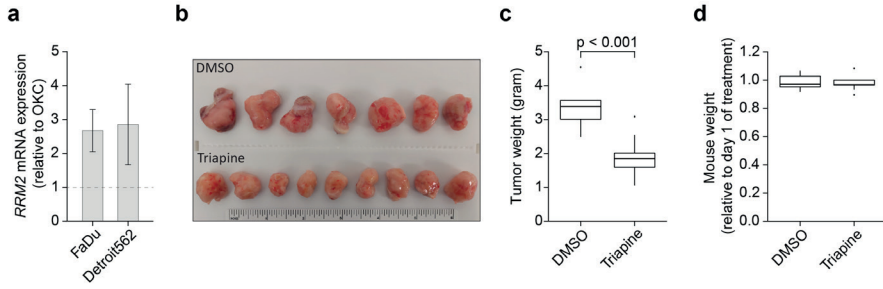


Figure S3 | Effects of triapine on *in vivo* tumor growth

a RRM2 expression values in FaDu and Detroit562 cells, relative to primary OKC.

b Tumors harvested on day 17 post 1st treatment of either DMSO or triapine treated mice.

c Tumor weight in grams of either DMSO or triapine treated mice.

d Mouse weight in grams relative to day 1 of treatment of either DMSO or triapine treated mice.

Chapter 5

Discovery of *ORA0V1* as a novel oncogene

Céline I Mahieu¹, Aaron D Tward¹

¹Department of Otolaryngology - Head and Neck Surgery, University of California
San Francisco, San Francisco, USA

Based on

ORA0V1, *CCND1*, and *MIR548K* are the driver oncogenes of the 11q13 amplicon in
squamous cell carcinoma (Molecular Cancer Research, 2024)



Abstract

Head and neck squamous cell carcinomas show frequent amplification of the 11q13 region, which harbors several potential oncogenes including *ORAOVI*. Little is known about *ORAOVI* in mammalian cells, hence we aimed here to gain insights into *ORAOVI* function. We show that *ORAOVI* is an essential gene in cancer cells, but not primary epithelial cells. Knockout of *ORAOVI* increases reactive oxygen species (ROS) levels in cancer cells, and overexpression of *ORAOVI* increases resistance against oxidative stress. Furthermore, we show that *ORAOVI* induces expression of thioredoxin, a redox protein that plays a central role in ROS homeostasis in many cancers. Thus, this work provides novel insights into *ORAOVI* function and shows that its contribution to development of HNSCC is likely through its ability to modulate reactive oxygen species via the thioredoxin pathway.

Introduction

Copy number alternations are a frequent event in cancer that can contribute to tumorigenesis through induction of expression of oncogenes present on the amplicon. Amplification of genes in the 11q13 region is one of the most frequent amplification in cancer, and is particularly enriched in squamous cell carcinomas (SCC)^{92,107,179,181,182}. In particular, around 25% of head and neck SCC (HNSCC) present with 11q13 amplifications⁹². HNSCC is a common and deadly disease, characterized by a heavy mutational burden and frequent copy number alterations. Despite advances in understanding the mutational landscape of HNSCC, treatment options are still limited. Increasing our understanding of the downstream consequences of oncogenic alterations might direct us to better treatment strategies. We previously found that *ORAOV1* is one of the main contributors to the oncogenic effects of the 11q13 amplicon. However, hitherto the role of *ORAOV1* in the development and progression of SCC has been largely overlooked and understanding of its function in both normal and cancer cells is limited. Here we aimed to get a better understanding of the role of *ORAOV1* in HNSCC tumorigenesis.

ORAOV1 function in SCC

ORAOV1 (oral cancer overexpressed, also known as *LTO1*) derives its name from its discovery in 2002, when it was identified as part of the 11q13 amplicon in HNSCC cells, located between *CCND1* and *FGF19*¹⁸⁴. The *CCND1/ORAOV1/FGF19* locus was found to be very well conserved across species³⁷⁰. Considering the location and correlation to expression of other genes on the 11q13 amplicon (see chapter 3), it is not surprising that in the following years several studies described an association between *ORAOV1* amplification/expression and lymph node metastasis, poor prognosis, or other clinical features in several cancer types^{193,371-373}. In 2008, a first study experimentally suggested that loss of *ORAOV1* in HNSCC inhibits growth of cancer cells through its effects on cell cycle and apoptosis, and subsequent studies have observed similar effects in other cancer cell lines, implying the necessity of *ORAOV1* for tumor growth^{193,374-376}. Some other studies have also suggested a role for *ORAOV1* in angiogenesis or proline metabolism in cancer cells, and ribosomal function in yeast cells^{195,196,377}. Furthermore, one group discovered 2 splice variants of *ORAOV1*, *ORAOV1-A* and *ORAOV1-B*, that are upregulated in cancer and play a role in the epithelial-mesenchymal transition (EMT) through TNF- α /NF- κ B pathways, respectively^{374,378}. More extensive work has been done on the *ORAOV1* orthologue *LTO* in both yeast and *Arabidopsis* models. Here, *LTO1* has been shown to protect cells against damage caused by reactive oxygen species (ROS)^{377,379-381}. Moreover, a recent study showed a functional link in esophageal SCC cell lines between *ORAOV1* and protection against ROS through its interaction with PYCR195.

Oxidative stress in cancer

ROS are inevitable side products of normal cell metabolism and are formed during reactions that require electron transfer. In these redox reactions – such as during mitochondrial oxidative phosphorylation – electrons can be transferred errantly onto O₂ derivatives, forming ROS³⁸². Normal cells keep a constant balance between ROS generation and scavenging through their variety of antioxidant regulatory systems. Low levels of ROS play an important function in cell signaling, as ROS can function as secondary messengers through oxidative modification of cysteine residues of specific proteins, thereby regulating gene expression, signal transduction, and cell growth³⁸³. Cancer cells often have increased ROS levels due to their high metabolic and proliferative rates. An increase in ROS levels during the early stages of tumorigenesis can have significant pro-tumorigenic effects, but persistently high ROS levels can induce apoptosis and senescence in tumor cells³⁸⁴⁻³⁸⁶. By increasing their antioxidant capacity, tumors can still benefit from the effects of ROS on proliferation, without getting harmed by its toxic effects³⁸⁴. Cells can control ROS through several antioxidant systems. These systems include enzymatic antioxidants (including superoxide dismutase, catalase, peroxiredoxin, and thioredoxin (TRX) systems) and non-enzymatic antioxidants (including glutathione synthesis and NADPH). The 2 most important systems used by cancer cells to combat disproportional high ROS levels are the NADPH-dependent glutathione and TRX systems³⁸⁴. Key elements of these systems, such as the thioredoxin protein (TXN) are often upregulated in cancer and expression is associated with poor prognosis³⁸⁷.

Thioredoxin

TXN is a small reductase that plays a key role in countering oxidative stress and is upregulated in many cancers^{384,388}. It is an essential part of the TRX system, which further consists of the thioredoxin reductase (TXNRD1) and a reduced form of NADPH. TXN works as a redox regulator by scavenging ROS through transferring electrons onto other proteins. In this process TXN gets oxidized, after which it needs to get reduced by TXNRD1 in a NADPH-dependent manner³⁸⁹. Through protecting against high ROS, TXN suppresses apoptosis and stimulates cell growth of cancer cells³⁹⁰. TXN is mostly located in the cytoplasm, but can also get transported to the nucleus³⁹¹. Here it can also interact with transcription factors, such as HIF1 α and AP-1, increasing their activity through enhancing their DNA binding capacity, stimulating angiogenesis and apoptosis resistance³⁹²⁻³⁹⁵. TXN levels are upregulated in many cancers and often correlate to worse survival³⁸⁸. This is also the case for HNSCC and other SCCs, where TXN levels are significantly higher in tumor samples compared to non-tumorigenic tissue^{396,397}.

Due to the importance of a balanced redox state for the health of cancer cells, treating tumors with anti-oxidant drugs is a potential treatment strategy^{388,398}. In this study, we

identify *ORAOV1* as an oncogene in HNSCC whose expression decreases ROS levels. Furthermore, we find that the antioxidant functions of *ORAOV1* are likely exerted through activation of TXN, opening up novel potential treatment strategies to treat *ORAOV1*-amplified HNSCCs.

Results

ORAOV1* is a pan-cancer essential gene and its upregulation is sufficient to drive SCC tumorigenesis *in vivo

The *ORAOV1* locus is in very close proximity to the *CCND1* locus on the 11q13 amplicon. While *CCND1* is a well characterized oncogene across multiple tumor types, the effects of *ORAOV1* amplification or overexpression have been less well characterized. However, nearly all tumors - both SCC and non-SCC - that have *CCND1* amplification also have amplification of *ORAOV1* (Fig 1a). Therefore, we aimed to establish whether *ORAOV1* has a role in tumorigenesis as well. Analysis of DepMap cell viability data across all tumor types identified that expression of *ORAOV1* is essential for cancer cell proliferation across all tumor types (Fig 1b). Additionally, whereas CRISPR knockout of *ORAOV1* in FaDu or Detroit562 cells significantly abrogates cell growth, knockout of *ORAOV1* in TP53/CDKN2A knockout primary oral keratinocytes (TC-OKC) or fibroblasts reveals that *ORAOV1* is dispensable for non-tumor cell proliferation (Fig 1c, Fig S1a, Fig S1b). This suggests that *ORAOV1* expression may be selectively necessary for proliferation of tumor cells

To determine whether expression of *ORAOV1* is not only necessary, but also sufficient to stimulate tumor growth, we next assessed the oncogenic driver potential of *ORAOV1 in vivo*. 11q13 amplification in HNSCC occurs primarily in a background of TP53 and CDKN2A loss⁹². Therefore, we engineered OKCs to carry TP53 and CDKN2A mutations (see chapter 2 and 3) and we injected these engineered TC-OKC overexpressing *ORAOV1* or mCherry (control) into NSG mice. Whereas only 1/12 of the control mice developed a tumor, overexpression of *ORAOV1* resulted in tumor formation in 7/11 mice (Fig 1d). This potential to induce tumorigenesis is almost equally strong to that of the established oncogene *CCND1* (9/11 mice, see chapter 3). Thus, *ORAOV1* is an independent contributor to tumorigenesis and overexpression of *ORAOV1* can be sufficient to induce tumor formation from TC-OKC.

***ORAOV1* regulates oxidative stress**

Little is known about the contribution of *ORAOV1* to tumorigenesis and the few papers on *ORAOV1* and cancer mostly focus on the clinical significance of *ORAOV1/11q13* amplification. Since we report a direct contribution of high *ORAOV1* to tumor growth, we next sought to attribute some functional role to *ORAOV1* overexpression in cancer.

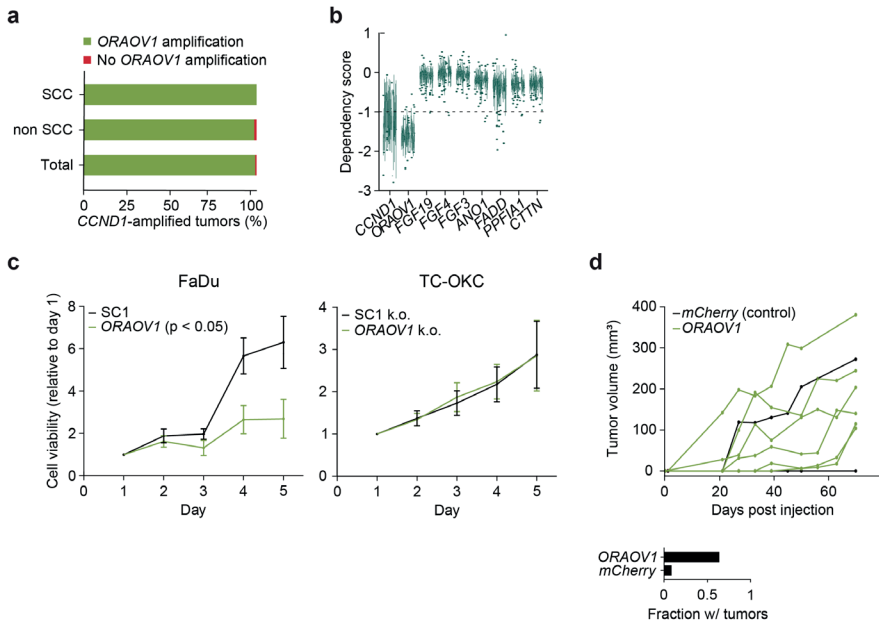


Figure 1 | Upregulation of ORAOV1 is sufficient to drive SCC tumorigenesis *in vivo*

- a Fraction of *CCND1* amplified tumors that carry *ORAOV1* amplification in SCC ($n = 238$) and non-SCC ($n = 382$) (TCGA, PanCancer Atlas).
- b Dependency scores on 11q13 genes for all cancer lines in database of CRISPR knockout screens from project Achilles (DepMap). Upper and lower whiskers represent the largest and smallest observed values within 1.5 times the interquartile range from the ends of the box. Scores below -1.0 show significant dependency.
- c Relative cell viability values based on Alamar Blue assay upon *ORAOV1* knockout in FaDu cells (left) and primary TC-OKC (right).
- d Top: *in vivo* tumor growth in NSG mice injected with 1E6 human TC-OKC cells overexpressing indicated gene (*mCherry*: $n = 12$, *ORAOV1*: $n = 11$) as measured with a caliper. Bottom: fraction of mice that developed tumors before endpoint.

Although not much is known about the function of ORAOV1 in mammalian cells, one study suggests its involvement in reactive oxygen species (ROS) metabolism¹⁹⁵, and several studies report that the *ORAOV1* ortholog LTO1 in *Arabidopsis* is essential for redox regulation^{379,399,400}. To explore the possibility that ORAOV1 has a similar role in HNSCC cells, we measured ROS levels in HNSCC cells with and without knockout of *ORAOV1*. *ORAOV1* knockout markedly increased ROS levels in cancer cells, supporting a role for *ORAOV1* in redox regulation in cancer cells (Fig 2a, Fig S2a).

Balanced redox regulation is an important feature of tumors, and upregulation of *ORAOV1* via 11q13 amplification may be one mechanism cancer cells utilize to regulate ROS levels^{92,384}. This is supported by our finding that expression of *ORAOV1* protects TC-OKCs from a loss in cell viability upon treatment with the oxidant tert-Butyl

hydroperoxide (TBHP) (Fig 2b). 11q13-mediated amplification of *ORAOV1* most often occurs after loss of *TP53* and *CDKN2A* in HNSCC. Therefore, we were interested to see how these mutations affect ROS levels. We engineered OKCs with dual *TP53* and *CDKN2A* mutations and measured ROS levels one week and six weeks after gene editing. TC-OKC accumulate higher ROS levels over time (Fig 2c), consistent with literature that shows *TP53* mutations increase ROS levels⁴⁰¹. Thus, for HNSCC, *ORAOV1* amplification and overexpression may help regulate ROS levels upon *TP53* and *CDKN2A* mutation during early tumorigenesis.

ORAOV1 induces *TXN* expression

To identify possible mechanisms through which *ORAOV1* counters oxidative stress, we overlaid the Reactive Oxygen Species Pathways GSEA Hallmark gene set with RNA-seq data of *ORAOV1* knockout FaDu cells. We found that loss of *ORAOV1* significantly decreases the level of *TXN* (Fig 2d, Fig S2b). To verify the RNA-seq data, we performed RT-qPCR on *ORAOV1* knockout FaDu and Detroit562 cells and found similar downregulation of *TXN* levels (Fig 2e). *TXN* is a key gene within the thioredoxin system to counter oxidative stress that is frequently upregulated in cancer²⁰. We found that in HNSCC cell lines - in comparison to TC-OKCs - *ORAOV1*-amplified lines have increased *TXN* levels (Fig 2f). These data is further supported by analysis of the full CCLE cell line panel, where cells with *ORAOV1* amplification show modest, but significantly higher *TXN* expression (Fig S2c)²⁶⁴. Furthermore, overexpression of *ORAOV1* in TC-OKCs increases *TXN* levels (Fig 2g). Finally, RT-qPCR analysis of *ORAOV1*-induced tumors in mice show that these tumors have a 5-fold upregulation of *TXN* compared to control cells, corroborating our results that *ORAOV1* induces *TXN* expression in cancer cells (Fig 2h).

To assess whether the growth effect of *ORAOV1* on cancer cells is through its effect on *TXN* expression, we engineered FaDu cells to carry either control (SC1), *ORAOV1*, *TXN*, or combined *ORAOV1* and *TXN* deleterious indels. Knockout of either *ORAOV1* or *TXN* individually resulted in decreased cell growth, but *TXN* knockout did not have an additive effect on the growth decrease upon *ORAOV1* knockout (Fig 2i), suggesting these genes function through a shared pathway. Thus, the *ORAOV1-TXN* signaling axis may be a key regulator of oxidative stress in SCC.

Together, these data demonstrate that 11q13 amplification-induced overexpression of *ORAOV1* is a potent oncogenic event for SCC tumorigenesis. High levels of *ORAOV1* may regulate oxidative stress levels through the thioredoxin pathway, potentially representing a critical pathway to target for anti-cancer therapy.

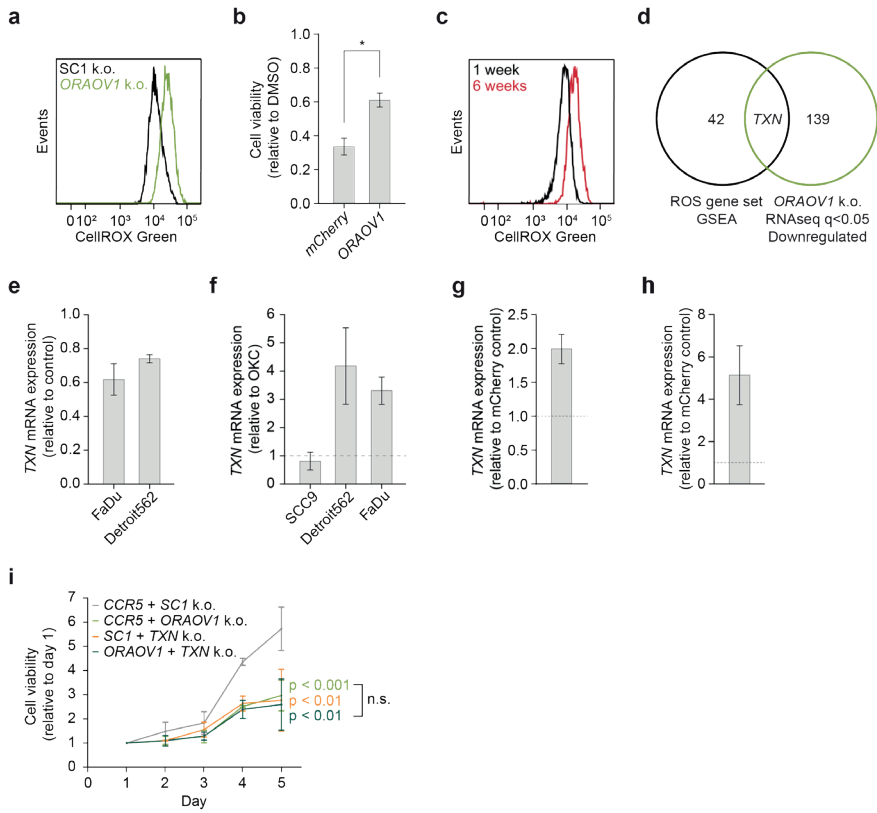


Figure 2 | ORAOV1 regulates oxidative stress, possibly through the TXN pathway

a ROS levels as measured by CellROX Green in FaDu cells upon *ORAOV1* knockout.

b Cell viability values based on Alamar Blue assay of mCherry or *ORAOV1* overexpressing TC-OKC after 72 hours of treatment with 150 nM TBHP, relative to DMSO.

c ROS levels as measured by CellROX Green in TC-OKC 1 week or 6 weeks post engineering.

d Venn diagram showing overlap between genes in the Reactive Oxygen Species Pathways GSEA Hallmark gene set and genes downregulated ($q < 0.05$) in the RNAseq dataset upon *ORAOV1* knockout in FaDu cells

e *TXN* expression values in FaDu and Detroit562 cells upon *ORAOV1* knockout

f *TXN* expression values in SCC9, Detroit562, and FaDu cells relative to OKC

g *TXN* expression values in OKC upon *ORAOV1* overexpression.

h *TXN* expression values of dissected *ORAOV1*-induced tumors, relative to dissected mCherry tumor.

i Relative cell viability values based on Alamar Blue assay upon knockout of Controls SC1+*CCR5*, *CCR5*+*ORAOV1*, SC1+*TXN*, or *ORAOV1*+*TXN* in FaDu cells. P values calculated with two-way ANOVA test.

Discussion

In this study we identified *ORAOV1* as a pan-cancer essential oncogene. Amplification of *ORAOV1* through 11q13 might have a role in tumor maintenance of SCCs through balancing oxidative stress levels via upregulation of the TXN pathway.

Historically, it has been assumed that *CCND1* is the main contributor to the oncogenic effects of the 11q13 amplification, despite the fact that virtually all tumors with *CCND1* amplification also carry *ORAOV1* amplification. We identified that following loss of *TP53* and *CDKN2A*, *ORAOV1* amplification is sufficient to induce tumor growth in mice, and here we show that *ORAOV1* is exclusively essential to tumor cells, in conjunction with previous studies who found the necessity of *ORAOV1* for tumor growth^{193,374-376}. Previous studies in cell lines show that *ORAOV1* also protects against apoptosis, suggesting that the effect of *ORAOV1* loss on cell growth might be (partially) due to decreased inhibition of apoptosis^{193,194,375,376}. Our results indicating that loss of *ORAOV1* does not affect primary cell growth, make *ORAOV1* and its downstream activities a potential target in 11q13-amplified SCCs.

We found that loss of *ORAOV1* increases ROS levels in cancer cells, and that overexpression of *ORAOV1* protects primary cells against oxidative stress, fitting with results from previous studies in yeast and *Arabidopsis*, as well as one recent study in esophageal SCC cell lines, but also with its protective role against apoptosis^{195,377,379-381}. Functionally, we found that *ORAOV1* expression directly affects expression of the redox protein TXN. TXN plays a central role in ROS homeostasis in cancer and is frequently found upregulated in SCCs^{384,388}. TXN cooperates with TXNRD1 to lower oxidative stress levels. Although we saw little to no effects of *ORAOV1* on *TXNRD1* expression (data not shown), it is notable that *TXNRD1* is also found to be upregulated in cancers, including HNSCC and ESCC, and correlates to a poor prognosis^{402,403}. This further supports the role of the thioredoxin system in HNSCC. Thus, amplification of *ORAOV1* and downstream activation of *TXN* may represent a generalizable mechanism through which cancer cells deal with oxidative stress during tumorigenesis.

Increased capacity to deal with oxidative stress can impact current treatment strategies, as dysregulation of pathways that deal with oxidative stress can contribute to drug resistance. For example, frequently used chemotherapeutics such as carboplatin and cisplatin, but also radiation therapies, (partially) rely on the induction of oxidative stress for their cytotoxic effect on cancer cells⁴⁰⁴⁻⁴⁰⁶. Thus, if *ORAOV1* amplification reduces oxidative stress, its amplification could have a role in resistance against chemotherapeutics.

Due to the limited number of studies that focused on *ORAOV1* in cancer, not much is known yet about the effect *ORAOV1* has on cancer development and drug resistance.

However, several studies have shown that TXN can induce chemoresistance^{407,408}. Furthermore, one study in cervical SCC showed that *TXN* levels are increased upon cisplatin treatment and that high levels correlate to a poor response³⁹⁷. Lastly, treatment with the TXN inhibitor PX-12 prevented resistance to radiotherapy in colorectal cancer⁴⁰⁹. Future studies should examine whether *ORAOVI* or TXN inhibition can synergize with chemotherapies for the treatment of 11q13-amplified HNSCCs.

The increased ROS levels in cancer cells can also be exploited to treat cancer cells directly. The high proliferation rate of cancer cells results in high ROS production and the cancer cells need to balance these levels to prevent cell death through oxidative stress. Since balancing this redox state is essential to cancer cell health, targeting the reducing power of cancer cells is a potential treatment strategy. Cancer cells might be more susceptible to this treatment compared to normal cells, due to their higher baseline ROS levels, which can tilt them over the edge towards apoptosis faster upon decreased reducing power.

Although we and others showed that inhibition of *ORAOVI* inhibits tumor growth, there are no (pre)clinical studies performed yet to support this strategy. However, inhibition of the TXN pathway has recently been explored as a strategy for treatment of several cancer types^{388,398,410}. However, the TXN system is highly redundant with the GSH system, and inhibition of the one system might be compensated by activation of the other. Therefore, treatment strategies frequently target both together. This combined inhibition yields potent, synergistic effects as stand-alone treatment or as a potentiator for chemotherapeutics^{387,411-414}.

In earlier stages of tumorigenesis, ROS levels can actually play a favorable function in tumor development, suggesting that treatment with antioxidants would be better in these stages. However, moderate levels of ROS are also essential for signaling, proliferation, and normal cell health, so this is a critical balance⁴¹⁵. Moreover, treatment with anti-oxidant in later stages might actually stimulate tumor growth^{416,417}. Therefore, targeting the antioxidant system is typically regarded as the better strategy.

In summary, in the present study we identified that the frequently amplified *ORAOVI* gene can induce tumorigenesis and protect against oxidative stress, potentially through regulation of the TXN pathway. This *ORAOVI-TXN* signaling axis represents a potential target for (combination) therapy of the treatment of 11q13-amplified HNSCCs.

Material and Methods

Cell culture

FaDu (ATCC cat#HTB-43, male) and Detroit562 (ATCC cat#CCL-138, female) cells were grown in Eagle's Minimal Essential Medium with L-glutamine (Fisher Scientific cat#50983283) supplemented with 10% FBS (Corning cat#MT35010CV) and 1% Penicillin/Streptomycin (P/S, Corning cat#MT30002CI). SCC-9 (ATCC cat#CRL-1629, male) cells were cultured in Dulbecco's Modified Eagle medium (DMEM):F12 (Gibco cat#11039021) supplemented with 400 ng/mL hydrocortisone (EMD Millipore cat#386698), 10% FBS, and 1% P/S. HEK293T (ATCC cat#CRL-3216, female) cells were grown in DMEM (Gibco cat#12491023) supplemented with 5% FBS and 1% P/S. All cell lines were purchased and authenticated at ATCC in 2016 and tested yearly for mycoplasma through PCR. Human primary fibroblasts were isolated and collected from patient derived skin samples and cultured in DMEM supplemented with 5% FBS and 1% P/S. Human primary keratinocytes were collected and isolated from patient derived mucosal samples and cultured in Medium 154 and Keratinocyte Serum Free Medium (1:1, Life Technologies cat#M154500 and cat#17005042), supplemented with 5 mL/L Human Keratinocyte Growth Supplement (Life Technologies cat#S0015), 25 mg/L Bovine Pituitary Extract (Life Technologies cat#17005042), 2.5 µg/L EGF Human Recombinant (Life Technologies cat#17005042), and 1% P/S. No cells were passaged for longer than 5 weeks.

Table 1 | CRISPR crRNA sequences and primers for TIDE analysis

Target gene	crRNA sequence	Forward primer	Reversed primer
CCR5	AACACCAGTGAGTAGAGCGG	TGCTTGGCCAAAAGAGAGT	CGATTGTCAGGAGGATGATG
CDKN2A	TAACTATTCGGTGCCTTGGG	GACTCCCTTTTATCCCAAACG	CCAGTCTCCTTCTTGCCAAC
ORAOV1	CATATTCGATGCCATCGTGA	CCATGTACAGGCTGCTTTGG	ACCAGGCTGAGCAGATGTTT
SC1	TTGGTCCCACGATGACCCAC	GATCGAGGTCCACTCTGAGC	GGTGTGTGTACTGGGGAAC
TP53	CCATTGTTCAATATCGTCCG	ACTGACCGTGCAAGTCACAG	CCCCTCTGAGTCAGGAAACA
TXN	TAGTTGACTTCTCAGCCACG	n.a.*	n.a.*

* no PCR possible due to poly-T sequence. Knockout confirmed with qPCR.

Genome engineering

To generate gene knockouts, cells were transfected via electroporation using the MaxCyte ATX electroporation platform with Clustered Regularly Interspaced Short Palindromic Repeat (CRISPR) Cas9- ribonucleoproteins (RNPs) and gene-specific guideRNAs (table 1). For electroporation, sub-confluent cells were trypsinized and washed 1x in DMEM and 1x in Opti-MEM (Life Technologies cat#31985070). Cells

were resuspended to a concentration of 2.5×10^7 cells/mL in Opti-MEM. crRNAs and Alt-R CRISPR-Cas9 tracrRNA (Integrated DNA Technologies) were hybridized in a 1:1 ratio to a final concentration of $50 \mu\text{M}$. crRNA:tracrRNA were complexed with Cas9-RNP at a 1:1:1 ratio for 20 minutes at room temperature and subsequently mixed with the cells to a final concentrations of $2.5 \mu\text{M}$ crRNA:Cas9 and 2.0×10^7 cells/mL. Cells were electroporated in $25 \mu\text{l}$ or $400 \mu\text{l}$ reactions with the 'Optimization 7' (keratinocytes, fibroblasts, Detroit562, and SCC-9) or 'DLD-1' (FaDu) electroporation protocols. After electroporation, cells were immediately collected from the processing assembly, plated into a 6 well plate and recovered 20 minutes at 37°C , before resuspending in 2 mL culture medium. Transfection efficiency was determined 24 hrs post electroporation through flow cytometry. After 96 hours, gene disruption was confirmed through TIDE (Tracking of Indels by Decomposition¹²⁸) analysis (primers: **table 1**). To control for multiple edits in the amplified 11q13 region, a negative control "Safe Control" SC1 crRNA was designed to target the 11q13 region in a non-coding and non-regulating region.

Exogenous 11q13 gene constructs and cloning

To clone overexpression constructs, RNA was purified from oral keratinocytes (OKCs) and total cDNA was synthesized with poly-A specific primers using SuperScript III First-Strand Synthesis System (Invitrogen cat#18080051) according to the manufacturer's instructions. To create Gateway compatible PCR products of the gene of interest, coupled to an mCherry tag through a T2A sequence, primers were designed with AttB and T2A adapters (**table 2**). PCRs were performed to create AttB-gene-T2A and T2A-mCherry-AttB products from whole genome cDNA (*ORA0V1*) or plasmid DNA (mCherry:pHR_Gal4UAS_pGKmCherry, Addgene cat#79124) as template. PCR products were purified and coupled in a subsequent PCR. Full *attB* products were cloned into the pDONR221 Vector (ThermoFisher Scientific cat#12536017) using Gateway Technology according to the manufacturer's instruction. Coding sequences were transferred into the pLEX_307 vector (Addgene cat#41392). As negative control, pLEX_307-EBFP was generated.

Table 2 | Lentiviral overexpression cloning primers

Gene for fusion cloning pLEX_307		
Target gene		AttB insert forward primer / T2A insert reversed primer
ORAOV1	AttB Forward	GGGGACAAGTTTGTACAAAAAGCAGGCTTAATGGCTGGCAGTCAGGAC
	T2A Reversed	CACGTCACCCGATGTTAGCAGACTTCCCTCTGCCCTCTCCGCTTCCAATGAAAGTCCGGAACCTTCTGC
Label for fusion cloning pLEX_307		
Label		T2A insert forward primer / AttB insert reversed primer
mCherry	T2A Forward	CTAACATGCGGTGACGTGGAGGAGAATCCCGCCCTGCTAGCATGGTGAGCAAGGGCGAGG
	AttB Reversed	GGGGACCACTTTGTACAAGAAAGCTGGGTTTTACTTGTACAGCTCGTCCATGCC
Label only cloning pLEX_307		
Label		AttB insert forward primer / AttB insert reversed primer
mCherry	AttB Forward	GGGGACAAGTTTGTACAAAAAGCAGGCTTAATGGTGAGCAAGGGCGAG
	AttB Reversed	GGGGACCACTTTGTACAAGAAAGCTGGGTTTTACTTGTACAGCTCGTCCATGCC

Lentiviral production and infection

HEK293T cells were transfected with 750 ng transfer plasmid, 375 ng psPAX2 (Addgene cat#12259), 750 ng pMD2.G (Addgene cat#12260), and 5.5 μ l Lipofectamin 2000 Transfection reagent (Life Technologies cat#11668027) per mL culture medium. Medium was replaced 16 hours post transfection and viral supernatant was collected 72 hours later, filtered through a 0.45 μ m PVDF filter (MilliporeSigma cat#SLHVM33RS), concentrated using LentiX concentrator (Takara Bio cat#631231) and stored at -80°C . Cells were transduced with viral pellets resuspended in appropriate medium with 8 μ g/ml Polybrene Transfection reagent (EMD Millipore cat#TR1003G) for 16 hours.

RT-qPCR

For Reversed Transcriptase quantitative PCR (RT-qPCR), RNA was isolated with the RNeasy Plus Mini Kit (Qiagen cat#74136) and converted into cDNA using SuperScript III First-Strand Synthesis SuperMix for qRT-PCR (Thermo Fisher Scientific cat#11752250). PrimeTime qPCR Probe-based assays and Gene Expression Master Mix were purchased from Integrated DNA Technologies with 6-FAM/ZEN/IBFQ labeling (table 3). *ACTB* probes and primers for loading control were designed with JOE NHS/ZEN/3' IBFQ labeling to allow multiplex RT-qPCR. 10 μ l RT-qPCR reactions were prepared containing 500 nM of each primer (gene of interest, *ACTB*: forward and reversed), 250 nM of each probe, 5 μ l Mastermix, and 10-50 ng cDNA. Reactions were run in triplicates on the Quantstudio 6 (Applied Biosystems). Relative gene expression levels were calculated using the ΔCT method against *ACTB*.

Table 3 | RT-qPCR probes and assays

RT-qPCR			
Target gene	Probe sequence	Forward primer	Reversed primer
ACTB	AGTTTCGTGGATGCCACAGGACTC	CACTCTTCCAGCCTTCCTTC	GTACAGGTCTTTGCGGATGT
Target gene	Assay number		
ORAOV1	Hs.PT.58.40145225		
TXN	Hs.PT.58.14778418		

Cell viability assays

Cells were seeded into Black Greiner Cellstar 96 well plates (Sigma-Aldrich cat#M9936). Starting at 72 hours after plating or drug treatment, cells were incubated with 10% Alamar Blue (Bio-Rad cat#100234-634) according to the manufacturer's instruction. Fluorescence was read out on a GloMax Explorer plate reader (Promega) at an excitation of 520 nm and emission of 580-640 nm. Cell viability was calculated relative to untreated or day 1 condition.

Drug treatments

Tert-Butyl hydroperoxide (TBHP, Life Technologies cat#180340050) was diluted in water and added to the culture media at 150 nM for 72 hours.

Reactive oxygen species assays

ROS levels were detected using CellROX Green flow cytometry assay kits (Life Technologies cat#C10492). Cells were concentrated 5×10^5 cells/mL in complete medium. Negative controls were incubated with N-acetylcysteine at 1000 μ M for 60 minutes at 37°C, positive controls were incubated with TBHP hydroperoxide at 400 μ M for 30 minutes at 37°C. CellROX Green reagent was added at 500 nM for 40 minutes at 37°C. Samples were analyzed by flow cytometry.

In vivo experiments

NOD *scid* gamma (NSG) mice were purchased from the Jackson laboratory (cat#005557). All experimental procedures were approved by and in compliance with UCSF IACUC. *TP53* and *CDKN2A* knockout OKCs were transduced with pLEX_307 virus to induce expression of target genes. 6 days post transduction, cells were resuspended in a 1:1 ratio of Matrigel and OKC culture medium at a concentration of 1.0×10^7 cells/mL. NSG mice (mixed male and female) were subcutaneously injected in the hind flank with 1.0×10^6 cells. Tumor growth was monitored weekly until endpoint

and tumors were measured using a caliper. Tumors were dissected and origin was confirmed through RT-qPCR on target genes.

RNA-seq analysis

Cells were transfected as indicated and RNA was collected 6 days after. RNA-sequencing libraries were prepared with the QuantSeq 3' mRNA-Seq Library Prep Kit (Lexogen cat#015.24) kit according to the manufacturer's instructions. Library quality was assessed with a High Sensitivity DNA Assay on the Agilent 2100 Bioanalyzer. Samples were sequenced by the Center of Advanced Technologies (UCSF) on the HiSeq SE50/65 (Illumina). Samples of sufficient quality were analyzed for Differential Expression analysis using the DESeq2 pipeline.

TCGA and CCLE data analyses

Publicly available copy number and gene expression data from TCGA was accessed through cBioportal¹⁷⁸. For overall *CCND1* and *ORAOVI* amplification frequencies in tumors, TCGA PanCancer data was analyzed²⁶⁵. For *TXN* expression in cell lines, data from the Cancer Cell Line Encyclopedia (CCLE) were analyzed²⁶⁴. For cancer dependency analysis, the Cancer Dependency Map was accessed via the depmap package for R. DepMap Release: DepMap, Broad (2019): DepMap 19Q3 Public. Dataset doi:10.6084/m9.figshare.9201770.v2 (CRISPR knockout screens from project Achilles244).

Statistical analysis

All data are represented as mean \pm SEM unless stated otherwise. All experiments were independently reproduced at least 3 times. Statistical significance is indicated as follows: * $p < 0.05$, ** $p < 0.01$, *** $p < 0.001$

Data availability

RNA-sequencing data generated in this study are publicly available at the Gene Expression Omnibus under accession code GSE216849.

Acknowledgements

This work was supported, in part, by the US National Institutes of Health (NIH) grant ROI-DE029890 (A.T.). The authors thank Andrew Mancini, René Bernards, Vicente Planells Palop, and Nancy Joseph for helpful discussions, and Ellee Vikram and Andrea Yeung for technical assistance.

Author Contributions

C.I.M. and A.D.T. conceived of research. C.I.M. designed and executed all *in vitro* and *in vivo* studies, performed all data analyses, and wrote the manuscript. A.D.T. supervised the study.

Conflict of interest

The authors declare no competing interest.

Supplemental data

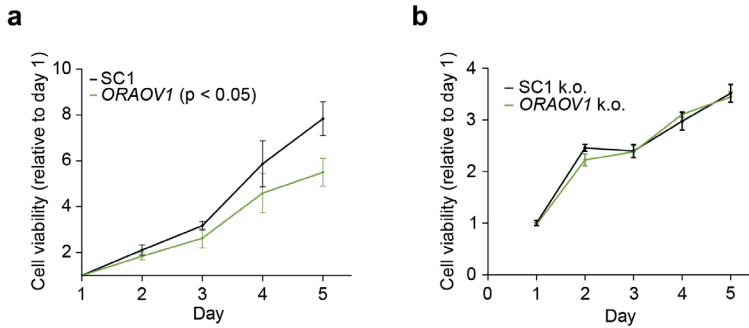


Figure S1 | Primary fibroblasts are not dependent on ORAOV1

- a Relative cell viability values based on Alamar Blue assay upon *ORAOV1* knockout in Detroit562 cells.
- b Relative cell viability values based on Alamar Blue assay upon *ORAOV1* knockout in primary human fibroblasts. Data from representative replicate.

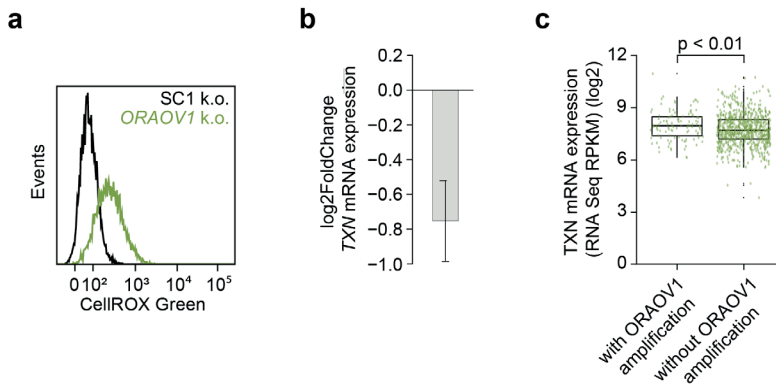


Figure S2 | ORAOV1 regulates oxidative stress

- a ROS levels as measured by CellROX Green in Detroit562 cells upon *ORAOV1* knockout.
- b Log₂FoldChange of *TXN* expression upon *ORAOV1* knockout in FaDu cells (RNAseq, $q < 0.05$).
- c *TXN* mRNA expression levels in CCL6 cell lines either with ($n = 114$) or without ($n = 847$) *ORAOV1* amplification.

Chapter 6

General discussion



PART I

Keratinocyte Engineering and its Application in Disease Modeling and Cell Therapy

Summary

Loss of normal keratinocyte function is the cause of a significant number of epidermal or oral diseases and conditions, as detailed in **Chapter 1**. Development of representative genetic models is crucial to gain a better understanding of these disorders, such as epidermolysis bullosa (EB) and squamous cell carcinoma (SCC). Additionally, engineered keratinocyte-based cell therapies are a promising option to treat a variety of dermal conditions, such as burn wounds. However, the lack of efficient genome engineering strategies currently limits the generation of engineered keratinocytes for such purposes. In **Chapter 2** we present a novel electroporation-based cell engineering workflow for efficient transfection of primary keratinocytes with CRISPR RNPs and demonstrate its use in both cancer modeling and the development of novel allogeneic cell therapies.

Our main results include:

- 1 Delivery of mRNA and CRISPR-RNPs to primary adult keratinocytes derived from four distinct anatomical sites with efficiencies between 97% and 100%, without compromising cell viability or cell morphology
- 2 Genome editing efficiencies upon CRISPR RNP transfection in primary adult keratinocytes between 85% and 100%, in a fast, robust, scalable, and GMP-compatible manner
- 3 A proof of concept for the generation of hypimmune universal donor primary adult keratinocytes for the use in cell therapies

Overall, we present a highly efficient and fast workflow for the generation of engineered keratinocytes, facilitating future developments for disease modeling and the field of keratinocyte-based cell therapies.

Transfecting and engineering primary keratinocytes

Genetic alterations in keratinocytes are the cause of many types of genodermatoses and all squamous cell carcinomas, yet the use of genetically engineered primary keratinocytes to study these diseases is very limited. This lack of use can be attributed to the fragile nature of primary keratinocytes, making it challenging to isolate, culture, and transfect these cells. Analysis of publications using CRISPR-Cas9 technologies in human cells during the period of 2013-2022 showed that of approximately 18,000 studies, only 51 (0.3%) were done with keratinocytes⁴¹⁸. Moreover, of these 51, the

majority used immortalized keratinocyte variations, and only 12 studies total applied CRISPR-Cas9 technologies in true primary keratinocytes. Virtually all these studies had to include additional lengthy purification steps post-editing, adding a further challenge to the cell engineering process when considering the fragility and short lifespan of adult keratinocytes. Thus, delivery efficiency of genome engineering machinery is the main limiting factor in the generation of engineered keratinocytes⁴¹⁸.

Currently, lentiviral or adenoviral delivery are the most frequently used delivery methods owing to their higher efficiency. However, these methods have significant off target and safety concerns⁴¹⁹. Adeno-associated virus (AAV) is generally a safer option, but comes with a smaller loading capacity, restricting the options of engineering machineries^{420,421}. Therefore, development of efficient, non-viral delivery methods is crucial to enable high quality studies with engineered keratinocytes. In **Chapter 2** we describe an electroporation-based method to efficiently transfect and engineer keratinocytes with CRISPR RNPs where we routinely achieve 90-100% transfection and editing efficiencies. This approach enables the generation of engineered keratinocytes for the development of proper disease models and cell therapies.

Improved disease modeling

Proper disease models are imperative to study the genetic predispositions that are essential for disease development⁴²¹. Primary patient material is ideal, but this material is scarce, cells can be challenging to isolate, and for most disorders it is not possible to get an isogenic control/mutant pair⁴⁷. Therefore, most current studies aiming to model epithelial diseases use a variety of immortalized keratinocyte lines⁴¹⁸. However, these models often show abnormal stratification and differentiation, aneuploidy, and have limited usefulness in studying disorders that affect proliferation and differentiation⁴²². Instead, true primary keratinocytes from healthy donors can be engineered to precisely mimic genetic alterations as they occur in disease without undesired background alterations, building valuable models for both monogenic - as well as more complex polygenic - epithelial diseases. These models can be used to enhance our understanding of disease risk- and progression, as well as for the development and validation of potential therapeutic strategies⁴⁷.

In contrast to genodermatoses, squamous cell carcinomas are caused by a multitude of genetic alterations that can highly differ from patient-to-patient⁹². Throughout this thesis we show several examples of knockouts of tumor suppressor genes. Specifically, in **Chapter 3** we show that by stacking genetic alterations in the order that they frequently occur in patients, we can mimic the process of oncogenic transformation from normal to tumor-forming cells. Although it is well characterized which mutations frequently occur in SCCs⁹¹⁻⁹³, it is less clear which mutations at minimum can form the switch to an aggressive phenotype. Due to the high variety and near-endless possibilities for mutational combinations, it is a momentous job to study these

combinations individually. However, with the highly efficient engineering process we present here, high-throughput screens utilizing CRISPR guideRNA libraries can begin to interrogate these questions. Furthermore, through knockout of oncogenes in primary cells in parallel with knockout of the same genes in cancer cells, we reveal several cancer-specific sensitivities (Chapter 4 and Chapter 5). Thus, the ability to engineer primary keratinocytes alongside cancer cells provides a great platform for the uncovering of cancer-specific sensitivities and potential treatment options.

Engineered primary keratinocytes cultures are a valuable tool for the initial screening of genotypic- and phenotypic effects of certain mutations. However, culturing in a 2D context does not fully represent the 3D environment in which the cells naturally operate⁴²¹. Therefore, application of engineered keratinocytes in 3D and *in vivo* cultures would be an even more powerful disease model. In our work described in Chapter 3 we use a combination of several 2D, 3D, and *in vivo* models with manipulated keratinocytes- and keratinocyte-derived cell lines to assess different growth characteristics upon manipulation. For example, the organotypic model (such as used in Chapter 3) can be used in combination with engineered primary keratinocytes in either suspension or spheroid formation^{47,423,424}. This 3D skin model accurately represents the multicellular organization as found in epithelial tissues and is a good platform to test novel therapeutics^{47,423}. Other alternatives include skin-on-a-chip models and pluripotent stem cell-derived skin organoids^{425,426}. However, these 3D models too are restricted by their limited culture life and still lack an *in vivo* context with mesenchymal tissue and responses such as angiogenesis.

The use of mouse models can overcome these limitations – provided they are used with appropriate ethical considerations. Genetic mouse models exist for some disorders, but their development is time-consuming, they are limited by the amount of genetic alterations, and they do not represent human tissue. Instead, mouse xenograft models with engineered human keratinocytes, either grown in suspension or in a 3D context, can be used to study human keratinocyte behavior *in vivo*. In our work in Chapter 3, Chapter 4, and Chapter 5 we show that the transplantation of human keratinocytes to immunocompromised mice only results in *in vivo* tumor formation upon a specific subset of oncogenic alterations. To study complex cell interactions beyond internal (tumor) growth behavior, 3D xenograft models can be used. The skin-humanized mouse model consists of bio-engineered human keratinocytes on a human plasma/fibroblast containing scaffold that is “stitched” on immunodeficient mice^{47,427-429}. This comprehensive model can be used to study human skin in both normal and pathogenic context^{430,431}. The combination of these diverse modelling techniques and enhanced genome engineering possibilities (discussed below) provides a plethora of possibilities to increase our understanding of genetic epithelial disorders.

Future perspectives of the use of CRISPR-Cas technologies

In the work presented in this thesis on engineering primary keratinocytes, we have focused on the use of CRISPR-Cas9 as the flagship technology for genome engineering. However, in recent years there have been significant advances in CRISPR-based genome engineering technologies⁴³². These advances have improved the editing capabilities, targeting scope, and specificity of genome editors through both the discovery of novel Cas enzymes and genetic modification to the original Cas9 backbone, e.g. through broadening of the PAM compatibility, altering the nuclease activity, or addition of new functional elements⁴³². The editors with the most interest from both research- and clinical perspectives include Cas12a nucleases, base editors, prime editors, and RNA editors (see **Textbox 1**). Although these variations are typically less efficient than the highly optimized Cas9 nuclease, they have a variety of advantages - e.g. higher specificity, different nuclease activity, easier delivery - that make them a preferred option for disease modeling or cell therapy development. Due to the relative novelty of these CRISPR-based engineering techniques and the hitherto challenges in keratinocyte transfection, there is a dearth of studies using these CRISPR variants in primary keratinocytes. However, these technologies expand disease modeling to beyond 'simple' loss of function mutation to include protein-function altering mutations. To illustrate, these mutations could be dominant negative mutations as found in many keratin genes - resulting in a number of genodermatoses, including specific types of EB or Pachyonychia Congenita^{431,433,434} - or gain of function mutations in oncogenes such as EGFR, HRAS, or PIK3CA that are frequently mutated in head and neck squamous cell carcinoma (HNSCC)⁹¹⁻⁹³.

Engineered keratinocytes in cell therapy

The development of the advanced CRISPR technologies combined with the enhanced delivery efficiency that we describe here, can drive the development of novel keratinocyte-based gene- and cell therapies forward. We find that engineered keratinocytes are an exciting cell type to develop autologous and allogeneic cell therapies with. In **Chapter 2** we propose the use of hypo-immune allogeneic keratinocytes as an alternative to autologous epidermal grafts to stimulate regeneration of the epidermal layer upon wounding. Results from current approaches using epidermal grafts to stimulate re-epithelization are encouraging - as both autologous and allogeneic approaches provide their own healing benefits¹¹³.

Textbox 1 | CRISPR-Cas based genome editing However, we believe that the use of hypoimmune allogeneic cells can combine best of both worlds: the enhanced and long-term healing of autologous approaches, and the universality, reduced patient burden, and instant availability of allogeneic approaches.

Cas9. The standard Cas9 nuclease is a large, multidomain Class 2 Type II CRISPR nuclease that creates double strand breaks with a blunt ends upon target recognition⁴³⁵. Cas9 is the most developed and optimized Cas protein with therefore strong nuclease activity. Cas9 is primarily useful for efficient gene knockouts.

Cas12a. Cas12a is a Class 2 Type V CRISPR nuclease that creates staggered (“sticky”) ends upon target cutting. It exhibits less off-target activity and is significantly smaller than Cas9^{436,437}. The size of Cas9 can be a limiting factor in the efficient delivery of the genome editing machinery, and therefore smaller Cas variants are gaining interest - in particular Cas12a^{438,439}. Editing efficiencies are lower than with typical Cas9, but several attempts to improve the range and efficiency of Cas12a show that these limitations can be overcome^{440, 441}. Due to its smaller size and reduced off-target activity, Cas12a has a better safety profile and is gaining a lot of momentum for use in the field of gene and cell therapy.

Base editors. Base editors typically consist of a catalytically impaired Cas9 nickase (nCas9) that is fused to a single strand DNA deaminase. Ultimately, complex activity results in a single base pair conversion. There are two types of base editors: cytosine base editors (CBE) that convert C•G to T•A and adenine base editors (ABE) that convert A•T to G•C^{442,443}. Upon target recognition through the guideRNA, the editor will induce the specific conversion. Importantly, all compatible bases within the editing window will get edited. This non-specificity, together with the limited type of conversions possible, constrains the usability of these editors. However, base editors are more efficient than prime editors (discussed below) and improvements towards smaller editing windows are being made. Thus, when the editing window allows for it and the conversion of interest is possible through either the CBE or ABE, base editors are a valuable tool to induce a single nucleotide conversion.

Prime editors. Prime editors are fusion enzymes typically consisting of a Cas9 nickase (nCas9), a reverse transcriptase, and a prime editing guideRNA (pegRNA)⁴³². The nickase creates a single strand cut upstream of the PAM sequence, resulting in an overhang. The transcriptase subsequently directly copies the desired sequence from the pegRNA into the target locus, replacing the original sequence while installing insertions, deletions, and other possible conversions. As such, in theory, prime editors could be the ultimate genome editor tool. Compared to for example Cas9-based homology directed repair, prime editing is more efficient and has less off target effects. Moreover, prime editing does not create any double strand breaks, avoiding off target edits and activation of P53 signaling⁴⁴⁴⁻⁴⁴⁶. However, prime editing is less efficient than base editing.

RNA editors. RNA editors form an alternative to the genome editing approaches described above. RNA-targeting nucleases such as Cas7-II or Cas13 only induce transient alterations as they target RNA, reducing the risk of genotoxicity⁴⁴⁷⁻⁴⁵⁰. Moreover, RNA editors such as Cas13 can be easily used in non-dividing cells - e.g. differentiating keratinocytes - whereas many DNA nucleases are mostly suitable for dividing cells.

Currently, the majority of cell therapy approaches targeting diseases such as RDEB utilize first-generation editing technologies including TALEN-mediated editing or standard Cas9 editing^{55,124-126}. By expanding the genome editing toolbox, novel strategies to develop a broad portfolio of keratinocyte-based cellular medicines are on the horizon. For example, multiplexing standard Cas9 gene editing alongside Cas12a editing and prime editing can enable single-step manufacturing workflows for highly engineered keratinocyte-based products with enhanced safety profiles. These “next generation” keratinocyte engineering strategies can reduce manufacturing cost and risk while enabling the development of tailored cellular therapeutics for the spectrum of genodermatoses.

PART II

Dissecting the 11q13 Amplification in Head and Neck Squamous Cell Carcinoma

Summary

Over 25% of Head and Neck Squamous Cell Carcinomas display amplification of genes in the 11q13 region, yet it is unclear which genetic elements of the amplicon are the key driver events in these tumors. In **Chapter 3** we describe a comparative analysis on the contribution of each 11q13 gene to HNSCC tumorigenesis and the identification of three critical drivers of the amplicon. In **Chapter 4** and **Chapter 5**, we further analyze the mechanism behind these critical drivers and explore potential therapeutic strategies.

Our main findings include

- 1 *CCND1*, *ORAOVI*, and *MIR548K* are the critical drivers of the 11q13 amplicon in HNSCC. These genes have distinct effects on tumorigenesis.
- 2 *MIR548K* contributes to the epithelial-mesenchymal transition.
- 3 Primary keratinocytes are exclusively dependent on *CCND2*, whereas *CCND1* amplification induces cyclin D1 oncogene addiction in cancer cells.
- 4 *CCND1* amplification drives the cell cycle in a CDK4/6/RB1-independent fashion.
- 5 *CCND1* amplification induces *RRM2* expression, conferring a dependency on *RRM2*.
- 6 *ORAOVI* is a potent oncogene that is capable of initiating *in vivo* tumor formation at a level similar to *CCND1*.
- 7 *ORAOVI* regulates reactive oxygen species through activation of the thioredoxin pathway.

Thus, 11q13 amplification drives tumorigenesis through a combination of at least three independent oncogenic events. Through better understanding of the individual contributions, we find dependencies on these genes and their downstream mechanisms that are unique to the cancer cells. Exploiting these weaknesses could be a novel therapeutic approach for 11q13-amplified HNSCC.

The 11q13 amplicon in HNSCC

In **Chapter 3** we identify 3 genes - *CCND1*, *ORAOVI*, and *MIR548K* - as key-drivers of the 11q13 amplification in HNSCC. Whereas *CCND1* is generally accepted as a key oncogene, we find that *ORAOVI* and *MIR548K* also have independent effects on tumorigenesis. *CCND1* and *ORAOVI* have the strongest effect on tumor growth, and we find that nearly all tumors - SCC and non-SCC - with *CCND1* amplification also

carry *ORAOVI* amplification. Thus, *ORAOVI* may be a novel pan-cancer oncogene, and our findings on its function might be broader applicable to other cancer types as well. In contrast, *MIR548K* amplification seems more specific towards SCCs, indicating a possible SCC-specific function.

Furthermore, we find that amplification of 11q13 might be a critical oncogenic event in SCC tumorigenesis, as *TP53* and *CDKN2A* mutations are insufficient to robustly grow tumors. However, additional overexpression of either *CCND1* or *ORAOVI* results in frequent tumor formation. Indeed, loss of *TP53* and *CDKN2A* can already be present in normal skin or premalignant lesions, whereas the 11q13 amplification is exclusively found in later stages of tumorigenesis^{101,107,247}. Normal skin presents with patches of cells that have different oncogenic mutations, yet are constrained to behave like normal cells due to competition and limitations in the proliferating compartment, limiting clonal growth in the epidermis^{103,104}. Hence, although *TP53* and *CDKN2A* mutations might give cells a proliferative advantage due to loss of tumor suppressor activity, an additional pure oncogenic event - such as 11q13 amplification - is likely required to push cells towards a more aggressive state and overcome the restraints of the epidermal compartment. Thus, amplification of the 11q13 region might be a driver event in nearly a quarter of all HNSCCs and identifying its mechanism of oncogenesis is important to reveal novel therapeutic approaches for this subset of HNSCCs.

Interactions on the 11q13 amplicon

The 11q13 amplicon is a gene-dense region that is well conserved between species³⁷⁰. Generally, genes often cluster together in functionally similar or coherent gene clusters and conservation of chromosomal proximity between genes throughout evolution is a strong indicator for functional coupling⁴⁵¹⁻⁴⁵⁴. The observation that the 11q13 region is not only well conserved, but also nearly always co-amplified, suggests potential cooperation between genes on the amplicon. Mechanisms of cooperation can include co-regulation of genes by nearby elements, such as enhancers or transcription factors, but also functional convergence in a shared pathway or cellular process. Computational screening for regulating elements on the amplicon did not reveal any candidate areas. Additionally, gene-expression analysis upon perturbation of gene expression did not reveal any indications of co-regulation between 11q13 genes either. Functionally however, we identified *RRM2* and *TXN* activation as two of the major altered downstream effects with oncogenic potential of the 11q13 amplification. This is remarkable since *TXN* was originally discovered as activator of the ribonucleotide reducing function of the RNR enzyme, of which *RRM2* is the rate-limiting subunit⁴⁵⁵. Since this initial discovery, it has become apparent that in its function as electron donor for RNR, *TXN* is also essential in nucleotide synthesis⁴⁵⁶. Several drugs that directly target the *TXN* pathway have been shown to also affect RNR activity⁴⁵⁷⁻⁴⁵⁹. As such, these drugs killed cancer cells through the induction of both oxidative stress as well as replicative stress. The interaction between *TXN* and RNR has previously been

shown to contribute to cancer malignancy, implying potential cooperation between these genes⁴⁶⁰.

Thus, *ORAOV1* amplification – through increased activity of the thioredoxin pathway – might enhance *CCND1*-induced *RRM2* activity. Of note, *ORAOV1* has previously been found to physically interact with *PYCR1* and *PYCR2*¹⁹⁵, two proteins that are part of the *RRM2B* complex⁴⁶¹. As explained in **Chapter 4**, the RNR complex typically consists of *RRM1* and *RRM2*. However, under high stress conditions such as upon DNA damage or high oxidative stress levels, *RRM2B* expression can get favored over *RRM2*, resulting in a *RRM1-RRM2B* complex that protects against further DNA damage and oxidative stress in a *PYCR*-dependent fashion⁴⁶¹⁻⁴⁶³. It is unclear whether *ORAOV1* is involved in the interaction between *PYCR* and *RRM2B*, but if so, it would provide a link between *ORAOV1* and the RNR complex in both normal and high stress conditions. However, *RRM2B* expression and binding to *RRM1* is *TP53*-dependent⁴⁶²⁻⁴⁶⁴. Since *11q13* amplification virtually always occurs in a *TP53*-mutant background, RNR activation through this pathway is likely to be less active in these HNSCC tumors, and therefore might be more dependent on the *ORAOV1-TXN* axis.

Implications for therapy

11q13 amplification is a frequent event in SCC and correlates with a poor prognosis, yet is not being clinically used for diagnosis, prognosis, or treatment strategy. However, even with just relatively simple non-invasive diagnostic tools such as saliva-based biosensors⁴⁶⁵, the presence of the amplification can aid in diagnosis and determination of therapeutic strategy as *11q13*-amplified tumors tend to be more aggressive and in a more advanced stage. Furthermore, since *11q13* amplification might be a determining factor in cancer development, direct targeting of amplicon-induced oncogenic pathways provides potential targeted treatment options.

Currently, there is a good understanding of the mutational landscape of HNSCCs, yet this understanding has not translated to improvement or development of sufficient targeted therapies⁴⁶⁶. Especially for *11q13*-amplification bearing tumors, the options are limited as the amplification negatively correlates with efficacy of PD-1 blockade therapy^{248,249}. An in-depth molecular understanding of the oncogenic signaling upon frequent genetic alterations can provide further insights into potential treatment strategies.

For example, in **Chapter 4** we show that *11q13* amplification induces *CCND1*-oncogene addiction, but that this addiction is independent from *CDK4/6*. Moreover, we show that normal keratinocytes are highly dependent on *CCND2*. Historically, cyclin D1-activity has been targeted through *CDK4-6* inhibitors such as Palbociclib. However, these drugs target both cyclin D1 and cyclin D2, thus also affecting non-cancerous cells. Moreover, the *11q13*-amplified cells are less dependent on the *CDK4-6* functions

of cyclin D1. Therefore, we propose the direct targeting of cyclin D1 as a preferred strategy. Targeting oncoproteins such as cyclin D1 is an attractive therapeutic option due to the strong effect of these proteins on tumorigenesis. However, direct targeting of cyclin D1 is currently challenging due to the absence of enzymatic activity of the protein⁹⁵. Therefore, we explored further downstream mechanisms of the 11q13 amplifications. Our results in **Chapter 3**, **Chapter 4**, and **Chapter 5** indicate that *CCND1* and *ORAOV1* are the biggest drivers of proliferation on the 11q13 amplicon, and that they exert their effects at least partially through *RRM2* and *TXN*, respectively. As *RRM2* and *TXN* may cooperate with one another during tumorigenesis, targeting the interaction between these two proteins may potentially neutralize the oncogenic effect exhibited by the 11q13 amplicon. Thus, interventions targeting these pathways provides novel potential therapeutic approaches and future studies should investigate these options further.

Current approaches to treat HNSCC are reliant on surgery, radiation and chemotherapeutics such as cisplatin. However, patients often develop resistance over the course of treatment^{68,467} and almost half of patients have diseases recurrence within two years. Therapy resistance is - like with most cancers - therefore one of the big challenges to overcome in the therapeutic approaches for HNSCCs. An increased understanding of genetic and cellular alterations that are predictive of therapy resistance and approaches to target these alterations can significantly contribute to improved patient outcome⁴⁶⁸. There are currently no studies reported that directly investigate a potential link between 11q13 amplification and therapy resistance. However, the poor prognosis and frequent recurrence of disease of 11q13-amplified HNSCC suggests aggressiveness and therapy-evading properties in these tumors. Mechanisms of resistance, whether intrinsic or acquired, are very diverse and hard to predict and therefore challenging to anticipate. Cellular processes implicated in therapy resistance work through evasion of cell death and include increased reactive oxygen species capacity and bypassing the DNA Damage Response, amongst others. Targeting mechanisms of resistance in HNSCC will increase long-term treatment responses and improve patient outcomes.

Both *RRM2* and *TXN* expression have been reported to be upregulated in therapeutically resistant cells, and both proteins are mediators of this resistance^{351,407,408,469}. High *RRM2* levels protect against DNA damage induced apoptosis and as such can induce chemoresistance³⁵¹. Similarly, *TXN* levels have been reported to be increased upon cisplatin treatment and *TXN* levels correlate to a poor response to treatment of cervical SCC397. Mechanistically, this is likely due to the effect *TXN* has on oxidative stress, as these chemotherapeutics induce apoptosis - partially - in a oxidative-stress dependent manner in HNSCC^{404,406}.

Thus, amplification of the 11q13 region may contribute to a mechanism of resistance to frequently used chemotherapeutics through the downstream effectors *RRM2* and

TXN. Therefore, it is worthwhile to further explore combinatorial treatment strategies that combine chemotherapeutics with targeting 11q13 effectors.

Previous studies report that inhibition of RRM2 indeed sensitizes cancer cells to several types of therapy, including radiation and chemotherapy^{317,318,349,351}. Moreover, several clinical trials show that inhibition of RNR activity is most effective in combination with radiation or chemotherapy^{355-358,365-367}. Similarly, co-treatment with the TXN inhibitor PX12 can overcome resistance to chemotherapeutics or radiotherapy in multiple myeloma and colorectal cancer, respectively^{469,470}. Thus, the genetic dissection of the 11q13 amplicon in HNSCC reveals novel potential strategies to treat 11q13-amplified tumors and overcome therapy resistance.

Modeling and interpreting copy number alterations in cancer

CNAs are a frequent and important event in tumorigenesis, affecting approximately 30% of the genome of cancer cells⁴⁷¹⁻⁴⁷⁴. The pattern of these CNAs is linked to clinical outcome, suggesting a selection for specific genetic functions^{239,471,472,475}. CNAs are challenging to model and study, and in the past decades research has mostly focused on known driver genes of the CNA, thereby disregarding the effect that co-amplified or co-deleted genes might pose on the tumorigenic process. However, it has become apparent that these “passenger” genes can have significant effects on the tumorigenic process^{476,477}. Thus, it is important to consider each CNA as a whole without simplifying it to a single driver element. However, just a single CNA might already contain hundreds of genetic elements, making it challenging to identify the driver events in these CNAs. Generally, the importance of a CNA can be determined based on a balance between the frequency with which it occurs in cancer versus the instability of the chromosomal region and computational approaches can decipher these different structural signatures⁴⁷⁸⁻⁴⁸¹.

As opposed to single nucleotide variations, CNAs need two breakpoints in the DNA followed by some type of genetic rearrangement. There are several mechanism that can regulate breakpoints, including epigenetic regulation^{482,483}. It is possible that this regulation dictates the length of CNA. However, the different frequencies in which they can occur in different cancer types argues for specific selective pressures and poses the regulators merely as enabling. This is further supported by the finding that chromosomal deletions are bordered by deletion-limiting genes: essential genes that limit the extent of the amplification⁴⁸⁴. This argues that functionality of elements affects the extent of the amplicon.

In the presented work we dissected the 11q13 amplicon through a combination of computational and experimental approaches and found that there are 3 driver elements located on the amplicon. We found that not only strong oncogenic effects by the known oncogenic “driver” *CCND1*, but also by the “passenger” neighbor

gene *ORAOVI*. However, other genes that were nearly equally frequently amplified - such as *FGF19* - had no effect on SCC tumorigenesis, despite known functions in hepatocellular carcinoma^{199,200}. Studies on other amplifications in other cancer types have found similar patterns of cooperation on amplicons. For example, analysis of the 14q13 amplicon in lung cancer identified three transcription factors that cooperate to stimulate oncogenic proliferation⁴⁸⁵.

Genomic deletions also typically span multiple genes and in recent years research has started to look more closely at the genomic loci alongside the driver tumor suppressor genes. Tumor suppressor genes can be inactivated both through a loss of function mutation or through chromosomal deletion, and the question has been raised whether these two types of mutations have a similar effect. Inactivation of *CDKN2A* is one of the most frequent events across cancer and occurs both through a single nucleotide mutation or through larger chromosomal deletion. The latter results in co-deletion with several genes, including a cluster of interferon genes. Recent studies have found that this co-deletion of interferon genes serves in the tumors immune escape implying a biologically additive function to copy number deletions over mutations^{486,487}.

In conclusion, we propose that a comprehensive approach for the functional analysis of copy number alterations in cancer *must* be employed in order to truly determine the impact of a CNA in cancer. The reductionist approach that many have previously used to study CNAs in cancer can inaccurately ascribe all tumor-promoting functions of a CNA to a single well-described gene while ignoring the less studied genes on the amplicon. The 11q13 amplicon is a perfect example of this phenomenon. *CCND1* - a well-known pan-cancer oncogene - has dominated studies of 11q13 while an equally potent oncogene - *ORAOVI*, as described here - has been almost entirely ignored. By utilizing a comprehensive approach in our study of the 11q13 amplicon, we have not only increased our understanding of this common CNA but also identify new pathways that can be evaluated for therapeutic intervention. Overall, we hope this work can be used as a blueprint for the dissection of other CNAs in cancer, elucidating driver elements and mechanisms of these frequent oncogenic events.

Appendix

References

Nederlandse samenvatting

Curriculum Vitae

Dankwoord



References

- 1 Groeger, S. & Meyle, J. Oral mucosal epithelial cells. *Front. Immunol.* **10**, 1-22 (2019).
- 2 Madison, K. C. Barrier function of the skin: 'La Raison d'Être' of the epidermis. *J. Invest. Dermatol.* **121**, 231-241 (2003).
- 3 Proksch, E., Brandner, J. M. & Jensen, J. M. The skin: An indispensable barrier. *Exp. Dermatol.* **17**, 1063-1072 (2008).
- 4 Bikle, D. D., Nemanic, M. K., Gee, E. & Elias, P. 1,25-Dihydroxyvitamin D3 production by human keratinocytes. Kinetics and regulation. *J. Clin. Invest.* **78**, 557-566 (1986).
- 5 Zimmerman, A., Bai, L. & Ginty, D. D. The gentle touch receptors of mammalian skin. *Science (80-)*. **346**, 950-954 (2014).
- 6 Nakamura, K. Central circuitries for body temperature regulation and fever. *Am. J. Physiol. - Regul. Integr. Comp. Physiol.* **301**, (2011).
- 7 Driskell, R. R., Jahoda, C. A. B., Chuong, C. M., Watt, F. M. & Horsley, V. Defining dermal adipose tissue. *Exp. Dermatol.* **23**, 629-631 (2014).
- 8 Bikle, D. D., Xie, Z. & Tu, C. L. Calcium regulation of keratinocyte differentiation. *Expert Rev. Endocrinol. Metab.* **7**, 461-472 (2012).
- 9 Fuchs, E. Epidermal differentiation: The bare essentials. *J. Cell Biol.* **111**, 2807-2814 (1990).
- 10 Szpaderska AM, Zuckerman, J. & DiPietro, L. Differential Injury Responses in Oral Mucosal and Cutaneous Wounds. *J Dent Res* **82**, 621-626 (2003).
- 11 Chen, L. *et al.* Positional differences in the wound transcriptome of skin and oral mucosa. *BMC Genomics* **11**, 1-15 (2010).
- 12 Turabelidze, A. *et al.* Intrinsic differences between oral and skin keratinocytes. *PLoS One* **9**, 1-10 (2014).
- 13 Elias, P. M. Epidermal Lipids, Barrier Function, and Desquamation. *J. Invest. Dermatol.* **80**, S44-S49 (1983).
- 14 Nemes, Z. & Steinert, P. M. Bricks and mortar of the epidermal barrier. *Exp. Mol. Med.* **31**, 5-19 (1999).
- 15 Blanpain, C. & Fuchs, E. Epidermal stem cells of the skin. *Annu. Rev. Cell Dev. Biol.* **22**, 339-373 (2006).
- 16 Page, M. E., Lombard, P., Ng, F., Göttgens, B. & Jensen, K. B. The epidermis comprises autonomous compartments maintained by distinct stem cell populations. *Cell Stem Cell* **13**, 471-482 (2013).
- 17 Candi, E., Schmidt, R. & Melino, G. The cornified envelope: A model of cell death in the skin. *Nat. Rev. Mol. Cell Biol.* **6**, 328-340 (2005).
- 18 Moltrasio, C., Romagnuolo, M. & Marzano, A. V. Epigenetic Mechanisms of Epidermal Differentiation. *Int. J. Mol. Sci.* **23**, (2022).
- 19 Li, J. & Sen, G. L. Post-Transcriptional Mechanisms Regulating Epidermal Stem and Progenitor Cell Self-Renewal and Differentiation. *J. Invest. Dermatol.* **136**, 746-752 (2016).
- 20 Slominski, A. T., Zmijewski, M. A., Plonka, P. M., Szaflarski, J. P. & Paus, R. How UV Light Touches the Brain and Endocrine System Through Skin, and Why. *Endocrinology* **159**, 1992-2007 (2018).
- 21 Kypriotou, M., Huber, M. & Hohl, D. The human epidermal differentiation complex: Cornified envelope precursors, S100 proteins and the 'fused genes' family. *Exp. Dermatol.* **21**, 643-649 (2012).
- 22 Abhishek, S. & Krishnan, S. P. Epidermal differentiation complex: A review on its epigenetic regulation and potential drug targets. *Cell J* **18**, 1-6 (2016).
- 23 Koster, M. I. *et al.* P63 Induces Key Target Genes Required for Epidermal Morphogenesis. *Proc. Natl. Acad. Sci. U. S. A.* **104**, 3255-3260 (2007).

- 24 Yang, A. *et al.* P63 Is Essential for Regenerative Proliferation in Limb, Craniofacial and Epithelial Development. *Nature* **398**, 714-718 (1999).
- 25 Truong, A. B., Kretz, M., Ridky, T. W., Kimmel, R. & Khavari, P. A. P63 Regulates Proliferation and Differentiation of Developmentally Mature Keratinocytes. *Genes Dev.* **20**, 3185-3197 (2006).
- 26 Soares, E. & Zhou, H. Master regulatory role of p63 in epidermal development and disease. *Cell. Mol. Life Sci.* **75**, 1179-1190 (2018).
- 27 Nguyen, B. C. *et al.* Cross-regulation between Notch and p63 in keratinocyte commitment to differentiation. *Genes Dev.* **20**, 1028-1042 (2006).
- 28 Koh, L. F., Ng, B. K., Bertrand, J. & Thierry, F. Transcriptional control of late differentiation in human keratinocytes by TAp63 and Notch. *Exp. Dermatol.* **24**, 754-760 (2015).
- 29 Moriyama, M. *et al.* Multiple Roles of Notch Signaling in the Regulation of Epidermal Development. *Dev. Cell* **14**, 594-604 (2008).
- 30 Watt, F. M., Estrach, S. & Ambler, C. A. Epidermal Notch signalling: differentiation, cancer and adhesion. *Curr. Opin. Cell Biol.* **20**, 171-179 (2008).
- 31 Blanpain, C., Lowry, W. E., Pasolli, H. A. & Fuchs, E. Canonical notch signaling functions as a commitment switch in the epidermal lineage. *Genes Dev.* **20**, 3022-3035 (2006).
- 32 Eckert, R. L. *et al.* Keratinocyte survival, differentiation, and death: Many roads lead to mitogen-activated protein kinase. *J. Investig. Dermatology Symp. Proc.* **7**, 36-40 (2002).
- 33 Pastar, I. *et al.* Epithelialization in Wound Healing: A Comprehensive Review. *Adv. Wound Care* **3**, 445-464 (2014).
- 34 Dekoninck, S. & Blanpain, C. Stem cell dynamics, migration and plasticity during wound healing. *Nat. Cell Biol.* **21**, 18-24 (2019).
- 35 Aragona, M. *et al.* Defining stem cell dynamics and migration during wound healing in mouse skin epidermis. *Nat. Commun.* **8**, (2017).
- 36 Park, S. *et al.* Tissue-scale coordination of cellular behaviour promotes epidermal wound repair in live mice. *Nat. Cell Biol.* **19**, 155-163 (2017).
- 37 El-Serafi, A. T., El-Serafi, I., Steinvall, I., Sjöberg, F. & Elmasry, M. A Systematic Review of Keratinocyte Secretions: A Regenerative Perspective. *Int. J. Mol. Sci.* **23**, (2022).
- 38 Brazil, J. C., Quiros, M., Nusrat, A. & Parkos, C. A. Innate immune cell-epithelial crosstalk during wound repair. *J. Clin. Invest.* **129**, 2983-2993 (2019).
- 39 Roupé, K. M. *et al.* Injury is a major inducer of epidermal innate immune responses during wound healing. *J. Invest. Dermatol.* **130**, 1167-1177 (2010).
- 40 Rousselle, P., Braye, F. & Dayan, G. Re-epithelialization of adult skin wounds: Cellular mechanisms and therapeutic strategies. *Adv. Drug Deliv. Rev.* **146**, 344-365 (2019).
- 41 Andreadis, S. T., Hamoen, K. E., Yarmush, M. L. & Morgan, J. R. Keratinocyte growth factor induces hyperproliferation and delays differentiation in a skin equivalent model system. *FASEB J.* **15**, 898-906 (2001).
- 42 Tang, A. & Gilchrist, B. A. Regulation of keratinocyte growth factor gene expression in human skin fibroblasts. *J. Dermatol. Sci.* **11**, 41-50 (1996).
- 43 Rubin, J. S. *et al.* Purification and characterization of a newly identified growth factor specific for epithelial cells. *Proc. Natl. Acad. Sci. U. S. A.* **86**, 802-806 (1989).
- 44 Honari, S. Topical therapies and antimicrobials in the management of burn wounds. *Crit. Care Nurs. Clin. North Am.* **16**, 1-11 (2004).
- 45 Feramisco, J. D., Sadreyev, R. I., Murray, M. L., Grishin, N. V. & Tsao, H. Phenotypic and genotypic analyses of genetic skin disease through the online mendelian inheritance in man (OMIM) database. *J. Invest. Dermatol.* **129**, 2628-2636 (2009).
- 46 Morren, M. A. *et al.* Challenges in Treating Genodermatoses: New Therapies at the Horizon. *Front. Pharmacol.* **12**, 1-25 (2022).

- 47 Gálvez, V. *et al.* Efficient CRISPR-Cas9-Mediated Gene Ablation in Human Keratinocytes to Recapitulate Genodermatoses: Modeling of Netherton Syndrome. *Mol. Ther. - Methods Clin. Dev.* **18**, 280-290 (2020).
- 48 Descargues, P. *et al.* Corneodesmosomal cadherins are preferential targets of stratum corneum trypsin- and chymotrypsin-like hyperactivity in Netherton syndrome. *J. Invest. Dermatol.* **126**, 1622-1632 (2006).
- 49 Egelrud, T. *et al.* hK5 and hK7, two serine proteinases abundant in human skin, are inhibited by LEKTI domain 6. *Br. J. Dermatol.* **153**, 1200-1203 (2005).
- 50 Deraison, C. *et al.* LEKTI Fragments Specifically Inhibit KLK5, KLK7, and KLK14 and Control Desquamation through a pH-dependent Interaction. *Mol. Biol. Cell* **18**, 3607-3619 (2007).
- 51 Fine, J. D. *et al.* Inherited epidermolysis bullosa: Updated recommendations on diagnosis and classification. *J. Am. Acad. Dermatol.* **70**, 1103-1126 (2014).
- 52 Lunstrum, G. P., Sakai, L. Y., Keene, D. R., Morris, N. P. & Burgeson, R. E. Large complex globular domains of Type VII procollagen contribute to the structure of anchoring fibrils. *J. Biol. Chem.* **261**, 9042-9048 (1986).
- 53 Sakai, L. Y., Keene, D. R., Morris, N. P. & Burgeson, R. E. Type VII collagen is a major structural component of anchoring fibrils. *J. Cell Biol.* **103**, 1577-1586 (1986).
- 54 Latella, M. C. *et al.* Correction of Recessive Dystrophic Epidermolysis Bullosa by Transposon-Mediated Integration of COL7A1 in Transplantable Patient-Derived Primary Keratinocytes. *J. Invest. Dermatol.* **137**, 836-844 (2017).
- 55 Bonafont, J. *et al.* Clinically Relevant Correction of Recessive Dystrophic Epidermolysis Bullosa by Dual sgRNA CRISPR/Cas9-Mediated Gene Editing. *Mol. Ther.* **27**, 986-998 (2019).
- 56 Wu, W. *et al.* Efficient in vivo gene editing using ribonucleoproteins in skin stem cells of recessive dystrophic epidermolysis bullosa mouse model. *Proc. Natl. Acad. Sci. U. S. A.* **114**, 1660-1665 (2017).
- 57 Choquet, H., Ashrafzadeh, S., Kim, Y., Asgari, M. M. & Jorgenson, E. Genetic and environmental factors underlying keratinocyte carcinoma risk. *JCI Insight* **5**, 1-14 (2020).
- 58 Johnson, D. E. *et al.* Head and neck squamous cell carcinoma. *Nat. Rev. Dis. Prim.* **6**, (2020).
- 59 Bray, F. *et al.* Global cancer statistics 2018: GLOBOCAN estimates of incidence and mortality worldwide for 36 cancers in 185 countries. *CA. Cancer J. Clin.* **68**, 394-424 (2018).
- 60 Sung, H. *et al.* Global Cancer Statistics 2020: GLOBOCAN Estimates of Incidence and Mortality Worldwide for 36 Cancers in 185 Countries. *CA. Cancer J. Clin.* **71**, 209-249 (2021).
- 61 Ferlay, J. *et al.* Estimating the global cancer incidence and mortality in 2018: GLOBOCAN sources and methods. *Int. J. Cancer* **144**, 1941-1953 (2019).
- 62 Smeets, S. J. *et al.* Genome-wide DNA copy number alterations in head and neck squamous cell carcinomas with or without oncogene-expressing human papillomavirus. *Oncogene* **25**, 2558-2564 (2006).
- 63 Slebos, R. J. C. *et al.* Gene expression differences associated with human papillomavirus status in head and neck squamous cell carcinoma. *Clin. Cancer Res.* **12**, 701-709 (2006).
- 64 Braakhuis, B. J. M. *et al.* Genetic patterns in head and neck cancers that contain or lack transcriptionally active human papillomavirus. *J. Natl. Cancer Inst.* **96**, 998-1006 (2004).
- 65 Ang, K. K. *et al.* Human Papillomavirus and Survival of Patients with Oropharyngeal Cancer. *N. Engl. J. Med.* **363**, 31-36 (2010).
- 66 Fakhry, C. *et al.* Improved survival of patients with human papillomavirus-positive head and neck squamous cell carcinoma in a prospective clinical trial. *J. Natl. Cancer Inst.* **100**, 261-269 (2008).

- 67 Ragin, C. C. R. & Taioli, E. Survival of squamous cell carcinoma of the head and neck in relation to human papillomavirus infection: Review and meta-analysis. *Int. J. Cancer* **121**, 1813-1820 (2007).
- 68 Bos, T., Ratti, J. A. & Harada, H. Targeting Stress-Response Pathways and Therapeutic Resistance in Head and Neck Cancer. *Front. Oral Heal.* **2**, 1-12 (2021).
- 69 Fang, M., Huang, W., Mo, D., Zhao, W. & Huang, R. Association of Five Snps in Cytotoxic T-Lymphocyte Antigen 4 and Cancer Susceptibility: Evidence from 67 Studies. *Cell. Physiol. Biochem.* **47**, 414-427 (2018).
- 70 Cadoni, G. *et al.* A review of genetic epidemiology of head and neck cancer related to polymorphisms in metabolic genes, cell cycle control and alcohol metabolism. *Acta Otorhinolaryngol. Ital.* **32**, 1-11 (2012).
- 71 Schultz, J. *et al.* Induction chemotherapy with TPF (Docetaxel, Carboplatin and Fluorouracil) in the treatment of locally advanced squamous cell carcinoma of the head and neck. *Oncol. Rep.* **24**, 1213-1216 (2010).
- 72 Vermorcken, J. B. *et al.* Cisplatin, Fluorouracil, and Docetaxel in Unresectable Head and Neck Cancer. *N. Engl. J. Med.* **357**, 1695-1704 (2007).
- 73 Bernier, J. *et al.* Postoperative irradiation with or without concomitant chemotherapy for locally advanced head and neck cancer. *Cancer/Radiotherapie* **9**, 203-204 (2005).
- 74 Cooper, J. S. *et al.* Postoperative Concurrent Radiotherapy and Chemotherapy for High-Risk Squamous-Cell Carcinoma of the Head and Neck. *N. Engl. J. Med.* **350**, 1937-1944 (2004).
- 75 Bonner, J. A. *et al.* Radiotherapy plus cetuximab for locoregionally advanced head and neck cancer: 5-year survival data from a phase 3 randomised trial, and relation between cetuximab-induced rash and survival. *Lancet Oncol.* **11**, 21-28 (2010).
- 76 Mehanna, H. *et al.* Radiotherapy plus cisplatin or cetuximab in low-risk human papillomavirus-positive oropharyngeal cancer (De-ESCALaTE HPV): an open-label randomised controlled phase 3 trial. *Lancet* **393**, 51-60 (2019).
- 77 Gillison, M. L. *et al.* Radiotherapy plus cetuximab or cisplatin in human papillomavirus-positive oropharyngeal cancer (NRG Oncology RTOG 1016): a randomised, multicentre, non-inferiority trial. *Lancet* **393**, 40-50 (2019).
- 78 Ferris, R. L. *et al.* Nivolumab for Recurrent Squamous-Cell Carcinoma of the Head and Neck. *N. Engl. J. Med.* **375**, 1856-1867 (2016).
- 79 Seiwert, T. Y. *et al.* Safety and clinical activity of pembrolizumab for treatment of recurrent or metastatic squamous cell carcinoma of the head and neck (KEYNOTE-012): an open-label, multicentre, phase 1b trial. *Lancet Oncol.* **17**, 956-965 (2016).
- 80 Chaturvedi, A. K. *et al.* Human papillomavirus and rising oropharyngeal cancer incidence in the United States. *J. Clin. Oncol.* **29**, 4294-4301 (2011).
- 81 Pulte, D. & Brenner, H. Changes in Survival in Head and Neck Cancers in the Late 20th and Early 21st Century: A Period Analysis. *Oncologist* **15**, 994-1001 (2010).
- 82 Belbin, T. J. *et al.* Molecular classification of head and neck squamous cell carcinoma using cDNA microarrays. *Cancer Res.* **62**, 1184-1190 (2002).
- 83 Keck, M. K. *et al.* Integrative analysis of head and neck cancer identifies two biologically distinct HPV and three non-HPV subtypes. *Clin. Cancer Res.* **21**, 870-881 (2015).
- 84 Chung, C. H. *et al.* Molecular classification of head and neck squamous cell carcinomas using patterns of gene expression. *Cancer Cell* **5**, 489-500 (2004).
- 85 Leemans, C. R., Snijders, P. J. F. & Brakenhoff, R. H. The molecular landscape of head and neck cancer. *Nat. Rev. Cancer* **18**, 269-282 (2018).
- 86 Hanahan, D. & Weinberg, R. A. Hallmarks of cancer: The next generation. *Cell* **144**, 646-674 (2011).

- 87 Merlo, L. M. F., Pepper, J. W., Reid, B. J. & Maley, C. C. Cancer as an evolutionary and ecological process. *Nat. Rev. Cancer* **6**, 924-935 (2006).
- 88 Garraway, L. A. & Lander, E. S. Lessons from the cancer genome. *Cell* **153**, 17-37 (2013).
- 89 Paulson, T. G., Almasan, A., Brody, L. L. & Wahl, G. M. Gene Amplification in a p53-Deficient Cell Line Requires Cell Cycle Progression under Conditions That Generate DNA Breakage. *Mol. Cell. Biol.* **18**, 3089-3100 (1998).
- 90 Zhu, C. *et al.* Unrepaired DNA breaks in p53-deficient cells lead to oncogenic gene amplification subsequent to translocations. *Cell* **109**, 811-821 (2002).
- 91 Stransky, N. *et al.* The mutational landscape of head and neck squamous cell carcinoma. *Science (80-.)* **333**, 1157-1160 (2011).
- 92 Lawrence, M. S. *et al.* Comprehensive genomic characterization of head and neck squamous cell carcinomas. *Nature* **517**, 576-582 (2015).
- 93 Chung, C. H. *et al.* Genomic alterations in head and neck squamous cell carcinoma determined by cancer gene-targeted sequencing. *Ann. Oncol.* **26**, 1216-1223 (2015).
- 94 Levine, A. J. & Oren, M. The first 30 years of p53: Growing ever more complex. *Nat. Rev. Cancer* **9**, 749-758 (2009).
- 95 Musgrove, E. A., Caldon, C. E., Barraclough, J., Stone, A. & Sutherland, R. L. Cyclin D as a therapeutic target in cancer. *Nat. Rev. Cancer* **11**, 558-572 (2011).
- 96 van Kempen, P. M. W. *et al.* Clinical relevance of copy number profiling in oral and oropharyngeal squamous cell carcinoma. *Cancer Medicine* vol. 4 1525-1535 at <https://doi.org/10.1002/cam4.499> (2015).
- 97 Westra, W. H. *et al.* Human Cancer Biology Inverse Relationship between Human Papillomavirus-16 Infection and Disruptive p53 Gene Mutations in Squamous Cell Carcinoma of the Head and Neck. **14**, 366-369 (2008).
- 98 Michaud, D. S. *et al.* High-risk HPV types and head and neck cancer. *Int. J. Cancer* **135**, 1653-1661 (2014).
- 99 Rampias, T., Sasaki, C., Weinberger, P. & Psyrris, A. E6 and E7 gene silencing and transformed phenotype of human papillomavirus 16-positive oropharyngeal cancer cells. *J. Natl. Cancer Inst.* **101**, 412-423 (2009).
- 100 Califano, J. *et al.* Genetic progression model for head and neck cancer: Implications for field cancerization. *Cancer Res.* **56**, 2488-2492 (1996).
- 101 Martincorena, I. *et al.* High burden and pervasive positive selection of somatic mutations in normal human skin. *Science (80-.)* **348**, 880-886 (2015).
- 102 Fowler, J. C. *et al.* Selection of oncogenic mutant clones in normal human skin varies with body site. *Cancer Discov.* **11**, 340-361 (2021).
- 103 Hall, M. W. J., Jones, P. H. & Hall, B. A. Relating evolutionary selection and mutant clonal dynamics in normal epithelia. *J. R. Soc. Interface* **16**, (2019).
- 104 Murai, K. *et al.* Epidermal Tissue Adapts to Restrain Progenitors Carrying Clonal p53 Mutations. *Cell Stem Cell* **23**, 687-699.e8 (2018).
- 105 Martincorena, I. *et al.* Somatic mutant clones colonize the human esophagus with age. *Science (80-.)* **917**, 911-917 (2018).
- 106 Bhattacharya, A. *et al.* Two distinct routes to oral cancer differing in genome instability and risk for cervical node metastasis. *Clin. Cancer Res.* **17**, 7024-7034 (2011).
- 107 Veeramachaneni, R. *et al.* Analysis of head and neck carcinoma progression reveals novel and relevant stage-specific changes associated with immortalisation and malignancy. *Sci. Rep.* **9**, 1-17 (2019).
- 108 Lorsch, B. J. R., Collins, F. S. & Lippincott-schwartz, J. Fixing problems with cell lines. *Science (80-.)* **346**, 1452-1453 (2014).
- 109 Geraghty, R. J., Davis, J. M., Downward, J., Freshney, R. I. & Knezevic, I. Guidelines for the use of cell lines in biomedical research. *Br. J. Cancer* **111**, 1021-1046 (2014).

- 110 Alston-Roberts, C. *et al.* Cell line misidentification: The beginning of the end. *Nature Reviews Cancer* vol. 10 441-448 at <https://doi.org/10.1038/nrc2852> (2010).
- 111 Green, H., Kehinde, O. & Thomas, J. Growth of cultured human epidermal cells into multiple epithelia suitable for grafting. *Proc. Natl. Acad. Sci. U. S. A.* **76**, 5665-5668 (1979).
- 112 O'Connor, N. E., Mulliken, J. B., Banks-Schlegel, S., Kehinde, O. & Green, H. Grafting of burns with cultured epithelium prepared from autologous epidermal cells. *Lancet* **317**, 75-78 (1981).
- 113 Petrof, G., Abdul-Wahab, A. & McGrath, J. A. Cell therapy in dermatology. *Cold Spring Harb. Perspect. Med.* **4**, (2014).
- 114 Cirodde, A. *et al.* Cultured epithelial autografts in massive burns: A single-center retrospective study with 63 patients. *Burns* **37**, 964-972 (2011).
- 115 Sood, R. *et al.* Cultured epithelial autografts for coverage of large burn wounds in eighty-eight patients: The Indiana university experience. *J. Burn Care Res.* **31**, 559-568 (2010).
- 116 Hefton, J. M., Finkelstein, J. L., Madden, M. R. & Thomas Shires, G. Grafting of Burn Patients With Allografts of Cultured Epidermal Cells. *Lancet* **322**, 428-430 (1983).
- 117 Brain, A. *et al.* Survival of cultured allogenic keratinocytes transplanted to deep dermal bed assessed with probe specific for Y chromosome. *Br. Med. J.* **298**, 917-919 (1989).
- 118 Burt, A. M. *et al.* Survival of cultured allografts in patients with burns assessed with probe specific for Y chromosome. *Br. Med. J.* **298**, 915-917 (1989).
- 119 Dickerson, J. E. *et al.* Cell Persistence of Allogeneic Keratinocytes and Fibroblasts Applied in a Fibrin Matrix to Acute, Full Thickness Wounds. *Cell Med.* **4**, 149-152 (2013).
- 120 Osborn, M. J. *et al.* Base Editor Correction of COL7A1 in Recessive Dystrophic Epidermolysis Bullosa Patient-Derived Fibroblasts and iPSCs. *J. Invest. Dermatol.* **140**, 338-347.e5 (2020).
- 121 Phillips, T. J., Bhawan, J., Leigh, I. M., Baum, H. J. & Gilchrist, B. A. Cultured epidermal autografts and allografts: A study of differentiation and allograft survival. *J. Am. Acad. Dermatol.* **23**, 189-198 (1990).
- 122 Wendt, J. R., Ulich, T. & Rao, P. N. Long-term survival of human skin allografts in patients with immunosuppression. *Plast. Reconstr. Surg.* **113**, 1347-1354 (2004).
- 123 Hancock, K. & Leigh, I. M. Cultured keratinocytes and keratinocyte grafts. *Br. Med. J.* **299**, 1179-1180 (1989).
- 124 Mencia, Á. *et al.* Deletion of a Pathogenic Mutation-Containing Exon of COL7A1 Allows Clonal Gene Editing Correction of RDEB Patient Epidermal Stem Cells. *Mol. Ther. - Nucleic Acids* **11**, 68-78 (2018).
- 125 Chamorro, C. *et al.* Gene Editing for the Efficient Correction of a Recurrent COL7A1 Mutation in Recessive Dystrophic Epidermolysis Bullosa Keratinocytes. *Mol. Ther. - Nucleic Acids* **5**, e307 (2016).
- 126 Izmiryan, A. *et al.* Ex Vivo COL7A1 Correction for Recessive Dystrophic Epidermolysis Bullosa Using CRISPR/Cas9 and Homology-Directed Repair. *Mol. Ther. - Nucleic Acids* **12**, 554-567 (2018).
- 127 Kocher, T. *et al.* Improved Double-Nicking Strategies for COL7A1-Editing by Homologous Recombination. *Mol. Ther. - Nucleic Acids* **18**, 496-507 (2019).
- 128 Brinkman, E. K., Chen, T., Amendola, M. & Van Steensel, B. Easy quantitative assessment of genome editing by sequence trace decomposition. *Nucleic Acids Res.* **42**, 1-8 (2014).
- 129 Hammerman, P. S. *et al.* Comprehensive genomic characterization of squamous cell lung cancers. *Nature* **489**, 519-525 (2012).
- 130 Chang, D. & Shain, A. H. The landscape of driver mutations in cutaneous squamous cell carcinoma. *npj Genomic Med.* **6**, 1-10 (2021).

- 131 Shi, H., Smits, J. P. H., van den Bogaard, E. H. & Brewer, M. G. Research Techniques Made Simple: Delivery of the CRISPR/Cas9 Components into Epidermal Cells. *J. Invest. Dermatol.* **141**, 1375-1381.e1 (2021).
- 132 Jayarajan, V., Kounatidou, E., Qasim, W. & Di, W. L. Ex vivo gene modification therapy for genetic skin diseases—recent advances in gene modification technologies and delivery. *Exp. Dermatol.* **30**, 887-896 (2021).
- 133 Distler, J. H. W. *et al.* Nucleofection: A new, highly efficient transfection method for primary human keratinocytes. *Exp. Dermatol.* **14**, 315-320 (2005).
- 134 Kim, S., Kim, D., Cho, S. W., Kim, J. & Kim, J. S. Highly efficient RNA-guided genome editing in human cells via delivery of purified Cas9 ribonucleoproteins. *Genome Res.* **24**, 1012-1019 (2014).
- 135 Liang, X. *et al.* Rapid and highly efficient mammalian cell engineering via Cas9 protein transfection. *J. Biotechnol.* **208**, 44-53 (2015).
- 136 Tartaglia-Polcini, A. *et al.* SPINK5, the defective gene in Netherton syndrome, encodes multiple LEKTI isoforms derived from alternative pre-mRNA processing. *J. Invest. Dermatol.* **126**, 315-324 (2006).
- 137 Thomas, A. C. *et al.* ABCA12 Is the Major Harlequin Ichthyosis Gene. *J. Invest. Dermatol.* **126**, 2408-2413 (2006).
- 138 Walker, J. A. & Upadhyaya, M. Emerging therapeutic targets for neurofibromatosis type 1. *Expert Opin. Ther. Targets* **22**, 419-437 (2018).
- 139 Anzalone, A. V. *et al.* Search-and-replace genome editing without double-strand breaks or donor DNA. *Nature* **576**, 149-157 (2019).
- 140 Kim, E. H. & Lee, S. H. Efficacy of Cultured Allogeneic Keratinocytes in Treatment of Deep Second-Degree Burn. *J. Burn Care Res.* **42**, 533-537 (2021).
- 141 Petrof, G. *et al.* Potential of Systemic Allogeneic Mesenchymal Stromal Cell Therapy for Children with Recessive Dystrophic Epidermolysis Bullosa. *J. Invest. Dermatol.* **135**, 2319-2321 (2015).
- 142 Rashidghamat, E. *et al.* Phase I/II open-label trial of intravenous allogeneic mesenchymal stromal cell therapy in adults with recessive dystrophic epidermolysis bullosa. *J. Am. Acad. Dermatol.* **83**, 447-454 (2020).
- 143 Wagner, J. E. *et al.* Bone Marrow Transplantation for Recessive Dystrophic Epidermolysis Bullosa. *N. Engl. J. Med.* **363**, 629-639 (2010).
- 144 Torikai, H. *et al.* Toward eliminating HLA class I expression to generate universal cells from allogeneic donors. *Blood* **122**, 1341-1349 (2013).
- 145 Gornalusse, G. G. *et al.* HLA-E-expressing pluripotent stem cells escape allogeneic responses and lysis by NK cells. *Nat. Publ. Gr.* **35**, 765-772 (2017).
- 146 Teklemariam, T., Zhao, L. & Hantash, B. M. Heterologous expression of mutated HLA-G1 reduces alloreactivity of human dermal fibroblasts. *Regen. Med.* **9**, 775-784 (2014).
- 147 Tamoutounour, S. *et al.* Keratinocyte-intrinsic MHCII expression controls microbiota-induced Th1 cell responses. *Proc. Natl. Acad. Sci. U. S. A.* **116**, 23643-23652 (2019).
- 148 Carr, M. M., McVittie, E., Guy, K., Gawkrödger, D. J. & Hunter, J. a. MHC class II antigen expression in normal human epidermis. *Immunology* **59**, 223-7 (1986).
- 149 Coleman, N. & Stanley, M. A. Analysis of HLA-DR expression on keratinocytes in cervical neoplasia. *Int. J. Cancer* **56**, 314-319 (1994).
- 150 Albanesi, C., Cavani, A. & Girolomoni, G. Interferon- γ -stimulated human keratinocytes express the genes necessary for the production of peptide-loaded MHC class II molecules. *J. Invest. Dermatol.* **110**, 138-142 (1998).
- 151 Aubock, J., Romani, N., Grubauer, G. & Fritsch, P. HLA-DR expression on keratinocytes is a common feature of diseased skin. *Br. J. Dermatol.* **114**, 465-472 (1986).

- 152 Lampert, I. A. Expression of HLA-DR (Ia like) antigen on epidermal keratinocytes in human dermatoses. *Clin Exp Immunol* **57**, 93-100 (1984).
- 153 Todd, D. J., Handley, J., Walsh, M., Dolan, O. & Burrows, D. Keratinocyte expression of class II MHC antigens in long-lasting allergic patch test reaction. *Contact Dermatitis* **26**, 22-26 (1992).
- 154 Griffiths, C. E. M., Voorhees, J. J. & Nickoloff, B. J. Gamma interferon induces different keratinocyte cellular patterns of expression of HLA-DR and DQ and intercellular adhesion molecule-I (ICAM-I) antigens. *Br. J. Dermatol.* **120**, 1-7 (1989).
- 155 Czernielewski, J. M. & Bagot, M. Class II MHC antigen expression by human keratinocytes results from lympho-epidermal interactions and gamma-interferon production. *Clin. Exp. Immunol.* **66**, 295-302 (1986).
- 156 Barker, J. N. W. N., Ophir, J. & MacDonald, D. M. Keratinocyte HLA-DR expression: the relationship to dermal lymphocytic infiltration. *Clin. Exp. Dermatol.* **12**, 397-399 (1987).
- 157 Deuse, T. *et al.* Hypoimmunogenic derivatives of induced pluripotent stem cells evade immune rejection in fully immunocompetent allogeneic recipients. *Nat. Biotechnol.* **37**, (2019).
- 158 Schlottmann, F., Strauss, S., Hake, K., Vogt, P. M. & Bucan, V. Down-Regulation of MHC Class I Expression in Human Keratinocytes Using Viral Vectors Containing USII Gene of Human Cytomegalovirus and Cultivation on Bovine Collagen-Elastin Matrix (Matriderm[®]): Potential Approach for an Immune-Privileged Skin Substitu. *Int. J. Mol.* **20**, (2019).
- 159 Mestrallet, G. *et al.* Immunosuppressive Properties of Epidermal Keratinocytes Differ According to Their Immaturity Status. *Front. Immunol.* **13**, 1-8 (2022).
- 160 Mestrallet, G. *et al.* Human keratinocytes inhibit cd4+ t-cell proliferation through tgfb1 secretion and surface expression of hla-g1 and pd-l1 immune checkpoints. *Cells* **10**, 1-18 (2021).
- 161 Esteban-Vives, R. *et al.* In vitro keratinocyte expansion for cell transplantation therapy is associated with differentiation and loss of basal layer derived progenitor population. *Differentiation* **89**, 137-145 (2015).
- 162 Van Den Bogaard, E. H. *et al.* Rho kinase inhibitor Y-27632 prolongs the life span of adult human keratinocytes, enhances skin equivalent development, and facilitates lentiviral transduction. *Tissue Eng. - Part A* **18**, 1827-1836 (2012).
- 163 Gandham, V. D. *et al.* Effects of Y27632 on keratinocyte procurement and wound healing. *Clin. Exp. Dermatol.* **38**, 782-786 (2013).
- 164 Fortunel, N. O. *et al.* KLF4 inhibition promotes the expansion of keratinocyte precursors from adult human skin and of embryonic-stem-cell-derived keratinocytes. *Nat. Biomed. Eng.* **3**, 985-997 (2019).
- 165 Mou, H. *et al.* Dual SMAD Signaling Inhibition Enables Long-Term Expansion of Diverse Epithelial Basal Cells. *Cell Stem Cell* **19**, 217-231 (2016).
- 166 Harkin, D. G., Dawson, R. A. & Upton, Z. Optimized delivery of skin keratinocytes by aerosolization and suspension in fibrin tissue adhesive. *Wound Repair Regen.* **14**, 354-363 (2006).
- 167 Duncan, C. O. *et al.* In vitro transfer of keratinocytes: Comparison of transfer from fibrin membrane and delivery by aerosol spray. *J. Biomed. Mater. Res. - Part B Appl. Biomater.* **73**, 221-228 (2005).
- 168 Kirsner, R. S. *et al.* Spray-applied cell therapy with human allogeneic fibroblasts and keratinocytes for the treatment of chronic venous leg ulcers: A phase 2, multicentre, double-blind, randomised, placebo-controlled trial. *Lancet* **380**, 977-985 (2012).
- 169 Kirsner, R. S. *et al.* Durability of healing from spray-applied cell therapy with human allogeneic fibroblasts and keratinocytes for the treatment of chronic venous leg ulcers: A 6-month follow-up. *Wound Repair Regen.* **21**, 682-687 (2013).

- 170 Horch, R. E., Bannasch, H., Kopp, J., Andree, C. & Stark, G. B. Single-cell suspensions of cultured human keratinocytes in fibrin-glue reconstitute the epidermis. *Cell Transplant.* **7**, 309-317 (1998).
- 171 Velander, P. *et al.* Cell Suspensions of Autologous Keratinocytes or Autologous Fibroblasts Accelerate the Healing of Full Thickness Skin Wounds in a Diabetic Porcine Wound Healing Model. *J. Surg. Res.* **157**, 14-20 (2009).
- 172 Gravante, G. *et al.* A randomized trial comparing ReCell® system of epidermal cells delivery versus classic skin grafts for the treatment of deep partial thickness burns. *Burns* **33**, 966-972 (2007).
- 173 Kirsner, R. S. *et al.* Phase 3 evaluation of HP802-247 in the treatment of chronic venous leg ulcers. *Wound Repair Regen.* **24**, 894-903 (2016).
- 174 Steinstraesser, L. *et al.* Skin Electroporation of a Plasmid Encoding hCAP-18 / LL-37 Host Defense Peptide Promotes Wound Healing. *Mol. Ther.* **22**, 734-742 (2014).
- 175 Lin, M. P. *et al.* Delivery of plasmid DNA expression vector for keratinocyte growth factor-1 using electroporation to improve cutaneous wound healing in a septic rat model. *Wound Repair Regen.* **14**, 618-624 (2006).
- 176 Bussi, M., Valente, G., Curato, M. P., Carlevato, M. T. & Cortesina, G. Is transposed skin transformed in major head and neck mucosal reconstruction? *Acta Otolaryngol.* **115**, 348-351 (1995).
- 177 Reilly, J. S., Behringer, W. H. & Trocki, I. Intraoral keloid: Complication of forehead flap. *Otolaryngol. - Head Neck Surg.* **88**, 139-141 (1980).
- 178 Cerami, E. *et al.* The cBio Cancer Genomics Portal: An open platform for exploring multidimensional cancer genomics data. *Cancer Discov.* **2**, 401-404 (2012).
- 179 Hoadley, K. A. *et al.* Cell-of-Origin Patterns Dominate the Molecular Classification of 10,000 Tumors from 33 Types of Cancer. *Cell* **173**, 291-304 (2018).
- 180 Lidereau, R. *et al.* Amplification of the int-2 gene in primary human breast tumors. *Oncogene Res.* **2**, 285-291 (1988).
- 181 Gerstung, M. *et al.* The evolutionary history of 2,658 cancers. *Nature* **578**, 122-128 (2020).
- 182 Zhang, W. *et al.* The chromosome 11q13.3 amplification associated lymph node metastasis is driven by miR-548k through modulating tumor microenvironment. *Mol. Cancer* **17**, 1-18 (2018).
- 183 Shuster, M. I. *et al.* A consistent pattern of RIN1 rearrangements in oral squamous cell carcinoma cell lines supports a breakage-fusion-bridge cycle model for 11q13 amplification. *Genes, Chromosom. Cancer* **28**, 153-63 (2000).
- 184 Huang, X., Gollin, S. M., Raja, S. & Godfrey, T. E. High-resolution mapping of the 11q13 amplicon and identification of a gene, TAOS1, that is amplified and overexpressed in oral cancer cells. *Proc. Natl. Acad. Sci. U. S. A.* **99**, 11369-11374 (2002).
- 185 Jarmuz-Szymczak, M. *et al.* Heterogeneity of 11q13 region rearrangements in laryngeal squamous cell carcinoma analyzed by microarray platforms and fluorescence in situ hybridization. *Mol. Biol. Rep.* **40**, 4161-4171 (2013).
- 186 Choi, Y. J. *et al.* The Requirement for Cyclin D Function in Tumor Maintenance. *Cancer Cell* **22**, 438-451 (2012).
- 187 Zwijnen, R. M. L. *et al.* CDK-independent activation of estrogen receptor by cyclin D1. *Cell* **88**, 405-415 (1997).
- 188 Zwijnen, R. M. L., Buckle, R. S., Hijmans, E. M., Loomans, C. J. M. & Bernards, R. Ligand-independent recruitment of steroid receptor coactivators to estrogen receptor by cyclin D1. *Genes Dev.* **12**, 3488-3498 (1998).
- 189 Knudsen, K. E., Cavenee, W. K. & Arden, K. C. D-type cyclins complex with the androgen receptor and inhibit its transcriptional transactivation ability. *Cancer Res.* **59**, 2297-2301 (1999).

- 190 Reutens, A. T. *et al.* Cyclin D1 binds the androgen receptor and regulates hormone-dependent signaling in a p300/CBP-associated factor (P/CAF)-dependent manner. *Mol. Endocrinol.* **15**, 797-811 (2001).
- 191 Fu, M. *et al.* Cyclin D1 inhibits peroxisome proliferator-activated receptor γ -mediated adipogenesis through histone deacetylase recruitment. *J. Biol. Chem.* **280**, 16934-16941 (2005).
- 192 Bienvenu, F. *et al.* Transcriptional role of cyclin D1 in development revealed by a genetic-proteomic screen. *Nature* **463**, 374-378 (2010).
- 193 Ha, S. Y., Yeo, S. Y., Lee, K. W. & Kim, S. H. Validation of ORAOV1 as a new treatment target in hepatocellular carcinoma. *J. Cancer Res. Clin. Oncol.* **147**, 423-433 (2021).
- 194 Jiang, L. *et al.* Oral cancer overexpressed 1 (ORAOV1): A regulator for the cell growth and tumor angiogenesis in oral squamous cell carcinoma. *Int. J. Cancer* **123**, 1779-1786 (2008).
- 195 Togashi, Y. *et al.* Frequent amplification of *oraov1* gene in esophageal squamous cell cancer promotes an aggressive phenotype via proline metabolism and ros production. *Oncotarget* **5**, 2962-2973 (2014).
- 196 Zhao, X. *et al.* RNAi-mediated downregulation of oral cancer overexpressed 1 (ORAOV1) inhibits vascular endothelial cell proliferation, migration, invasion, and tube formation. *J. Oral Pathol. Med.* **45**, 256-261 (2016).
- 197 Kir, S., Kliewer, S. A. & Mangelsdorf, D. J. Roles of FGF19 in liver metabolism. *Cold Spring Harb. Symp. Quant. Biol.* **76**, 139-144 (2011).
- 198 Fukumoto, S. Actions and mode of actions of FGF19 subfamily members. *Endocr. J.* **55**, 23-31 (2008).
- 199 Sawey, E. T. *et al.* Identification of a Therapeutic Strategy Targeting Amplified FGF19 in Liver Cancer by Oncogenomic Screening. *Cancer Cell* vol. 19 347-358 at <https://doi.org/10.1016/j.ccr.2011.01.040> (2011).
- 200 Desnoyers, L. R. *et al.* Targeting FGF19 inhibits tumor growth in colon cancer xenograft and FGF19 transgenic hepatocellular carcinoma models. *Oncogene* **27**, 85-97 (2008).
- 201 Gao, L. *et al.* FGF19 amplification reveals an oncogenic dependency upon autocrine FGF19/FGFR4 signaling in head and neck squamous cell carcinoma. *Oncogene* 2394-2404 (2018).
- 202 Li, F. *et al.* Enhanced autocrine FGF19/FGFR4 signaling drives the progression of lung squamous cell carcinoma, which responds to mTOR inhibitor AZD2104. *Oncogene* **39**, 3507-3521 (2020).
- 203 Zhang, X. *et al.* FGF19 genetic amplification as a potential therapeutic target in lung squamous cell carcinomas. *Thorac. Cancer* **8**, 655-665 (2017).
- 204 Jung, J. *et al.* Dynamic modulation of ANO1/TMEM16A HCO₃⁻ permeability by Ca²⁺/calmodulin. *Proc. Natl. Acad. Sci. U. S. A.* **110**, 360-365 (2013).
- 205 Yang, Y. D. *et al.* TMEM16A confers receptor-activated calcium-dependent chloride conductance. *Nature* **455**, 1210-1215 (2008).
- 206 Ayoub, C. *et al.* ANO1 amplification and expression in HNSCC with a high propensity for future distant metastasis and its functions in HNSCC cell lines. *Br. J. Cancer* **103**, 715-726 (2010).
- 207 Duvvuri, U. *et al.* TMEM16A induces MAPK and contributes directly to tumorigenesis and cancer progression. *Cancer Res.* **72**, 3270-3281 (2012).
- 208 Godse, N. R. *et al.* TMEM16A/ANO1 inhibits apoptosis via downregulation of Bim expression. *Clin. Cancer Res.* **23**, 7324-7332 (2017).
- 209 Ruiz, C. *et al.* Enhanced expression of ANO1 in head and neck squamous cell carcinoma causes cell migration and correlates with poor prognosis. *PLoS One* **7**, (2012).

- 210 Shiwerski, D. J. *et al.* To 'grow' or 'go': TMEM16A expression as a switch between tumor growth and metastasis in SCCHN. *Clin. Cancer Res.* **20**, 4673-4688 (2014).
- 211 Lee, E. W. *et al.* Ubiquitination and degradation of the FADD adaptor protein regulate death receptor-mediated apoptosis and necroptosis. *Nat. Commun.* **3**, (2012).
- 212 Ranjan, K. & Pathak, C. FADD regulates NF- κ B activation and promotes ubiquitination of cFLIP L to induce apoptosis. *Sci. Rep.* **6**, 1-16 (2016).
- 213 Kischkel, F. C. *et al.* Cytotoxicity-dependent APO-1 (Fas/CD95)-associated proteins form a death-inducing signaling complex (DISC) with the receptor. *EMBO J.* **14**, 5579-5588 (1995).
- 214 Kischkel, F. C. *et al.* Death Receptor Recruitment of Endogenous Caspase-10 and Apoptosis Initiation in the Absence of Caspase-8. *J. Biol. Chem.* **276**, 46639-46646 (2001).
- 215 Liu, Y., Li, X., Zhou, X., Wang, J. & Ao, X. FADD as a key molecular player in cancer progression. *Mol. Med.* **28**, (2022).
- 216 Mouasni, S. & Tourneur, L. FADD at the Crossroads between Cancer and Inflammation. *Trends Immunol.* **39**, 1036-1053 (2018).
- 217 Serra-Pages, C. *et al.* The LAR transmembrane protein tyrosine phosphatase and a coiled-coil LAR-interacting protein co-localize at focal adhesions. *EMBO J.* **14**, 2827-2838 (1995).
- 218 Riehn, M., Klopocki, E., Molkentin, M., Reinhardt, R. & Burmeister, T. A BACH2-BCL2L1 Fusion Gene Resulting from a Lymphoma Cell Line BLUE-1. *Cancer* **396**, 389-396 (2011).
- 219 Shen, J. C. *et al.* Inhibitor of growth 4 suppresses cell spreading and cell migration by interacting with a novel binding partner, liprin α . *Cancer Res.* **67**, 2552-2558 (2007).
- 220 Pehkonen, H. *et al.* Liprin- α 1 modulates cancer cell signaling by transmembrane protein CD82 in adhesive membrane domains linked to cytoskeleton. *Cell Commun. Signal.* **16**, 1-14 (2018).
- 221 Pehkonen, H. *et al.* Liprin- α 1 is a regulator of vimentin intermediate filament network in the cancer cell adhesion machinery. *Sci. Rep.* **6**, 1-15 (2016).
- 222 Chen, Z. *et al.* Up-regulated miR-548k promotes esophageal squamous cell carcinoma progression via targeting long noncoding RNA-LET. *Exp. Cell Res.* **362**, 90-101 (2018).
- 223 Lin, J. *et al.* An NF90/long noncoding RNA-LET/miR-548k feedback amplification loop controls esophageal squamous cell carcinoma progression. *J. Cancer* **10**, 5139-5152 (2019).
- 224 Song, Y. *et al.* Identification of genomic alterations in oesophageal squamous cell cancer. *Nature* **508**, 91-95 (2014).
- 225 Van Rossum, A. G. S. H. *et al.* Alternative Splicing of the Actin Binding Domain of Human Cortactin Affects Cell Migration. *J. Biol. Chem.* **278**, 45672-45679 (2003).
- 226 Schuurig, E., Verhoeven, E., Litvinov, S. & Michalides, R. J. A. M. The Product of the EMS1 Gene, Amplified and Overexpressed in Human Carcinomas, is Homologous to a v-src Substrate and is Located in Cell-Substratum Contact Sites. *Mol. Cell. Biol.* **13**, 2891-2898 (1993).
- 227 Schuurig, E. D. *et al.* Characterization of the EMS1 Gene and its Product, Human Cortactin. *Cell Commun. Adhes.* **6**, 185-209 (1998).
- 228 Hong Wu and J. Thomas Parsons. Cortactin, an 80/85-Kilodalton pp60 src Substrate, is a Filamentous Actin-binding Protein Enriched in the Cell Cortex. *J. Cell Biol.* **120**, 1417-1426 (1993).
- 229 Wu, H., Reynolds, A. B., Kanner, S. B., Vines, R. R. & Parsons, J. T. Identification and Characterization of a Novel Cytoskeleton-Associated pp60src Substrate. **11**, 5113-5124 (1991).
- 230 Weaver, A. M. *et al.* Cortactin promotes and stabilizes Arp2/3-induced actin filament network formation. *Curr. Biol.* **11**, 370-374 (2001).
- 231 Weed, S. A. *et al.* Cortactin localization to sites of actin assembly in lamellipodia requires interactions with F-actin and the Arp2/3 complex. *J. Cell Biol.* **151**, 29-40 (2000).

- 232 Su, C. M. *et al.* Vascular Endothelial Growth Factor-C Upregulates Cortactin and Promotes Metastasis of Esophageal Squamous Cell Carcinoma. *Ann. Surg. Oncol.* **21**, 767-775 (2014).
- 233 Rothschild, B. L. *et al.* Cortactin overexpression regulates actin-related protein 2/3 complex activity, motility, and invasion in carcinomas with chromosome 11q13 amplification. *Cancer Res.* **66**, 8017-8025 (2006).
- 234 Clark, E. S., Brown, B., Kochaishvili, A., Yarbrough, W. G. & Weaver, A. M. Aggressiveness of HNSCC tumors depends on expression levels of cortactin, a gene in the 11q13 amplicon. *Oncogene* **28**, 431-444 (2009).
- 235 Ni, Q. F. *et al.* Cortactin promotes colon cancer progression by regulating ERK pathway. *Int. J. Oncol.* **47**, 1034-1042 (2015).
- 236 Timpson, P., Lynch, D. K., Schramek, D., Walker, F. & Daly, R. J. Cortactin overexpression inhibits ligand-induced down-regulation of the epidermal growth factor receptor. *Cancer Res.* **65**, 3273-3280 (2005).
- 237 Timpson, P. *et al.* Aberrant expression of cortactin in head and neck squamous cell carcinoma cells is associated with enhanced cell proliferation and resistance to the epidermal growth factor receptor inhibitor gefitinib. *Cancer Res.* **67**, 9304-9314 (2007).
- 238 Kim, J. *et al.* Integrated genomic characterization of oesophageal carcinoma. *Nature* **541**, 169-174 (2017).
- 239 Noorlag, R. *et al.* The diagnostic value of 11q13 amplification and protein expression in the detection of nodal metastasis from oral squamous cell carcinoma: a systematic review and meta-analysis. *Virchows Arch.* **466**, 363-373 (2015).
- 240 Noorlag, R. *et al.* Amplification and protein overexpression of cyclin D1: Predictor of occult nodal metastasis in early oral cancer. *Head Neck* **36**, 1391 (2014).
- 241 Kim, R. D. *et al.* First-in-human phase I study of figogatinib (BLU-554) validates aberrant FGF19 signaling as a driver event in hepatocellular carcinoma. *Cancer Discovery* vol. 9 1696-1707 at <https://doi.org/10.1158/2159-8290.CD-19-0555> (2019).
- 242 Huang, C. *et al.* Proteogenomic insights into the biology and treatment of HPV-negative head and neck squamous cell carcinoma. *Cancer Cell* **39**, 361-379.e16 (2021).
- 243 Vörsmann, H. *et al.* Development of a human three-dimensional organotypic skin-melanoma spheroid model for in vitro drug testing. *Cell Death Dis.* **4**, (2013).
- 244 Meyers, R. M. *et al.* Computational correction of copy number effect improves specificity of CRISPR-Cas9 essentiality screens in cancer cells. *Nat. Genet.* **49**, 1779-1784 (2017).
- 245 Cavallaro, U. & Christofori, G. Cell adhesion and signalling by cadherins and Ig-CAMs in cancer. *Nat. Rev. Cancer* **4**, 118-132 (2004).
- 246 Subramanian, A. *et al.* Gene set enrichment analysis: A knowledge-based approach for interpreting genome-wide expression profiles. *Proc. Natl. Acad. Sci. U. S. A.* **102**, 15545-15550 (2005).
- 247 Wei, L. *et al.* Ultradeep sequencing differentiates patterns of skin clonal mutations associated with sun-exposure status and skin cancer burden. *Sci. Adv.* **7**, 1-13 (2021).
- 248 Chen, Y. *et al.* CCND1 Amplification Contributes to Immunosuppression and Is Associated With a Poor Prognosis to Immune Checkpoint Inhibitors in Solid Tumors. *Front. Immunol.* **11**, 1-11 (2020).
- 249 Dou, S. *et al.* EGFR Mutation and 11q13 Amplification Are Potential Predictive Biomarkers for Immunotherapy in Head and Neck Squamous Cell Carcinoma. *Front. Immunol.* **13**, 1-7 (2022).
- 250 Ormandy, C. J., Musgrove, E. A., Hui, R., Daly, R. J. & Sutherland, R. L. Cyclin D1, EMS1 and 11q13 amplification in breast cancer. *Breast Cancer Res. Treat.* **78**, 323-335 (2003).
- 251 Schuurig, E. The involvement of the chromosome 11q13 region in human malignancies: cyclin D1 and EMS1 are two new candidate oncogenes - a review. *Gene* **159**, 83-96 (1995).

- 252 Hui, R. *et al.* EMS1 amplification can occur independently of CCND1 or INT-2 amplification at 11q13 and may identify different phenotypes in primary breast cancer. *Oncogene* **15**, 1617-1623 (1997).
- 253 Sood, P., Krek, A., Zavolan, M., Macino, G. & Rajewsky, N. Cell-type-specific signatures of microRNAs on target mRNA expression. *Proc. Natl. Acad. Sci. U. S. A.* **103**, 2746-2751 (2006).
- 254 Hsin, J.-P., Lu, Y., Loeb, G. B., Leslie, C. S. & Rudensky, A. Y. The effect of cellular context on miR-155-mediated gene regulation in four major immune cell types. *Nat. Immunol.* **19**, 1137-1145 (2018).
- 255 Farh, K. K. H. *et al.* The widespread impact of mammalian microRNAs on mRNA repression and evolution. *Science (80-)*. **310**, 1817-1821 (2005).
- 256 Hsu, M. Y. *et al.* E-cadherin expression in melanoma cells restores keratinocyte-mediated growth control and down-regulates expression of invasion-related adhesion receptors. *Am. J. Pathol.* **156**, 1515-1525 (2000).
- 257 Vlemminckx, K., Vakaet, L., Mareel, M., Fiers, W. & Van Roy, F. Genetic manipulation of E-cadherin expression by epithelial tumor cells reveals an invasion suppressor role. *Cell* **66**, 107-119 (1991).
- 258 Uhlén, M. *et al.* Tissue-based map of the human proteome. *Science (80-)*. **347**, (2015).
- 259 Yadollahi-Farsani, M., Amini-Farsani, Z., Moayedi, F., Khazaei, N. & yaghoobi, H. MiR-548k suppresses apoptosis in breast cancer cells by affecting PTEN/PI3K/AKT signaling pathway. *IUBMB Life* **548** (2022) doi:10.1002/iub.2688.
- 260 Weinstein, I. B. Addiction to oncogenes—the Achilles heel of cancer. *Science (80-)*. **297**, 63-64 (2002).
- 261 Shan, J., Zhao, W. & Gu, W. Suppression of Cancer Cell Growth by Promoting Cyclin D1 Degradation. *Mol. Cell* **36**, 469-476 (2009).
- 262 Campbell, J. *et al.* Large-Scale Profiling of Kinase Dependencies in Cancer Cell Lines. *Cell Rep.* **14**, 2490-2501 (2016).
- 263 Hu, Y. & Smyth, G. K. ELDA: Extreme limiting dilution analysis for comparing depleted and enriched populations in stem cell and other assays. *J. Immunol. Methods* **347**, 70-78 (2009).
- 264 Barretina, J. *et al.* The Cancer Cell Line Encyclopedia enables predictive modelling of anticancer drug sensitivity. *Nature* **483**, 603-607 (2012).
- 265 Campbell, P. J. *et al.* Pan-cancer analysis of whole genomes. *Nature* **578**, 82-93 (2020).
- 266 Ally, A. *et al.* Comprehensive and Integrative Genomic Characterization of Hepatocellular Carcinoma. *Cell* **169**, 1327-1341 (2017).
- 267 Matthews, H. K., Bertoli, C. & de Bruin, R. A. M. Cell cycle control in cancer. *Nat. Rev. Mol. Cell Biol.* **23**, 74-88 (2022).
- 268 Qie, S. & Diehl, J. A. Cyclin D1, cancer progression, and opportunities in cancer treatment. *J. Mol. Med.* **94**, 1313-1326 (2016).
- 269 Musgrove, E. A. Cyclins: Roles in mitogenic signaling and oncogenic transformation. *Growth Factors* **24**, 13-19 (2006).
- 270 Jirawatnotai, S. *et al.* A function for cyclin D1 in DNA repair uncovered by protein interactome analyses in human cancers. *Nature* **474**, 230-234 (2011).
- 271 Chen, H. Z., Tsai, S. Y. & Leone, G. Emerging roles of E2Fs in cancer: an exit from cell cycle control. *Nat. Rev. Cancer* **9**, (2009).
- 272 Aggarwal, P. *et al.* Nuclear accumulation of cyclin D1 during S phase inhibits Cul4-dependent Cdt1 proteolysis and triggers p53-dependent DNA rereplication. *Genes Dev.* **21**, 2908-2922 (2007).
- 273 Matsuura, I. *et al.* Cyclin-dependent kinases regulate the antiproliferative function of Smads. *Nature* **430**, 226-231 (2004).

- 274 Tchakarska, G. & Sola, B. The double dealing of cyclin D1. *Cell Cycle* **19**, 163-178 (2020).
- 275 Shen, R. *et al.* Cyclin D1-Cdk4 Induce Runx2 Ubiquitination and Degradation. *J. Biol. Chem.* **281**, 16347-16353 (2006).
- 276 Nakajima, K. *et al.* Coordinated regulation of differentiation and proliferation of embryonic cardiomyocytes by a jumonji (Jarid2) -cyclin D1 pathway. *Development* **178**, 1771-1782 (2011).
- 277 Kehn, K. *et al.* Functional consequences of cyclin D1/BRCA1 interaction in breast cancer cells. *Oncogene* 5060-5069 (2007) doi:10.1038/sj.onc.1210319.
- 278 Lazaro, J., Bailey, P. J. & Lassar, A. B. Cyclin D - cdk4 activity modulates the subnuclear localization and interaction of MEF2 with SRC-family coactivators during skeletal muscle differentiation. *Genes Dev.* 1792-1805 (2002) doi:10.1101/gad.U-9988R.cytes.
- 279 Neuman, E. *et al.* Cyclin D1 stimulation of estrogen receptor transcriptional activity independent of cdk4. *Mol. Cell. Biol.* **17**, 5338-5347 (1997).
- 280 Wang, C. *et al.* Cyclin D1 Repression of Peroxisome Proliferator-Activated Receptor Gamma Expression and Transactivation. *Mol. Cell. Biol.* **23**, 6159-6173 (2003).
- 281 Ganter, B., Fu, S. & Lipsick, J. S. D-type cyclins repress transcriptional activation by the v-Myb but not the c-Myb DNA-binding domain. *EMBO J.* **17**, 255-268 (1998).
- 282 Horstmann, S., Ferrari, S. & Klempnauer, K. H. Regulation of B-Myb activity by cyclin D1. *Oncogene* **19**, 298-306 (2000).
- 283 Hirai, H. & Sherr, C. J. Interaction of D-type cyclins with a novel myb-like transcription factor, DMP1. *Mol. Cell. Biol.* **16**, 6457-6467 (1996).
- 284 Inoue, K. & Sherr, C. J. Gene Expression and Cell Cycle Arrest Mediated by Transcription Factor DMP1 Is Antagonized by D-Type Cyclins through a Cyclin-Dependent-Kinase-Independent Mechanism. *Mol. Cell. Biol.* **18**, 1590-1600 (1998).
- 285 Lamb, J. *et al.* A Mechanism of Cyclin D1 Action Encoded in the Patterns of Gene Expression in Human Cancer. *Cell* **114**, 323-334 (2003).
- 286 Skapek, S. X., Rhee, J., Kim, P. S., Novitch, B. G. & Lassar, A. B. Cyclin-mediated inhibition of muscle gene expression via a mechanism that is independent of pRB hyperphosphorylation. *Mol. Cell. Biol.* **16**, 7043-7053 (1996).
- 287 Wen, M. A. R. K. E. E., McMahon, C., Suthiphongchai, T., Drenzo, J. & Ewen, M. E. P/CAF associates with cyclin D1 and potentiates its activation of the estrogen receptor. *Proc. Natl. Acad. Sci. U. S. A.* **96**, 5382-5387 (1999).
- 288 Lin, H. M., Zhao, L. & Cheng, S. Y. Cyclin D1 Is a Ligand-independent Co-repressor for Thyroid Hormone Receptors. *J. Biol. Chem.* **277**, 28733-28741 (2002).
- 289 Li, Z. *et al.* Alternative cyclin D1 splice forms differentially regulate the DNA damage response. *Cancer Res.* **70**, 8802-8811 (2010).
- 290 Shimura, T. *et al.* Cyclin D1 overexpression perturbs DNA replication and induces replication-associated DNA double-strand breaks in acquired radioresistant cells. *Cell Cycle* **12**, 773-782 (2013).
- 291 Chen, S. & Li, L. Degradation strategy of cyclin D1 in cancer cells and the potential clinical application. *Front. Oncol.* **12**, 1-10 (2022).
- 292 Deshpande, A., Sicinski, P. & Hinds, P. W. Cyclins and cdks in development and cancer: A perspective. *Oncogene* **24**, 2909-2915 (2005).
- 293 Malumbres, M. & Barbacid, M. Cell cycle, CDKs and cancer: A changing paradigm. *Nat. Rev. Cancer* **9**, 153-166 (2009).
- 294 Keum, J. S. *et al.* Cyclin D1 overexpression is an indicator of poor prognosis in resectable non-small cell lung cancer. *Br. J. Cancer* **81**, 127-132 (1999).
- 295 Ibrahim, H. M. *et al.* Prognostic Value of Cyclin D1 and CD44 Expression in Gastric Adenocarcinoma. *J. Gastrointest. Cancer* **50**, 370-379 (2019).

- 296 Almangush, A. *et al.* Prognostic biomarkers for oral tongue squamous cell carcinoma: A systematic review and meta-analysis. *Br. J. Cancer* **117**, 856-866 (2017).
- 297 Shan, Y. S. *et al.* Cyclin D1 overexpression correlates with poor tumor differentiation and prognosis in gastric cancer. *Oncol. Lett.* **14**, 4517-4526 (2017).
- 298 Lin, H. *et al.* Significantly upregulated TACSTD2 and Cyclin D1 correlate with poor prognosis of invasive ductal breast cancer. *Exp. Mol. Pathol.* **94**, 73-78 (2013).
- 299 Tetsu, O. & McCormick, F. Beta-Catenin regulates expression of cyclinD1 in colon carcinomacells Osamu. *Nature* **398**, 422 (1999).
- 300 Takuwa, N., Fukui, Y. & Takuwa, Y. Cyclin D1 Expression Mediated by Phosphatidylinositol 3-Kinase through mTOR-p70 S6K -Independent Signaling in Growth Factor-Stimulated NIH 3T3 Fibroblasts. *Mol. Cell. Biol.* **19**, 1346-1358 (1999).
- 301 Shtutman, M. *et al.* The cyclin D1 gene is a target of the β -catenin/LEF-1 pathway. *Proc. Natl. Acad. Sci. U. S. A.* **96**, 5522-5527 (1999).
- 302 Diehl, J. A., Cheng, M., Roussel, M. F. & Sherr, C. J. Glycogen synthase kinase-3 β regulates cyclin D1 proteolysis and subcellular localization. *Genes Dev.* **12**, 3499-3511 (1998).
- 303 Guttridge, D. C., Albanese, C., Reuther, J. Y., Pestell, R. G. & Baldwin, A. S. NF- κ B Controls Cell Growth and Differentiation through Transcriptional Regulation of Cyclin D1. *Mol. Cell. Biol.* **19**, 5785-5799 (1999).
- 304 Poch, B. *et al.* Epidermal growth factor induces cyclin D1 in human pancreatic carcinoma: Evidence for a cyclin D1-dependent cell cycle progression. *Pancreas* **23**, 280-287 (2001).
- 305 Rowlands, T. M., Pechenkina, I. V., Hatsell, S. J., Pestell, R. G. & Cowin, P. Dissecting the roles of β -catenin and cyclin D1 during mammary development and neoplasia. *Proc. Natl. Acad. Sci. U. S. A.* **100**, 11400-11405 (2003).
- 306 Barbash, O. *et al.* Mutations in Fbx4 Inhibit Dimerization of the SCFFbx4 Ligase and Contribute to Cyclin D1 Overexpression in Human Cancer. *Cancer Cell* **14**, 68-78 (2008).
- 307 Lin, D. I. *et al.* Phosphorylation-dependent ubiquitination of cyclin D1 by the SCFFBX4- α Bcrystallin complex. *Mol Cell* **24**, 355-366 (2006).
- 308 Diehl, J. A., Zindy, F. & Sherr, C. J. Inhibition of cyclin D1 phosphorylation on threonine-286 prevents its rapid degradation via the ubiquitin-proteasome pathway. *Genes Dev.* **11**, 957-972 (1997).
- 309 Alt, J. R., Cleveland, J. L., Hannink, M. & Diehl, J. A. Phosphorylation-dependent regulation of cyclin D1 nuclear export and cyclin D1-dependent cellular transformation. *Genes Dev.* **14**, 3102-3114 (2000).
- 310 Bertoni, F., Rinaldi, A., Zucca, E. & Cavalli, F. Update on the molecular biology of mantle cell lymphoma. *Hematol. Oncol.* **1**, 22-27 (2006).
- 311 Wiest, T., Schwarz, E., Enders, C., Flechtenmacher, C. & Bosch, F. X. Involvement of intact HPV16 E6 / E7 gene expression in head and neck cancers with unaltered p53 status and perturbed pRb cell cycle control. *Oncogene* **21**, 1510-1517 (2002).
- 312 Edelman, M. J. *et al.* SWOG S1400C (NCT02154490)—A Phase II Study of Palbociclib for Previously Treated Cell Cycle Gene Alteration-Positive Patients with Stage IV Squamous Cell Lung Cancer (Lung-MAP Substudy). *J. Thorac. Oncol.* **14**, 1853-1859 (2019).
- 313 Adkins, D. R. *et al.* Palbociclib and cetuximab compared with placebo and cetuximab in platinum-resistant, cetuximab-naïve, human papillomavirus-unrelated recurrent or metastatic head and neck squamous cell carcinoma: A double-blind, randomized, phase 2 trial. *Oral Oncol.* **115**, 105192 (2021).
- 314 Oppelt, P. *et al.* Palbociclib and cetuximab in cetuximab-resistant human papillomavirus-related oropharynx squamous-cell carcinoma : A multicenter phase 2 trial. *Oral Oncol.* **114**, 105164 (2021).
- 315 Hinds, P. W., Dowdy, S. F., Eaton, E. N., Arnold, A. & Weinberg, R. A. Function of a human cyclin gene as an oncogene. *Proc. Natl. Acad. Sci. U. S. A.* **91**, 709-713 (1994).

- 316 Mazzu, Y. Z. *et al.* A novel mechanism driving poor-prognosis prostate cancer: Overexpression of the DNA repair gene, ribonucleotide reductase small subunit M2 (RRM2). *Clin. Cancer Res.* **25**, 4480–4492 (2019).
- 317 Wilson, E. A., Sultana, N., Shah, K. N., Elford, H. L. & Faridi, J. S. Molecular targeting of RRM2, NF- κ B, and mutant TP53 for the treatment of triple-negative breast cancer. *Mol. Cancer Ther.* **20**, 655–664 (2021).
- 318 Rasmussen, R. D. *et al.* BRCA1-regulated RRM2 expression protects glioblastoma cells from endogenous replication stress and promotes tumorigenicity. *Nat. Commun.* **7**, 13398 (2016).
- 319 Xiong, W. *et al.* RRM2 Regulates Sensitivity to Sunitinib and PD-1 Blockade in Renal Cancer by Stabilizing ANXA1 and Activating the AKT Pathway. *Adv. Sci.* **8**, 1–13 (2021).
- 320 Cory, J. *et al.* Structure-function relationships for a new series of pyridine-2-carboxaldehyde thiosemicarbazones on ribonucleotide reductase activity and tumor cell growth in culture and in vivo. *Advan Enzym. Regul* **35**, 55–68 (1995).
- 321 Kunos, C. A., Andrews, S. J., Moore, K. N., Chon, H. S. & Ivy, S. P. Randomized Phase II Trial of Triapine-Cisplatin-Radiotherapy for Locally Advanced Stage Uterine Cervix or Vaginal Cancers. *Front. Oncol.* **9**, 1–9 (2019).
- 322 Mannargudi, M. B. & Deb, S. Clinical pharmacology and clinical trials of ribonucleotide reductase inhibitors: is it a viable cancer therapy? *J. Cancer Res. Clin. Oncol.* **143**, 1499–1529 (2017).
- 323 Burnworth, B. *et al.* Gain of 11q/cyclin D1 overexpression is an essential early step in skin cancer development and causes abnormal tissue organization and differentiation. *Oncogene* **25**, 4399–4412 (2006).
- 324 Boukamp, P. Normal Keratinization in a Spontaneously Immortalized. *J. Cell Biol.* **106**, 761–771 (1988).
- 325 Burnworth, B. *et al.* The multi-step process of human skin carcinogenesis: A role for p53, cyclin D1, hTERT, p16, and TSP-1. *Eur. J. Cell Biol.* **86**, 763–780 (2007).
- 326 Padar, A. *et al.* Inactivation of Cyclin D2 Gene in Prostate Cancers by Aberrant Promoter Methylation. *Clin. Cancer Res.* **9**, 4730–4734 (2003).
- 327 Evron, E. *et al.* Loss of Cyclin D2 Expression in the Majority of Breast Cancers Is Associated with Promotor Hypermethylation. *Cancer Res.* **1**, 2782–2787 (2001).
- 328 Matsubayashi, H. *et al.* Methylation of Cyclin D2 Is Observed Frequently in Pancreatic Cancer but Is Also an Age-related Phenomenon in Gastrointestinal Tissues I. *Clin. Cancer Res.* **9**, 1446–1452 (2003).
- 329 Knudsen, E. S. *et al.* CDK/cyclin dependencies define extreme cancer cell-cycle heterogeneity and collateral vulnerabilities. *Cell Rep.* **38**, 110448 (2022).
- 330 Zhang, Q. *et al.* Cyclin D3 compensates for the loss of cyclin D1 during ErbB2-induced mammary tumor initiation and progression. *Cancer Res.* **71**, 7513–7524 (2011).
- 331 Laderian, B. & Fojo, T. CDK4/6 Inhibition as a therapeutic strategy in breast cancer: palbociclib, ribociclib, and abemaciclib. *Semin. Oncol.* **44**, 395–403 (2018).
- 332 Berger, A. C. *et al.* A Comprehensive Pan-Cancer Molecular Study of Gynecologic and Breast Cancers. *Cancer Cell* **33**, 690–705.e9 (2018).
- 333 Lee, Y. M. & Sicinski, P. Targeting cyclins and cyclin-dependent kinases in cancer: Lessons from mice, hopes for therapeutic applications in human. *Cell Cycle* **5**, 2110–2114 (2006).
- 334 Wei, Y., Huang, C., Wu, H. & Huang, J. Estrogen Receptor Beta (ER β) Mediated-CyclinD1 Degradation via Autophagy Plays an Anti-Proliferation Role in Colon Cells. *Int. J. Biol. Sci.* **15**, (2019).
- 335 Yang, W., Zhang, Y., Li, Y., Wu, Z. & Zhu, D. Myostatin Induces Cyclin D1 Degradation to Cause Cell Cycle Arrest through a Phosphatidylinositol 3-Kinase / AKT / GSK-3 β Pathway and Is Antagonized by Insulin-like Growth Factor 1*. *J. Biol. Chem.* **282**, 3799–3808 (2007).

- 336 Dale, B. *et al.* Advancing targeted protein degradation for cancer therapy. *Nature Reviews Cancer* vol. 21 638-654 at <https://doi.org/10.1038/s41568-021-00365-x> (2021).
- 337 Xiong, Y. *et al.* Bridged Proteolysis Targeting Chimera (PROTAC) Enables Degradation of Undruggable Targets. *J. Am. Chem. Soc.* **144**, 22622-22632 (2022).
- 338 Chabes, A. L., Bjo, S. & Thelander, L. S Phase-specific Transcription of the Mouse Ribonucleotide Reductase R2 Gene Requires Both a Proximal Repressive E2F-binding Site and an Upstream Promoter Activating Region *. *Journal Biol. Chem.* **279**, 10796-10807 (2004).
- 339 Angiolella, V. D. *et al.* Cyclin F-Mediated Degradation of Ribonucleotide Reductase M2 Controls Genome Integrity and DNA Repair. *Cell* **149**, 1023-1034 (2012).
- 340 Zhang, Y. W., Jones, T. L., Martin, S. E., Caplen, N. J. & Pommier, Y. Implication of checkpoint kinase-dependent up-regulation of ribonucleotide reductase R2 in DNA damage response. *J. Biol. Chem.* **284**, 18085-18095 (2009).
- 341 Gu, Z. *et al.* Palbociclib - based high - throughput combination drug screening identifies synergistic therapeutic options in HPV - negative head and neck squamous cell carcinoma. *BMC Med.* 1-22 (2022) doi:10.1186/s12916-022-02373-6.
- 342 Satow, R. *et al.* Combined functional genome survey of therapeutic targets for hepatocellular carcinoma. *Clin. Cancer Res.* **16**, 2518-2528 (2010).
- 343 Morikawa, T., Hino, R., Uozaki, H. & Maeda, D. Expression of ribonucleotide reductase M2 subunit in gastric cancer and effects of RRM2 inhibition in vitro. *Hum. Pathol.* **41**, 1742-1748 (2010).
- 344 Kretschmer, C. *et al.* Identification of early molecular markers for breast cancer. *Mol. Cancer* **10**, 1-11 (2011).
- 345 Grade, M. *et al.* A genomic strategy for the functional validation of colorectal cancer genes identifies potential therapeutic targets. *Int. J. Cancer* **128**, 1069-1079 (2011).
- 346 Ferrandina, G. *et al.* Expression of nucleoside transporters, deoxycytidine kinase, ribonucleotide reductase regulatory subunits, and gemcitabine catabolic enzymes in primary ovarian cancer. *Cancer Chemother. Pharmacol.* **65**, 679-686 (2010).
- 347 Wang, S. *et al.* Overexpression of RRM2 is related to poor prognosis in oral squamous cell carcinoma. *Oral Dis.* **27**, 204-214 (2021).
- 348 Wang, J., Yi, Y., Chen, Y., Xiong, Y. & Zhang, W. Potential mechanism of RRM2 for promoting Cervical Cancer based on weighted gene co-expression network analysis. *Int. J. Med. Sci.* **17**, (2020).
- 349 Jiang, X. *et al.* RRM2 silencing suppresses malignant phenotype and enhances radiosensitivity via activating cGAS / STING signaling pathway in lung adenocarcinoma. *Cell Biosci.* **11**, 1-20 (2021).
- 350 Xu, X. *et al.* Broad overexpression of ribonucleotide reductase genes in mice specifically induces lung neoplasms. *Cancer Res.* **68**, 2652-2660 (2008).
- 351 Zhan, Y. *et al.* Inhibiting RRM2 to enhance the anticancer activity of chemotherapy. *Biomed. Pharmacother.* **133**, 110996 (2021).
- 352 Wadler, S. *et al.* Phase I and pharmacokinetic study of the ribonucleotide reductase inhibitor, 3-aminopyridine-2-carboxaldehyde thiosemicarbazone, administered by 96-hour intravenous continuous infusion. *J. Clin. Oncol.* **22**, 1553-1563 (2004).
- 353 Murren, J. *et al.* Phase I and Pharmacokinetic Study of Triapine, a Potent Ribonucleotide Reductase Inhibitor, Administered Daily for Five Days in Patients with Advanced Solid Tumors. *Clin. Cancer Res.* **9**, 4092-4100 (2003).
- 354 Gojo, I. *et al.* Phase I and pharmacokinetic study of Triapine®, a potent ribonucleotide reductase inhibitor, in adults with advanced hematologic malignancies. *Leuk. Res.* **31**, 1165-1173 (2007).

- 355 Kunos, C. A. *et al.* Gynecologic Oncology Radiochemotherapy plus 3-aminopyridine-2-carboxaldehyde thiosemicarbazone (3-AP , NSC # 663249) in advanced-stage cervical and vaginal cancers ★ , ★★. *Gynecol. Oncol.* **130**, 75-80 (2013).
- 356 Kunos, C. *et al.* Ribonucleotide reductase inhibition restores platinum-sensitivity in platinum-resistant ovarian cancer: A Gynecologic Oncology Group Study. *J. Transl. Med.* **10**, 1-10 (2012).
- 357 Kunos, C. *et al.* Phase I trial of pelvic radiation, weekly cisplatin, and 3-aminopyridine-2-carboxaldehyde thiosemicarbazone (3-AP, NSC #663249) for locally advanced cervical cancer. *Clin. Cancer Res.* **16**, (2010).
- 358 Martin, L. K. *et al.* A dose escalation and pharmacodynamic study of triapine and radiation in patients with locally advanced pancreas cancer. *Int. J. Radiat. Oncol. Biol. Phys.* **84**, (2012).
- 359 Mortazavi, A. *et al.* A phase I study of prolonged infusion of triapine in combination with fixed dose rate gemcitabine in patients with advanced solid tumors. *Invest. New Drugs* **31**, 685-695 (2013).
- 360 Zeidner, J. F. *et al.* A phase II trial of sequential ribonucleotide reductase inhibition in aggressive myeloproliferative neoplasms. *Haematologica* **99**, 672-678 (2014).
- 361 Traynor, A. M. *et al.* A phase II trial of Triapine® (NSC# 663249) and gemcitabine as second line treatment of advanced non-small cell lung cancer: Eastern Cooperative Oncology Group Study 1503. *Invest. New Drugs* **28**, 91-97 (2010).
- 362 Ma, B. *et al.* A multicenter phase II trial of 3-aminopyridine-2-carboxaldehyde thiosemicarbazone (3-AP, Triapine®) and gemcitabine in advanced non-small-cell lung cancer with pharmacokinetic evaluation using peripheral blood mononuclear cells. *Invest. New Drugs* **26**, 169-173 (2008).
- 363 Ocean, A. J. *et al.* Phase II trial of the ribonucleotide reductase inhibitor 3-aminopyridine-2-carboxaldehydethiosemicarbazone plus gemcitabine in patients with advanced biliary tract cancer. *Cancer Chemother. Pharmacol.* **68**, 379-388 (2011).
- 364 Nutting, C. M. *et al.* Phase II study of 3-AP Triapine in patients with recurrent or metastatic head and neck squamous cell carcinoma. *Ann. Oncol.* **20**, 1275-1279 (2009).
- 365 Vanderveken, O. M. *et al.* Gemcitabine-Based Chemoradiation in the Treatment of Locally Advanced Head and Neck Cancer: Systematic Review of Literature and Meta-Analysis. *Oncologist* **21**, 59-71 (2016).
- 366 Zhang, L. *et al.* Gemcitabine plus cisplatin versus fluorouracil plus cisplatin in recurrent or metastatic nasopharyngeal carcinoma: a multicentre, randomised, open-label, phase 3 trial. *Lancet* **6736**, 1-10 (2016).
- 367 Zhang, Y. *et al.* Gemcitabine and Cisplatin Induction Chemotherapy in Nasopharyngeal Carcinoma. *N. Engl. J. Med.* **381**, 1124-1135 (2019).
- 368 Raguse, J. D., Gath, H. J., Bier, J., Reiss, H. & Oettle, H. Gemcitabine in the treatment of advanced head and neck cancer. *Clin. Oncol.* **17**, 425-429 (2005).
- 369 Gilbert, L. A. *et al.* CRISPR-mediated modular RNA-guided regulation of transcription in eukaryotes. *Cell* **154**, 442 (2013).
- 370 Katoh, M. & Katoh, M. Evolutionary conservation of CCND1-ORA0V1-FGF19-FGF4 locus from zebrafish to human. *Int. J. Mol. Med.* **12**, 45-50 (2003).
- 371 Kang, J. U. & Koo, S. H. ORA0V1 is a probable target within the 11q13.3 amplicon in lymph node metastases from gastric adenocarcinoma. *Int. J. Mol. Med.* **29**, 81-87 (2012).
- 372 Li, M., Cui, X., Shen, Y. & Dong, H. ORA0V1 overexpression in esophageal squamous cell carcinoma and esophageal dysplasia : a possible biomarker of progression and poor prognosis in esophageal carcinoma ★ , ★★. *Hum. Pathol.* **46**, 707-715 (2015).
- 373 Xia, J., Chen, Q., Li, B. & Zeng, X. Amplifications of TAOS1 and EMS1 genes in oral carcinogenesis: association with clinicopathological features. *Oral Oncol.* **43**, 508-514 (2007).

- 374 Jiang, L. *et al.* ORAOV1-A correlates with poor differentiation in oral cancer. *J. Dent. Res.* **88**, 433-438 (2009).
- 375 Jiang, L. *et al.* Oral cancer overexpressed 1 (ORAOV1) regulates cell cycle and apoptosis in cervical cancer HeLa cells. *Mol. Cancer* **9**, 1-9 (2010).
- 376 Qin, Y. *et al.* VP2 of infectious bursal disease virus induces apoptosis via triggering oral cancer overexpressed 1 (ORAOV1) protein degradation. *Front. Microbiol.* **8**, 1-19 (2017).
- 377 Zhai, C. *et al.* The function of ORAOV1/LTO1, a gene that is overexpressed frequently in cancer: Essential roles in the function and biogenesis of the ribosome. *Oncogene* **33**, 484-494 (2014).
- 378 Luo, X. *et al.* ORAOV1-B Promotes OSCC Metastasis via the NF- κ B-TNF α Loop. *J. Dent. Res.* **100**, 858-867 (2021).
- 379 Lu, Y. *et al.* A chloroplast membrane protein LTO1/AtVKOR involving in redox regulation and ROS homeostasis. *Plant Cell Rep.* **32**, 1427-1440 (2013).
- 380 Wu, J. *et al.* Functional redox links between lumen thiol oxidoreductase1 and serine/threonine-protein kinase STN7. *Plant Physiol.* **186**, 964-976 (2021).
- 381 Lu, Y. *et al.* Thylakoid membrane oxidoreductase LTO1/AtVKOR is involved in ABA-mediated response to osmotic stress in Arabidopsis. *Physiol. Plant.* **154**, 28-38 (2015).
- 382 Finkel, T. & Holbrook, N. J. Oxidants, Oxidative Stress and Biology of Ageing. *Nature* **408**, 239-247 (2000).
- 383 Sies, H. & Jones, D. P. Reactive oxygen species (ROS) as pleiotropic physiological signalling agents. *Nat. Rev. Mol. Cell Biol.* **21**, 363-383 (2020).
- 384 Hayes, J. D., Dinkova-Kostova, A. T. & Tew, K. D. Oxidative Stress in Cancer. *Cancer Cell* **38**, 167-197 (2020).
- 385 Reczek, C. R. *et al.* A CRISPR screen identifies a pathway required for paraquat-induced cell death. *Nat. Chem. Biol.* **13**, 1274-1279 (2017).
- 386 Redza-Dutordoir, M. & Averill-Bates, D. A. Activation of apoptosis signalling pathways by reactive oxygen species. *Biochim. Biophys. Acta - Mol. Cell Res.* **1863**, 2977-2992 (2016).
- 387 Benhar, M., Shytaj, I. L., Stamler, J. S. & Savarino, A. Dual targeting of the thioredoxin and glutathione systems in cancer and HIV. *J. Clin. Invest.* **126**, 1630-1639 (2016).
- 388 Jia, J. J., Geng, W. S., Wang, Z. Q., Chen, L. & Zeng, X. S. The role of thioredoxin system in cancer: strategy for cancer therapy. *Cancer Chemother. Pharmacol.* **84**, 453-470 (2019).
- 389 Lu, J. & Holmgren, A. The thioredoxin superfamily in oxidative protein folding. *Antioxidants Redox Signal.* **21**, 457-470 (2014).
- 390 Baker, A., Payne, C. M., Briehl, M. M. & Powis, G. Thioredoxin, a gene found overexpressed in human cancer, inhibits apoptosis in vitro and in vivo. *Cancer Res.* **57**, 5162-5167 (1997).
- 391 Arai, R. J. *et al.* Nitric oxide induces thioredoxin-1 nuclear translocation: Possible association with the p21Ras survival pathway. *Biochem. Biophys. Res. Commun.* **348**, 1254-1260 (2006).
- 392 Welsh, S. J. *et al.* The thioredoxin redox inhibitors 1-methylpropyl 2-imidazolyl disulfide and pleurotin inhibit hypoxia-induced factor 1 α and vascular endothelial growth factor formation. *Mol. Cancer Ther.* **2**, 235-243 (2003).
- 393 Zhao, L. *et al.* The overexpression and nuclear translocation of Trx-1 during hypoxia confers on HepG2 cells resistance to DDP, and GL-V9 reverses the resistance by suppressing the Trx-1/Ref-1 axis. *Free Radic. Biol. Med.* **82**, 29-41 (2015).
- 394 Hirota, K. *et al.* Ap-1 transcriptional activity is regulated by a direct association between thioredoxin and Ref-1. *Proc. Natl. Acad. Sci. U. S. A.* **94**, 3633-3638 (1997).
- 395 Gurusamy, N., Malik, G., Gorbunov, N. V. & Das, D. K. Redox activation of Ref-1 potentiates cell survival following myocardial ischemia reperfusion injury. *Free Radic. Biol. Med.* **43**, 397-407 (2007).

- 396 Zhu, X., Huang, C. & Peng, B. Overexpression of thioredoxin system proteins predicts poor prognosis in patients with squamous cell carcinoma of the tongue. *Oral Oncol.* **47**, 609-614 (2011).
- 397 Zhu, H. *et al.* Expression of thioredoxin 1 and peroxiredoxins in squamous cervical carcinoma and its predictive role in NACT. *BMC Cancer* **19**, 1-9 (2019).
- 398 Zhang, J., Li, X., Han, X., Liu, R. & Fang, J. Targeting the Thioredoxin System for Cancer Therapy. *Trends Pharmacol. Sci.* **38**, 794-808 (2017).
- 399 Du, J. J., Zhan, C. Y., Lu, Y., Cui, H. R. & Wang, X. Y. The conservative cysteines in transmembrane domain of AtVKOR/LTO1 are critical for photosynthetic growth and photosystem II activity in Arabidopsis. *Front. Plant Sci.* **6**, 1-9 (2015).
- 400 Karamoko, M., Cline, S., Redding, K., Ruiz, N. & Hamel, P. P. Lumen thiol oxidoreductase1, a disulfide bond-forming catalyst, is required for the assembly of photosystem II in Arabidopsis. *Plant Cell* **23**, 4462-4475 (2011).
- 401 Maillet, A. & Pervaiz, S. Redox regulation of p53, redox effectors regulated by p53: A subtle balance. *Antioxidants Redox Signal.* **16**, 1285-1294 (2012).
- 402 Tang, B., Zhang, Q., Liu, K. & Huang, Y. Exosomal circRNA FNDC3B promotes the progression of esophageal squamous cell carcinoma by sponging miR-490-5p and regulating thioredoxin reductase 1 expression. *Bioengineered* **13**, 13829-13848 (2022).
- 403 Iwasawa, S. *et al.* Upregulation of thioredoxin reductase 1 in human oral squamous cell carcinoma. *Oncol. Rep.* **25**, 637-644 (2011).
- 404 Yu, W. *et al.* Cisplatin generates oxidative stress which is accompanied by rapid shifts in central carbon metabolism. *Sci. Rep.* 1-12 (2018) doi:10.1038/s41598-018-22640-y.
- 405 Valko, M., Rhodes, C. J., Moncol, J., Izakovic, M. & Mazur, M. Free radicals, metals and antioxidants in oxidative stress-induced cancer. *Chem. Biol. Interact.* **160**, 1-40 (2006).
- 406 He, P. J. *et al.* Oxidative stress induced by carboplatin promotes apoptosis and inhibits migration of HN-3 cells. *Oncol. Lett.* **16**, 7131-7138 (2018).
- 407 Li, C. *et al.* Over-expression of Thioredoxin-1 mediates growth, survival, and chemoresistance and is a druggable target in diffuse large B-cell lymphoma. *Oncotarget* **3**, 314-326 (2012).
- 408 Yamada, M., Tomida, A., Yoshikawa, H., Taketani, Y. & Tsuruo, T. Increased expression of thioredoxin/adult T-cell leukemia-derived factor in cisplatin-resistant human cancer cell lines. *Clin. Cancer Res.* **2**, 427-432 (1996).
- 409 Yu, L. *et al.* TXN inhibitor impedes radioresistance of colorectal cancer cells with decreased ALDH1L2 expression via TXN/NF- κ B signaling pathway. *Br. J. Cancer* **127**, 637-648 (2022).
- 410 Stafford, W. C. *et al.* Irreversible inhibition of cytosolic thioredoxin reductase 1 as a mechanistic basis for anticancer therapy. *Science Translational Medicine* vol. 10 at <https://doi.org/10.1126/scitranslmed.aaf7444> (2018).
- 411 Harris, I. S. *et al.* Glutathione and Thioredoxin Antioxidant Pathways Synergize to Drive Cancer Initiation and Progression. *Cancer Cell* **27**, 211-222 (2015).
- 412 Fath, M. A., Ahmad, I. M., Smith, C. J., Spence, J. & Spitz, D. R. Enhancement of carboplatin-mediated lung cancer cell killing by simultaneous disruption of glutathione and thioredoxin metabolism. *Clin. Cancer Res.* **17**, 6206-6217 (2011).
- 413 Mandal, P. K. *et al.* Loss of thioredoxin reductase 1 renders tumors highly susceptible to pharmacologic glutathione deprivation. *Cancer Res.* **70**, 9505-9514 (2010).
- 414 Simons, A. L. *et al.* Inhibition of glutathione and thioredoxin metabolism enhances sensitivity to perifosine in head and neck cancer cells. *J. Oncol.* **2009**, (2009).
- 415 Holmström, K. M. & Finkel, T. Cellular mechanisms and physiological consequences of redox-dependent signalling. *Nat. Rev. Mol. Cell Biol.* **15**, 411-421 (2014).

- 416 Bagati, A. *et al.* KLF9-dependent ROS regulate melanoma progression in stage-specific manner. *Oncogene* **38**, 3585–3597 (2019).
- 417 Wiel, C. *et al.* BACH1 Stabilization by Antioxidants Stimulates Lung Cancer Metastasis. *Cell* **178**, 330–345.e22 (2019).
- 418 Smits, J. P. H. *et al.* CRISPR-Cas9-Based Genomic Engineering in Keratinocytes: From Technology to Application. *JID Innov.* **2**, 100082 (2022).
- 419 Bushman, F. D. Retroviral Insertional Mutagenesis in Humans: Evidence for Four Genetic Mechanisms Promoting Expansion of Cell Clones. *Mol. Ther.* **28**, 352–356 (2020).
- 420 Zaiss, A.-K. *et al.* Differential Activation of Innate Immune Responses by Adenovirus and Adeno-Associated Virus Vectors. *J. Virol.* **76**, 4580–4590 (2002).
- 421 Asmamaw Mengstie, M. Viral Vectors for the in Vivo Delivery of CRISPR Components: Advances and Challenges. *Front. Bioeng. Biotechnol.* **10**, 1–6 (2022).
- 422 Schoop, V. M., Mirancea, N. & Fusenig, N. E. Epidermal organization and differentiation of HaCat keratinocytes in organotypic coculture with human dermal fibroblasts. *J. Invest. Dermatol.* **112**, 343–353 (1999).
- 423 Vörsmann, H. *et al.* Development of a human three-dimensional organotypic skin-melanoma spheroid model for in vitro drug testing. *Cell Death Dis.* **4**, 719 (2013).
- 424 Smits, J. P. H. *et al.* Immortalized N/TERT keratinocytes as an alternative cell source in 3D human epidermal models. *Sci. Rep.* **7**, 1–14 (2017).
- 425 Lee, J. *et al.* Hair-bearing human skin generated entirely from pluripotent stem cells. *Nature* **582**, 399–404 (2020).
- 426 Ahn, J. *et al.* Modeling of three-dimensional innervated epidermal like-layer in a microfluidic chip-based coculture system. *Nat. Commun.* **14**, 1–14 (2023).
- 427 Escámez, M. J. *et al.* An in vivo model of wound healing in genetically modified skin-humanized mice. *J. Invest. Dermatol.* **123**, 1182–1191 (2004).
- 428 Llamas, S. G. *et al.* Human plasma as a dermal scaffold for the generation of a completely autologous bioengineered skin. *Transplantation* **77**, 350–355 (2004).
- 429 Del Rio, M. *et al.* A preclinical model for the analysis of genetically modified human skin in vivo. *Hum. Gene Ther.* **13**, 959–968 (2002).
- 430 Aufvenne, K. *et al.* Long-term faithful recapitulation of transglutaminase 1-deficient lamellar ichthyosis in a skin-humanized mouse model, and insights from proteomic studies. *J. Invest. Dermatol.* **132**, 1918–1921 (2012).
- 431 García, M. *et al.* Development of skin-humanized mouse models of pachyonychia congenita. *J. Invest. Dermatol.* **131**, 1053–1060 (2011).
- 432 Anzalone, A. V., Koblan, L. W. & Liu, D. R. Genome editing with CRISPR-Cas nucleases, base editors, transposases and prime editors. *Nat. Biotechnol.* **38**, 824–844 (2020).
- 433 Kowalewski, C. *et al.* A novel autosomal partially dominant mutation designated G476D in the keratin 5 gene causing epidermolysis bullosa simplex Weber-Cockayne type: A family study with a genetic twist. *Int. J. Mol. Med.* **20**, 75–78 (2007).
- 434 Kocher, T. *et al.* Cut and Paste: Efficient Homology-Directed Repair of a Dominant Negative KRT14 Mutation via CRISPR/Cas9 Nickases. *Mol. Ther.* **25**, 2585–2598 (2017).
- 435 Jinek, M. *et al.* A programmable dual-RNA-guided DNA endonuclease in adaptive bacterial immunity. *Science (80-.)*. **337**, 816–821 (2012).
- 436 Kleinstiver, B. P. *et al.* Genome-wide specificities of CRISPR-Cas Cpf1 nucleases in human cells. *Nat. Biotechnol.* **34**, 869–874 (2016).
- 437 Kim, D. *et al.* Genome-wide analysis reveals specificities of Cpf1 endonucleases in human cells. *Nat. Biotechnol.* **34**, 863–868 (2016).
- 438 Ran, F. A. *et al.* In vivo genome editing using Staphylococcus aureus Cas9. *Nature* **520**, 186–191 (2015).

- 439 Zetsche, B. *et al.* Cpf1 Is a Single RNA-Guided Endonuclease of a Class 2 CRISPR-Cas System. *Cell* **163**, 759-771 (2015).
- 440 Bin Moon, S. *et al.* Highly efficient genome editing by CRISPR-Cpf1 using CRISPR RNA with a uridylate-rich 3'-overhang. *Nat. Commun.* **9**, (2018).
- 441 Gao, L. *et al.* Engineered Cpf1 variants with altered PAM specificities. *Nat. Biotechnol.* **35**, 789-792 (2017).
- 442 Komor, A. C., Kim, Y. B., Packer, M. S., Zuris, J. A. & Liu, D. R. Programmable editing of a target base in genomic DNA without double-stranded DNA cleavage. *Nature* **533**, 420-424 (2016).
- 443 Gaudelli, N. M. *et al.* Programmable base editing of T to G C in genomic DNA without DNA cleavage. *Nature* **551**, 464-471 (2017).
- 444 Kosicki, M., Tomberg, K. & Bradley, A. Repair of double-strand breaks induced by CRISPR-Cas9 leads to large deletions and complex rearrangements. *Nat. Biotechnol.* **36**, 765-771 (2018).
- 445 Haapaniemi, E., Botla, S., Persson, J., Schmierer, B. & Taipale, J. CRISPR-Cas9 genome editing induces a p53-mediated DNA damage response. *Nat. Med.* **24**, 927-930 (2018).
- 446 Enache, O. M. *et al.* Cas9 activates the p53 pathway and selects for p53-inactivating mutations. *Nat. Genet.* **52**, 662-668 (2020).
- 447 Özcan, A. *et al.* Programmable RNA targeting with the single-protein CRISPR effector Cas7-11. *Nature* **597**, 720-725 (2021).
- 448 Abudayyeh, O. O. *et al.* A cytosine deaminase for programmable single-base RNA editing. *Science (80-.)*. **365**, 382-386 (2019).
- 449 Cox, D. B. T. *et al.* RNA editing with CRISPR-Cas13. *Science (80-.)*. **358**, 1019-1027 (2017).
- 450 Abudayyeh, O. O. *et al.* C2c2 is a single-component programmable RNA-guided RNA-targeting CRISPR effector. *Science (80-.)*. **353**, (2016).
- 451 Al-Shahrour, F. *et al.* Selection upon genome architecture: Conservation of functional neighborhoods with changing genes. *PLoS Comput. Biol.* **6**, (2010).
- 452 Lee, J. M. & Sonnhammer, E. L. L. Genomic gene clustering analysis of pathways in eukaryotes. *Genome Res.* **13**, 875-882 (2003).
- 453 Overbeek, R., Fonstein, M., D'Souza, M., Push, G. D. & Maltsev, N. The use of gene clusters to infer functional coupling. *Proc. Natl. Acad. Sci. U. S. A.* **96**, 2896-2901 (1999).
- 454 Yanai, I., Mellor, J. C. & DeLisi, C. Identifying functional links between genes using conserved chromosomal proximity. *Trends Genet.* **18**, 176-179 (2002).
- 455 Laurent, T. C., Moore, E. C. & Reichard, P. Enzymatic Synthesis of Deoxyribonucleotides. *Journal Biol. Chem.* **239**, 3436-3444 (1964).
- 456 Muri, J. *et al.* The thioredoxin-I system is essential for fueling DNA synthesis during T-cell metabolic reprogramming and proliferation. *Nat. Commun.* **9**, 1-16 (2018).
- 457 Ren, X. *et al.* The combination of ascorbate and menadione causes cancer cell death by oxidative stress and replicative stress. *Free Radic. Biol. Med.* **134**, 350-358 (2019).
- 458 Hashemy, S. I., Ungerstedt, J. S., Zahedi Avval, F. & Holmgren, A. Motexafin gadolinium, a tumor-selective drug targeting thioredoxin reductase and ribonucleotide reductase. *J. Biol. Chem.* **281**, 10691-10697 (2006).
- 459 Haffo, L. *et al.* Inhibition of the glutaredoxin and thioredoxin systems and ribonucleotide reductase by mutant p53-targeting compound APR-246. *Sci. Rep.* 1-10 (2018) doi:10.1038/s41598-018-31048-7.
- 460 Lou, M. *et al.* Physical interaction between human ribonucleotide reductase large subunit and thioredoxin increases colorectal cancer malignancy. *J. Biol. Chem.* **292**, 9136-9149 (2017).

- 461 Kuo, M. L. *et al.* PYCR1 and PYCR2 Interact and Collaborate with RRM2B to Protect Cells from Overt Oxidative Stress. *Sci. Rep.* **6**, 1-15 (2016).
- 462 Kuo, M. L. *et al.* RRM2B suppresses activation of the oxidative stress pathway and is Up-regulated by P53 during senescence. *Sci. Rep.* **2**, 1-9 (2012).
- 463 Tanaka, H. *et al.* A ribonucleotide reductase gene involved in a p53-dependent cell-cycle checkpoint for DNA damage. *Nature* **404**, (2000).
- 464 Zhou, B. *et al.* The Human Ribonucleotide Reductase Subunit hRRM2 Complements p53R2 in Response to UV-Induced DNA Repair in Cells with Mutant p53. *Cancer Res.* **63**, 6583-6594 (2003).
- 465 Zhang, D., Wang, Y., Jin, X., Xiao, Q. & Huang, S. A label-free and ultrasensitive electrochemical biosensor for oral cancer overexpressed l gene via exonuclease III-assisted target recycling and dual enzyme-assisted signal amplification strategies. *Analyst* **147**, 2412-2424 (2022).
- 466 Harten, A. M. Van & Brakenhoff, R. H. Targeted Treatment of Head and Neck (Pre) Cancer: Preclinical Target Identification and Development of Novel Therapeutic Applications. *Cancers (Basel)*. **13**, (2021).
- 467 Alshafi, E. *et al.* Clinical update on head and neck cancer: molecular biology and ongoing challenges. *Cell Death Dis.* **10**, (2019).
- 468 Vasan, N., Baselga, J. & Hyman, D. M. A view on drug resistance in cancer. *Nature* **575**, 299-309 (2019).
- 469 Zheng, Z. *et al.* Inhibition of thioredoxin activates mitophagy and overcomes adaptive bortezomib resistance in multiple myeloma. *J. Hematol. Oncol.* **11**, 1-15 (2018).
- 470 Raininga, P. V., Di Trapani, G., Vuckovic, S., Bhatia, M. & Tonissen, K. F. Erratum: Inhibition of thioredoxin 1 leads to apoptosis in drug-resistant multiple myeloma (*Oncotarget* (2015) 6 (15410-15424) DOI: 10.18632/oncotarget.3795). *Oncotarget* **12**, 948-949 (2021).
- 471 Beroukhi, R. *et al.* The landscape of somatic copy-number alteration across human cancers. *Nature* **463**, 899-905 (2010).
- 472 Zack, T. I. *et al.* Pan-cancer patterns of somatic copy number alteration. *Nat. Genet.* **45**, 1134-1140 (2013).
- 473 Vasudevan, A. *et al.* Aneuploidy as a promoter and suppressor of malignant growth. *Nat. Rev. Cancer* **21**, 89-103 (2021).
- 474 Stratton, M. R., Campbell, P. J. & Futreal, P. A. The cancer genome. *Nature* **458**, 719-724 (2009).
- 475 Smith, J. C. & Sheltzer, J. M. Systematic identification of mutations and copy number alterations associated with cancer patient prognosis. *Elife* **7**, 1-26 (2018).
- 476 Kumar, S. *et al.* Passenger Mutations in More Than 2,500 Cancer Genomes: Overall Molecular Functional Impact and Consequences. *Cell* **180**, 915-927.e16 (2020).
- 477 Muller, F. L., Aquilanti, E. A. & Depinho, R. A. Collateral Lethality: A New Therapeutic Strategy in Oncology. *Trends in Cancer* **1**, 161-173 (2015).
- 478 Bignell, G. R. *et al.* Signatures of mutation and selection in the cancer genome. *Nature* **463**, 893-898 (2010).
- 479 Rajaram, M. *et al.* Two Distinct Categories of Focal Deletions in Cancer Genomes. *PLoS One* **8**, (2013).
- 480 Cox, C. *et al.* A survey of homozygous deletions in human cancer genomes. *Proc. Natl. Acad. Sci. U. S. A.* **102**, 4542-4547 (2005).
- 481 Cheng, J. *et al.* Pan-cancer analysis of homozygous deletions in primary tumours uncovers rare tumour suppressors. *Nat. Commun.* **8**, 1-14 (2017).
- 482 Weckselblatt, B. & Rudd, M. K. Human Structural Variation: Mechanisms of Chromosome Rearrangements. *Trends Genet.* **31**, 587-599 (2015).

- 483 Clarke, T. L. *et al.* Histone lysine methylation dynamics control EGFR DNA copy-number amplification. *Cancer Discov.* **10**, 306–325 (2020).
- 484 Pertesi, M. *et al.* Essential genes shape cancer genomes through linear limitation of homozygous deletions. *Commun. Biol.* **2**, 1–11 (2019).
- 485 Kendall, J. *et al.* Oncogenic cooperation and coamplification of developmental transcription factor genes in lung cancer. *Proc. Natl. Acad. Sci. U. S. A.* **104**, 16663–16668 (2007).
- 486 Peng, Y. *et al.* Co-occurrence of CDKN2A/B and IFN-I homozygous deletions correlates with an immunosuppressive phenotype and poor prognosis in lung adenocarcinoma. *Mol. Oncol.* **16**, 1746–1760 (2022).
- 487 Barriga, F. M. *et al.* MACHETE identifies interferon-encompassing chromosome 9p21.3 deletions as mediators of immune evasion and metastasis. *Nat. Cancer* **3**, 1367–1385 (2022).
- 488 Eisenberg, E., Natarajan, E. & Formaker, B. K. Oral mucosa and mucosal sensation. in *Pocket Dentistry* (2015).
- 489 Ji, H. & Li, X. K. Oxidative Stress in Atopic Dermatitis. *Oxid. Med. Cell. Longev.* **2016**, (2016).
- 490 Lawton, S. Skin I: the structure and functions of the skin. *Nurs. Times* **115**, 2019 (2019).

Nederlandse samenvatting

Het genoom bevat alle genetische informatie die bepaalt hoe cellen en organen zich gedragen. Het genoom bestaat uit DNA: een lange streng met codes die bepaalde erfelijke eigenschappen bevatten. Deze codes zijn genen en elk gen wordt vertaald naar een eiwit. Eiwitten zijn de functionele eenheden in de cellen, die via complexe patronen en samenwerkingen er bijvoorbeeld voor zorgen dat cellen gaan groeien, vermenigvuldigen, of afsterven. In mensen is het DNA specifiek georganiseerd en verdeeld over 46 chromosomen. In gezonden cellen is hetzelfde DNA altijd gelokaliseerd op hetzelfde stuk van het specifieke chromosoom. Veel ziektes ontstaan door fouten in het DNA. Voorbeelden van dit soort fouten zijn kleine veranderingen in de code van een gen ('mutatie'), verwijdering van een stuk DNA waar een gen op ligt ('deletie'), of het ontstaan van meerdere kopieën van een stuk DNA ('amplificatie'). In het geval van amplificatie kunnen cellen van een bepaald stukje chromosoom - en dus alle genen die op dit stukje liggen - wel zes of acht kopieën hebben, in plaats van de gebruikelijke twee. Algemeen genomen zorgen mutaties en deleties voor inactivatie van de activiteit van genen, terwijl amplificatie juist zorgt voor overactiviteit van deze genen.

In dit proefschrift beschrijven we de functionele ontleding van een stuk DNA op chromosoom 11, dat in 25% van alle hoofd-halstumoren is geamplificeerd.

In **hoofdstuk 1** introduceren we hoe huid- en mondweefsel is opgebouwd en hoe fouten in het DNA kunnen resulteren in ziektes, waaronder hoofd-hals kanker. De huid bestaat uit verschillende lagen en elke laag bestaat uit verschillende type cellen. De bovenste laag is de epidermis en deze bestaat voor ongeveer 90% uit 1 cel type: de keratinocyt. Keratinocyten vormen de bouwstenen van deze huidlaag en zijn daarmee belangrijk voor de beschermen van het lichaam tegen zowel de omgeving (UV-straling, pathogenen) als bijvoorbeeld tegen uitdroging. In de mond-, neus- en keelholte is een soortgelijk weefsel aanwezig: het slijmvlies. Dit slijmvlies is opgebouwd uit hetzelfde type keratinocyten, met slechts kleine verschillen die bijvoorbeeld de hardheid en vochtigheid van het weefsel beïnvloeden. Keratinocyten spelen een belangrijke rol in diverse dermatologische aandoeningen en hoofd-hals tumoren.

Jaarlijks worden bijna een miljoen mensen gediagnosticeerd met hoofd-hals kanker en meer dan de helft van deze patiënten overlijdt aan de ziekte. Een beter begrip op moleculair niveau van het ontstaan en de progressie van deze tumoren kan bijdragen aan de ontwikkeling van nieuwe behandelingsplannen. Hoofd-hals tumoren ontstaan uit keratinocyten die door een samenspel van diverse mutaties, deleties en amplificaties ongeremd kunnen vermenigvuldigen. Hoewel elke tumor een andere combinatie van deze veranderingen heeft, komen bepaalde veranderingen vaker voor dan andere. De frequentie waarmee een verandering voorkomt is indicatief voor het belang van de verandering. 25% van alle hoofd-hals tumoren heeft amplificatie

van een specifiek stuk DNA op chromosoom 11, de 11q13 regio. Dit stuk DNA bevat meerdere genen, maar het is onduidelijk welke van deze genen bijdragen aan de ontwikkeling en progressie van de tumoren. In dit proefschrift beschrijven we de systematische analyse van de bijdrage van alle genen in de 11q13 regio en beschrijven we nieuwe inzichten in de moleculaire functie van de belangrijkste genen. Voor deze systematische analyse maken we o.a. gebruik van nieuwe, representatieve modellen met normale keratinocyten.

In **hoofdstuk 2** beschrijven we allereerst een nieuwe methode voor het efficiënt bezorgen van o.a. CRISPR-Cas9 machinerie in keratinocyten. CRISPR-Cas9 machinerie kan gebruikt worden om heel specifiek bepaalde veranderingen in het DNA aan te brengen, zoals mutaties en deleties. We laten zien dat we met deze nieuwe bezorgingsmethode het DNA heel efficiënt kunnen aanpassen. Deze aangepaste cellen kunnen vervolgens gebruikt worden in diverse toepassingen, waaronder het accuraat modelleren van veranderingen in het DNA in kanker. Ook gebruiken we deze methode om 2 genen die belangrijk zijn voor herkenning door het immuunsysteem te inactiveren. Deze aangepaste cellen kunnen daardoor niet herkend worden door het immuunsysteem als 'niet lichaamseigen' en daardoor gebruikt worden als celtherapie voor patiënten met condities waarin de huid wonden niet (voldoende) zelf kan dichten, zoals brandwonden of epidermolysis bullosa.

In **hoofdstuk 3** analyseren we de bijdrage van alle genen op de 11q13 amplificatie in hoofd-hals kanker. Daartoe analyseren we eerst diverse patiënten datasets met informatie over de amplificatie en expressie (activatie) status van de 11q13 regio. Naar aanleiding van die data definiëren we eerst de 11q13 amplificatie tot een regio van tien genen en daarna concluderen we dat slechts zeven van de tien genen geactiveerd zijn door de amplificatie. Vervolgens doen we verscheidene experimenten met zowel kankercellen als normale cellen, waarbij we de expressie van deze zeven genen veranderen en vervolgens celgroei en invasie meten. Hieruit concluderen we dat drie genen in de 11q13 regio (*CCND1*, *ORAOVI*, en *MIR548K*) de belangrijkste bijdragen leveren aan tumor groei- en/of uitzaaing. *CCND1* en *ORAOVI* bevinden zich direct naast elkaar aan het ene einde van de amplificatie, terwijl *MIR548K* zich aan het andere einde bevindt. We beschrijven dat deze drie genen onafhankelijk van elkaar een effect hebben op tumorgroei en de verhoogde activatie van elk van deze genen – met name *CCND1* en *ORAOVI* – is voldoende om tumorgroei in muizen te stimuleren. We concluderen dat door de combinatie van deze drie effecten, de amplificatie van de 11q13 regio een bepalende factor is in tumorgroei en prognose van hoofd-hals kanker.

In **hoofdstuk 4** onderzoeken we de functie van geamplificeerd *CCND1* in hoofd-hals kanker. *CCND1* is een bekend kankergen dat celdeling stimuleert en activatie van dit gen draagt bij aan de ontwikkeling van vele soorten kanker. We ontdekken dat kankercellen met de 11q13 amplificatie afhankelijk zijn van de verhoogde *CCND1* levels, maar dat normale keratinocyten dat niet zijn. Het remmen van *CCND1* remt

daardoor alleen groei van kankercellen, en niet van normale cellen. Er zijn nog geen medicijnen om *CCND1* direct te remmen. Echter, een van de bekendste functies van *CCND1* in de celdeling is de interactie met twee andere eiwitten: CDK4 en CDK6. Hier bestaan wel medicijnen tegen. Onverwachts zien we echter dat de kankercellen minder gevoelig zijn voor deze medicijnen dan de normale cellen. Met diverse andere experimenten beschrijven we vervolgens dat in de cellen met de 11q13 amplificatie, *CCND1* een functie heeft die onafhankelijk is van deze CDK4 en CDK6 eiwitten. Om te detecteren of *CCND1* in deze cellen een ander target heeft wat wel geremd kan worden, analyseren we twee grote genexpressie datasets. De eerste bevat data van patiënten met of zonder de 11q13 amplificatie, de tweede bevat zelf gegenereerde data van de veranderde genexpressie als *CCND1* wordt geïnactiveerd in cellen met de 11q13 amplificatie. Door analyse in de overlap tussen deze datasets identificeren we dat *CCND1* de expressie van een ander gen, *RRM2*, stimuleert. Inactivatie van *RRM2* remt specifiek de groei van cellen met hoge *CCND1* levels en remming van *RRM2* met een medicijn remt de groei van deze tumoren in muizen. Samenvattend beschrijven we in dit hoofdstuk nieuwe inzichten en strategieën voor het remmen van hoofd-hals tumoren met de 11q13 amplificatie.

In hoofdstuk 5 onderzoeken we de rol van *ORAOVI* in tumoren met de 11q13 amplificatie. *ORAOVI* ligt direct naast *CCND1* op het DNA, maar daar waar *CCND1* een bekend kankergen is, is over *ORAOVI* heel weinig bekend. Hier beschrijven we echter dat bijna alle tumoren – niet alleen hoofd-hals tumoren – die *CCND1* amplificatie hebben, ook *ORAOVI* amplificatie hebben en afhankelijk zijn van hoge *ORAOVI* levels. Er is weinig bekend over de functie van *ORAOVI* in menselijke cellen, maar een vergelijkbaar gen is in planten belangrijk voor de regulering van oxidatieve stress levels in de cellen. Inactivatie van *ORAOVI* in kankercellen resulteert inderdaad in verhoogde oxidatieve stress levels, terwijl activatie van *ORAOVI* cellen juist beschermt tegen deze oxidatieve stress.

Kankercellen delen veelvuldig, wat gepaard gaat met verhoogde oxidatieve stress levels. Kankercellen ontwikkelen daarom diverse mechanismes om hiermee om te gaan en een van de bekendste mechanismes is via activatie van thioredoxin – wat een anti-oxidatieve werking heeft. Via analyse van genexpressie patronen na inactivatie van *ORAOVI* identificeren we dat *ORAOVI* de expressie van thioredoxin stimuleert. We concluderen dat de amplificatie van *ORAOVI* – via thioredoxin – de kankercellen beschermt tegen hoge stress levels.

In hoofdstuk 6 bediscussiëren we de resultaten en conclusies uit dit proefschrift. We beschrijven de uitdagingen en daaruit voortvloeiende tekortkomingen omtrent het gebruik van normale keratinocyten in het modelleren van genetische huidziekten en kanker. De efficiënte bezorgingsmethode van CRISPR-Cas machinerie die we hier beschrijven kan deze uitdagingen deels wegnemen. In combinatie met vernieuwde technologie omtrent modificatie van het DNA en 3D- en muis-modellen, vormen

normale keratinocyten een uitstekend celtype om vele huidziektes mee te modelleren en nieuwe therapieën te testen.

Vervolgens beschrijven we hoe de ontleding van de genen in de 11q13 regio kan bijdragen aan nieuwe ideeën voor het behandelen van hoofd-hals tumoren met de 11q13 amplificatie. Zo suggereren we dat voor specifiek dit type tumoren het direct remmen van *CCND1* beter is dan het remmen van *CCND1* activiteit met *CDK4/CDK6* remmers. Andere opties zijn het remmen van *RRM2* of *TXN* activiteit. Bovendien kunnen deze laatste opties theoretisch bijdragen aan het voorkomen van resistentie tegen bijvoorbeeld chemotherapieën, aangezien voor beide genen in andere kankersoorten al is aangetoond dat hun verhoogde activiteit resulteert in chemoresistentie. Tot slot beschrijven we dat de eerst bekende functie van *TXN* het activeren van *RRM2* activiteit is. Hieraan verbinden we de conclusie dat *ORAOV1* - door middel van *TXN* activatie - bijdraagt aan de door de *CCND1*-geactiveerde *RRM2* activiteit. Dit duidt op mogelijke coöperatie tussen deze twee genen op de 11q13 amplificatie.

De analyse van de genen in de 11q13 regio zoals beschreven in dit proefschrift geeft nieuwe inzichten in de bijdrage van de 11q13 amplificatie in hoofd-hals kanker en geeft richting aan vervolgonderzoeken die de effectiviteit van de nieuw geïdentificeerde targets kunnen verifiëren.

Curriculum Vitae

Céline Ismay Mahieu was born on July 18 1992 in Utrecht, the Netherlands. She graduated from secondary school at Het Nieuwe Lyceum (Bilthoven) in 2010. She continued her education at Utrecht University, where she pursued a Bachelor's degree in Biomedical Sciences. She finalized this degree with a research project in the lab of Prof. Dr. Saskia van Mil at the department of Molecular Cancer Research, UMC Utrecht on the role of FXR signaling in Ulcerative Colitis.

In 2013, Céline started with her Master's program in Cancer, Stem Cells & Developmental Biology at Utrecht University. As part of this program, she performed two internships. For her first internship, she worked at the lab of Prof. Dr. Boudewijn Burgering at the department of Molecular Cancer Research, UMC Utrecht, focusing on cyclin-dependent kinase inhibitors in FOXO signaling. For her final internship, Céline worked at the lab of Prof. Andrei Goga at the department of Cell and Tissue Biology at the University of California, San Francisco. Here she worked on the contribution of fatty acid oxidation to the progression of triple negative breast cancers. After she finished her internship, she continued as a junior specialist for an additional 8 months, where she further developed her project regarding the role of *FABP5* in MYC-driven triple negative breast cancers. Céline obtained her Master's degree in 2016.

In 2018, Céline started her PhD-trajectory in the lab of Dr. Aaron Tward at the department of Otolaryngology and Head and Neck Surgery at the University of California, San Francisco (in collaboration with Prof. Dr. René Bernards at the Division of Molecular Carcinogenesis at the Netherlands Cancer Institute). Here she worked on several projects involving functional genomics of head and neck squamous cell carcinoma and primary cell engineering. As part of her PhD she also initiated and led a collaboration with MaxCyte to develop a workflow for efficient genome engineering of primary keratinocytes. The results of her PhD research are presented in this thesis.

Dankwoord

Like every PhD-trajectory, this one has been quite the journey. Literally, as I spent almost 5 years 9000 kilometers away from my homebase. Figuratively, as I started with ideas and concepts on what my PhD should be like, and quickly learned I had to mold these ideas to what was realistic, while pushing on what was possible.

Along the way I found a lot of people who helped and supported me. Thank you all for being part of this.

First of I'd like to thank **Aaron**. We met when I was still an intern on the same floor during a joint lab meeting. When I contacted you about the possibilities of doing a PhD in your lab, you immediately bombarded me with ideas. Despite your attempts to lure me over to the ear-side, I stuck at 'team cancer'. You gave me all the freedom and trust to explore whatever I was interested in, as long as I could tell 'what is the question'. Thank you for the opportunity and trust. Keep Living The Dream!

Rene, bedankt voor je oprechte interesse in mijn PhD project en het vormen van de link naar mijn thuis universiteit. Je ideeën en vragen tijdens onze meetings van de afgelopen jaren zijn zo waardevol geweest. Bedankt dat je mijn PhD bijstuurde en bereikbaar was als het even nodig was.

Beste **beoordelingscommissie**, bedankt voor jullie tijd om mijn proefschrift te beoordelen.

Everyone in the **Tward lab**, present and past. **Vicente**, super post-doc/lab-dad. When I interviewed with you, we had a terrible connection because I was camping in the mountains. I thought that was a bad omen, but little did I know that just a year later I would be doing that exact thing together with you. It's been amazing working with you, learning from you, exploring California together, and forcing our European lifestyle on those Boston people ;). **Stacey**, I've been so impressed with your scientific rigor and endless willingness to help and teach. Your kindness and warmth made me feel home in the lab right away. I wish our times in the lab had overlapped for longer, but I'm so excited for this new Boston chapter for you! **Sonia**, my fellow-PhD student (although Team Ear). I'm so glad I had you to complain with, cry with, yell with, but mostly laugh with. You are so smart and I'm excited to follow your journey towards your ENT specialty. Sorry I never wanted to do a marathon with the lab. I'd rather eat croissants. **Ellee**, the lab would have crumbled without you. It has been amazing watching you grow over the years, both in professional and personal settings. Especially this last year, I've been so happy I had you next to me fight the fight and I cherish our strategically planned back-to-back TC sessions. I wish you everything good in your next chapter of becoming an amazing MD. I have no doubt you're gonna kill it. **Nancy**, spirit animal. I admire your excitement and scientific knowledge. You

don't buy bullshit but you do drink wine. I'm so grateful to have worked with you. I'm definitely coming back for more Napa trips. **Elijah, Ramin, Kevin, Sarah, Kimberly, David, Catherine, Andrea, Douwe, Amar, and Xian** (you've just become honorary Tward lab at this point): thank you for all your input, help, laughs, and changing the liquid nitrogen tanks when I didn't want to.

All the labs on HSE7, but particularly the Smith and Chang labs. For generously sharing equipment and tolerating our beeping-everything. **Bogdan, Eileen, Noura, Ian, and Yesai**: I miss our happy hours more than anything and my only regret is that we didn't start those earlier. Thank you for providing a real lab community. Bogdan, you deserve an extra shout-out. This is the shout-out.

The **Selleri lab**, for always tolerating me using every piece of equipment you have. Is it even a real lab day if I don't show up? **Licia**, thank you for facilitating, and always being so kind and supportive whenever we ran into each other. **Maurizio**, thank you for teaching me mouse handling. **Brandon**, always willing to help. **Marta**, I can't even pinpoint what to thank you for exactly, but I guess it comes down to being a friend. Thank you for your words of wisdom that put everything in perspective, moral support, and picnicks in the park. The weekend meetups with you, Vicente, and Chloe have been a real beacon in this last year and my main source of stress relieve.

The **Goga lab**, where I started my UCSF adventure as a research intern back in 2015 and where I continued showing up randomly. **Andrei**, thank you for your support over the years.

MaxCyte, in particular **Daniel, Lesley, James, and Caroline**: thank you for our wonderful collaboration, supporting me, and providing me with so many opportunities to share our work. I've really enjoyed this process - and the dinners.

Then there have been many people outside the lab who have kept me sane and make this San Francisco experience one to never forget.

My dear **Improv at UCSF** family. How far we've come from our first class and what an important part of feeling home in San Francisco. **Miki and Rosalba**, I loved being a team with you. I am so proud of the shows and classes we put down and I can't wait for all the visits you promised to pay me. **Elise**, one day I hope to be on stage with you again. Until then, I'll patiently watch you nail starting your own lab at the NIH. **Neha, Will, Erika, Marcell, Ale**: thank you all!

Kelly, we zagen elkaar niet zo vaak, maar wel op de juiste momenten. Dank voor al je openheid en zo tof om te zien dat je uithoudingsvermogen wordt beloond met je eigen lab in San Diego! Zo verdiend!

Roman and Krystal, there's not going to be sufficient pages in this thesis to thank you enough. Roman, you are to blame for it all. You have been an amazing mentor - turning into an equally amazing friend. I'm so honored you will make it all the way to Utrecht to stand by me during my defense. Krystal, you are so inspiring. Strong female scientist who knows what she wants (and particularly what not!). I feel so cool being able to call you two 'friends'.

John and Christina, I cherish the game nights and extensive cheese platters at your place.

Eric, thank you for sharing all your miRNA expertise when I really didn't want to go down that rabbit hole.

Francesca and Marcus, penthouse buddies. Being able to signal to each other with our living room lights has been one of lives greatest pleasures. I'm so happy to explore this next European chapter in parallel with you. Francesca, you are such a fantastic scientist and valuable friend, and I miss our wine and decorative chocolates nights.

Stijn en Lisa, ik ben zo dankbaar dat San Francisco ons heeft samengebracht. Onze avonturen hebben me zo veel gebracht. Heel fijn om jullie nog steeds - relatief - dicht bij te hebben. *I like you as much as I like mountains.*

Knowing that somewhere back home - or in Europe, at least - there is this collection of people patiently waiting for my return and cheering me on, has been a great feeling.

Cinzia and Ana, years pass but I know you're there! **Maanlanding, Lisa en Rik, Marjon, Rineke**: wat fijn dat ik jullie weer wat vaker kan zien!

Iris, we kennen elkaar al meer dan 12 jaar (!), toch voelt het of onze vriendschap juist in de afgelopen jaren echt gegroeid is. Een avondje bij jou op de bank met een goede fles wijn doet wonderen. En dat ligt echt meer aan jou dan aan de wijn. De Grote Problemen Des Levens zijn met jou heerlijk te relativeren en helpen mij altijd weer gewoon te doen wat ik zelf wil. Dat is zo waardevol. Ik vind het heel fijn om jou bij mijn zijde te hebben tijdens mijn verdediging.

Lieve **familie**, sorry dat ik al jullie kringverjaardagen heb gemist.

Guyon, altijd mijn broertje, altijd oeverloze kletsverhalen. Ik vind het fascinerend hoe wij zo onze eigen weg zijn gegaan, op het oog erg verschillend, maar uiteindelijk eigenlijk best hetzelfde. "Of ik nou al bijna klaar was". Kon ik ook aan jou vragen. En inmiddels kunnen we dat allebei bevestigen. En jij zelfs nog iets eerder dan ik. Shit. Wel goed van ons hè.

Papa, dankjewel voor al je support. Hoewel het vast niet makkelijk is om je dochter naar de andere kant van de wereld te zien vertrekken, heb ik me altijd enorm gesteund gevoeld in die keuze. Uiteindelijk ben ik natuurlijk ook erfelijk belast met die drang naar bergen en avontuur. Jouw bezoekjes in San Francisco waar ik mijn wereld en uitzichten met je kon delen, vond ik fantastisch. Jij en mama hebben me altijd gestimuleerd om te bereiken wat ik kan, te doen wat ik wil, en te dromen wat ik zal. Zo'n warm thuisfront en vangnet is een enorme luxe waar ik zo dankbaar voor ben. Het is de basis voor alles. Dankjewel.

Andrew, I am so grateful to have you as my partner and live this wonderful adventurous life with you. Your faith and support continuously push me further, both scientifically and in life. Throughout this crazy PhD, you were there to come home to. You were the one that could always show me I was doing just fine when I was not able to see that by myself. Whether its about science or life, you always strive for better and bolder. When I propose a hike, you propose a multi-day backpacking trip. When we go camping, we go camping in Alaska. And I enjoy nothing more than going on these crazy adventures with you. I am so excited to see what else life has in store for us.

Mama, voor jou.

Ik mis je elke dag in alles wat ik doe.

Maar het gaat goed, want ik lijk op jou.

Céline

